



Mag. rer. nat. Wolf-Dieter Lienhart

**Biochemical characterisation of NAD(P)H:quinone
oxidoreductase 1 variants involved in cancer development and
resistance to chemotherapy.**

DISSERTATION

zur Erlangung des akademischen Grades

Doktor der Naturwissenschaften

eingereicht an der

Technischen Universität Graz

Betreuer

Univ.-Prof. Mag. rer. nat. Dr. rer. nat. Peter Macheroux

Institut für Biochemie
Technische Universität Graz

Gelbes Gold hat seinen Preis;
Wissen ist unbezahlbar.

Chinesische Weisheit

I have never been disappointed upon asking
microorganisms for whatever I wanted.

Kin'ichiro Sakaguchi

Acknowledgements

First I want to thank my supervisor Peter Macheroux for giving me the chance to start working in this amazing project. I am grateful that he facilitated to guide the project predominantly autonomous and to test exciting new technics and methods assisted with feedback and new thoughts from him. Whenever problems occurred and I needed new inspiration I could talk to Peter Macheroux and I returned with new ideas and knowledge.

I would like to thank all my former and current colleagues at the institute for being my friends and for the great working atmosphere. Some people of the institute especially contributed something to my work. Alexandra Binter, Venugopal Gudipati, Karin Koch and Emilia Strandback helped me in the lab by contributing new ideas and also practical help in the project. Silvia Wallner was always kindly answering every question and helping with the lab equipment and the procedures for experiments.

Sincere thanks to Karl Gruber and Michael Uhl for their support with the crystallisation of the protein even if the crystallisation screenings appeared to be quite labour-intensive in the beginning of the work.

I am grateful to Klaus Zangger and Sergio Pulido for all the help and the support of the project and providing a new focus on the experiments.

Furthermore I want to thank David Rantasa and Geraldine Zenz for all the help in the project during their work.

I want to thank Karina Hauer for supporting me all the years. A life without you is unthinkable for me and I am thinking forward to our common and scientific future. I am thankful that Karina made my life so wonderful. Moreover I want to thank my parents Dieter and Gertrude Lienhart for their encouragement during my whole life.

Finally I would like to thank all the people helping me, talking to me and giving me new inspirations and ideas but are not mentioned namely.

Tabel of contents

Acknowledgements	iii
Prefix.....	- 1 -
Abstract	- 2 -
Kurzfassung	- 3 -
STATUTORY DECLARATION.....	- 4 -
Chapter 1: Introduction.....	- 5 -
The flavoproteome of the yeast <i>Saccharomyces cerevisiae</i>	- 6 -
Author Contributions.....	- 6 -
The human flavoproteome.....	- 17 -
Author Contributions.....	- 17 -
Supporting Information	- 31 -
Chapter 2: NAD(P)H:quinone oxidoreductase 1.....	- 33 -
Collapse of the native structure caused by a single amino acid exchange in human NAD(P)H:quinone oxidoreductase 1	- 34 -
Author Contributions.....	- 34 -
The impact of human <i>NQO1*3</i> , coding for NAD(P)H:quinone oxidoreductase 1 R139W, on the catalytic competence, structure and stability of the cancer associated flavoenzyme	- 49 -
Author Contributions.....	- 49 -
Chapter 3: Additional publications.....	- 66 -
Biocatalytic Enantioselective Oxidative C-C Coupling by Aerobic C-H Activation.....	- 67 -
Author Contributions.....	- 67 -
Biocatalytic Organic Synthesis of optically pure (<i>S</i>)-Scoulerine and Berbine and Benzylisoquinoline Alkaloids	- 74 -
Author Contributions.....	- 74 -
Appendix.....	- 87 -
Curriculum Vitae	- 88 -
Publications	- 90 -
Papers:.....	- 90 -
Presentations:.....	- 90 -
Posters:.....	- 90 -

Prefix

Abstract

NAD(P)H:quinone oxidoreductase 1 (NQO1; EC 1.6.99.2) is an essential flavoenzyme in the antioxidant defence system. Thereby NQO1 is catalysing the two electron reduction of quinones to hydroquinones without the formation of semiquinones. Semiquinones can lead to the formation of reactive oxygen species promoting the development of cancer. Furthermore NQO1 is stabilising various tumour suppressors for instance p33, p53 and p73, and prevents the proteasomal degradation by the 20S proteasome altogether leading to an antineoplastic effect.

A high number of tumours have increased levels of NQO1 turning the enzyme to a promising target for chemotherapy. Various chemotherapeutic prodrugs like mitomycin c are activated by NQO1 and thus cause an increased cytotoxic effect in tumour tissue.

Two frequent single nucleotide polymorphisms (SNPs) are occurring in the human population, to be specific a cytosine-thymine exchange in position 609 (NQO1 609C>T; NQO1*2) and an exchange in position 465 (NQO1 465C>T; NQO1*3). Even though the amino acid exchanges are not in or near the active site, both SNPs are found to be connected with a higher risk for specific cancers and an elevated toxicity of benzene.

One common SNP, namely NQO1*2, leads to a proline to serine exchange in position 187 (NQO1 P187S). Depending on the ethnic population the homozygous polymorphism can be found in 4 to 20% of the population and is even more increased in cancer patients. Furthermore chemotherapeutic prodrugs targeting NQO1 do not work in an appropriate way because of diminished functionality of the enzyme. Previous studies have already shown a decreased enzyme activity but structural information was lacking and thus no satisfactory explanation for the altered behaviour could be provided. Our crystal structure revealed a structure that appeared to be identical to the wildtype NQO1. Nevertheless NMR measurements revealed a higher flexibility of the C-terminal region of the protein leading to a destabilisation and a loss of enzyme activity and stability.

In the case of NQO1*3, arginine in position 139 is replaced by tryptophan. Due to the minor frequency of this variant fewer studies are available for this variant. Reduced activity as well as an accumulation of an alternatively spliced form of the mRNA was shown by whole cell studies. But it was still unclear if the exchange of the charged arginine to an aromatic tryptophan at the protein surface will have any effect on the protein's stability and/or function. Our experiments have shown that the main cause of the elevated cancer risk appears to be erroneous splicing because the biochemical and structural properties of the variant are very similar to those of wild-type enzyme.

Current screenings are already testing for these SNPs and the development of drugs that stabilise for example the NQO1 P187S variant could be useful approaches to improve cancer therapy.

Keywords: quinone reductase, flavoprotein, NQO1; NQO1 P187S; NQO1 R139W; cancer development; SNP

Kurzfassung

Die NAD(P)H:Chinon Oxidoreduktase 1 (NQO1; EC 1.6.99.2) ist ein wichtiges enzymatisches Antioxidans. NQO1 katalysiert eine Zweielektronenübertragung vom FAD-Cofaktor auf Chinone wodurch eine Bildung von reaktiven, radikalischen Zwischenstufen (Semichinone) verhindert wird. Des Weiteren bindet es an Tumorsuppressoren wie zum Beispiel p33, p53 und p73 und verhindert dadurch deren Abbau durch das 20S Proteasom. Diese Funktionen und die Tatsache, dass zahlreiche Tumorzelllinien einen erhöhten NQO1 Spiegel aufweisen, machen das Enzym zu einem vielversprechenden Ziel für die Chemotherapie. Man macht sich die Aktivität von NQO1 bereits zu Nutze indem man Chemotherapeutika, wie zum Beispiel Mitomycin C einsetzt. Diese werden als inaktive Vorläufersubstanz aufgenommen und werden erst im Zielgewebe durch NQO1 aktiviert.

In der Gensequenz von NQO1 treten zwei Einzelnukleotid-Polymorphismen (SNPs) an den Positionen 609 (NQO1 609C>T; NQO1*2) und 465 (NQO1 465C>T; NQO1*3) gehäuft auf. Obwohl die veränderten Aminosäuren nicht im aktiven Zentrum des Proteins lokalisiert sind, zeigen betroffene Personen ein erhöhtes Krebsrisiko und eine verstärkte Toxizität von Benzol.

Im Fall von NQO1*2 ist die Aminosäure Prolin in Position 187 zu Serin ausgetauscht (NQO1 P187S). Diese Variante ist mit 4% bis zu 20% sehr weit verbreitet. Zahlreiche Studien zeigten bereits, dass diese Proteinvariante eine verringerte katalytische Aktivität aufweist. Daher werden chemotherapeutische Vorläufersubstanzen nicht mehr ausreichend durch NQO1 umgesetzt, wodurch eine erfolgreiche Krebsbehandlung erschwert wird. Diese Studien lieferten jedoch keine eindeutige Erklärung für das unterschiedliche Verhalten der Variante. Die erste Kristallstruktur von NQO1 P187S zeigte, dass dessen Struktur identisch mit dem Wildtyp ist. Weitere Untersuchungen mittels NMR zeigten jedoch, dass der C-Terminus von NQO1 P187S flexibler ist und daher zu einer Destabilisierung des Proteins und folglich zu einem Verlust der Enzymaktivität führt.

Bei NQO1*3 wird auf Position 139 ein Arginin mit einem Tryptophan ausgetauscht. Da diese Variante weitaus seltener verbreitet ist, existieren weniger Studien. Aber auch hier zeigten Experimente mit Krebszellen, dass eine verminderte Chinon-Reduktase-Aktivität vorliegt. Des Weiteren wurde ein gehäuftes Auftreten einer alternativ prozessierten mRNA beobachtet. Unsere Experimente zeigten, dass vermutlich die fehlerhafte Prozessierung der pre-mRNA der Hauptgrund für das erhöhte Krebsrisiko bei Trägern dieser Variante darstellt, da weder die Proteinstabilität noch die Enzymaktivität wesentlich beeinflusst sind.

Die erhaltenen Daten zeigen, dass eine Überprüfung von Krebspatienten bezüglich ihrer NQO1 Genvariante und Medikamente die zur Stabilisierung von NQO1 P187S beitragen, eine vielversprechende Möglichkeit zur Verbesserung der Krebstherapie darstellen.

Schlagwörter: Chinonreduktase; Flavoprotein; NQO1; NQO1 P187S; NQO1 R129W; Krebsentstehung; SNP

EIDESSTÄTTLICHE ERKLÄRUNG

Ich erkläre an Eides statt, dass ich die vorliegende Arbeit selbstständig verfasst, andere als die angegebenen Quellen/Hilfsmittel nicht benutzt, und die den benutzten Quellen wörtlich und inhaltlich entnommenen Stellen als solche kenntlich gemacht habe.

STATUTORY DECLARATION

I declare that I have authored this thesis independently, that I have not used other than the declared sources / resources, and that I have explicitly marked all material which has been quoted either literally or by content from the used sources.

Graz,

.....

Chapter 1: Introduction

The flavoproteome of the yeast *Saccharomyces cerevisiae*

Author Contributions

The manuscript has been published in *BIOCHIMICA ET BIOPHYSICA ACTA* (2014), Volume 1844, Number 3, Pages 534-544. The literature search and the writing of the paper was a cooperation among the authors.



ELSEVIER

Contents lists available at ScienceDirect

Biochimica et Biophysica Acta

journal homepage: www.elsevier.com/locate/bbapap

Review

The flavoproteome of the yeast *Saccharomyces cerevisiae*

Venugopal Gudipati, Karin Koch, Wolf-Dieter Lienhart, Peter Macheroux*

Graz University of Technology, Institute of Biochemistry, Petersgasse 12, A-8010 Graz, Austria

ARTICLE INFO

Article history:

Received 4 November 2013

Received in revised form 18 December 2013

Accepted 21 December 2013

Available online 27 December 2013

Keywords:

Iron metabolism

Mitochondrion

Redox balance

tRNA-modifications

Membrane transporters

ABSTRACT

Genome analysis of the yeast *Saccharomyces cerevisiae* identified 68 genes encoding flavin-dependent proteins (1.1% of protein encoding genes) to which 47 distinct biochemical functions were assigned. The majority of flavoproteins operate in mitochondria where they participate in redox processes revolving around the transfer of electrons to the electron transport chain. In addition, we found that flavoenzymes play a central role in various aspects of iron metabolism, such as iron uptake, the biogenesis of iron–sulfur clusters and insertion of the heme cofactor into apocytochromes. Another important group of flavoenzymes is directly (Dus1-4p and Mto1p) or indirectly (Tyw1p) involved in reactions leading to tRNA-modifications. Despite the wealth of genetic information available for *S. cerevisiae*, we were surprised that many flavoproteins are poorly characterized biochemically. For example, the role of the yeast flavodoxins Pst2p, Rfs1p and Ycp4p with regard to their electron donor and acceptor is presently unknown. Similarly, the function of the heterodimeric Aim45p/Cir1p, which is homologous to the electron-transferring flavoproteins of higher eukaryotes, in electron transfer processes occurring in the mitochondrial matrix remains to be elucidated. This lack of information extends to the five membrane proteins involved in riboflavin or FAD transport as well as FMN and FAD homeostasis within the yeast cell. Nevertheless, several yeast flavoproteins, were identified as convenient model systems both in terms of their mechanism of action as well as structurally to improve our understanding of diseases caused by dysfunctional human flavoprotein orthologs.

© 2013 The Authors. Published by Elsevier B.V. Open access under [CC BY-NC-ND license](http://creativecommons.org/licenses/by-nc-nd/3.0/).

1. Introduction to the history of Flavoprotein discovery

The yeast *Saccharomyces cerevisiae* played a central role in the discovery of flavoproteins as Otto Warburg and his collaborators were the first to isolate a “yellow ferment” from yeast cells [1]. Further studies by Theorell led to the concept of reversible association of co-enzyme and apo-enzyme to form the active holo-enzyme [2]. The isolation of other (new) yellow ferments from yeast prompted the renaming of the original ferment in to “old yellow ferment” (old yellow enzyme = OYE) [3]. Although it was demonstrated that OYE is reduced by NADPH [1,4] the physiological electron accepting substrate(s) remains uncertain despite its reported role in the maintenance of the cytoskeleton [5]. This may have contributed

to the persistent use of OYE instead of the official classification as NAD(P)H dehydrogenase (EC 1.6.99.1).

Despite the elusive nature of the physiological substrate(s), OYE rapidly developed in to an important model flavoenzyme culminating in the determination of the nucleotide sequence of *oye2* and *oye3* as well as the elucidation of its three-dimensional structure by X-ray crystallography [6–8]. The detailed biochemical characterisation of OYE also led to the identification of a number of artificial substrates, such as *N*-ethylmaleimide, cyclohex-2-enone and nitroolefins [8–10]. All of these substrates share a common structural motif consisting of an electron-withdrawing group (e.g. a carbonyl or nitro group) in α -position of a carbon–carbon double bond. The remarkably broad range of accepted substrates rendered OYE an ideal tool for biocatalytic applications exploited in numerous studies [11–15]. These efforts were further stimulated by the discovery of OYE homologs in many eubacteria as well as plant species in the 1990s [16–23]. Plant OYE homologs were of particular interest because of their well-defined role in the biosynthesis of the plant hormone jasmonate, which plays a crucial role in the plant’s defense response to pathogens [24,25]. In all reported cases, the natural substrates exhibited the structural motif discovered in previous studies with yeast OYE. Hence, the yeast enzyme also became the paradigm for the class of “ene-reductases” now widely used for the synthesis of a variety of useful chemicals. Curiously, the broad range of activated “enes” accepted by OYEs as substrates is in stark contrast to its

Abbreviations: DHAP, dihydroxy acetone phosphate; DHBp, 3,4-dihydroxy-2-butanone-4-phosphate; DRAP, 2,5-diamino-6-(ribosylamino)-4-(3H)-pyrimidinone 5'-phosphate; ER, endoplasmic reticulum; ETC, electron transport chain; Gly3p, glycerol 3-phosphate; gluSA, γ -glutamic acid semialdehyde; Mia(40), mitochondrial intermembrane space import and assay/oxidoreductase 40; ORF, open reading frame; Q, ubiquinone

* Corresponding author. Tel.: +43 316 873 6450; fax: +43 316 873 6952.

E-mail address: peter.macheroux@tugraz.at (P. Macheroux).

1570-9639 © 2013 The Authors. Published by Elsevier B.V. Open access under [CC BY-NC-ND license](http://creativecommons.org/licenses/by-nc-nd/3.0/).
<http://dx.doi.org/10.1016/j.bbapap.2013.12.015>

Table 1
Yeast flavoproteins and genes.

No.	E.C.	Enzyme	Cofactor	Structure clan (family) ^a	Localization	Abbrev.	Syst. name
1	1.1.2.3	L-Lactate:cytochrome c oxidoreductase (flavocytochrome b ₂)	FMN/heme	TIM_barrel (FMN_dh)	Mito. intermembr. sp.	<i>cyb2</i>	YML054C
2	1.1.2.4	D-Lactate dehydrogenase	FAD/heme	–	I. mito. membr. Mito. matrix Cytoplasm	<i>ddl1</i> <i>ddl2</i> <i>ddl3</i>	YDL174C YDL178W YEL071W
3	1.1.3.37	D-Arabino-1,4-lactone oxidase	8α-(N3-His) -FAD	<i>FAD_PCMH</i>	O. mito. membr.	<i>alo1</i>	YML086C
4	1.1.5.3	Glycerol-3-phosphate dehydrogenase	FAD	<i>NADP_Rossmann (DAO)</i>	I. mito. membr.	<i>gut2</i>	YIL155C
5	1.3.1.90	tRNA dihydrouridine synthase	FMN	<i>TIM_barrel (Dus)</i>	Nucleus Nucleus/cytoplasm Nucleus/cytoplasm	<i>dus1</i> <i>dus2</i> <i>dus3</i>	YML080W YNR015W YLR401C
						<i>dus4</i>	YLR405W
6	1.3.3.1	Dihydroorotate dehydrogenase	FMN	<i>TIM_barrel (DHO_dh)</i>	Cytoplasm	<i>ura1</i>	YKL216W
7	1.3.3.4	Protoporphyrinogen IX oxidase	FAD	<i>NADP_Rossmann (Amino_oxidase)</i>	I. mito. membr.	<i>hem14</i>	YER014W
8	1.3.3.6	Acyl-CoA oxidase	FAD	<i>Acyl-CoA_dh (ACOX, acyl-CoA_dh_1)</i>	Peroxisome	<i>pox1</i>	YGL205W
9	1.3.5.1	Succinate dehydrogenase	8α-(N3-His) -FAD/2Fe-2S/	<i>NAPH_Rossmann (FAD_binding_2)</i>	I. mito. membr.	<i>sdh1</i>	YKL148C
		Flavoprotein subunit A				<i>sdh1b</i>	YJL045W
		Protein required for flavinylation of sdh			I. mito. membr.	<i>emi5</i>	YOL071W
10	1.4.1.14	NAD-dependent glutamate synthase	FMN/3Fe-4S	<i>Glu_synthase/ Glu_syn_central</i>	Mito. matrix	<i>glt1</i>	YDL171C
11	1.4.3.5	Pyridoxal 5'-phosphate oxidase	FMN	FMN-binding	Mito. intermembr. sp.	<i>pdx3</i>	YBR035C
		Pyridoxine 5'-phosphate oxidase		(Pyridox_oxidase)			
12	1.4.3.17	Polyamine oxidase	FAD	<i>NADP_Rossmann (FAD_binding_2)</i>	cytoplasm	<i>fms1</i>	YMR020W
13	1.5.1.20	Methylenetetrahydrofolate reductase	FAD	<i>FAD_oxidored (MTHFR)</i>	–	<i>met12</i>	YPL023C
					Mito.	<i>met13</i>	YGL125W
14	1.5.5.1	Electron-transferring flavoprotein-ubiquinone oxidoreductase	FAD/4Fe-4S	<i>4Fe-4S (ETF_QO)</i>	I. mito. membr.	<i>cir2</i>	YOR356W
15	–	Electron transferring flavoprotein	FAD	<i>FAD_DHS (ETF_alpha)</i>	Mito. matrix	<i>aim45</i>	YPR004C
16	1.5.99.8	Proline dehydrogenase	FAD	<i>FAD_oxidored (Pro_dh)</i>	Mito. matrix	<i>put1</i>	YLR142W
17	1.6.2.2	Cytochrome-b5 reductase	FAD	<i>FAD_Lum_binding (FAD_binding_6)</i>	ER & o. mito. membr. ER & plasma membr.	<i>cbr1</i> <i>pga3</i>	YIL043C YML125C
18	1.6.2.4	NADPH-hemoprotein reductase	FMN/heme	Flavoprotein	O. mito. membr.	<i>ncp1</i>	YHR042W
		(cytochrome P450 reductase)	FAD	(Flavodoxin_1) <i>FAD_Lum_binding (FAD_binding_1)</i>	ER & plasma membr.		
19	1.6.5.2	NAD(P)H quinone oxidoreductase	FMN	Flavoprotein	cytoplasm	<i>lot6</i>	YLR011W
				(Flavodoxin_2)			
20	1.6.5.9	NADH-ubiquinone oxidoreductase (rotenone-insensitive)	FAD/Fe-S	<i>NADP_Rossmann (Pyr_redox_2)</i>	I. mito. membr.	<i>ndi1</i>	YML120C
21	1.6.99.1	NADPH dehydrogenase	FMN	TIM_barrel (Oxidored_FMN)	Cytoplasm	<i>oye2</i>	YHR179W
						<i>oye3</i>	YPL171C
22	1.–.–	External NADH dehydrogenase	FAD	–	I. mito. membr.	<i>nde1</i>	YMR145C
					I. mito. membr.	<i>nde2</i>	YDL085W
23	1.6.–	NADPH-dep. diflavin oxidoreductase	FMN	Flavoprotein (Flavodoxin_1)	Mito. matrix	<i>tah18</i>	YPR048W
			FAD	<i>FAD_Lum_binding (FAD_binding_1)</i>			
24	–	5-Carboxymethylaminomethylation of uridine (heterodimer with Mss1p)	FAD	<i>GIDA</i>	Mito.	<i>mta1</i>	YGL236C
25	–	Wybutosine biosynthesis, a tRNA-modification	FMN/4Fe-4S	Flavoprotein	ER	<i>tyw1</i>	YPL207W
26	1.8.1.2	Sulphite reductase (beta subunit)	FMN/heme	Flavoprotein (Flavodoxin_1)	Cytoplasm	<i>met5</i>	YJR137C
			FAD	<i>FAD_Lum_binding (FAD_binding_1)</i>			
27	1.8.1.4	Dihydropolyl dehydrogenase	FAD	<i>NADP_Rossmann (Pyr_redox_2)</i>	Mito. matrix	<i>lpd1</i>	YFL018C
28	1.8.1.7	Glutathione-disulfide reductase	FAD	<i>NADP_Rossmann (Pyr_redox_2)</i>	Cytoplasm & mito.	<i>glr1</i>	YPL091W
29	1.8.1.9	Thioredoxin-disulfide reductase	FAD	<i>NADP_Rossmann (Pyr_redox_2)</i>	Cytoplasm & mito. intermembr. sp.	<i>trr1</i>	YDR353W
					Cytoplasm & mito. cytoplasm microtubule	<i>trr2</i> <i>irc15</i>	YHR106W YPL017C
30	–	Microtubule associated protein	FAD	<i>NADP_Rossmann? (Pyr_redox_2)</i>			
31	1.8.3.2	Sulfhydryl oxidase	FAD/Fe-S cluster/ Heme	Erv1_Alr	Mito. intermembr. sp. ER membr.	<i>erv1</i> <i>erv2</i>	YGR029W YPR037C
32	1.8.4.–	Endoplasmic oxidoreductin 1	FAD	Ero1	ER & ER membr.e	<i>ero1</i>	YML130C
33	1.14.12.17	Nitric oxide oxidoreductase (flavo-hemoglobin)	FAD/heme	<i>FAD_Lum_Binding (FAD_binding_6)</i>	Cytoplasm	<i>yhb1</i>	YGR234W
34	1.14.13.–	Oxidase of thiols in the ER	FAD	–	Mito. matrix		
35	1.14.13.9	Kynurenine 3-monooxygenase	FAD	–	ER membr. O. mito. membr.	<i>fmo1</i> <i>bnr4</i>	YHR176W YBL098W

Table 1 (continued)

No.	E.C.	Enzyme	Cofactor	Structure clan (family) ^a	Localization	Abbrev.	Syst. name
				NADP_Rossmann (FAD_Binding_3)			
36	1.14.99.7	Squalene monooxygenase	FAD	–	ER membr.	<i>erg1</i>	YGR175C
37	1.14.99.–	Monooxygenase in coenzyme Q biosyn.	FAD	–	I. mito. membr.	<i>coq6</i>	YGR255C
38	1.–.–.–	Ferric reductase	FAD/heme	–	Plasma membr.	<i>fre1</i>	YLR214W
					Plasma membr.	<i>fre2</i>	YKL220C
					Plasma membr.	<i>fre3</i>	YOR381W
					Plasma membr.	<i>fre4</i>	YNR060W
					Plasma membr.	<i>fre5</i>	YOR384W
					Vacuole membr.	<i>fre6</i>	YLL051C
					Plasma membr.	<i>fre7</i>	YOL152W
					–	<i>fre8</i>	YLR047C
39	1.–.–.–	NADPH oxidase	FAD/heme	–	Perinucl. ER membr.	<i>aim14</i>	YGL160W
40	1.–.–.–	NAD(P)H-dep. heme reductase	FAD	–	Inner mito. membr.	<i>cyc2</i>	YOR037W
41	2.2.1.6	Acetolactate synthase	FAD/TPP	FAD_DHS (TPP_enzyme_M)	Mito.	<i>iv2</i>	YMR108W
42	2.3.1.86	Fatty acid synthase, subunit β , chain I	FMN	Not reported	Cytoplasm & mito.	<i>fas1</i>	YKL182W
43	4.1.1.36	4'-Phosphopantothienoylcysteine decarboxylase (forms a heterotrimeric complex with Sis2p and Vhs3p)	FMN	Flavoprotein	Cytoplasm	<i>cab3</i>	YKL088W
44	4.1.99.3	Deoxyribodipyrimidine photo-lyase	FAD	<i>HUP (DNA_photolyase)</i>	Cytoplasm, mito. & nucleus	<i>phr1</i>	YOR386W
45	4.2.3.5	Chorismate synthase	FMN	Chorismate_synt	Cytoplasm	<i>aro2</i>	YGL148W
46	–	Flavodoxin-like protein	FMN	Flavoprotein (Flavodoxin_1)	Cytoplasm, mito.	<i>pst2</i>	YDR032C
	–	Flavodoxin-like protein	FMN	Flavoprotein (Flavodoxin_1)	Cytoplasm	<i>rfs1</i>	YBR052C
	–	flavodoxin-like protein	FMN	Flavoprotein (Flavodoxin_1)	Cytoplasm, mito.	<i>ycp4</i>	YCR004C
47	–	Apoptosis-inducing factor	FAD	–	O. mito. membr., plasma membr. & nucleus	<i>aif1</i>	YNR074C

Abbreviations used in Table 1: biosyn., biosynthesis; dh, dehydrogenase; degr., degradation; dep., dependent; i., inner; ER, endoplasmic reticulum; mito., mitochondrion; o., outer; perinucl., perinuclear; red., reductase; sp., space.

^a Pfam classification given in plain text is for yeast proteins and those in italics are for homologs from other species.

invoked physiological role as a reductase of disulphide bonds in oxidatively damaged proteins of the cytoskeleton, such as actin [5].

2. General aspects of the yeast flavoproteome

The yeast genome contains 68 genes encoding for a flavin-dependent protein and thus 1.1% of all yeast proteins (5885 protein-encoding genes [26]) have a requirement for either FMN or FAD. Owing to the presence of several flavoprotein families, which will be discussed further below, these 68 genes give rise to 47 defined biochemical roles. Thirty-five flavoproteins require FAD (74%) and fifteen require FMN (26%). Yeast also possesses three diflavin enzymes, which harbor both FMN and FAD (Table 1). The utilization of FMN and FAD in yeast flavoproteins is very similar to the distribution found in a global analysis across all kingdoms of life [27] and does not have the bias towards FAD as found for the human flavoproteome [28]. Covalent flavinylation, which is statistically found in ca. 10% of flavoproteins, is underrepresented in the yeast flavoproteome with only two enzymes, succinate dehydrogenase (Sdh1p) and L-arabinono-1,4-lactone oxidase (Alo1p) featuring a covalent bond between the N(3)-nitrogen of a histidine residue and the 8-methyl group of the isoalloxazine ring system (Table 1). Both of these enzymes operate in yeast mitochondria and are located in the inner (Sdh1p) and outer (Alo1p) membrane. The scarcity of covalent flavoproteins is linked to the relative absence of the structural clan FAD_PCMH (with the exception of Alo1p), which features many examples of mono- and even bi-covalent flavinylation [27,28].

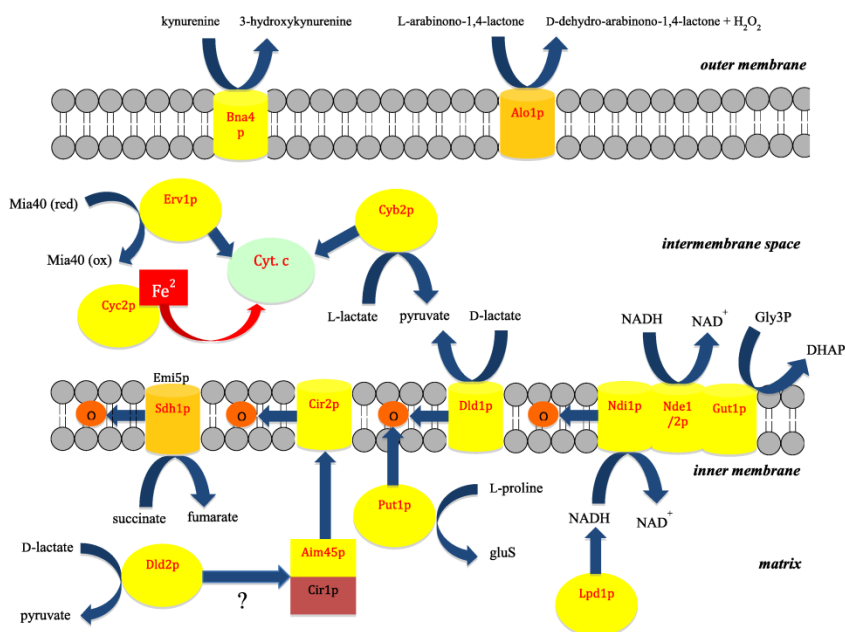
Structural information through X-ray crystallographic analysis is available for about one third of yeast flavoproteins listed in Table 1 (plain font in column "Structure clan/family"). In addition, the three-dimensional structure can be inferred from the known structure of homologs from other species (italics in column "Structure clan/family"). In some cases the structure of yeast flavoproteins served as paradigms for a family of enzymes, for example yeast OYEs [6,29] and more recently kynurenine monooxygenase [30].

The general difficulties to elucidate the structure of integral or membrane associated proteins is also seen for flavoproteins (see Table 1).

Table 1 also provides information on the localisation of flavoproteins in the yeast cell. More than half of yeast flavoproteins (36 entries in Table 1) operate in the mitochondrion. Many of these are directly participating in redox reactions connected to the electron transport chain (ETC) (see also next section). Seventeen flavoproteins are located in the cytoplasm and only a few in the nucleus (Dus1-4p, Phr1p, Aif1p), endoplasmic reticulum (Aim14p, Cbr1p, Erg1p, Ero1p, Erv2p, Fmo1p, Ncp1p, Pga3p, Tyw1p) or the peroxisome (Pox1p). Requirement for the same flavoenzyme activity in different cellular compartments is either satisfied by expression of isozymes (e.g. Dld1-3p are found in either the cytoplasm, the inner mitochondrial membrane or the matrix) or the same flavoenzyme is present in multiple compartments (e.g. Cbr1p, Pga3p, Ncp1p, Trr1/2p, Yhb1p, Fas1p, Phr1p, Aif1p).

3. Flavoproteins, the stewards of iron

A remarkable result of our analysis concerns the multi-layered relationship between flavins and iron. As discussed in more detail in the next section, flavin-dependent ferric reductases (Fre1p-8p) are essential for reduction of ferric iron (and copper), which is prerequisite for iron (and copper) uptake by yeast transporters (permeases). Moreover, in several flavoproteins the flavin is responsible for the reduction of either heme iron or an iron-sulfur cluster (Table 1 and Scheme 1). Prominent examples include succinate dehydrogenase (Sdh1p), (Aim1p), nitric oxide oxidoreductase and L-lactate:cytochrome c oxidoreductase (flavocytochrome b₂). In addition to this intramolecular electron transfer, two yeast flavoproteins, Cyc2p and Tah18p, are involved in intermolecular electron transfer. In the case of Cyc2p, which is located in the inner mitochondrial membrane with its FAD-containing active site exposed to the intermembrane space, the enzyme reduces Fe(III) and participates in the incorporation of the heme prosthetic group into apocytochrome c and c1 [31,32]. Similarly, the diflavin reductase Tah18p forms a complex



Scheme 1. Flavoproteins in mitochondrial redox processes. Flavoproteins are represented by yellow spheres (soluble flavoproteins in the matrix or intermembrane space) or barrels (inner or outer mitochondrial membrane). Flavoproteins with a covalently bound FAD (Sdh1p in the inner and Alo1p in the outer membrane) are shown in light orange. Cytochrome c is shown as a light green sphere. Curved blue arrows indicate redox reactions and straight arrows electron transfer. For further explanations and comments see main text. Several flavoproteins appear to participate in a multi-protein complex in the inner mitochondrial membrane [57]. For clarity, we have shown only a complex consisting of Ndi1p, Nde1/2p and Gut1p. Abbreviations used are: DHAP, dihydroxy acetone phosphate; Gly3p, glycerol 3-phosphate; GluSA, γ -glutamic acid semialdehyde; Mia(40), mitochondrial intermembrane space import and assay/oxidoreductase 40 (ox, oxidized; red, reduced); Q, ubiquinone.

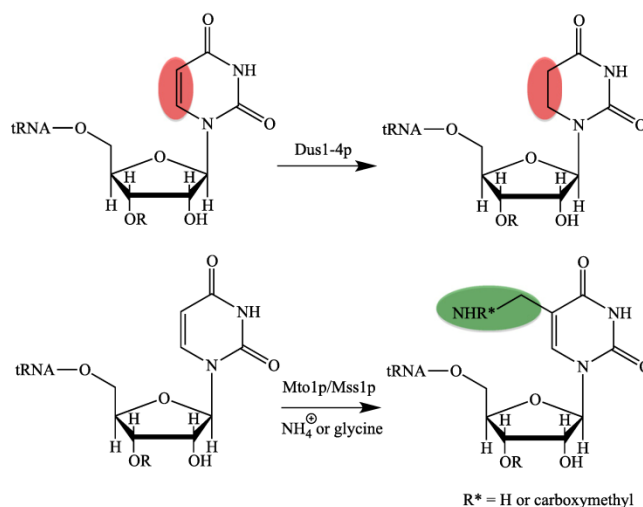
with Dre2p and provides electrons derived from NADPH to support the biosynthesis of two iron–sulfur clusters [33]. Recently, Tah18p was reported to be involved in NO generation in yeast and hence it is conceivable that it has more clients than Dre2p [34]. Thus flavoproteins fulfill various crucial tasks ranging from iron uptake, delivery of electrons to the mitochondrial electron transport chain, reduction of cytochrome-dependent reductases, biogenesis of iron–sulfur clusters and insertion of the heme cofactor into apocytochromes.

4. Flavoprotein families in yeast

As mentioned above, the yeast flavoproteome contains several families of flavoproteins, which catalyze identical or similar reactions. The largest group are the ferric/cupric reductases encoded by *fre1*–*8* (see Table 1, entry 38). *Fre1* and *fre2* are metalloregulated by either iron or copper availability and the encoded metalloreductases reduce Fe(III) and Cu(II) at the expense of NADPH [35]. In addition to *fre1* and *fre2*, the yeast genome contains six homologous genes, termed *fre3*–*8*. *Fre3*–*6* are regulated by iron whereas *fre7* is copper-regulated [36,37]. *Fre8* and the homologous *aim14* are not regulated by iron or copper suggesting a different role for these proteins [36]. Recently, it was demonstrated that *aim14* encodes an NADPH-oxidase, which produces superoxide in the endoplasmic reticulum [38] and it is thus conceivable that *fre8* also encodes an enzyme with similar properties. This notion is also supported by pair-wise sequence alignments showing the highest identity (30.6%) and similarity (56.5%) on the amino acid level between *fre8* and *aim14* within this family of flavoproteins [36]. Again, these functions highlight the importance of flavoenzymes for iron uptake and reduction as introduced in the previous section.

The second largest family comprise four tRNA-dihydrouridine synthases encoded by *dus1*–*4* (Table 1, entry 5). The reduction of uracils to dihydrouridines in tRNA is one of the most common modifications of nucleosides in tRNA in all kingdoms of life [39]. A recent mechanistic study employing Dus2p revealed that reduction of uracil to dihydrouracil (see Scheme 2, top) is promoted by other tRNA modifications suggesting that tRNA maturation may occur in an ordered fashion [40]. Cytoplasmic tRNA in *S. cerevisiae* contains dihydrouridine in the D loop at positions 16, 17, 20, 20A, 20B and at the base of the variable arm at position 47. The four yeast enzymes exclusively reduce uracils in specific positions in tRNA: Dus1p reduces uracils in positions 16 and 17, Dus2p in position 20, Dus3p in position 47 and Dus4p in positions 20a and 20b. Thus these four enzymes are sufficient to generate all dihydrouridine modifications known in yeast [41]. In humans, only one dihydrouridine synthase homologous to yeast Dus2p (42% identity) was identified so far, which reduces uracil in tRNA for phenylalanine [28,42]. The human enzyme appears to be upregulated in malignant tissues resulting in higher levels of dihydrouridine [42]. Despite its putative role in malignancy the specificity and exact role of the human enzyme remains unclear.

In addition to reduction of uracil, the flavoenzyme Mto1p (also termed GidA) is involved in the biosynthesis of modifications at the C5-position of the uracil base in tRNAs [43,44]. Depending on the nitrogen source, ammonia or glycine, this reaction leads to the formation of either 5-aminomethyl- or 5-carboxymethylaminomethyluridine (Scheme 2, bottom). This modification occurs at the wobble position in mitochondrial tRNAs for lysine, glutamate and glutamine [44]. Detailed characterization of the bacterial protein complex of MnmE and MnmG (homolog of Mto1p) led to a mechanistic proposal in which the FAD-dependent MnmG serves a dual function during the reaction [43,45]. In this model,



Scheme 2. Flavoproteins in tRNA-modification. Top, reaction catalyzed by tRNA-dihydrouridine synthase (Dus1-4p); Bottom, reaction catalyzed by Mto1p/Mss1p. Depending on the substrate, ammonia or glycine, the side chain in position 5' of the uracil base is aminomethyl or carboxymethylaminomethyl. "R" represents the next 3'-nucleotide in the tRNA molecule.

methylene tetrahydrofolate bound to MnmE reacts with either ammonia or glycine to form a methylene amino group at N-5 of the tetrahydrofolate cofactor. Then, FAD oxidizes the carbon–nitrogen bond to yield an imine, which is then nucleophilically attacked by the uracil base of the tRNA substrate. In the next step the reduced FAD transfers a hydride to the imine to reduce the carbon–nitrogen double bond thus completing the biosynthesis of the C-5 side chain (see Scheme 2). Thus MnmG combines two canonical flavin-dependent reactions – oxidation of amines and reduction of double bonds – to catalyze the biosynthesis of the amino methyl or carboxymethylaminomethyl side chain.

Recently, yet another flavin-dependent enzyme encoded by *tyw1* (Table 1, entry 25) was discovered that catalyzes the second step in the biosynthesis of wybutosine-modified tRNA [46]. This enzyme belongs to the radical SAM superfamily characterized by the presence of a [4Fe–4S] cluster and a S-adenosylmethionine (SAM) domain [47]. Catalytic activity requires reduction of the [4Fe–4S] cluster in order to initiate one-electron transfer for reductive cleavage of SAM to generate the 5'-deoxyadenosyl radical [48]. In vivo, flavodoxins or ferredoxins might act as potential electron donors to convert [4Fe–4S]²⁺ to [4Fe–4S]⁺ and therefore it is conceivable that the N-terminal flavodoxin domain of Tyw1p relays electrons from an external electron donor such as NAD(P)H or an electron transfer protein to the [4Fe–4S] cluster. Such a functional role is supported by the finding that deletion of the flavodoxin domain abolishes TYW1p activity [49].

Interestingly, the yeast genome contains three homologous genes, *pst1*, *rfs1* and *ycp4* encoding three highly similar flavodoxin-like proteins (Table 1, entry 46) [50]. Although none of the proteins was functionally characterized with respect to their electron transfer properties and physiological redox partners they were found to act as transcriptional regulators of *spi1*, a gene responding to various environmental stimuli [51]. The lack of information on yeast flavodoxins is very surprising in view of the abundance of structural (148 structures of wild-type and variants in the pdb) and biochemical studies available for bacterial flavodoxins. Therefore, the current state of affairs for yeast flavodoxin-like proteins is very unsatisfactory and clearly warrants further investigations to define their biochemical and structural properties.

The family of D-lactate dehydrogenases comprising three enzymes, Dld1-3p, will be discussed in the context of redox processes in the next section.

5. Yeast flavoproteins in redox balancing

More than a quarter of yeast flavoproteins listed in Table 1 participate in redox reactions in the mitochondrion. As shown in Scheme 1, transfer of electrons into the ETC can either occur through electron donation to cytochrome c (cyt. c) in the intermembrane space or directly by reduction of ubiquinone to ubiquinol in the inner mitochondrial membrane. The latter route is clearly the dominating process in yeast mitochondria. Electrons transferred to NAD⁺ in the isocitrate, α -ketoglutarate and malate dehydrogenase reactions of the tricarboxylic acid cycle enter the ETC. via the NADH:ubiquinone oxidoreductase Ndi1p ("internal NADH dehydrogenase"). In contrast to complex I of higher eukaryotes this membrane-bound enzyme does not engage in proton translocation resulting in lower phosphorylation efficiency. The oxidation of succinate to fumarate is catalyzed by a canonical membrane-bound succinate dehydrogenase in which the covalently linked FAD becomes reduced by the substrate and the electrons are passed on to ubiquinone via an iron–sulfur cluster and heme relay system. The Sdh1p subunit of yeast succinate dehydrogenase (complex II) is one of only two flavin-dependent proteins exhibiting a covalent linkage (see Table 1, entry 9). Typically, covalent flavinylation is a spontaneous co- or posttranslational process. However, in the case of Sdh1p the assistance of Emi1p (Sdh5p) is required, which is conserved in higher eukaryotes and hence appears to be essential for complex II assembly [52,53]. Yeast also possesses a heterodimeric electron transfer flavoprotein (Aim45p/Cir1p) located in the mitochondrial matrix, which communicates with a membrane-bound electron transferring flavoprotein ubiquinone oxidoreductase (Cir2p). The latter flavoprotein feeds electrons received from Aim45p/Cir1p into the ETC. The clients for Aim45p/Cir1p, however, remain elusive as most electron donor proteins, such as the acyl-Co dehydrogenases involved in β -oxidation or amino acid degradation, are not present in *S. cerevisiae*. A potential candidate, L-proline dehydrogenase (Put1p), evidently feeds electrons from L-proline oxidation directly into the ETC. by reduction of ubiquinone to ubiquinol (see Scheme 1) [54].

Cytosolic NADH generated for example by the glycolytic enzyme glyceraldehyde 3-phosphate dehydrogenase is oxidized by either Nde1p or Nde2p ("external NADH:ubiquinone oxidoreductases") and the electrons serve to reduce ubiquinone (Scheme 1). The

mitochondrial ETC. can also be fuelled by the glycerol 3-phosphate shuttle: glycerol is first phosphorylated by glycerol kinase (Gut1p) in the cytosol and then transported to the intermembrane space to become oxidized by the membrane-bound glycerol 3-phosphate dehydrogenase (Gut2p) [55,56]. Several of the membrane-bound flavoproteins involved in substrate oxidation and electron transfer form a large supramolecular complex containing Nde1p, Nde2p and Gut2p and therefore inter-protein electron transfer may also occur prior to ubiquinone reduction [57].

Yeast possesses three D-lactate dehydrogenases (Dldp1-3, see Table 1), which operate in different compartments of the cell: Dld1p is located in the inner mitochondrial membrane, Dld2p in the matrix and Dld3 in the cytosol [58,59]. D-lactate is produced by the glyoxalase pathway that detoxifies methylglyoxal adventitiously generated by non-enzymatic elimination of hydrogen and phosphate from the enediol intermediate of triose phosphates [60]. Since this detoxification pathway is active in the cytosol and the mitochondrial matrix D-lactate dehydrogenase activity is required in these compartments to oxidize D-lactate to pyruvate (Scheme 1). Oxidation of D-lactate by the D-lactate dehydrogenase (Dld2p) localized in the mitochondrial matrix is coupled to ATP synthesis and therefore Dld2p apparently donates substrate-derived electrons to the ETC [61]. However, it is currently unknown whether electrons are directly used to reduce ubiquinone or transferred to the heterodimeric Aim45p/Cir2p electron transfer complex (Scheme 1).

The involvement of flavoproteins in central mitochondrial redox processes is also reflected by the fact that the flavin oxidation state oscillates in synchronized aerobically grown yeast cultures. During the oxidative phase of the culture the increase of flavin fluorescence indicates that more flavoproteins become oxidized whereas in the reductive phase of the internal rhythm a decrease of flavin fluorescence indicates a shift to the reduced state [62,63].

6. Flavin biosynthesis and transport

The biosynthesis of riboflavin in *S. cerevisiae* utilizes the canonical precursors, GTP and ribulose 5-phosphate. However, riboflavin biosynthesis deviates from the bacterial pathway in that deamination and reduction of the initial metabolite, 2,5-diamino-6-(ribosylamino)-4-(3H)-pyrimidinone 5'-phosphate (DRAP), take place in reverse order (www.kegg.jp). Briefly, in the first step GTP is converted by GTP cyclohydrolase II, encoded by *rib1*, to DRAP, which is reduced by Rib7p to 2,5-diamino-6-(ribitylamino)-4-(3H)-pyrimidinone 5'-phosphate (Table 2 and Scheme 3). This reaction is followed by deamination to 5-amino-6-ribitylamino-2,4-(1H,3H)-pyrimidinedione 5'-phosphate catalyzed by Rib2p [64]. After dephosphorylation by an unidentified

phosphatase condensation with 3,4-dihydroxy-2-butanone-4-phosphate (DHAB) occurs. The latter metabolite is synthesized from ribulose 5-phosphate by DHBP synthase (encoded by *rib3*). The condensation reaction is catalyzed by lumazine synthase (encoded by *rib4*) and yields 6,7-dimethyl-8-(1-D-ribityl)lumazine [65,66]. In the final reaction, riboflavin synthase (encoded by *rib5*) uses two molecules of 6,7-dimethyl-8-(1-D-ribityl)-lumazine where one acts as donor and the other as acceptor of four carbon atoms leading to the generation of the isoalloxazine ring of one molecule of riboflavin [67]. The coenzyme forms of riboflavin, FMN and FAD, are synthesized from riboflavin by riboflavin kinase (Fmn1p) and FAD synthetase (Fad1p), respectively [68,69].

In addition to de novo biosynthesis, yeast is also capable of riboflavin uptake from the medium and it was shown that a plasma membrane flavin transporter, encoded by *mch5*, is regulated by the proline-dependent transcription factor Put3p [70,71]. Since proline utilization depends on the FAD-dependent proline dehydrogenase Put1p (Table 1) upregulation of *Mch5p* suggests that riboflavin uptake is necessary under these conditions to meet the cellular demand for flavin coenzymes.

Despite the wealth of genetic and biochemical information available on riboflavin biosynthesis in the cytosol, transport to other compartments, in particular the mitochondrion as the dominant organelle for flavoenzyme catalyzed reactions, remains controversial [53]. Based on the finding that yeast mitochondria possess riboflavin kinase but no FAD synthetase activity, Tzagaloff et al. [72] proposed a model according to which the carrier protein Flx1p acts as a "flavin antiporter" by exchanging FMN from the mitochondrial matrix with FAD from the cytosol. In contrast to this model, Barile and co-workers claim that riboflavin is transported into mitochondria where both FMN and FAD can be synthesized and are even exported back to the "extramitochondrial phase" [73,74]. More recent data from Pallotta indicated that mitochondria can also hydrolyze FAD and FMN to riboflavin and are thus capable of balancing the pools of riboflavin, FMN and FAD [75]. Yeast FAD synthetase (Fad1p) is essential and deletion of *fad1* makes yeast unviable. The localization of yeast FAD1p is still unclear, although recent studies on human FAD synthetase isoform 1 (hFADS1) suggest a mitochondrial localization in eukaryotes [76].

In addition to *flx1* and *mch5*, yeast possesses three *flc* genes encoding putative transporters of flavins (Table 2). These transporters are responsible for FAD transport into the endoplasmic reticulum (ER) where several flavoenzymes (e.g. Ero1p, Erv2p and Fmo1p) are involved in the redox balance of thiols and disulfide linkages [77]. However, the exact role and localisation of Flc1-3p in yeast are currently not fully understood.

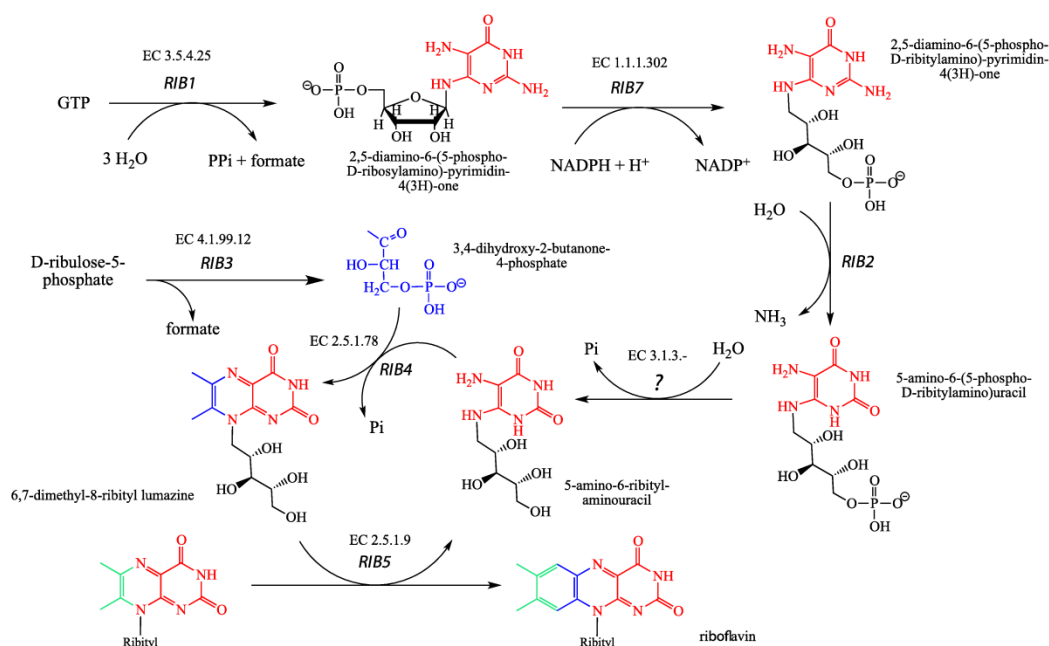
An alternative mechanism for assembling the holo-flavoenzyme is realized for the sole peroxisomal flavoenzyme, acyl-CoA oxidase

Table 2
Yeast flavin transporters and biosynthesis.

No.	E.C.	Protein/enzyme	Substrate/ligand	Structure clan (family) ^a	Abbrev.	Syst. name
<i>Transporters</i>						
1	–	FAD transmembrane transporter	FAD	–	<i>flx1</i>	YIL134W
2	–	FAD transporter (into ER)	FAD	–	<i>flc1</i>	YPL221W
3	–	FAD transporter (into ER)	FAD	–	<i>flc2</i>	YAL053W
4	–	FAD transporter (into ER)	FAD	–	<i>flc3</i>	YGL139W
5	–	Plasma-membrane riboflavin transporter	Riboflavin	–	<i>mch5</i>	YOR306C
<i>Biosynthesis of riboflavin, FMN and FAD</i>						
1	3.5.4.25	GTP cyclohydrolase II (1st step)	–	<i>GTP cyclohydrolase II</i>	<i>rib1</i>	YBL033C
2	1.1.1.302	DRAP reductase (2nd step)	–	DHFred (RibD_C)	<i>rib7</i>	YBR153W
3	–	Deaminase (3rd step)	–	DHFred (RibD_C)	<i>rib2</i>	YOR066C
4	4.1.99.12	DHBP synthase (4th step)	–	DHBP_synthase	<i>rib3</i>	YDR487C
5	2.5.1.78	Lumazine synthase (5th step)	–	DMRL_synthase	<i>rib4</i>	YOL143C
6	2.5.1.9	Riboflavin synthase (6th step)	–	FAD_Lum_binding (Lum_binding)	<i>rib5</i>	YBR256C
7	2.7.1.26	Riboflavin kinase	Riboflavin	Flavokinase	<i>fmn1</i>	YDR236C
8	2.7.7.2	FAD-adenylyl transferase (synthetase)	FMN	HUP (PAPS_reduct)	<i>fad1</i>	YDL045C

Abbreviations used in Table 2 are: DHBP, 3,4-dihydroxy-2-butanone-4-phosphate; DRAP, 2,5-diamino-6-ribosylamino-4(3H)-pyrimidinone 5'-phosphate.

^a Pfam classification given in plain text is for yeast proteins and those in italics are for homologs from other species.



Scheme 3. Biosynthesis of riboflavin in *S. cerevisiae*. GTP and D-ribose-5-phosphate serve as building blocks for the biosynthesis of 5-amino-6-ribityl-aminouracil and 3,4-dihydroxy-2-butanone-4-phosphate, respectively. These two compounds are then used by Rib4p to synthesize 6,7-dimethyl-8-ribityl lumazine. Two molecules 6,7-dimethyl-8-ribityl lumazine are converted by Rib5p to riboflavin and 5-amino-6-ribityl-aminouracil which serves again as substrate for Rib4p. This way all atoms of the dimethylbenzene moiety are derived from 3,4-dihydroxy-2-butanone-4-phosphate (colored in blue and green) while remainder of riboflavin is derived from GTP (colored in red).

(Pox1p). In this case, the holo-enzyme is formed in the cytosol, then binds to the import receptor Pex5p and, following an unknown import pathway, is transported into the peroxisome [78,79].

7. Yeast flavoproteins as models for human diseases

The yeast *S. cerevisiae* has been used as a model organism for studying fundamental biological processes for some time [80]. In 1997, Botstein and colleagues showed that nearly 31% of yeast open reading frames (ORF) have a homologue in mammalian genomes [81]. Since the number of annotated ORFs has almost doubled since 1997 this percentage is likely to have risen significantly. Moreover, an estimated 30% of human genes implicated in human diseases have a yeast homologue [82]. In a recent review, we have documented that fifty human flavoproteins are implicated in human diseases [28]. As shown in Table 3, nearly half of the disease-related human flavoproteins possess a yeast homologue. Interestingly, the majority of disease-related human flavoproteins operate in the mitochondrion [28]. Owing to the similarity of mitochondrial processes in eukaryotes it is conceivable that the yeast homologs located in mitochondria (see Table 3) may be particularly suitable as models for an improved understanding of human mitochondrial diseases.

Functional assignments based on sequence similarity generated ambiguities for several flavoproteins. For example, the yeast D-lactate dehydrogenases (Dld1-3p) show remarkable similarity to human D-2-hydroxyglutarate dehydrogenase and to a much lesser degree to alkylidihydroxyacetone phosphate synthase. Similarly, the yeast glutamate synthase, Glt1p, exhibits similarity to human dihydropyrimidine dehydrogenase (see Table 3). On the other hand the yeast NAD(P)H: quinone oxidoreductase Lot6p shows only a very low similarity to the human ortholog (P = 1) although it possesses a similar structure and

function [83–86]. These examples illustrate the need for biochemical characterization to provide a solid basis for comparative functional studies.

Yeast deletion strains were also used as convenient models to investigate the impact of mutations discovered in human genes. Examples are deletions of the genes *ura1*, *sdh1*, *ldp1* and *coq6*, leading to auxotrophic yeast strains, which were complemented with the orthologous human gene to investigate the functional impairment of mutations [87–90]. Yeast was also utilized as a host for heterologous expression of the human gene encoding 3 β -hydroxysterol Δ 24-reductase (DHCR24). Desmosterolosis, a rare autosomal recessive disorder is caused by mutations in the gene encoding DHCR24. Heterologous expression of the human *DHCR24* gene bearing different missense mutations confirmed their role in desmosterolosis [91].

A genetic screen in yeast suggested that kynurenine 3-monooxygenase may be a useful therapeutic target for Huntington disease [92]. This has prompted structural studies with the yeast enzyme leading to the elucidation of its X-ray crystal structure, which may serve as a model to investigate the structural basis of inhibitor binding [30]. Similarly, the crystal structure of the yeast flavin-containing monooxygenase Fmo1p proved useful as a model to understand the effect of mutations in human FMO3 that cause trimethylaminuria (“fish-odor” syndrome) [93].

8. Concluding remarks

Our analysis of the yeast flavoproteome has highlighted the importance of flavin-dependent enzymes in mitochondrial redox processes. Many of these mitochondrial enzymes have human homologs involved in diseases and thus genetically manipulated yeast strains (e.g. gene deletions) have potential as convenient model systems. On the other hand,

Table 3
Yeast flavoproteins as human disease models.

No.	E.C.	Human enzyme	Disease	OMIM	Yeast homolog	E value ^a
1	1.1.5.3	Glycerol 3-phosphate dh	Diabetes mellitus, type 2	138430	Cut2p	7.3 e – 124
2	1.1.99-	D-2-Hydroxyglutarate dh	D-2-Hydroxyglutaric aciduria	605176	Dld1p Dld2p Dld3p	1.9 e – 39 8.7 e – 128 3.3 e – 112
3	1.3.1.2	Dihydropyrimidine dh	Deficiency	612779	Glt1p	2.7 e – 14
4	1.3.5.2	Dihydroorotate dh	Miller syn.	126064	Ura1p	2.0 e – 6
5	1.3.3.4	Protoporphyrinogen IX ox.	Variety porphyria	600923	Hem1p	7.2 e – 20
6	1.3.3.6	Acyl-CoA ox.	Deficiency	609751	Pox1p	2.0 e – 45
7	1.3.5.1	Succinate dh	Complex II deficiency,	600857	Sdh1p	3.9 e – 219
		Flavoprotein subunit A	Leigh syn., paraganglioma 5		Sdh1bp	3.0 e – 214
8	1.4.3.4	Monoamine ox	Brunner syn., antisocial behavior, autism	309850	Fms1p	7.8 e – 11
9	1.4.3.5	Pyridoxine 5'-phosphate ox.	Encephalopathy	603287	Pdx3p	5.1 e – 36
10	1.5.1.20	Methylenetetrahydrofolate red.	Homocystinuria, neural tube defects, schizophrenia	607093	Met12p Met13p	2.9 e – 98 7.5 e – 122
11	1.5.5.1	Electron-transferring flavo-protein ubiquinone oxidored.	Glutaric acidemia IIC	231675	Cir2p	8.0 e – 157
12	–	Electron-transferring flavoprot.	Glutaric acidemia IIA Glutaric acidemia IIB	608053 130410	Aim45p	8.5 e – 66
13	1.5.99.8	Proline dh	Hyperprolinemia type I, schizophrenia	606810	Put1p	8.7 e – 12
14	1.6.2.2	Cytochrome-b5 red.	Methemoglobinemia types I & II	613213	Cbr1p	1.9 e – 30
15	1.6.2.4	NADPH-hemoprotein red. (cytochrome P450 red.)	Antley-Bixler syn.,	124015	Ncp1p	2.4 e – 86
16	1.6.5.2	NAD(P)H:quinone oxidored.	Benzene toxicity, breast cancer	125860	Lot6p	1
17	1.8.1.4	Dihydropolpyl dh	Leigh syn., maple syrup urine disease	238331	Lpd1p	2.8 e – 147
18	1.8.1.7	Glutathione-disulfide red.	Hemolytic anemia	138300	Clr1p	1.4 e – 104
19	1.14.13.8	Flavin-containing monooxy.	Trimethylaminuria	136132	Fmo1p	4.8 e – 27
20	1.14.13.39	Nitric-oxide synthase	Hypertension	163729	Tah18p	9.6 e – 27
				163730		
21	1.14.99.-	Monooxy. in coenzyme Q	Deficiency, nephrotic syn.	614647	Coq6p	7.0 e – 55
22	1.16.1.8	Methionine synthase red.	Homocystinuria, neural tube	602568	Met5p	0.24
23	2.5.1.26	Alkyldihydroxyacetone Phosphate synthase	Rhizomelic chondrodysplasia Punctata type 3	603051	Dld1p Dld2p Dld3p	2.1 e – 25 4.4 e – 16 1.1 e – 15
24	–	Apoptosis inducing protein	Combined oxidative phosphorylation deficiency	300169	Aif1p	8.8 e – 4

Abbreviations used in Table 3: dh, dehydrogenase; flavoprot., flavoprotein; monooxy., monooxygenase; ox, oxidase; oxidored., oxidoreductase; red., reductase; syn., syndrome.

^a E value; expect value, was generated by searching of *Saccharomyces* Genome Database (SGD; <http://www.yeastgenome.org>) open reading frames (DNA or protein) against human protein sequences using the SGD WU_Blast2 program.

many yeast flavoenzymes are barely characterized with regard to their biochemical properties, such as substrate specificity, kinetic parameters and reaction partners. This deficit is clearly illustrated by the yeast flavodoxin-like proteins and the electron-transferring flavoprotein, none of which were characterized in any biochemical or structural detail. Similarly, our understanding of riboflavin uptake and trafficking between cellular compartments as well as flavin homeostasis are at an early stage necessitating further studies. Since these processes are also poorly understood in humans, yeast lends itself as a valuable model organism to gain insight into uptake, transport and trafficking of this vital vitamin.

9. Methods

The names and gene abbreviations of yeast flavoproteins were recently compiled for a review article [27]. This list of flavoproteins was updated using the information available in the *Saccharomyces* genome database (<http://www.yeastgenome.org/>). This database was also used to extract information on viability of gene knock-outs and localisation of flavoproteins in the yeast cell. Structural information was obtained from the protein database (<http://www.pdb.org>).

Acknowledgments

We thank the Austrian Research Fund (FWF) for financial support through project P22361 and the PhD program "Molecular Enzymology" (W901).

References

- [1] O. Warburg, W. Christian, Über das gelbe Ferment und seine Wirkungen, *Biochem. Z.* 266 (1933) 377–392.
- [2] H. Theorell, O. Warburg, Reindarstellung (Kristallisation) des gelben Atmungsfermentes und die reversible Spaltung desselben, *Biochem. Z.* 272 (1934) 155–156.
- [3] E. Haas, O. Warburg, Isolierung eines neuen gelben Ferments, *Biochem. Z.* 298 (1938) 378–390.
- [4] V. Massey, L.M. Schopfer, Reactivity of Old Yellow Enzyme with alpha-NADPH and other pyridine nucleotide derivatives, *J. Biol. Chem.* 261 (1986) 1215–1222.
- [5] B.K. Haarer, D.C. Amberg, Old Yellow Enzyme protects the actin cytoskeleton from oxidative stress, *Mol. Biol. Cell* 15 (2004) 4522–4531.
- [6] K.M. Fox, P.A. Karplus, Old Yellow Enzyme at 2 Å resolution: overall structure, ligand binding, and comparison with related flavoproteins, *Structure* 2 (1994) 1089–1105.
- [7] Y.S. Niino, S. Chakraborty, B.J. Brown, V. Massey, A new Old Yellow Enzyme of *Saccharomyces cerevisiae*, *J. Biol. Chem.* 270 (1995) 1983–1991.
- [8] K. Stott, K. Saito, D.J. Thiele, V. Massey, Old Yellow Enzyme. The discovery of multiple isozymes and a family of related proteins, *J. Biol. Chem.* 268 (1993) 6097–6106.
- [9] Y. Meah, V. Massey, Old Yellow Enzyme: stepwise reduction of nitro-olefins and catalysis of aci-nitro tautomerization, *Proc. Natl. Acad. Sci. U. S. A.* 97 (2000) 10733–10738.
- [10] A.D. Vaz, S. Chakraborty, V. Massey, Old Yellow Enzyme: aromatization of cyclic enones and the mechanism of a novel dismutation reaction, *Biochemistry* 34 (1995) 4246–4256.
- [11] M. Hall, C. Stueckler, W. Kroutil, P. Macheroux, K. Faber, Asymmetric bioreduction of activated alkenes using cloned 12-oxophytodienoate reductase isoenzymes OPR-1 and OPR-3 from *Lycopersicon esculentum* (tomato): a striking change of stereoselectivity, *Angew. Chem. Int. Ed.* 46 (2007) 3934–3937.
- [12] A. Muller, R. Sturmer, B. Hauer, B. Rosche, Stereospecific alkyne reduction: novel activity of Old Yellow Enzymes, *Angew. Chem. Int. Ed.* 46 (2007) 3316–3318.
- [13] R. Sturmer, B. Hauer, M. Hall, K. Faber, Asymmetric bioreduction of activated C=C bonds using enoate reductases from the Old Yellow Enzyme family, *Curr. Opin. Chem. Biol.* 11 (2007) 203–213.
- [14] R.E. Williams, N.C. Bruce, 'New uses for an old enzyme' – the Old Yellow Enzyme family of flavoenzymes, *Microbiology* 148 (2002) 1607–1614.
- [15] R.E. Williams, D.A. Rathbone, N.S. Scrutton, N.C. Bruce, Biotransformation of explosives by the Old Yellow Enzyme family of flavoproteins, *Appl. Environ. Microbiol.* 70 (2004) 3566–3574.
- [16] F. Schaller, E.W. Weiler, Molecular cloning and characterization of 12-oxophytodienoate reductase, an enzyme of the octadecanoid signaling pathway from *Arabidopsis thaliana*. Structural and functional relationship to yeast Old Yellow Enzyme, *J. Biol. Chem.* 272 (1997) 28066–28072.
- [17] J. Strassner, A. Fürholz, P. Macheroux, N. Amrhein, A. Schaller, A homolog of Old Yellow Enzyme in tomato: Spectral properties and substrate specificity of the recombinant protein, *J. Biol. Chem.* 274 (1999) 35067–35073.

- [18] C.E. French, N.C. Bruce, Bacterial morphinone reductase is related to Old Yellow Enzyme, *Biochem. J.* 312 (1995) 671–678.
- [19] T.B. Fitzpatrick, N. Amrhein, P. Macheroux, Characterization of YqjM, an Old Yellow Enzyme homolog from *Bacillus subtilis*, *J. Biol. Chem.* 278 (2003) 19891–19897.
- [20] O. Adachi, K. Matsushita, E. Shinagawa, M. Ameyama, Occurrence of old yellow enzyme in *Gluconobacter suboxydans*, and the cyclic regeneration of NADP, *J. Biochem.* 86 (1979) 699–709.
- [21] C.E. French, S. Nicklin, N.C. Bruce, Sequence and properties of pentaerythritol tetranitrate reductase from *Enterobacter cloacae* PB2, *J. Bacteriol.* 178 (1996) 6623–6627.
- [22] J.R. Snape, N.A. Walkley, A.P. Morby, S. Nicklin, G.F. White, Purification, properties, and sequence of glycerol trinitrate reductase from *Agrobacterium radiobacter*, *J. Bacteriol.* 179 (1997) 7796–7802.
- [23] D.S. Blehert, B.G. Fox, G.H. Chambliss, Cloning and sequence analysis of two *Pseudomonas* flavoprotein xenobiotic reductases, *J. Bacteriol.* 181 (1999) 6254–6263.
- [24] J. Strassner, F. Schaller, U. Frick, G.A. Howe, E.E. Weiler, N. Amrhein, P. Macheroux, A. Schaller, Characterization and cDNA-microarray expression analysis of 12-oxophytodienoate reductases reveals differential roles for octadecanoid biosynthesis in the local versus the systemic wound response, *Plant J.* 32 (2002) 585–601.
- [25] A. Stintzi, J. Browse, The *Arabidopsis* male-sterile mutant, *opr3*, lacks the 12-oxophytodienoic acid reductase required for jasmonate synthesis, *Proc. Natl. Acad. Sci. U. S. A.* 97 (2000) 10625–10630.
- [26] A. Goffeau, B.G. Barrell, H. Bussey, R.W. Davis, B. Dujon, H. Feldmann, F. Galibert, J.D. Hoheisel, C. Jacq, M. Johnston, E.J. Louis, H.W. Mewes, Y. Murakami, P. Philippson, H. Tettelin, S.G. Oliver, Life with 6000 genes, *Science* 274 (1996) 546–563.
- [27] P. Macheroux, B. Kappes, S.E. Ealick, Flavogenomics—a genomic and structural view of flavin-dependent proteins, *FEBS J.* 278 (2011) 2625–2634.
- [28] W.D. Lienhart, V. Gudipati, P. Macheroux, The human flavoproteome, *Arch. Biochem. Biophys.* 535 (2013) 150–162.
- [29] K.M. Fox, P.A. Karplus, Crystallization of Old Yellow Enzyme illustrates an effective strategy for increasing protein crystal size, *J. Mol. Biol.* 234 (1993) 502–507.
- [30] M. Amaral, C. Levy, D.J. Heyes, P. Lafite, T.F. Outeiro, F. Giorgini, D. Leys, N.S. Scrutton, Structural basis of kynurenic acid 3-monooxygenase inhibition, *Nature* 496 (2013) 382–385.
- [31] D.G. Bernard, S. Quevillon-Cheruel, S. Merchant, B. Guiard, P.P. Hamel, Cyc2p, a membrane-bound flavoprotein involved in the maturation of mitochondrial c-type cytochromes, *J. Biol. Chem.* 280 (2005) 39852–39859.
- [32] V. Corvest, D.A. Murray, M. Hirasawa, D.B. Knaff, B. Guiard, P.P. Hamel, The flavoprotein Cyc2p, a mitochondrial cytochrome c assembly factor, is a NAD(P)H-dependent haem reductase, *Mol. Microbiol.* 83 (2012) 968–980.
- [33] N. Soler, E. Delagoutte, S. Miron, C. Facca, D. Baille, D. d'Autreaux, G. Craescu, Y.M. Frapart, D. Mansuy, G. Baldacci, M.E. Huang, L. Vernis, Interaction between the reductase Tah18 and highly conserved Fe-S containing Dre2 C-terminus is essential for yeast viability, *Mol. Microbiol.* 82 (2011) 54–67.
- [34] A. Nishimura, N. Kawahara, H. Takagi, The flavoprotein Tah18-dependent NO synthesis confers high-temperature stress tolerance on yeast cells, *Biochem. Biophys. Res. Commun.* 430 (2013) 137–143.
- [35] A. Dancis, D.G. Roman, G.J. Anderson, A.G. Hinnebusch, R.D. Klausner, Ferric reductase of *Saccharomyces cerevisiae*: molecular characterization, role in iron uptake, and transcriptional control by iron, *Proc. Natl. Acad. Sci. U. S. A.* 89 (1992) 3869–3873.
- [36] E. Georgatou, D. Alexandraki, Regulated expression of the *Saccharomyces cerevisiae* Fre1p/Fre2p Fe/Cu reductase related genes, *Yeast* 15 (1999) 573–584.
- [37] L.J. Martins, L.T. Jensen, J.R. Simon, G.L. Keller, D.R. Winge, Metalloregulation of FRE1 and FRE2 homologs in *Saccharomyces cerevisiae*, *J. Biol. Chem.* 273 (1998) 23716–23721.
- [38] M. Rinnerthaler, S. Buttner, P. Laun, G. Heeren, T.K. Felder, H. Klinger, M. Weinberger, K. Stolze, T. Grousl, J. Hasek, O. Benada, I. Frydlova, A. Klocker, B. Simon-Nobbe, B. Jansko, H. Breitenbach-Koller, T. Eisenberg, C.W. Gourel, F. Madeo, W.C. Burthans, M. Breitenbach, Yno1p/Aim14p, a NADPH-oxidase ortholog, controls extramitochondrial reactive oxygen species generation, apoptosis, and actin cable formation in yeast, *Proc. Natl. Acad. Sci. U. S. A.* 109 (2012) 8658–8663.
- [39] M. Sprinzl, C. Steegborn, F. Hubel, S. Steinberg, Compilation of tRNA sequences and sequences of tRNA genes, *Nucleic Acids Res.* 24 (1996) 68–72.
- [40] L.W. Rider, M.B. Ottsen, S.G. Gattis, B.A. Palffy, Mechanism of dihydrouridine synthase 2 from yeast and the importance of modifications for efficient tRNA reduction, *J. Biol. Chem.* 284 (2009) 10324–10333.
- [41] F. Xing, S.L. Hiley, T.R. Hughes, E.M. Phizicky, The specificities of four yeast dihydrouridine synthases for cytoplasmic tRNAs, *J. Biol. Chem.* 279 (2004) 17850–17860.
- [42] T. Kato, Y. Daigo, S. Hayama, N. Ishikawa, T. Yamabuki, T. Ito, M. Miyamoto, S. Kondo, Y. Nakamura, A novel human tRNA-dihydrouridine synthase involved in pulmonary carcinogenesis, *Cancer Res.* 65 (2005) 5638–5646.
- [43] M.E. Armengod, I. Moukadiri, S. Prado, R. Ruiz-Parrita, A. Benitez-Paez, M. Villarroya, R. Lomas, M.J. Garzon, A. Martinez-Zamora, S. Meseguer, C. Navarro-Gonzalez, Enzymology of tRNA modification in the bacterial MnmEG pathway, *Biochimie* 94 (2012) 1510–1520.
- [44] X. Wang, Q. Yan, M.X. Guan, Mutation in MTO1 involved in tRNA modification impairs mitochondrial RNA metabolism in the yeast *Saccharomyces cerevisiae*, *Mitochondrion* 9 (2009) 180–185.
- [45] I. Moukadiri, S. Prado, J. Piera, A. Velazquez-Campoy, G.R. Bjork, M.E. Armengod, Evolutionarily conserved proteins MnmE and GidA catalyze the formation of two methyluridine derivatives at tRNA wobble positions, *Nucleic Acids Res.* 37 (2009) 7177–7193.
- [46] L. Li, X. Jia, D.M. Ward, J. Kaplan, Yap5 protein-regulated transcription of the TYW1 gene protects yeast from high iron toxicity, *J. Biol. Chem.* 286 (2011) 38488–38497.
- [47] H.J. Sofia, G. Chen, B.G. Hetzler, J.F. Reyes-Spindola, N.E. Miller, Radical SAM, a novel protein superfamily linking unresolved steps in familiar biosynthetic pathways with radical mechanisms: functional characterization using new analysis and information visualization methods, *Nucleic Acids Res.* 29 (2001) 1097–1106.
- [48] S.C. Wang, P.A. Frey, S-adenosylmethionine as an oxidant: the radical SAM superfamily, *Trends Biochem. Sci.* 32 (2007) 101–110.
- [49] Y. Suzuki, A. Noma, T. Suzuki, M. Senda, T. Senda, R. Ishitani, O. Nureki, Crystal structure of the radical SAM enzyme catalyzing tricyclic modified base formation in tRNA, *J. Mol. Biol.* 372 (2007) 1204–1214.
- [50] R. Grandori, J. Carey, Six new candidate members of the alpha/beta twisted open-sheet family detected by sequence similarity to flavodoxin, *Protein Sci.* 3 (1994) 2185–2193.
- [51] F. Cardona, H. Orozco, S. Friant, A. Aranda, M. del Olmo, The *Saccharomyces cerevisiae* flavodoxin-like proteins Ycp4 and Rfs1 play a role in stress response and in the regulation of genes related to metabolism, *Arch. Microbiol.* 193 (2011) 515–525.
- [52] H.X. Hao, O. Khalimonchuk, M. Schradner, N. Dephoure, J.P. Bayley, H. Kunst, P. Devilee, C.W. Cremers, J.D. Schifman, B.G. Bentz, S.P. Gygi, D.R. Winge, H. Kremer, J. Rutter, SDH5, a gene required for flavination of succinate dehydrogenase, is mutated in paraganglioma, *Science* 325 (2009) 1139–1142.
- [53] H.J. Kim, D.R. Winge, Emerging concepts in the flavinylation of succinate dehydrogenase, *Biochim. Biophys. Acta* 1827 (2013) 627–636.
- [54] J. Lopes, M.J. Pinto, A. Rodrigues, F. Vasconcelos, R. Oliveira, The *Saccharomyces cerevisiae* genes, AIM45, YGR207c/CIR1 and YOR356w/CIR2, are involved in Cellular Redox State Under Stress Conditions, *Open Microbiol. J.* 4 (2010) 75–82.
- [55] R. Ansell, K. Granath, S. Hohmann, J.M. Thevelein, L. Adler, The two isoenzymes for yeast NAD⁺-dependent glycerol 3-phosphate dehydrogenase encoded by GPD1 and GPD2 have distinct roles in osmoadaptation and redox regulation, *EMBO J.* 16 (1997) 2179–2187.
- [56] M. Grauslund, J.M. Lopes, B. Ronnow, Expression of GUT1, which encodes glycerol kinase in *Saccharomyces cerevisiae*, is controlled by the positive regulators Adr1p, Ino2p and Ino4p and the negative regulator Opi1p in a carbon source-dependent fashion, *Nucleic Acids Res.* 27 (1999) 4391–4398.
- [57] X. Grandier-Vazeille, K. Bathany, S. Chaigepain, N. Camougrand, S. Manon, J.M. Schmitter, Yeast mitochondrial dehydrogenases are associated in a supramolecular complex, *Biochemistry* 40 (2001) 9758–9769.
- [58] A. Chelstowska, Z. Liu, Y. Jia, D. Amberg, R.A. Butow, Signalling between mitochondria and the nucleus regulates the expression of a new D-lactate dehydrogenase activity in yeast, *Yeast* 15 (1999) 1377–1391.
- [59] E.E. Rojo, B. Guiard, W. Neupert, R.A. Stuart, Sorting of D-lactate dehydrogenase to the inner membrane of mitochondria. Analysis of topogenic signal and energetic requirements, *J. Biol. Chem.* 273 (1998) 8040–8047.
- [60] M.J. Penninckx, C.J. Jaspers, M.J. Legrain, The glutathione-dependent glyoxalase pathway in the yeast *Saccharomyces cerevisiae*, *J. Biol. Chem.* 258 (1983) 6030–6036.
- [61] M.L. Pallotta, D. Valenti, M. Iacovino, S. Passarella, Two separate pathways for D-lactate oxidation by *Saccharomyces cerevisiae* mitochondria which differ in energy production and carrier involvement, *Biochim. Biophys. Acta* 1608 (2004) 104–113.
- [62] D.B. Murray, K. Haynes, M. Tomita, Redox regulation in respiring *Saccharomyces cerevisiae*, *Biochim. Biophys. Acta* 1810 (2011) 945–958.
- [63] D.B. Murray, S. Roller, H. Kuriyama, D. Lloyd, Clock control of ultradian respiratory oscillation found during yeast continuous culture, *J. Bacteriol.* 183 (2001) 7253–7259.
- [64] A. Urban, I. Ansmant, Y. Motorin, Optimisation of expression and purification of the recombinant Yol066 (Rib2) protein from *Saccharomyces cerevisiae*, *J. Chromatogr. B Anal. Technol. Biomed. Life Sci.* 786 (2003) 187–195.
- [65] C. Jin, A. Barrientos, A. Tzagoloff, Yeast dihydroxybutanone phosphate synthase, an enzyme of the riboflavin biosynthetic pathway, has a second unrelated function in expression of mitochondrial respiration, *J. Biol. Chem.* 278 (2003) 14698–14703.
- [66] J.J. Garcia-Ramirez, M.A. Santos, J.L. Revuelta, The *Saccharomyces cerevisiae* RIB4 gene codes for 6,7-dimethyl-8-ribityllumazine synthase involved in riboflavin biosynthesis. Molecular characterization of the gene and purification of the encoded protein, *J. Biol. Chem.* 270 (1995) 23801–23807.
- [67] M.A. Santos, J.J. Garcia-Ramirez, J.L. Revuelta, Riboflavin biosynthesis in *Saccharomyces cerevisiae*. Cloning, characterization, and expression of the RIB5 gene encoding riboflavin synthase, *J. Biol. Chem.* 270 (1995) 437–444.
- [68] M.A. Santos, A. Jimenez, J.L. Revuelta, Molecular characterization of FMN1, the structural gene for the monofunctional flavokinase of *Saccharomyces cerevisiae*, *J. Biol. Chem.* 275 (2000) 28618–28624.
- [69] M. Wu, B. Repetto, D.M. Glerum, A. Tzagoloff, Cloning and characterization of FAD1, the structural gene for flavin adenine dinucleotide synthetase of *Saccharomyces cerevisiae*, *Mol. Cell. Biol.* 15 (1995) 264–271.
- [70] P. Reihl, J. Stolz, The monocarboxylate transporter homolog Mch5p catalyzes riboflavin (vitamin B2) uptake in *Saccharomyces cerevisiae*, *J. Biol. Chem.* 280 (2005) 39809–39817.
- [71] A. Spitzner, A.F. Perzlmaier, K.E. Geillinger, P. Reihl, J. Stolz, The proline-dependent transcription factor Put3 regulates the expression of the riboflavin transporter MCH5 in *Saccharomyces cerevisiae*, *Genetics* 180 (2008) 2007–2017.
- [72] A. Tzagoloff, J. Jang, D.M. Glerum, M. Wu, FLX1 codes for a carrier protein involved in maintaining a proper balance of flavin nucleotides in yeast mitochondria, *J. Biol. Chem.* 271 (1996) 7392–7397.

- [73] M.L. Pallotta, C. Brizio, A. Friatianni, C. De Virgilio, M. Barile, S. Passarella, *Saccharomyces cerevisiae* mitochondria can synthesise FMN and FAD from externally added riboflavin and export them to the extramitochondrial phase, *FEBS Lett.* 428 (1998) 245–249.
- [74] V. Bafunno, T.A. Giancaspero, C. Brizio, D. Bufano, S. Passarella, E. Boles, M. Barile, Riboflavin uptake and FAD synthesis in *Saccharomyces cerevisiae* mitochondria: involvement of the Flx1p carrier in FAD export, *J. Biol. Chem.* 279 (2004) 95–102.
- [75] M.L. Pallotta, Evidence for the presence of a FAD pyrophosphatase and a FMN phosphohydrolase in yeast mitochondria: a possible role in flavin homeostasis, *Yeast* 28 (2011) 693–705.
- [76] E.M. Torchetti, C. Brizio, M. Colella, M. Galluccio, T.A. Giancaspero, C. Indiveri, M. Roberti, M. Barile, Mitochondrial localization of human FAD synthetase isoform 1, *Mitochondrion* 10 (2010) 263–273.
- [77] O. Protchenko, R. Rodriguez-Suarez, R. Androphy, H. Bussey, C.C. Philpott, A screen for genes of heme uptake identifies the FLC family required for import of FAD into the endoplasmic reticulum, *J. Biol. Chem.* 281 (2006) 21445–21457.
- [78] A.T. Klein, M. van den Berg, G. Bottger, H.F. Tabak, B. Distel, *Saccharomyces cerevisiae* acyl-CoA oxidase follows a novel, non-PTS1, import pathway into peroxisomes that is dependent on Pex5p, *J. Biol. Chem.* 277 (2002) 25011–25019.
- [79] S. Subramani, Hitchhiking fads en route to peroxisomes, *J. Cell Biol.* 156 (2002) 415–417.
- [80] D. Drubin, The yeast *Saccharomyces cerevisiae* as a model organism for the cytoskeleton and cell biology, *Cell Motil. Cytoskeleton* 14 (1989) 42–49.
- [81] D. Botstein, S.A. Chervitz, J.M. Cherry, Yeast as a model organism, *Science* 277 (1997) 1259–1260.
- [82] F. Foury, Human genetic diseases: a cross-talk between man and yeast, *Gene* 195 (1997) 1–10.
- [83] R. Li, M.A. Bianchet, P. Talalay, L.M. Amzel, The three-dimensional structure of NAD(P)H:quinone reductase, a flavoprotein involved in cancer chemoprotection and chemotherapy: Mechanism of the two-electron reduction, *Proc. Natl. Acad. Sci. U. S. A.* 92 (1995) 8846–8850.
- [84] D. Liger, M. Graille, C.-Z. Zhou, N. Leulliot, S. Quevillon-Cheruel, K. Blondeau, J. Janin, H. van Tilbeurgh, Crystal structure and functional characterization of yeast YLR011wp, an enzyme with NAD(P)H-FMN and ferric iron reductase activities, *J. Biol. Chem.* 279 (2004) 34890–34897.
- [85] S. Sollner, R. Nebauer, H. Ehammer, A. Prem, S. Deller, B.A. Palfey, G. Daum, P. Macheroux, Lot6p from *Saccharomyces cerevisiae* is a FMN-dependent reductase with a potential role in quinone detoxification, *FEBS J.* 274 (2007) 1328–1339.
- [86] S. Sollner, P. Macheroux, New roles of flavoproteins in molecular cell biology: an unexpected role for quinone reductases as regulators of proteasomal degradation, *FEBS J.* 276 (2009) 4313–4324.
- [87] N. Burnichon, J.J. Briere, R. Libe, L. Vescovo, J. Riviere, F. Tissier, E. Jouanno, X. Jeunemaitre, P. Benit, A. Tzagoloff, P. Rustin, J. Bertherat, J. Favier, A.P. Gimenez-Roqueplo, SDHA is a tumor suppressor gene causing paraganglioma, *Hum. Mol. Genet.* 19 (2010) 3011–3020.
- [88] S.F. Heeringa, G. Chernin, M. Chaki, W. Zhou, A.J. Sloan, Z. Ji, L.X. Xie, L. Salvati, T.W. Hurd, V. Vega-Warner, P.D. Killen, Y. Raphael, S. Ashraf, B. Övunc, D.S. Schoeb, H.M. McLaughlin, R. Airik, C.N. Vlangos, R. Gbadegesin, B. Hinkes, P. Saisawat, E. Trevisson, M. Doimo, A. Casarin, V. Pertegato, G. Giorgi, H. Prokisch, A. Rotig, G. Nurnberg, C. Becker, S. Wang, F. Ozaltin, R. Topaloglu, A. Bakkaloglu, S.A. Bakkaloglu, D. Muller, A. Beissert, S. Mir, A. Berdeli, S. Varpizen, M. Zenker, V. Matejas, C. Santos-Ocana, P. Navas, T. Kusakabe, A. Kispert, S. Akman, N.A. Soliman, S. Krick, P. Mundel, J. Reiser, P. Nurnberg, C.F. Clarke, R.C. Wiggins, C. Faul, F. Hildebrandt, COQ6 mutations in human patients produce nephrotic syndrome with sensorineural deafness, *J. Clin. Invest.* 121 (2011) 2013–2024.
- [89] J. Rainger, H. Bengani, L. Campbell, E. Anderson, K. Sokhi, W. Lam, A. Riess, M. Ansari, S. Smithson, M. Lees, C. Mercer, K. McKenzie, T. Lengfeld, B. Gener Querol, P. Branney, S. McKay, H. Morrison, B. Medina, M. Robertson, J. Kohlhase, C. Gordon, J. Kirk, D. Wiczorek, D.R. Fitzpatrick, Miller (Genee-Wiedemann) syndrome represents a clinically and biochemically distinct subgroup of postaxial acrofacial dysostosis associated with partial deficiency of DHODH, *Hum. Mol. Genet.* 21 (2012) 3969–3983.
- [90] R.A. Vaubel, P. Rustin, G. Isaya, Mutations in the dimer interface of dihydroipoamide dehydrogenase promote site-specific oxidative damages in yeast and human cells, *J. Biol. Chem.* 286 (2011) 40232–40245.
- [91] H.R. Waterham, J. Koster, G.J. Romeijn, R.C. Hennekam, P. Vreken, H.C. Andersson, D.R. FitzPatrick, R.I. Kelley, R.J. Wanders, Mutations in the 3beta-hydroxysterol Delta24-reductase gene cause desmosterolosis, an autosomal recessive disorder of cholesterol biosynthesis, *Am. J. Hum. Genet.* 69 (2001) 685–694.
- [92] F. Giorgini, P. Guidetti, Q. Nguyen, S.C. Bennett, P.J. Muchowski, A genomic screen in yeast implicates kynurenine 3-monooxygenase as a therapeutic target for Huntington disease, *Nat. Genet.* 37 (2005) 526–531.
- [93] C.K. Yeung, E.T. Adman, A.E. Rettie, Functional characterization of genetic variants of human FMO3 associated with trimethylaminuria, *Arch. Biochem. Biophys.* 464 (2007) 251–259.

The human flavoproteome

Author Contributions

The manuscript has been published in ARCHIVES OF BIOCHEMISTRY AND BIOPHYSICS (2013), Volume 535, Number 2, Pages 150-162. The literature search and the writing of the paper was a cooperation among the authors.



Review

The human flavoproteome

Wolf-Dieter Lienhart, Venugopal Gudipati, Peter Macheroux*

Graz University of Technology, Institute of Biochemistry, Petersgasse 12, A-8010 Graz, Austria

ARTICLE INFO

Article history:

Received 17 December 2012

and in revised form 21 February 2013

Available online 15 March 2013

Keywords:

Coenzyme A

Coenzyme Q

Folate

Heme

Pyridoxal 5'-phosphate

Steroids

Thyroxine

Vitamins

ABSTRACT

Vitamin B₂ (riboflavin) is an essential dietary compound used for the enzymatic biosynthesis of FMN and FAD. The human genome contains 90 genes encoding for flavin-dependent proteins, six for riboflavin uptake and transformation into the active coenzymes FMN and FAD as well as two for the reduction to the dihydroflavin form. Flavoproteins utilize either FMN (16%) or FAD (84%) while five human flavoenzymes have a requirement for both FMN and FAD. The majority of flavin-dependent enzymes catalyze oxidation–reduction processes in primary metabolic pathways such as the citric acid cycle, β -oxidation and degradation of amino acids. Ten flavoproteins occur as isozymes and assume special functions in the human organism. Two thirds of flavin-dependent proteins are associated with disorders caused by allelic variants affecting protein function. Flavin-dependent proteins also play an important role in the biosynthesis of other essential cofactors and hormones such as coenzyme A, coenzyme Q, heme, pyridoxal 5'-phosphate, steroids and thyroxine. Moreover, they are important for the regulation of folate metabolites by using tetrahydrofolate as cosubstrate in choline degradation, reduction of *N*-5,10-methylenetetrahydrofolate to *N*-5-methyltetrahydrofolate and maintenance of the catalytically competent form of methionine synthase. These flavoenzymes are discussed in detail to highlight their role in health and disease.

© 2013 Elsevier Inc. Open access under [CC BY-NC-ND license](http://creativecommons.org/licenses/by-nc-nd/3.0/).

Introduction

Vitamin B₂ (or riboflavin) is an essential dietary requirement for humans (*Homo sapiens sapiens*) because the biosynthesis of this compound is absent. The daily requirement for vitamin B₂ was estimated to be 1.1 mg and 1.3 mg for adult females and males, respectively, but may vary depending on metabolic challenges and the efficiency of riboflavin uptake. Dietary riboflavin is taken up in the human gastrointestinal tract by poorly characterized

transporters (Table 1, entry #74). Vitamin B₂ is not used in any human enzyme *per se* but is chemically modified to the flavin mononucleotide (FMN)¹ and flavin adenine dinucleotide form by riboflavin kinase (EC 2.7.1.26) and FAD synthetase (EC 2.7.7.2), respectively. FMN and FAD as well as excess riboflavin are excreted in the urine. Chastain and McCormick have also detected trace amounts of 7-hydroxy- and 8-hydroxy-flavins in human urine which are generated through as yet unknown catabolic reactions [1]. In addition, they have also found 8-sulfonyl-flavin which is supposedly released from enzymes bearing a covalent thioester linkage, e.g. monoamine oxidase A and B (MAOA and MAOB, Table 1).

FMN and FAD possess a tricyclic heteroaromatic isoalloxazine ring that can reversibly accept and donate one or two electrons. Thus the majority of the enzymes utilizing FMN or FAD catalyze reduction–oxidation (“redox”) reactions in metabolic transformations. In fact, the majority of human flavoenzymes belongs to the oxidoreductases with only two example each for a transferase and lyase, respectively (Table 1, entries #65–68). Flavoenzymes may either use FMN or FAD as cofactor and most are specific for one or the other. In the case of human flavoproteins only twelve use FMN and 64 FAD as cofactor amounting to ca. 16% and 84% of the flavoenzymes, respectively (note that five enzymes utilize both FMN and FAD). In a global analysis of FMN and FAD usage in flavoproteins it was noted that 25% of flavoenzymes utilize FMN [2], hence the human flavoproteome has a clear bias towards FAD-dependent enzymes.

* Corresponding author. Address: Graz University of Technology, Institute of Biochemistry, Petersgasse 12, A-8010 Graz, Austria. Fax: +43 316 873 6952.

E-mail address: peter.macheroux@tugraz.at (P. Macheroux).

¹ Abbreviations used: ACAD9 acyl-CoA dehydrogenase isoform 9; ACADS, short-chain acyl-CoA dehydrogenase; ACADL, long-chain acyl-CoA dehydrogenase; ACADM, medium-chain acyl-CoA dehydrogenase; DHCR24, 3 β -hydroxysterol Δ^{24} -reductase; DMGDH, dimethylglycine dehydrogenase; ETF, electron transferring flavoprotein; ETFDH, electron-transferring flavoprotein ubiquinone oxidoreductase; FMO3, flavin-containing monooxygenase isoform 3; FOXRED1, FAD-dependent oxidoreductase; MSmethionine synthase; MTHFR, *N*-5,10-methylene-tetrahydrofolate reductase; MTRR, methionine synthase reductase; OMIM, Online Mendelian Inheritance in Man; MAOA, monoamine oxidase isozyme A; MAOB, monoamine oxidase isozyme B; MS, methionine synthase; MSR, methionine synthase reductase; MTHFR, *N*-5,10-methylenetetrahydrofolate reductase; NQO1, NAD(P):quinone oxidoreductase; PANK, panthothenate kinase; PDB, protein data base; PLP, pyridoxal 5'-phosphate; PNPO, pyridoxal 5'-phosphate oxidase; PPOX, protoporphyrinogen IX oxidase; PPCD, 4'-phosphopantothienylcysteine decarboxylase; PPCS, phosphopantothienylcysteine synthase; SARDH, sarcosine dehydrogenase; SQLE, squalene monooxygenase; THF, tetrahydrofolate; VP, variegate porphyria.

Table 1
Human flavoproteins.

No.	E.C.	Enzyme	Cofactor	Structure clan (family) ^a	Gene symbol	Gene location
1	1.1.1.28	D-lactate dehydrogenase	FAD	FAD_PCMH (FAD_binding_4)	DHDH	16q23.1
2	1.1.1.204	Xanthine dehydrogenase	FAD	FAD_PCMH (FAD_binding_5)	XDH	2p23.1
3	1.1.1.15	(S)-2-hydroxy-acid oxidase	FMN	TIM_barrel (FMN_dh)	HAO1 HAO2	20p12.3 1p12
4	1.1.5.3	Glycerol 3-phosphate dehydrogenase	FAD	NADP_Rossmann (DAO)	GPD2	2q24.1
5	1.1.99.1	Choline dehydrogenase	FAD	---	CHDH	3p21.1
6	1.1.99.2	L-hydroxyglutarate dehydrogenase	FAD	---	LHGDH	14q21.3
7	1.1.99.-	D-2-Hydroxyglutarate dehydrogenase	FAD	---	D2HGDH	2q37.3
8	1.2.3.1	Aldehyde oxidase	FAD	---	AOX1	2q33.1
9	1.3.1.2	Dihydropyrimidine dehydrogenase	FMN	TIM_barrel (DHO_dh)	DPYD	1p21.3
10	1.3.1.72	3 β -Hydroxysterol Δ^24 -reductase	FAD	NADP_Rossmann (Pyr_redox_2)	DHCR24	1p32.3
11	1.3.3.1	Dihydroorotate dehydrogenase	FMN	TIM_barrel (DHO_dh)	DHODH	16q22.2
12	1.3.3.4	Protoporphyrinogen IX oxidase	FAD	NADP_Rossmann (Amino_oxidase)	PPOX	1q23.3
13	1.3.3.6	Acyl-CoA oxidase	FAD	Acyl-CoA_dh (ACOX_acyl-CoA_dh_1)	ACOX1 ACOX2 ACOX3	17q25.1 3p14.3 4p16.1
14	1.3.3.-	Glutaryl-CoA oxidase	FAD	---	C7orf10	7p14.1
15	1.3.5.1	Succinate dehydrogenase	8 α -(N3-His)- -FAD	NAPL_Rossmann (FAD_binding_2)	SDHA	5p15.33
16	1.3.99.2	Flavoprotein subunit A	FAD	Acyl-CoA_dh (Acyl-CoA_dh_1)	ACADS	12q24.31
17	1.3.99.3	Short-chain-(butyryl)-acyl CoA dehydrogenase	FAD	Acyl-CoA_dh (Acyl-CoA_dh_1)	ACADM	1p31.1
18	1.3.99.7	Medium-chain acyl-CoA dehydrogenase	FAD	Acyl-CoA_dh (acyl-CoA_dh_1)	GCDH	19p13.2
19	1.3.99.10	Glutaryl-CoA dehydrogenase	FAD	Acyl-CoA_dh (acyl-CoA_dh_1)	IVD	15q15.1
20	1.3.99.12	Isovaleryl-CoA dehydrogenase	FAD	Acyl-CoA_dh (acyl-CoA_dh_1)	ACADSB	10q26.13
21	1.3.99.13	2-Methylbutyryl-CoA dehydrogenase	FAD	Acyl-CoA_dh (acyl-CoA_dh_1)	ACADL	2q34
22	1.3.99.-	Very long-chain acyl-CoA dh	FAD	Acyl-CoA_dh (acyl-CoA_dh_1)	ACADVL	17p13.1
23	1.3.99.-	Isobutyryl-CoA dehydrogenase	FAD	Acyl-CoA_dh (acyl-CoA_dh_1)	ACAD8	11q25
24	1.3.99.-	Long-chain-unsaturated-acyl-CoA dh (molecular chaperone of complex I)	FAD	Acyl-CoA_dh (acyl-CoA_dh_1)	ACAD9	3q21.3
25	1.3.99.-	Long- and branched-chain-acyl-CoA dh	FAD	Acyl-CoA_dh (acyl-CoA_dh_1)	ACAD10	12q24.1
26	1.3.99.-	C22-long-chain-acyl-CoA dehydrogenase	FAD	Acyl-CoA_dh (acyl-CoA_dh_1)	ACAD11	3q22.1
27	1.4.3.1	D-aspartate oxidase	FAD	NADP_Rossmann (DAO)	DDO	6q21
28	1.4.3.2	L-amino acid oxidase	FAD	NADP_Rossmann (Amino_oxidase)	LAO	19q13.3-q13.4
29	1.4.3.3	D-amino acid oxidase	FAD	NADP_Rossmann (DAO)	DAO	12q24.11
30	1.4.3.4	Monoamine oxidase	8 α -(Cys)-FAD	NADP_Rossmann (Amino_oxidase)	MAOA MAOB	Xp11.3 Xp11.3 ^b
31	1.4.3.5	Pyridoxal 5'-phosphate oxidase	FMN	FMN-binding (Pyridox_oxidase)	PNPO	17q21.32
32	1.4.3.-	Pyridoxine 5'-phosphate oxidase	FAD	NADP_Rossmann (Amino_oxidase)	RNLS	10q23.31
33	1.5.1.20	Catecholamine oxidase (renalase)	FAD	FAD_oxidored (MTHFR)	MTHFR	1p36.22
34	1.5.3.7	Methylenetetrahydrofolate reductase	8 α -(Cys)-FAD	NADP_Rossmann (DAO)	PIFOX	17q11.2
35	1.5.3.16	Spermine oxidase	FAD	NADP_Rossmann (Amino_oxidase)	SMO	20p13
36	1.5.5.1	Electron-transferring flavoprotein-ubiquinone oxidoreductase	FAD	4Fe-4S (ETF_LOD)	ETFDH	4q32.1
37	---	Electron transferring flavoprotein	FAD	HUB (ETF)	ETFA	15q24.2-q24.3
38	1.5.99.1	Sarcosine dehydrogenase	8 α -(N3-His)- -FAD	NADP_Rossmann (DAO)	SARDH	19q13.41 9q34.2
39	1.5.99.2	Dimethylglycine dehydrogenase	8 α -(N3-His)- -FAD	NADP_Rossmann (DAO)	DMGDH	5q14.1
40	1.5.99.-	Lysine-specific histone demethylase	FAD	NADP_Rossmann	KDM1A	1p36.12
41	1.5.99.8	Proline dehydrogenase	FAD	FAD_oxidored (Pro_dh)	PRODH	22q11.21

(continued on next page)

Table 1 (continued)

No.	E.C.	Enzyme	Cofactor	Structure clan (family) ^a	Gene symbol	Gene location
42	1.6.2.2	Cytochrome-b5 reductase	FAD	FAD_Lum_binding (FAD_binding_6)	CYB5R3	22q13.2
43	1.6.2.4	NADPH-hemoprotein reductase (cytochrome P450 reductase)	FMN	Flavoprotein (flavodoxin_1)	FOR	7q11.23
44	1.6.5.2	NAD(P)H dehydrogenase (quinone)	FAD	FAD_Lum_binding (FAD_binding_1)	NQO1	16q22.1
45	1.6.5.3	NADH-ubiquinone oxidoreductase of complex I, subunit UQOR1	FMN	Flavoprotein (flavodoxin_2)	NDUFV1	11q13.2
46	1.6.5.4	NADPH-dep. diflavin oxidoreductase 1	FMN	complexY_5TK	NDORI	9q34.3
47	1.6.5.5	tRNA dihydrouridine synthase	FAD	FAD_Lum_binding (FAD_binding_1)	DUS2L	16q22.1
48	1.8.1.4	Dihydrolypyl dehydrogenase	FMN	TIM_barrel (Dus)	DLD	7q31.1
49	1.8.1.7	Glutathione-disulfide reductase	FAD	NADP_Rossmann (Pyr_redox_2)	GSR	8p12
50	1.8.1.9	Thioredoxin-disulfide reductase	FAD	NADP_Rossmann (Pyr_redox_2)	TXNR1	12q28.3
51	1.8.1.10	ER flavoprotein associated with degr.	FAD	NADP_Rossmann (Pyr_redox_2)	TXNR2	22q11.21
52	1.8.3.2	Sulphydryl oxidase	FAD	---	TXNR3	3q21.3
53	1.8.3.5	Prenylcysteine oxidase	FAD	ErV1_Alf	FOXRED2	22q12.3
54	1.10.99.2	Ribosyl(dihydropyridinyl)amide dehydrogenase	FAD	---	GFER	16p13.3
55	1.14.13.8	Flavin-containing monooxygenases	FAD	Flavoprotein (flavodoxin_2)	PCYOX1	2p13.3
56	1.14.13.9	Kynurenine 3-monooxygenase	FAD	---	NQO2	6p25.2
57	1.14.13.39	Nitric-oxide synthase	FMN	---	FMO1	1q24.3
58	1.14.13.132	Squalene monooxygenase	FAD	Flavoprotein (flavodoxin_1)	FMO2	1q24.3
59	1.14.99.1	Monooxygenase in coenzyme Q biosyn.	FAD?	FAD_Lum_binding (FAD_binding_1)	FMO3	1q24.3
60	1.16.1.2	Ferritoxinase (biliverdin IX beta red.)	FMN?	---	FMO4	1q24.3
61	1.16.1.8	Methionine synthase reductase	FMN	---	FMO5	1q21.1
62	1.18.1.2	Ferredoxin-NADP ⁺ reductase	FAD	---	KMO	1q43
63	1.1.1.1	NAD(P)H oxidase cytochrome b558, beta subunit	FAD	Flavoprotein (flavodoxin_1)	NOS1	12q24.22
64	1.1.1.1	Thyroid oxidase / dual oxidase	FAD	FAD_Lum_binding (FAD_binding_1)	NOS2	17q11.2
65	2.2.1.6	Acetolactate synthase-like protein	FAD?	---	NOS3	7q36.1
66	2.5.1.26	Alkylidihydroxyacetone phosphate synthase	FAD	---	SQL	8q24.13
67	4.1.1.36	4-Phosphopantothencycysteine decarboxylase	FMN	N-terminal domain (1-215)	COO6	14q24.3
68	4.1.99.3	Cryptochrome	FAD	Flavoprotein (flavodoxin_1)	STEAP3	2q14.2
69	---	Apoptosis inducing protein	FAD	FAD_Lum_binding (FAD_binding_1)	MTRR	5p15.31
70	---	Apoptosis inducing protein	6-OH-FAD	---	FDXR	17q25.1
71	---	Iodotyrosine deiodinase	FMN	FAD_Lum_Binding (FAD_binding_6)	CYBB	Xp11.4
72	---	Axon guidance protein interacting with CasL	FAD	---	DUOX1	15q21.1
73	---	FAD-dependent oxidoreductase (molecular chaperone of complex 1)	FAD?	---	DUOX2	15q21.1
74	---	Riboflavin transporter	Riboflavin ^c	---	---	19p13.12
75	1.5.1.30	Riboflavin / FMN reductase	FMN ^b	FAD_PCMH (FAD_binding_4)	AGPS	2q31.2
76	2.7.1.26	Riboflavin kinase	riboflavin ^c	Flavoprotein	PPCDC	15q24.2
77	2.7.7.2	FAD-adenylyl transferase (synthetase)	FMN ^b	FAD-binding of DNA-photolyase	CRY1	12q23.3
				(FAD_binding_7)	CRY2	11p11.2
				NADP_Rossmann (Pyr_redox_2)	AFM1	Xq26.1
				Nitroreductase	AFM2	10q22.1
				NADP_Rossmann (FAD_binding_3)	IYD	6q25.1
				---	MICAL1	6q21
				---	MICAL2	11p15.3
				---	MICAL3	22q11.21
				---	FOXRED1	11q24.2
				---	SLC52A1	17p13.2
				---	SLC52A2	8q24.3
				---	SLC52A3	20p13
				NADP_Rossmann (NmrA-like)	BLVFB	19q13.2
				Flavokinase	RFK	9q21.13
				HDP (PAPS_reduct)	FLAD1	1q21.3

Abbreviations used: biosyn., biosynthesis; dh, dehydrogenase; degr., degradation; dep., dependent; ER, endoplasmic reticulum; red., reductase.

^a Pfam classification given in plain text is for the structure of human proteins and those in italics for structures of homologs.^b Duplicated pseudogene.^c Opposite orientation on chromosome.^d Substrate of transporter, modifying enzyme or reductase (entries 74–77).

Table 2
Disease-related human flavoproteins.

No.	E.C.	Enzyme	Disease	Metabolic function	Localisation	OMIM
1	1.1.1.204	Xanthine dehydrogenase	Xanthinuria type I	Purine degr.	Cytosol	607633
2	1.1.5.3	Glycerol 3-phosphate dehydrogenase	Diabetes mellitus type II	Electron transport	mito. i.	138430
3	1.1.99.1	Choline dehydrogenase	tooth agenesis, cleft lip sperm motility	Choline degr.	mito. i. membr.	[78–82]
4	1.1.99.2	L-2-Hydroxyglutarate dehydrogenase	L-2-Hydroxyglutaric aciduria	"Metabolite repair"	mito. membr.	609584
5	1.1.99.-	D-2-Hydroxyglutarate dehydrogenase	D-2-Hydroxyglutaric aciduria	"Metabolite repair"	Mitochondria	605176
6	1.3.1.2	Dihydropyrimidine dehydrogenase	Deficiency	Pyrimidine catab.	Cytosol	612779
7	1.3.1.72	3 β -Hydroxysterol Δ^24 -reductase	Desmosterolosis	Sterol biosyn.	ER membr.	606418
8	1.3.3.1	Dihydroorotate dehydrogenase	Miller syn.	Please specify the significance of footnote "a" cited in the Table 2, as a corresponding footnote text has not been provided.	mito. i. membr.	126064
9	1.3.3.4	Protoporphyrinogen IX oxidase	Variegate porphyria	Heme biosyn.	Mito. i. membr.	600923
10	1.3.3.6	Acyl-CoA oxidase	Deficiency	Lipid degr.	Peroxisomes	609751
11	1.3.3.-	Glutaryl-CoA oxidase	Glutaric aciduria III	Glutaryl degr.	Peroxisomes	231690
12	1.3.5.1	Succinate dehydrogenase	Complex II deficiency	Citric acid cycle	mito. i. membr.	600857
		Flavoprotein subunit A	Leigh syn. paraganglioma 5			
13	1.3.99.2	Short-chain- (butyryl-) acyl CoA dehydrogenase	Deficiency	β -Oxidation	mito. matrix	201470
14	1.3.99.3	Medium-chain acyl-CoA dehydrogenase	Deficiency	β -Oxidation	mito. matrix	607008
15	1.3.99.7	Glutaryl-CoA dehydrogenase	Glutaric acidemia	Lysine degr.	mito. matrix	608801
16	1.3.99.10	Isovaleryl-CoA dehydrogenase	Isovaleric acidemia	Leucine degr.	mito. matrix	607036
17	1.3.99.12	2-Methylbutyryl-CoA dehydrogenase	Deficiency	Isoleucine degr.	mito. matrix	600301
18	1.3.99.13	Long-chain-acyl-CoA dehydrogenase	Deficiency	β -Oxidation	mito. matrix	609576
19	1.3.99.-	Isobutyryl-CoA dehydrogenase	Deficiency	Valine degr.	mito. matrix	611283
20	1.3.99.-	Long-chain-unsaturated-acyl-CoA dehydrogenase	Deficiency	β -Oxidation	mito. matrix	611126
21	1.3.99.-	very long-chain acyl-CoA dehydrogenase	Deficiency	β -oxidation	mito. matrix	201475
22	1.4.3.3	D-amino acid oxidase	Schizophrenia? amyotrophic lateral sclerosis	Oxidation of D-serine	Peroxisomes	124050
23	1.4.3.4	Monoamine oxidase	Brunner syn. antisocial behaviour autism	Oxidation of neuro-transmitter	mito. o. membr.	309850
24	1.4.3.5	Pyridoxal 5'-phosphate oxidase	Encephalopathy	Vitamin B ₆ metab.	Cytosol	603287
25	1.4.3.-	Catecholamine oxidase (renalase)	Hypertension?	Oxidation	Secreted (Blood)	609360
26	1.5.1.20	Methylenetetrahydrofolate reductase	Homocystinuria neural tube defects schizophrenia	Folate metab.	Cytosol	607093
27	1.5.5.1	Electron-transferring flavoprotein-ubiquinone oxidoreductase	Glutaric acidemia IIC	Electron transport	mito. i. membr.	231675
28	-----	Electron transferring flavoprotein	Glutaric acidemia IIA	Electron transport	mito. matrix	608053
29	1.5.99.1	Sarcosine dehydrogenase	Glutaric acidemia IIB Sarcosinemia	Electron transport		130410
30	1.5.99.2	Dimethylglycine dehydrogenase	DMGDH-deficiency	Choline degr.	mito. matrix	604455
31	1.5.99.8	Proline dehydrogenase	Hyperprolinemia type I schizophrenia	Amino acid metab.	mito. matrix	605850
32	1.6.2.2	Cytochrome-b5 reductase	Methemoglobinemia type I and II	Heme metab.	membr. soluble (erythro.)	613213
33	1.6.2.4	NADPH-hemoprotein reductase (cytochrome P450 reductase)	Antley-Bixler syn. Disordered steroidogenesis	Electron donor to P450 enzymes	Microsomes (ER)	124015
34	1.6.5.2	NAD(P)H dehydrogenase (quinone)	Benzene toxicity breast cancer	Quinone detox p53 degr.	Cytosol	125860

(continued on next page)

Table 2 (continued)

No.	E.C.	Enzyme	Disease	Metabolic function	Localisation	OMIM
35	1.6.5.3	NADH-ubiquinone oxidoreductase	Complex I deficiency	Electron transport	mito. i. membr.	161015
36	1.8.1.4	Dihydrolipoyl dehydrogenase	Leigh syn. Maple syrup urine dis., III	Energy metab.	mito. matrix	238331
37	1.8.1.7	Glutathione-disulfide reductase	Hemolytic anemia	detox.	Cytosol (erythro.)	138300
38	1.8.3.2	Sulfhydryl oxidase	Myopathy	Disulfide redox balance	mito. im. space	600924
39	1.10.99.2	Ribosylidihyronicotinamide dehydrogenase	Breast cancer susceptibility	Quinone detox.	Cytosol	160998
40	1.14.13.8	flavin-containing monooxygenases	trimethylaminuria	detox.	microsomes (ER)	136132
41	1.14.13.39	Nitric-oxide synthase	Hypertension	Vasodilation	Cytosol	163729 163730
42	1.14.99.-	Monooxygenase in coenzyme Q biosyn.	Deficiency/nephrotic syn.	Coenzyme Q biosyn.	Golgi/mito.	614647
43	1.16.1.8	Methionine synthase reductase	Homocystinuria neural tube defects	Methionine biosyn.	Cytosol	602568
44	1.-.-.	NAD(P)H oxidase	Chronic granulomatous dis.	Generation of superoxide	Phagocytes (membr.)	300481
45	1.-.-.	Cytochrome b(558), beta subunit Thyroid oxidase/dual oxidase	Atypical mycobacteriosis Thyroid dishormonogenesis 6	Thyroid biosyn.	membr.	606759
46	2.5.1.26	Alkyldihydroxyacetone phosphate synthase	Rhizomelic chondrodysplasia punctata, type 3	Lipid biosyn.	Peroxisomes	603051
47	-----	Apoptosis inducing protein	Combined oxidative phosphorylation deficiency	Redox control	mito./nucleus	300169
48	-----	Iodotyrosine deiodinase	Thyroid dishormonogenesis type 4	Iodide salvage	Cytosol	612025
49	-----	FAD-dependent oxidoreductase	complex I deficiency Leigh syn.	Molecular chaperone	mito. matrix	613622
50	-----	Riboflavin transporter (member 3)	Brown-Vialetto-Van Laere syn. Fazio-Londe dis.	Riboflavin uptake	membr.	613350

Abbreviations used: biosyn., biosynthesis; catab., catabolism; degr., degradation; detox., detoxification; dim., diminished; dis., disease; metabol., metabolism; mito., mitochondrium; mito. i. membr., inner membrane of mitochondria; mito. o. membr., outer membrane of mitochondria; mito. im. space, mitochondrial intermembrane space; ER, endoplasmic reticulum; membr., membrane; syn., syndrome; erythro., erythrocytes.

Most flavoenzymes bind FMN or FAD non-covalently (90%). In six human flavoenzymes the FAD cofactor is covalently linked via the 8- α -methyl group to either the nitrogen (N-3) of a histidine (succinate, sarcosine and dimethylglycine dehydrogenase) or the sulfur of a cysteine residue (MAOA, MAOB and L-pipecolate oxidase). Interestingly, monocovalent attachment to the 6-position of the isoalloxazine ring system as well as bicovalent attachment to the 8- α and 6-position observed in several bacterial, fungal and plant flavoenzymes are absent in human flavoproteins. This is also reflected by the scarcity of flavoenzymes adopting a topology similar to the *p*-cresolmethylhydroxylase (clan FAD_PCMH, family FAD_binding_4) with D-lactate dehydrogenase (EC 1.1.1.28) and alkylidihydroxyacetone phosphate synthase (EC 2.5.1.26) as sole examples for this type of structure. Interestingly, these two enzymes represent a subset of flavoenzymes in this clan that does not engage in covalent linkage of the FAD cofactor, which in fact appears to be the rule rather than the exception in this structure family [2]. Overall, it is encouraging that the structure of more than half of the human flavoproteins was solved by X-ray crystallography (Table 1). In addition, in 23 cases the structure of the human protein can be inferred from the known structure of a homologous flavoprotein. This leaves only fifteen flavoproteins where currently no structural information is available (Table 1). The prevalence of the Rossmann-fold in FAD-dependent flavoenzymes previously noted [2] is also seen in the human FAD-dependent proteins (see Fig. S1). In contrast to the global fold distribution the structural clan Acyl-CoA_dh takes second place

and switches place with the clan FAD_PCMH. This is due to the relatively large number of acyl-CoA dehydrogenases (eleven) and acyl-CoA oxidases (three) compared to only three members in the FAD_PCMH clan. Flavoenzymes in the latter clan appear to be rare in mammals but are very prominent in metabolically active and diverse organisms such as bacteria, fungi and plants [2]. The most common structural clan found for human FMN-dependent proteins is Flavoprotein and TIM_barrel (five and four members, respectively, see Fig. S1) and reflects the general prevalence of these two clans in FMN-dependent flavoproteins [2].

The chromosomal location of the genes encoding flavoproteins is known for all flavoproteins (Table 1 and Fig. S2). They are uniformly distributed over the chromosomes with only chromosome 13, 18, 21 and Y lacking genes encoding flavoproteins (Table 1 and Fig. S2). Eleven flavoenzymes occur as isozymes encoded by multiple genes (2–5). In three cases (DUOX1–2, FMO1–5 and MAOA + B) the genes are on the same chromosome (15, 1 and X, respectively) whereas in all other cases (ACOX1–3, CRY1–2, HAO1–2, MICAL1–3, NOS1–3 and SLC52A1–3) the genes are on different chromosomes (Fig. S2).

Flavoenzymes in human diseases

A surprisingly large number of flavoproteins (ca. 60%) is associated with human disorders caused by mutations in the pertinent gene. Table 2 provides an overview of the 50 flavoproteins along

with their corresponding record number in OMIM. Since most flavoproteins are localized in the mitochondria the diseases are connected with deficiencies in mitochondrial processes. Other compartments, most notably peroxisomes and the endoplasmic reticulum, are also affected by some flavoprotein deficiencies or dysfunctions. In several cases flavoprotein deficiencies occur in connected metabolic pathways and therefore give rise to similar clinical manifestations. For example, glutaric acidemia (OMIM 608801) can be caused by a deficiency of glutaryl-CoA dehydrogenase (type I), electron transferring flavoprotein (type IIA and IIB) or electron-transferring flavoprotein-ubiquinone oxidoreductase (type IIC). Similarly, Leigh syndrome (OMIM 256000) may arise from a defect in any of the respiratory electron transfer complexes in the inner mitochondrial membrane and thus deficiency of complex I (containing the FMN-dependent NDUFV1) or complex II (containing the FAD-dependent subunit A) as well as FOXRED1, an FAD-containing molecular chaperone of complex I, may constitute the molecular cause of the disease.

Since mutations are generally irreversible, adverse effects on the biological function of an encoded protein are untreatable and therapeutic interventions rely on protein substitution or, in the future, gene therapy. For several flavoproteins it was found that the mutation led to an amino acid exchange affecting the binding affinity of the flavin cofactor. In these cases it is conceivable that high-dose riboflavin supplementation may increase the concentration of flavin cofactors and this in turn may increase the fraction of active holo-enzyme. Ames and coworkers have compiled a list of flavoenzymes with decreased cofactor affinity where this strategy may be exploited successfully [3]. Among the flavoenzymes discussed are *N*-5,10-methylenetetrahydrofolate reductase (EC 1.5.1.20, MTHFR), NAD(P):quinone oxidoreductase (EC 1.6.5.2, NQO1), protoporphyrinogen IX oxidase (EC 1.3.3.4, PPOX), electron transferring flavoprotein (ETF), electron-transferring flavoprotein ubiquinone oxidoreductase (EC 1.5.5.1, ETFDH), glutaryl-CoA oxidase (EC 1.3.3.-, C7orf10), short-, medium-, long-chain acyl-CoA dehydrogenases (EC 1.3.99.2, ACADS; EC 1.3.99.3, ACADM; EC 1.3.99.13, ACADL) and complex I (EC 1.6.5.3, NDUFV1) [3]. More recently, it was shown that the neurological disorders Brown-Vialetto-Van Laere and Fazio-Londe syndrome were caused by mutations in the gene encoding an intestinal riboflavin transporter [4,5]. Since this transporter is largely unexplored, the effect of the mutation on riboflavin transport efficiency is currently unknown. However, it appears that at least in some patients riboflavin supplementation ameliorates the symptoms and positively affects disease progression [4,6,7]. Apart from a few flavoproteins with decreased affinity for cofactor mentioned by Ames and coworkers [3] it is largely unknown how mutations in genes encoding flavoproteins impact cofactor binding. In view of the large number of flavoproteins involved in human diseases it is worthwhile investigating the mutational effects on cofactor binding to thoroughly evaluate the benefits of high-dose riboflavin supplementation therapy (see also discussion below).

Flavoenzymes in cofactor biogenesis and metabolism

FMN and FAD are synthesized in the human organism from riboflavin (vitamin B₂) by riboflavin kinase (EC 2.7.1.26) and FAD-adenylyl transferase (EC 2.7.7.2). Riboflavin is absorbed from nutrients as is the case for many other vitamins required to supply vitamin-derived coenzymes to the apo-forms of hundreds of enzymes in the human body. In this context, we were intrigued by the number of flavoenzymes that are involved in the biosynthesis of other cofactors such as coenzyme A, coenzyme Q (ubiquinone), heme and pyridoxal 5'-phosphate. Equally, flavoenzymes participate in the interconversion of various folate metabolites and hence

play an important role in one-carbon (C1-unit) metabolism. Moreover, flavoenzymes catalyze essential reactions in biosynthetic pathways leading to cell signaling molecules such as the steroid and thyroid hormones. These topics are discussed in more depths in the next sections.

Flavoenzymes in folate and cobalamin metabolism

Tetrahydrofolate (THF) is a 6-methylpterin derivative that is widely used to shuttle C1-units in metabolic reactions. THF loaded with a C1-unit occurs in various oxidation states such as *N*-5,10-methylene-THF and *N*-5-methyl-THF. Two FAD-dependent enzymes, dimethylglycine dehydrogenase (EC 1.5.99.2, DMGDH) and sarcosine dehydrogenase (EC 1.5.99.1, SARDH), generate *N*-5,10-methylene-THF from THF which is then converted to *N*-5-methyl-THF by *N*-5,10-methylene-THF reductase (EC 1.5.1.20, MTHFR) at the expense of NADPH (Fig. 1). *N*-5-methyl-THF in turn is utilized by methionine synthase (EC 2.1.1.13, MS) yielding THF and methionine by transferring the methyl group to homocysteine. The cobalamin cofactor of MS is susceptible to oxidation and hence methionine synthase reductase (EC 1.16.1.8, MSR) is required to regenerate methylcob(II)alamin from cob(II)alamin. Hence, these four flavin-dependent enzymes play a role in the interconversion of THF, *N*-5,10-methylene-THF and *N*-5-methyl-THF and are thus important to balance the pools of folate metabolites (Fig. 1).

DMGDH and SARDH also catalyze two consecutive reactions in choline catabolism (Fig. 1). DMGDH oxidizes dimethylglycine to sarcosine, which is further oxidized to glycine. Both enzymes use THF to capture the C-1 fragment released by the oxidative demethylation of substrates yielding *N*-5,10-methylene-THF [8]. Since these reactions occur in the mitochondrial matrix, electrons extracted from the substrate are delivered to the mitochondrial electron transport chain via electron transferring flavoprotein (ETF) and electron transferring flavoprotein ubiquinone oxidoreductase (EC 1.5.5.1). DMGDH and SARDH were reported to contain a covalently linked 8 α -(N3-His)-FAD cofactor [9,10] and hence belong to the small group of flavoproteins that bind the cofactor covalently (see Table 1). Unfortunately, the structure of these proteins is not known and therefore neither the mode of FAD binding nor the interaction with THF can be firmly established. Interestingly, a recently discovered lysine-specific histone demethylase (EC 1.5.99.-, KDM1A) related to flavin-dependent amine oxidases apparently does not utilize THF to capture the formyl group and hence the demethylation results in the generation of formaldehyde [11]. Since the lysine demethylation occurs in the nucleus and not in mitochondria, the enzyme donates the electrons to oxygen generating hydrogen peroxide as a by-product of the demethylation reaction. The fate of these two potentially harmful compounds in the nucleus is currently not known. A recent study showed that inhibitors of KDM1A selectively target cancer cells with pluripotent stem cell properties [12]. In light of these recent findings it can be concluded that aberrations in KDM1A regulation might lead to development of cancer.

Deficiency of DMGDH is apparently very rare and only a single case was reported so far (OMIM 605850, [13,14]). Binzak et al. identified a homozygous point mutation in a patient (326 A-G) resulting in a histidine to arginine exchange (H109R) in the encoded DMGDH [13]. It is noteworthy that the covalent linkage of the FAD cofactor is to H91 and hence the inactivity of the altered enzyme is probably not due to the inability to form the covalent linkage with the FAD cofactor. Detailed studies with the recombinant DMGDH H109R variant showed effects on both the specific activity (27 times lower) and K_m (65 times higher) [15]. Interestingly, fish odor was reported as a salient symptom of DMGDH deficiency which is typically ascribed to impaired *N*-oxygenation of

xenobiotics due to deficiency of flavin-containing monooxygenase isoform 3 (EC 1.14.13.8, FMO3) [16].

Sarcosinemia caused by a deficiency of SARDH [17] is also a rare metabolic disorder characterized by elevated levels of sarcosine in plasma and urine. The mutational frequency in the human SARDH gene apparently varies from 1:350000 to 1:3414. The clinical symptoms reported to be associated with SARDH deficiency include mental retardation and loss of speech (OMIM 268900). Recently, sarcosine was suggested to be a marker for the invasiveness of prostate cancer cell lines [18]. In the same study, it was also noted that reduced levels of SARDH activity led to the induction of an invasive phenotype in benign prostate epithelial cells. The connection of SARDH to cancer development and progression indicated by this study and the usefulness of sarcosine as a tumor marker is currently the subject of an intense scientific debate [19–21].

MTHFR connects the pool of *N*-5,10-methylene-THF, mainly derived from the glycine cleavage system (EC 2.1.2.10) and serine hydroxymethyltransferase (EC 2.1.2.1), with that of *N*-5-methyl-THF, which is used by MS to generate methionine from homocysteine (Fig. 1). This reaction not only provides an important building block for protein biosynthesis but also a substrate for the synthesis of *S*-adenosyl-methionine (SAM), an ubiquitous and powerful reagent in many biological methylation reactions. The MS reaction also regenerates THF, which then re-enters the reactions mentioned above capturing C1-units from glycine, serine, dimethylglycine and sarcosine. More than thirty deleterious mutations of the *MTHFR* gene are known as well as several common variants, like the 677C>T point mutation. *MTHFR* deficiency is connected to several serious diseases, such as neural tube defects, coronary heart disease and schizophrenia (OMIM 607093). Depending on the severity of the mutation hyperhomocysteinemia with homocystinuria or mild hyperhomocysteinemia is observed. The 677C>T polymorphism is of particular interest as it is recognized as the

most frequent genetic cause of homocysteinemia [22,23]. This common C to T mutation gives rise to a conservative amino acid replacement in position 222 of *MTHFR* (A222V). Surprisingly, the A222V variant possesses reduced thermostability and weaker affinity to the FAD cofactor. In the same study it was also reported that folate (and adenosylmethionine) increases the affinity of FAD, which in turn increases the thermostability of the A222V variant [24]. This positive interplay suggests that the status of folate and riboflavin may be critical in cases where cofactor affinity is compromised by the amino acid exchange (see discussion above).

Mechanistically, MS uses *N*-5-methyl-THF to methylate its cob(I)alamin cofactor which in turn transfers the methyl group to the thiol group of homocysteine (Fig. 1). The cob(I)alamin state is highly sensitive to oxidation rendering the enzyme inactive [25]. In order to restore the reduced active form of the cofactor, cob(II)alamin is reductively methylated by MSR using NADPH as electron source and SAM as methyl group donor [26,27]. Since MSR is required to maintain MS activity, it is not surprising that allelic variants resulting in MSR deficiency present similar symptoms, such as homocystinuria, as seen in MS and *MTHFR* deficiency. Accordingly, megaloblastic anemia, an increased risk for neural tube defect and Down syndrome are among the disorders caused by inherited MSR deficiency (OMIM 602568). A common polymorphism found in the MSR gene (allele frequency 0.51) results in a single amino acid replacement, I23M, and increases the risk for neural tube defects [25,28].

Recently, Matthews and coworkers suggested that MSR also plays a role as a chaperone for MS and also acts as an aquacobalamin reductase [29]. They reported that MSR stabilizes the apofactor of MS and promotes the association with methylcobalamin. In addition, MSR catalyzes the NADPH-dependent reduction of aquacobalamin to cob(II)alamin and thereby accelerates the formation of holo-MS. Hence, MSR exhibits multiple beneficial effects on MS. In this context, it is interesting to note that MSR was also

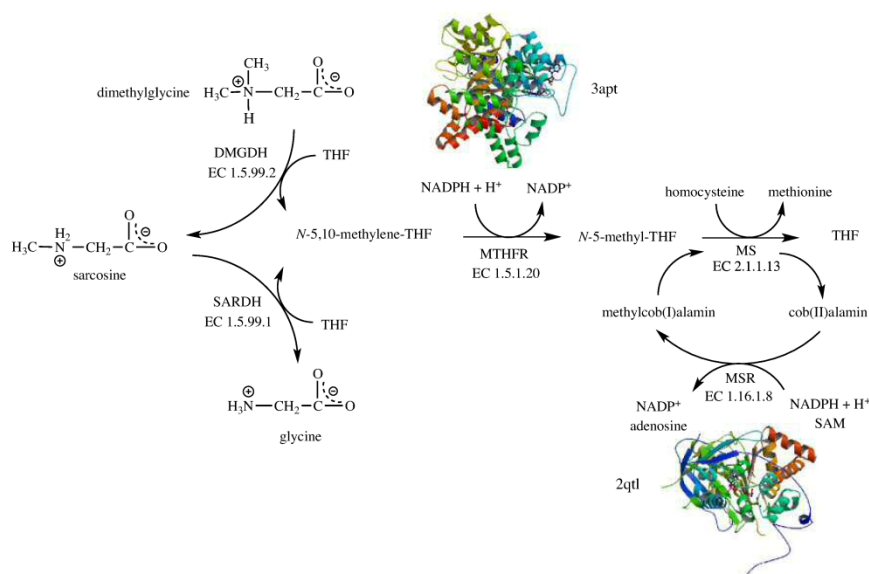


Fig. 1. Flavin-catalyzed reactions connected to folate metabolism: dimethylglycine dehydrogenase (EC 1.5.99.1, DMGDH), sarcosine dehydrogenase (EC 1.5.99.2, SARDH), *N*-5,10-methylene-tetrahydrofolate reductase (EC 1.5.1.20, MTHFR) and methionine synthase reductase (EC 1.16.1.8, MSR). Structures depicted are from the human methionine synthase reductase (2qtl) as well as the *N*-5,10-methylene-tetrahydrofolate reductase from *Thermus thermophilus* HB8 (3apt).

invoked as catalyst for the formation of adenosylcobalamin [25,30]. Recent evidence, however, suggests that reduction of Co^{2+} to Co^+ occurs by free dihydroflavins when cob(II)alamin is bound to human adenosyltransferase [31]. It is currently unknown whether this process is driven solely by free dihydroflavins or involves a specialized flavoprotein reductase *in vivo*.

Heme biosynthesis

The biosynthesis of heme from succinyl-CoA and glycine is initiated in the mitochondria and then proceeds in the cytosol to generate coproporphyrinogen III. This intermediate is transported back into mitochondria to complete the oxidation of the macrocycle by the FAD-dependent protoporphyrinogen IX oxidase (EC 1.3.3.4, PPOX). This reaction involves the six-electron oxidation of the methylene groups linking the pyrrole rings to methenyl groups thereby generating an extensively conjugated π -electron system (Fig. 2). As the isoalloxazine ring system can only handle two electrons at a time, the cofactor needs to run three times through the catalytic cycle of flavin reduction and reoxidation to complete the oxidation of protoporphyrinogen IX to protoporphyrin IX. This catalytic cycling was suggested to proceed by substrate oxidation and release of the dihydro- and tetrahydro-intermediates rather than continuous processing of a constantly bound substrate [32]. PPOX is located in the inner mitochondrial membrane and anchored by acylation to the leaflet oriented towards the intermembrane space [33,34]. Diminished PPOX activity results in variegate porphyria (VP), which belongs to a group of metabolic disturbances caused by genetic defects affecting heme biosynthesis (collectively called as *porphyrias*). Symptoms of autosomal dominant VP include acute abdominal pain, neurological manifestations and/or cutaneous photosensitivity [35]. Apparently, the disease is characterized by severe, sometimes life-threatening, crisis triggered by external factors (e.g. medication, toxins) [36]. Perhaps the most controversial case of VP was postulated for King George III (1738–1820) who suffered long episodes of mental and physical illness culminating in the Regency crisis (1788–1789). According to Macalpine & Hunter, King George III was afflicted by VP, a claim supported by several pieces of evidence collected on ancestors and descendants [37,38]. More recently, Cox et al. suggested that high concentrations of arsenic in the medication administered to the king may have triggered the episodes of VP [39].

The structure of the human enzyme was solved to 1.9 Å resolution (pdb code 3nks). Forty-seven variants of PPOX that were found to cause VP in humans were heterologously expressed in *Escherichia coli* and the properties of the variants studied *in vitro* [40]. Based on the observed effects and the locus of the amino acid in the structure of the enzyme the authors of that study classified

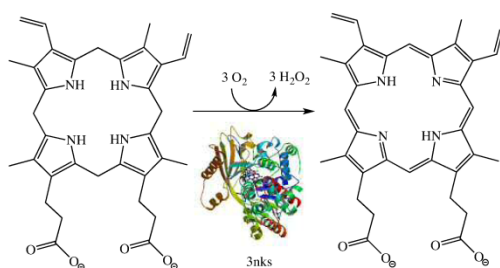


Fig. 2. The penultimate reaction in heme biosynthesis involves the six-electron oxidation of protoporphyrinogen-IX to protoporphyrin-IX by the FAD-dependent protoporphyrinogen-IX oxidase (EC 1.3.3.4, PPOX) (human structure: 3nks).

the variants according to their proposed effect on either FAD- or substrate binding or structural alterations of the protein. Interestingly, the Human Gene Mutation Database (www.hgmd.cf.ac.uk) lists more than 130 mutations, which appear to be uniformly distributed over the entire length of the gene and concern invariant amino acids as well as regions of variability.

Pyridoxal 5'-phosphate biosynthesis

Pyridoxal 5'-phosphate (PLP) serves as a cofactor in more than 140 distinct enzymatic activities and is arguably one of the most utilized vitamins in nature. According to a recent analysis, the human genome contains 68 genes encoding proteins with a structural fold typical for PLP-dependent enzymes [41]. Although functional assignment of these enzymes was not possible in all cases (14 remained unassigned) this result indicates that the supply of PLP is critical for the maintenance of numerous metabolic activities especially in pathways involving biochemical transformations of amino acids, e.g. PLP-dependent decarboxylations of amino acids to generate active amines and neurotransmitters. In humans, PLP is mainly generated by enzymatic phosphorylation and oxidation of pyridoxine and pyridoxamine. These two vitamers are available either from nutritional sources or are produced in the course of the degradation of PLP-containing enzymes. In the first step, they are phosphorylated by pyridoxal kinase and then oxidized by pyridoxine 5'-phosphate oxidase (EC 1.4.3.5, PNPO) to the active cofactor PLP (Fig. 3). The three-dimensional structures of the enzyme from several bacteria as well as the recombinant human enzyme were determined by X-ray crystallography ([42], pdb code 1nrg). Interestingly, the structure of the *E. coli* enzyme features two PLP binding sites, one in the active site near the flavin's isoalloxazine ring and a second closer to the surface of the dimeric protein ([43], pdb code 1g79). It is currently unclear whether the latter binding site is identical to the tight binding site identified by functional studies [43]. The human enzyme (261 amino acids) presumably also features a second tight binding site for PLP, however its exact location is currently not known [44]. Di Salvo et al. suggested that this second tight binding site might serve as transient storage for PLP, which is channeled to the apo-forms of PLP-dependent enzymes [44]. In support of this hypothesis, these authors reported that PNPO from *E. coli* interacts with several apo-forms of PLP-dependent enzymes with dissociation constants in the micromolar range (0.3–56 μM ; [44]). Although this appears to be an attractive process for the delivery of PLP to its target enzymes, it is unlikely that this is applicable to all human PLP-dependent enzymes because it would require a common docking site between the single PNPO and the 68 predicted enzymes. On the other hand, PNPO's cytosolic localization would enable the enzyme to deliver PLP directly to the apo-form of PLP-dependent enzymes *in statu nascendi*.

Several allelic variants of the PNPO gene were described (OMIM 603287). The reported mutations either lead to premature termination of protein biosynthesis (at position 174 [45]), extension of the protein by 28 amino acids (X262N) or splicing errors due to a mutation in intron 3 [46]. In addition, Mills et al., reported a point mutation in the PNPO gene resulting in the substitution of arginine in position 229 with tryptophan [46]. This R229W variant was recombinantly expressed and characterized by Musayev et al. [47]. They found that this variant is substantially compromised in its catalytic efficiency (ca. 850-fold) due to weaker binding of the substrate and decreased catalytic activity. Moreover, FMN possessed a 50-fold reduced affinity to the variant (see discussion above). These effects could be rationalized based on the involvement of the arginine residue in organizing important interactions in the active site of the enzyme. All of the reported mutations caused severe deficiency of PNPO activity resulting in neonatal epileptic encephalopathy. This disorder has a very poor prognosis

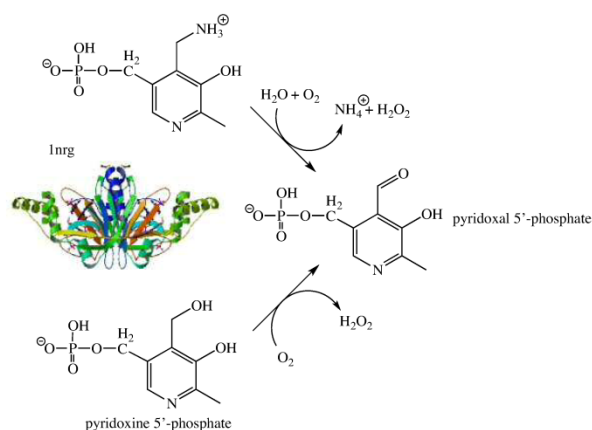


Fig. 3. Oxidation of pyridoxamine and pyridoxine 5'-phosphate to pyridoxal 5'-phosphate by the FMN-dependent pyridoxamine/pyridoxine 5'-phosphate oxidase (EC 1.4.3.5, PNPO), the last step of the PLP-biosynthesis. The structure shown is that of the human enzyme (1nrg).

postnatally and surviving children typically suffer from mental retardation.

PNPO expression in humans is prevalent in liver and kidney with most other tissues (brain, heart, muscle) having clearly reduced levels of mRNA [48]. Interestingly, abnormally low levels of PNPO activity were reported for some neoplastic cell lines, e.g. liver and neurally-derived tumors [49]. Whether and how these low PNPO activities are connected to tumorigenesis remains to be investigated.

Coenzyme A biosynthesis

Coenzyme A (CoA) biosynthesis from pantothenic acid (vitamin B₅) is a five-step enzymatic process. The third reaction in this universal reaction sequence is the decarboxylation of phosphopantothenoylcysteine to 4'-phosphopantotheine by phosphopantothenoylcysteine decarboxylase (EC 4.1.1.36; PPCD) as shown in Fig. 4 [50]. The structure of the human enzyme shows a non-covalently bound FMN per protomer of the trimeric protein [51]. In eukaryotes PPCD occurs as a monofunctional enzyme whereas in most bacteria – with the exception of streptococci and enterococci – PPCD is fused with phosphopantothenoylcysteine synthase (PPCS) the second enzyme of CoA biosynthesis [50]. In contrast to the reactions described above, the decarboxylation does not involve a net redox change. PPCD is one of the few examples where the flavin is not used for a reduction–oxidation reaction in a human flavoprotein (Table 1, entry #67). However, the flavin apparently plays a role as a transient electron acceptor during the reaction involving the transfer of charge from the substrate thiolate group to the isoalloxazine ring [52]. Currently, the OMIM database does not list any diseases related to a deficiency of PPCD. This may be partly due to the fact that approximately 4% of all enzymes utilize substrates linked to coenzyme A (e.g. acyl-CoAs) [53] and hence a deficiency in coenzyme A seriously compromises the viability of cells. This notion is supported by the fact that only the initial enzyme of coenzyme A biosynthesis, pantothenate kinase (EC 2.7.1.33, PANK), is linked to inherited diseases (OMIM 606157) but none of the other enzymes required. Interestingly, four isoforms of PANK were discovered in the human genome and therefore it appears likely that a deficiency of one isoform may be compensated at least partially by the others [54].

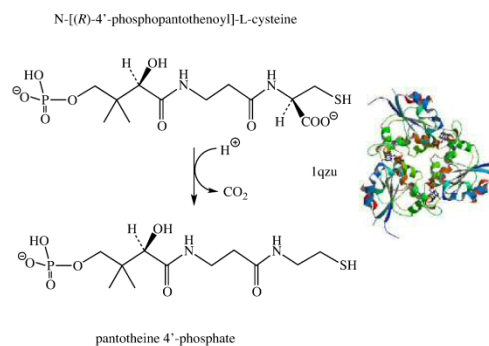


Fig. 4. Decarboxylation of N-[(R)-4'-phosphopantothenoyl]-L-cysteine to pantotheine 4'-phosphate by the FMN-dependent 4'-phosphopantothenoylcysteine decarboxylase (EC 4.1.1.36, PPCD). The structure shown is that of the human enzyme (1qzu).

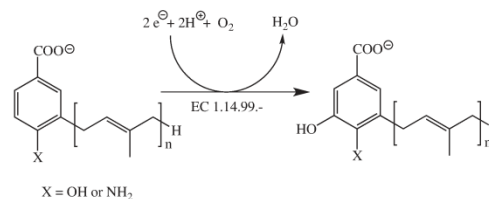


Fig. 5. Hydroxylation of the ubiquinone precursors in 5-position of the aromatic system by COQ6 (EC 1.14.99.-). In yeast, the electrons required for reduction of dioxygen are supplied by an NADPH-dependent ferredoxin reductase-ferredoxin system.

Coenzyme Q biosynthesis

Coenzyme Q or ubiquinone is an essential electron carrier in the mitochondrial electron transport chain shuttling electrons from complex I and II to complex III (see also section below). In contrast

to vitamin-derived coenzymes, ubiquinone is synthesized *de novo* from aromatic precursors such as *p*-hydroxybenzoic acid. In 2011, Pierrel and coworkers identified a FAD-dependent monooxygenase encoded by *coq6*, for the required hydroxylation in 5-position of a ubiquinone precursor in the yeast *Saccharomyces cerevisiae* (Fig. 5) [55]. A human homolog of *coq6* was recently discovered, which apparently catalyzes the hydroxylation in human ubiquinone biosynthesis (Table 1, entry #59) [56]. Flavin-dependent monooxygenases (hydroxylases) require a source of electrons for reduction of the flavin's isoalloxazine ring in order to enable the generation of hydroxylating 4 α -hydroperoxy intermediates. Based on the mode of flavin reduction, internal and external monooxygenases are distinguished which either use NAD(P)H or NADH directly for reduction or rely on the activity of an external NAD(P)H/NADH:FAD reductase to supply the reduced flavin cofactor [57]. In the case of yeast Coq6p, reduction of FAD is accomplished by ferredoxin reductase (termed Arh1) and ferredoxin (termed Yah1) at the expense of NADPH and thus has the character of an external reduction mode. It is currently unknown whether the human enzyme is reduced by the same mechanism. The human ortholog of *coq6* was discovered in search of the genetic cause of nephrotic syndrome [56] and several reports of coenzyme Q deficiency are compiled in the OMIM (614647).

Steroid biosynthesis

Steroid hormones play fundamental roles in developmental programs and homeostatic processes. Cholesterol, a central precursor for the biosynthesis of steroid hormones, bile acids and vitamin D, is synthesized from acetyl-CoA via the mevalonate pathway in a multistep pathway [58]. A crucial step in the biosynthesis is the cyclisation of the linear 2,3-oxidosqualene to the first tetracyclic ring system, lanosterol. The preceding reaction, catalyzed by squalene monooxygenase (EC 1.14.13.132, SQLE), enables this cyclisation by epoxidation of the 2,3-carbon-carbon double bond (Fig. 6, top) [59]. The oxygen atom introduced by SQLE remains in the molecule during processing to the steroid target structures and is important for the physical (amphiphilic character) and chemical properties (formation of esters). Although SQLE does not appear to be linked to an inherited disease, it was suggested earlier that the gene encoding SQLE is a candidate for Langer-Giedion syndrome, which is associated with mental retardation and microcephaly [60]. Interestingly, SQLE became a focus as a

drug target for antimycotic compounds in the 1980s [61]. More recently it is also discussed as a potentially useful target in hypercholesterolemic therapy [62,63]. Currently, treatment of hypercholesterolemia is dominated by statins, which inhibit 3-hydroxy-3-methylglutaryl CoA (HMG-CoA) reductase (EC 1.1.1.34), a central and rate-limiting enzyme in the mevalonate pathway. A major drawback of HMG-reductase inhibition results from the adverse effects on the biosynthesis of non-steroidal isoprenoids (e.g. ubiquinone) since the enzyme catalyzes an "early" step in the pathway. To alleviate this problem steps occurring after the committing reaction of steroid biosynthesis, i.e. the synthesis of squalene from farnesylpyrophosphate catalyzed by squalene synthase (EC 2.5.1.21) might be potentially useful targets for the design of new cholesterol lowering compounds. Because SQLE is the next enzyme of this metabolic branch point it is a suitable point of intervention to reduce the biosynthesis of cholesterol [62,63].

The ultimate reaction in cholesterol biosynthesis, the reduction of desmosterol, is catalyzed by 3 β -hydroxysterol Δ^{24} -reductase (EC 1.3.1.72, DHCR24). In contrast to SQLE, DHCR24 does not activate dioxygen for insertion into the substrate, but simply reduces the side-chain double bond at the expense of NADPH (Fig. 6, bottom). The gene encoding DHCR24 is a human homolog (also termed seldadin-1) of the *DIMINUTO/DWARF1* gene found in plants and *Caenorhabditis elegans* [64]. Several mutations in the human gene are known which result in reduced enzyme activity leading to desmosterolosis (OMIM 606418). Some of the mutations discovered are in or near the FAD binding site and hence may affect FAD binding. In other cases, however, the mutation is in less conserved areas and their effect on protein structure, folding or stability is unclear. Symptoms of the disease present at or shortly after birth and show a diverse range of developmental anomalies, such as failure to thrive, micro- or macrocephaly, psychomotor retardation, spasticity and seizures. The observed developmental and neurological defects correspond to the high expression of the gene in neuronal cells [64]. More recently it was also shown that DHCR24 is important for long bone growth in mice indicating that the enzyme's activity is also critical for the development of other tissues [65].

Thyroxine biosynthesis and iodine salvage

The thyroid gland produces two iodinated tyrosine-derived hormones, triiodothyronine (T₃) and thyroxine (T₄), which stimulate metabolism in most tissues. The initial biosynthetic reaction

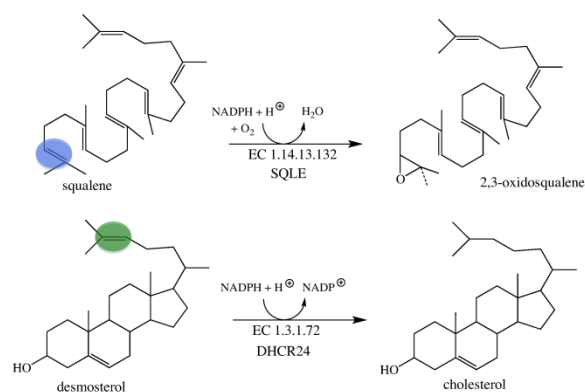


Fig. 6. Reactions of the two FAD-dependent enzymes in cholesterol biosynthesis. The reaction shown on top involves the insertion of an oxygen atom (blue circle) by SQLE (EC 1.14.13.132) and the reaction shown on the bottom the reduction of the side chain double bond (green circle) by DHCR24 (EC 1.3.1.72).

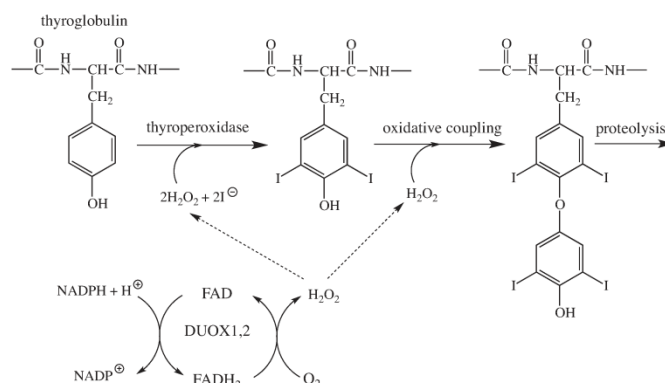


Fig. 7. Role of DUOX1 and 2 in the biosynthesis of thyroxine. The iodination of tyrosine residues and the coupling of two iodinated tyrosines require hydrogen peroxide, which is provided by the oxidation of reduced FAD with molecular dioxygen.

involves incorporation of iodine into tyrosine residues of thyroglobulin. In the next step, two neighboring diiodotyrosine residues are oxidatively coupled and the active hormones, T_3 and T_4 , are released by proteolytic cleavage of the precursor protein. The iodination and coupling reaction both require hydrogen peroxide, which is provided by two FAD-dependent thyroid oxidases (termed DUOX1 and 2) [66,67]. During turnover, FAD is reduced at the expense of NADPH and then reoxidized by dioxygen yielding hydrogen peroxide (Fig. 7). Several allelic variants were reported for DUOX2 leading to thyroid dysmorphogenesis 6 (OMIM 606759). How the resulting single amino acid exchange in the observed variants affect enzyme function is currently not known.

During the production of T_3 and T_4 substantial amounts of mono- and diiodotyrosine are released [68]. Because iodine is a precious trace element, it is recycled in a single reductive step catalyzed by an FMN-dependent dehalogenase (IYD, Fig. 8 [69]). The released iodine can then be reused by thyroperoxidase for incorporation into thyroglobulin (see above). Several allelic variants were reported for IYD, which severely compromise the dehalogenase activity of the enzyme leading to hypothyroidism (dysmorphogenesis 4, OMIM 612025) [70,71].

Flavoproteins providing assistance to other flavoproteins: Assembly of complex I

The human respiratory electron transport chain relies on complex I for electron transfer from NADH to ubiquinone coupled with proton translocation across the inner mitochondrial membrane. In the initial reaction NADH reduces the FMN cofactor in the NDUV1 subunit (EC 1.6.5.3) of complex I, which in turn passes the electrons to iron-sulfur clusters. The formation of complex I, which

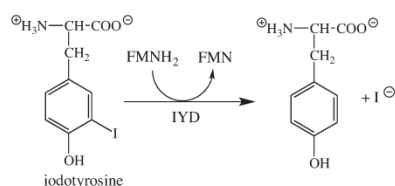


Fig. 8. Dehalogenation of iodotyrosine catalyzed by IYD. The mono- and diiodotyrosine residues released from thyroglobulin are substrates of the enzyme. Reductively released iodine is then reused by thyroperoxidase for incorporation into tyrosine residues of thyroglobulin.

consists of at least 36 nuclear- and seven mitochondrial-encoded subunits (OMIM 252010), requires several assembly factors, such as NDUFAF1 and NUBPL [72,73]. In addition, two FAD-dependent proteins recently emerged as critical factors for complex I assembly, ACAD9 and FOXRED1 (Table 1, entries #24 and #73, respectively). The exact role of the FAD-dependent OXidoREDuctase (FOXRED1) in assembly of complex I is not fully understood at the moment but it was clearly shown that it is essential for complex I activity in the inner mitochondrial membrane [72,74]. A BLASTp search identified two human FAD-dependent flavoproteins, SARDH and DMGDH, as related (22% and 21% identity, respectively) enzymes to FOXRED1. FOXRED1 comprises 486 amino acids and thus is much shorter than SARDH and DMGDH with 918 and 866 amino acids, respectively. The similarity of FOXRED1 to SARDH and DMGDH is found in the N-terminal part of the two dehydrogenases where FAD is covalently bound to a histidine. This amino acid residue is not conserved in FOXRED1 indicating that the FAD cofactor may not be covalently bound.

The discovery of FOXRED1 was closely associated with the search to identify the mechanism of complex I deficiency, leading for example to mitochondrial encephalopathy. Fassone et al. demonstrated that a point mutation in the FOXRED1 gene led to an amino acid exchange (R352W) in the putative FAD binding site [74]. According to their molecular model of the protein this amino acid exchange could prevent FAD binding and hence compromises the assumed chaperone activity of the protein.

ACAD9 (EC 1.3.99.-) was first described as an acyl-CoA dehydrogenase specific for long-chain unsaturated fatty acids [75,76]. Recent evidence however questions the involvement of ACAD9 in the degradation of long-chain fatty acids in the mitochondrial matrix and suggests a role in biogenesis of complex I instead [77]. Although recombinant ACAD9 possesses dehydrogenase activity *in vitro*, mutations in ACAD9 result in complex I deficiency rather than a disturbance of long-chain fatty acid metabolism [77].

Concluding remarks

Our analysis of the human flavoproteome has led to the identification of several areas where further research is required. Because riboflavin must be supplied by the diet uptake in the human intestine is an important process to make the vitamin available for the synthesis of FMN and FAD. Three poorly characterized transporters seem to be responsible for riboflavin uptake in the human intestine. The relative contribution and role of these

transporters is currently unclear and warrants further investigations. A better understanding of the uptake processes may also have therapeutic benefits as some inherited diseases feature reduced flavin affinity to the affected flavoproteins and thus are potentially treatable by riboflavin supplementation. Equally, little is known about flavin homeostasis and the processes leading to degradation and excretion of flavins.

Although many human flavoprotein structures were solved experimentally by X-ray crystallography or modeled using homologous structures several flavoproteins still elude structural characterisation. Many of these are associated with cellular membranes and are therefore more difficult to obtain by recombinant expression in heterologous hosts. Moreover, membrane integral or associated proteins are challenging for structure elucidation by X-ray crystallography due to their lipophilic character. In view of the important roles of membrane-associated flavoproteins in humans, the potential as drug targets (e.g. SQLE) and the involvement in diseases (e.g. DUOX1/2, IYD) determination of the “missing” structures are certainly rewarding goals.

We found that many genes encoding flavoproteins occur as allelic variants with the potential to cause severe human diseases (Table 2). The number of allelic variants covers a wide range from only a few to more than one hundred. With the exception of a few systematic studies our knowledge of the effect of the mutation on stability, structure and activity of the flavoprotein is incomplete. This lack of insight should be improved by detailed analyses of mutational effects on flavoprotein properties. In light of many indications that flavoprotein variants suffer from a reduced affinity to their cognate flavin cofactor this seems to be of particular importance because riboflavin supplementation may help to remedy symptoms in affected individuals.

Methods

The names and gene abbreviations of human flavoproteins, compiled for a previously published review article [2], were used to search for inherited diseases in the Online Mendelian Inheritance in Man data base (OMIM; <http://www.ncbi.nlm.nih.gov/omim>). This search constituted the basis for Table 2 where the most relevant entry in OMIM is provided as a six-digit number (right column). The reader is referred to these entries for a complete list of references pertaining to the diseases mentioned in this article.

Acknowledgments

We thank the Austrian Research Fund (FWF) for financial support through project P22361 and the PhD program “Molecular Enzymology” (W901).

Appendix A. Supplementary data

Supplementary data associated with this article can be found, in the online version, at <http://dx.doi.org/10.1016/j.abb.2013.02.015>.

References

- [1] J.L. Chastain, D.B. McCormick, *Am. J. Clin. Nutr.* 46 (1987) 830–834.
- [2] P. Macheroux, B. Kappes, S.E. Ealick, *FEBS J.* 278 (2011) 2625–2634.
- [3] B.N. Ames, I. Elson-Schwab, E.A. Silver, *Am. J. Clin. Nutr.* 75 (2002) 616–658.
- [4] A.M. Bosch, N.C. Abeling, L. IJlst, H. Knoester, W.L. van der Pol, A.E. Stromer, R.J. Wanders, G. Visser, F.A. Wijburg, M. Duran, et al., *Inherit. Metab. Dis.* 34 (2011) 159–164.
- [5] P. Green, M. Wiseman, Y.J. Crow, H. Houlden, S. Riphagen, J.P. Lin, F.L. Raymond, A.M. Childs, E. Sheridan, S. Edwards, et al., *Am. J. Hum. Gen.* 86 (2010) 485–489.
- [6] G. Anand, N. Hasan, S. Jayapal, Z. Huma, T. Ali, J. Hull, E. Blair, T. McShane, S. Jayawant, *Dev. Med. Child Neurol.* 54 (2012) 187–189.
- [7] A. Koy, F. Pillekamp, T. Hoehn, H. Waterham, D. Klee, E. Mayatepek, B. Assmann, *Pediatr. Neurol.* 46 (2012) 407–409.
- [8] A.J. Wittwer, C. Wagner, *J. Biol. Chem.* 256 (1981) 4102–4108.
- [9] R.J. Cook, K.S. Misono, C. Wagner, *J. Biol. Chem.* 259 (1984) 12475–12480.
- [10] R.J. Cook, K.S. Misono, C. Wagner, *J. Biol. Chem.* 260 (1985) 12998–13002.
- [11] F. Forneris, E. Battaglioli, A. Mattevi, C. Binda, *FEBS J.* 276 (2009) 4304–4312.
- [12] J. Wang, F. Lu, Q. Ren, H. Sun, Z. Xu, R. Lan, Y. Liu, D. Ward, J. Quan, T. Ye, et al., *Cancer Res.* 71 (2011) 7238–7249.
- [13] B.A. Binzak, R.A. Wevers, S.H. Moolenaar, Y.M. Lee, W.L. Hwu, J. Poggi-Bach, U.F. Engelke, H.M. Hoard, J.G. Vockley, *J. Vockley, Am. J. Hum. Gen.* 68 (2001) 839–847.
- [14] S.H. Moolenaar, J. Poggi-Bach, U.F. Engelke, J.M. Corstiaensen, A. Heerschap, J.G. de Jong, B.A. Binzak, J. Vockley, R.A. Wevers, *Clin. Chem.* 45 (1999) 459–464.
- [15] R.P. McAndrew, J. Vockley, J.J. Kim, *J. Inherit. Metab. Dis.* 31 (2008) 761–768.
- [16] E.P. Treacy, B.R. Akerman, L.M. Chow, R. Youil, C. Bibeau, J. Lin, A.G. Bruce, M. Knight, D.M. Danks, J.R. Cashman, et al., *Hum. Mol. Gen.* 7 (1998) 839–845.
- [17] M. Eschenbrenner, M.S. Jorns, *Genomics* 59 (1999) 300–308.
- [18] A. Sreekumar, L.M. Poisson, T.M. Rajendiran, A.P. Khan, Q. Cao, J. Yu, B. Laxman, R. Mehra, R.J. Lonigro, Y. Li, et al., *Nature* 457 (2009) 910–914.
- [19] L. Bohm, A.M. Serafin, P. Fernandez, G. Van der Watt, P.J. Bouic, J. Harvey, *S. Afr. Med. J.* 102 (2012) 677–679.
- [20] H.J. Issaq, T.D. Veenstra, *J. Sep. Sci.* 34 (2011) 3619–3621.
- [21] G. Lucarelli, M. Fanelli, A.M. Larocca, C.A. Germinario, M. Rutigliano, A. Vavallo, F.P. Selvaggi, C. Bettocchi, M. Battaglia, P. Dittono, *Prostate* 72 (2012) 1611–1621.
- [22] P. Frosst, H.J. Blom, R. Milos, P. Goyette, C.A. Sheppard, R.G. Matthews, G.J. Boers, M. den Heijer, L.A. Kluijtmans, L.P. van den Heuvel, et al., *Nat. Gen.* 10 (1995) 111–113.
- [23] P.M. Ueland, S. Hustad, J. Schneede, H. Refsum, S.E. Vollset, *Trends Pharmacol. Sci.* 22 (2001) 195–201.
- [24] K. Yamada, Z. Chen, R. Rozen, R.G. Matthews, *Proc. Natl. Acad. Sci. USA* 98 (2001) 14853–14858.
- [25] D. Leclerc, A. Wilson, R. Dumas, C. Gafuik, D. Song, D. Watkins, H.H. Heng, J.M. Rommens, S.W. Scherer, D.S. Rosenblatt, et al., *Proc. Natl. Acad. Sci. USA* 95 (1998) 3059–3064.
- [26] M.L. Ludwig, R.G. Matthews, *Annu. Rev. Biochem.* 66 (1997) 269–313.
- [27] H. Olteanu, R. Banerjee, *J. Biol. Chem.* 276 (2001) 35558–35563.
- [28] A. Wilson, R. Platt, Q. Wu, D. Leclerc, B. Christensen, H. Yang, R.A. Gravel, R. Rozen, *Mol. Gen. Metab.* 67 (1999) 317–323.
- [29] K. Yamada, R.A. Gravel, T. Toraya, R.G. Matthews, *Proc. Natl. Acad. Sci. USA* 103 (2006) 9476–9481.
- [30] N.A. Leal, H. Olteanu, R. Banerjee, T.A. Bobik, *J. Biol. Chem.* 279 (2004) 47536–47542.
- [31] P.E. Mera, J.C. Escalante-Semerena, *J. Biol. Chem.* 285 (2010) 2911–2917.
- [32] H.A. Dailey, *Biochem. Soc. Trans.* 30 (2002) 590–595.
- [33] S. Arnould, M. Takahashi, J.-M. Camadro, *Proc. Natl. Acad. Sci. USA* 96 (1999) 14825–14830.
- [34] J.C. Deybach, V. da Silva, B. Grandchamp, Y. Nordmann, *Eur. J. Biochem.* 194 (1985) 431–435.
- [35] S. Sassa, Br. J. Haematol. 135 (2006) 281–292.
- [36] H. Puy, L. Gouya, J.C. Deybach, *Lancet* 375 (2010) 924–937.
- [37] I. Macalpine, R. Hunter, *Br. Med. J.* 1 (1966) 65–71.
- [38] J.C.G. Röhl, M.J. Warren, D.M. Hunt, *Purple Secret, Genes, “Madness” and the Royal Houses of Europe*, Bantam Press, London, 1998.
- [39] T.M. Cox, N. Jack, S. Lofthouse, J. Watling, *Lancet* 366 (2005) 332–335.
- [40] X. Qin, Y. Tan, L. Wang, Z. Wang, B. Wang, X. Wen, G. Yang, Z. Xi, Y. Shen, *FASEB J.* 25 (2011) 653–664.
- [41] R. Percudani, A. Peracchi, *EMBO Rep.* 4 (2003) 850–854.
- [42] F.N. Musayev, M.L. Di Salvo, T.-P. Ko, V. Schirch, M.K. Safo, *Protein Sci.* 12 (2003) 1455–1463.
- [43] M.K. Safo, F.N. Musayev, M.L. Di Salvo, V. Schirch, *J. Mol. Biol.* 310 (2001) 817–826.
- [44] M.L. Di Salvo, R. Contestabile, M.K. Safo, *Biochim. Biophys. Acta* 1814 (2011) 1597–1608.
- [45] A. Ruiz, J. Garcia-Villoria, A. Ormazabal, J. Zschocke, M. Fiol, A. Navarro-Sastre, R. Artuch, M.A. Vilaseca, A. Ribes, *Mol. Gen. Metab.* 93 (2008) 216–218.
- [46] P.B. Mills, R.A. Surtees, M.P. Champion, C.E. Beesley, N. Dalton, P.J. Scambler, S.J. Heales, A. Briddon, I. Scheimberg, G.F. Hoffmann, et al., *Hum. Mol. Gen.* 14 (2005) 1077–1086.
- [47] F.N. Musayev, M.L. Di Salvo, M.A. Saavedra, R. Contestabile, M.S. Chatge, A. Haynes, V. Schirch, M.K. Safo, *J. Biol. Chem.* 284 (2009) 30949–30956.
- [48] J.H. Kang, M.L. Hong, D.W. Kim, J. Park, T.C. Kang, M.H. Won, N.I. Baek, B.J. Moon, S.Y. Choi, O.S. Kwon, *Eur. J. Biochem.* 271 (2004) 2452–2461.
- [49] E.O. Ngo, G.R. LePage, J.W. Thanassi, N. Meisler, L.M. Nutter, *Biochemistry* 37 (1998) 7741–7748.
- [50] M. Daugherty, B. Polanuyer, M. Farrell, M. Scholle, A. Lykidis, V. de Crecy-Lagard, A. Osterman, *J. Biol. Chem.* 277 (2002) 21431–21439.
- [51] N. Manoj, S.E. Ealick, *Acta Crystallogr.* 59 (2003) 1762–1766.
- [52] S. Steinbacher, P. Hernandez-Acosta, B. Bieseler, M. Blaesse, R. Huber, F.A. Culianez-Macia, T. Kupke, *J. Mol. Biol.* 327 (2003) 193–202.
- [53] T.P. Begley, C. Kinsland, E. Strauss, *Vitam. Horm.* 61 (2001) 157–171.
- [54] B. Zhou, S.K. Westaway, B. Levinson, M.A. Johnson, J. Gitschier, S.J. Hayflick, *Nat. Gen.* 28 (2001) 345–349.
- [55] M. Ozeir, U. Mühlenhoff, H. Weibert, R. Lill, M. Fontecave, F. Pierrel, *Chem. Biol.* 18 (2011) 1134–1142.

- [56] S.F. Heeringa, G. Chernin, M. Chaki, W. Zhou, A.J. Sloan, Z. Ji, L.X. Xie, L. Salviati, T.W. Hurd, V. Vega-Warner, et al., *J. Clin. Invest.* 121 (2011) 2013–2024.
- [57] W.J. van Berkel, N.M. Kamerbeek, M.W. Fraaije, *J. Biotech.* 124 (2006) 670–689.
- [58] G. Gibbons, K. Mitropoulos, N. Myant, *Biochemistry of Cholesterol*, Elsevier Biomedical, Amsterdam, 1982.
- [59] S. Yamamoto, K. Bloch, *J. Biol. Chem.* 245 (1970) 1670–1674.
- [60] M. Nagai, J. Sakakibara, K. Wakui, Y. Fukushima, S. Igarashi, S. Tsuji, M. Arakawa, T. Ono, *Genomics* 44 (1997) 141–143.
- [61] N.S. Ryder, M.C. Dupont, *Biochem. J.* 230 (1985) 765–770.
- [62] A. Belter, M. Skupinska, M. Giel-Pietraszuk, T. Grabarkiewicz, L. Rychlewski, J. Barciszewski, *Biol. Chem.* 392 (2011) 1053–1075.
- [63] A. Chugh, A. Ray, J.B. Gupta, *Prog. Lipid Res.* 42 (2003) 37–50.
- [64] I. Greeve, I. Hermans-Borgmeyer, C. Brellinger, D. Kasper, T. Gomez-Isla, C. Behl, B. Levkau, R.M. Nitsch, *J. Neurosci.* 20 (2000) 7345–7352.
- [65] R. Mirza, S. Qiao, K. Tateyama, T. Miyamoto, L. Xiuli, H. Seo, *J. Bone Miner. Metab.* 30 (2012) 144–153.
- [66] X. De Deken, D. Wang, M.C. Many, S. Costagliola, F. Libert, G. Vassart, J.E. Dumont, F. Miot, *J. Biol. Chem.* 275 (2000) 23227–23233.
- [67] C. Dupuy, R. Ohayon, A. Valent, M.S. Noel-Hudson, D. Deme, A. Virion, *J. Biol. Chem.* 274 (1999) 37265–37269.
- [68] J. Nunez, J. Pommier, *Vitam. Horm.* 39 (1982) 175–229.
- [69] J.E. Friedman, J.A. Watson Jr., D.W. Lam, S.E. Rokita, *J. Biol. Chem.* 281 (2006) 2812–2819.
- [70] G. Afink, W. Kulik, H. Overmars, J. de Randamie, T. Veenboer, A. van Cruchten, M. Craen, C. Ris-Stalpers, *J. Clin. Endocrinol. Metab.* 93 (2008) 4894–4901.
- [71] J.C. Moreno, W. Klootwijk, H. van Toor, G. Pinto, M. D'Alessandro, A. Leger, D. Goudie, M. Polak, A. Crutters, T.J. Visser, *N. Engl. J. Med.* 358 (2008) 1811–1818.
- [72] S.E. Calvo, E.J. Tucker, A.G. Compton, D.M. Kirby, G. Crawford, N.P. Burt, M. Rivas, C. Guiducci, D.L. Bruno, O.A. Goldberger, et al., High-throughput, pooled sequencing identifies mutations in NUBPL and FOXRED1 in human complex I deficiency, *Nat. Gen.* 42 (2010) 851–858.
- [73] C.J. Dunning, M. McKenzie, C. Sugiana, M. Lazarou, J. Silke, A. Connelly, J.M. Fletcher, D.M. Kirby, D.R. Thorburn, M.T. Ryan, *EMBO J.* 26 (2007) 3227–3237.
- [74] E. Fassone, A.J. Duncan, J.W. Taanman, A.T. Pagnamenta, M.I. Sadowski, T. Holand, W. Qasim, P. Rutland, S.E. Calvo, V.K. Mootha, et al., *Hum. Mol. Gen.* 19 (2010) 4837–4847.
- [75] R. Ensenauer, M. He, J.M. Willard, E.S. Goetzman, T.J. Corydon, B.B. Vandahl, A.W. Mohsen, G. Isaya, J. Vockley, *J. Biol. Chem.* 280 (2005) 32309–32316.
- [76] J. Zhang, W. Zhang, D. Zou, G. Chen, T. Wan, M. Zhang, X. Cao, *Biochem. Biophys. Res. Commun.* 297 (2002) 1033–1042.
- [77] J. Nouws, L. Nijtmans, S.M. Houten, M. van den Brand, M. Huynen, H. Venselaar, S. Hoefs, J. Gloerich, J. Kronick, T. Hutchin, et al., *Cell. Metab.* 12 (2010) 283–294.
- [78] A. Mostowska, B. Biedziak, I. Dunin-Wilczynska, A. Komorowska, P.P. Jagodzinski, *Birth Defects Res. A Clin. Mol. Teratol.* 91 (2011) 169–176.
- [79] A. Mostowska, K.K. Hozyasz, B. Biedziak, J. Misiak, P.P. Jagodzinski, *Eur. J. Oral. Sci.* 118 (2010) 325–332.
- [80] A. Mostowska, K.K. Hozyasz, P. Wojcicki, M. Dziegielewska, P.P. Jagodzinski, *J. Med. Genet.* 47 (2010) 809–815.
- [81] A.R. Johnson, C.N. Craciunescu, Z. Guo, Y.W. Teng, R.J. Thresher, J.K. Blusztajn, S.H. Zeisel, *FASEB J.* 24 (2010) 2752–2761.
- [82] A.R. Johnson, S. Lao, T. Wang, J.A. Galanko, S.H. Zeisel, *PLoS ONE* 7 (2012) e36047.

Supporting Information

Figure S1

Distribution of structural clans in human flavoproteins.

The y-axis indicates the number of representatives from Table 1 for each of the Pfam clans (see <http://pfam.sanger.ac.uk/>). The left and right panel is for FAD- and FMN-dependent flavoproteins, respectively.

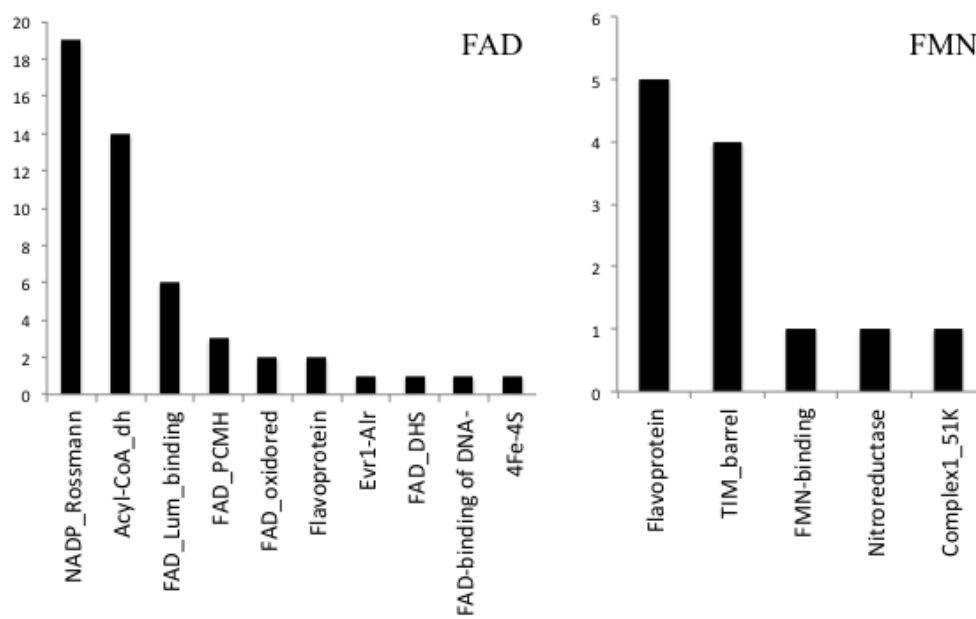
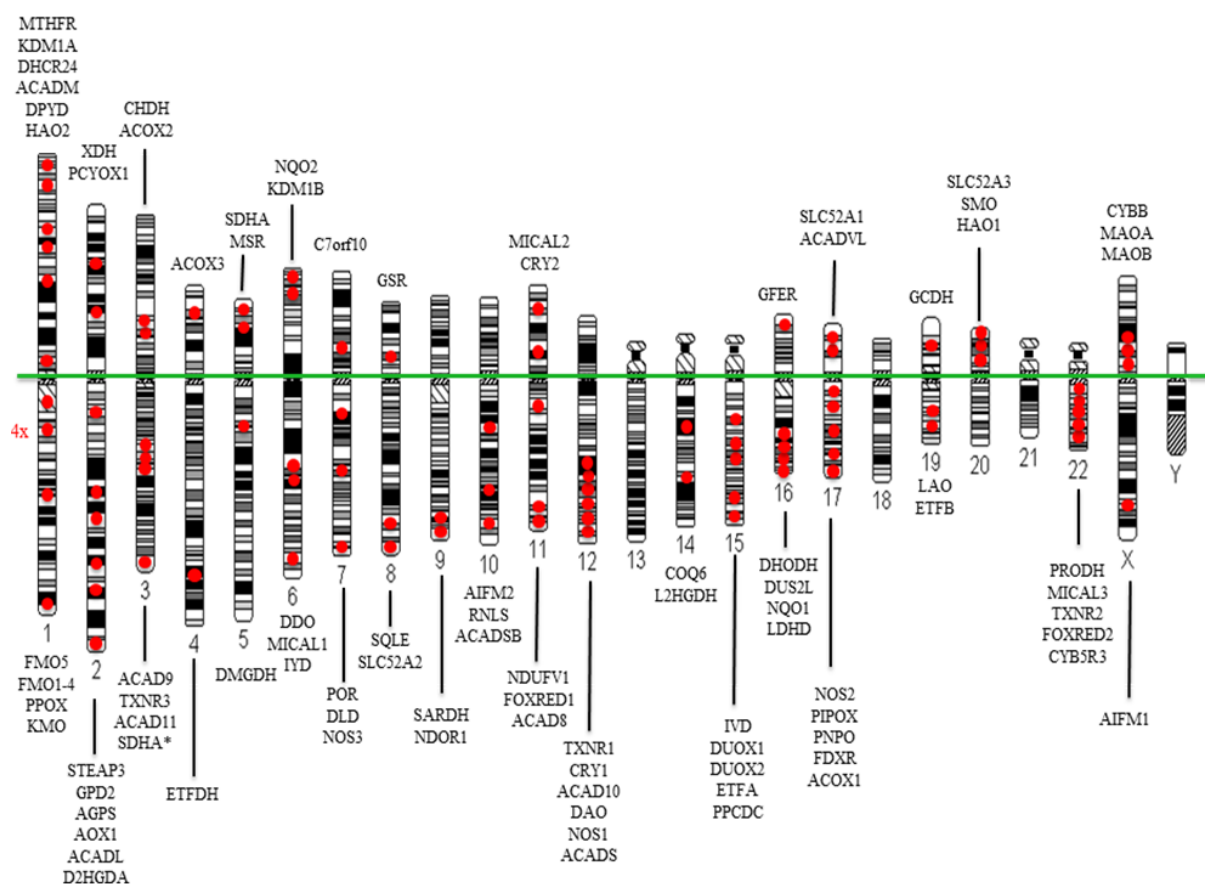


Figure S2

Chromosomal map of genes encoding flavoproteins.

The abbreviations used for the genes represented here by red spheres are given in Table 1. The gene symbols on top refer to the location above the green line (marking the centromere) and the gene symbols on the bottom to the location below the green line (from top to bottom)Figure S1:

Distribution of structural clans in human flavoproteins



Chapter 2:
NAD(P)H:quinone oxidoreductase 1

Collapse of the native structure caused by a single amino acid exchange in human NAD(P)H:quinone oxidoreductase 1

Author Contributions

The manuscript has been published in FEBS JOURNAL (2014), Volume 281, Number 20, Pages 4691-4704. The research was carried out in cooperation with the Institute of Molecular Biosciences (University of Graz, Austria), the Institute of Chemistry (University of Graz, Austria) and Institute of Chemistry and Technology of Materials (Graz University of Technology, Austria). Venugopal Gudipati (Institute of Biochemistry, Graz University of Technology, Austria) cloned the truncation mutants, expressed proteins and did the trypsin digestion followed by MALDI-MS measurements. Michael Karl Uhl (Institute of Molecular Biosciences, University of Graz, Austria) performed the crystallisation experiments and structure determination and refinement of the crystallisation data. Alexandra Binter (Institute of Biochemistry, Graz University of Technology, Austria) realised the stopped flow measurements. Sergio A. Pulido (Institute of Chemistry, University of Graz, Austria) performed the NMR relaxation time experiments. Robert Saf (Institute of Chemistry and Technology of Materials, Graz University of Technology, Austria) assisted with the MALDI-MS measurements. Klaus Zangger (Institute of Chemistry, University of Graz, Austria) performed NMR and HSQC measurements and assisted in writing this paper. Karl Gruber (Institute of Molecular Biosciences, University of Graz, Austria) helped with data interpretation and assisted in writing this paper. Peter Macheroux (Institute of Biochemistry, Graz University of Technology, Austria) managed the project and is responsible for the most part of the writing and correcting of the paper. My contribution consisted in cloning of the full length proteins and expression of the unlabelled and isotopically labelled proteins as well as doing measurements with ITC and spectrophotometer.

Collapse of the native structure caused by a single amino acid exchange in human NAD(P)H:quinone oxidoreductase¹

Wolf-Dieter Lienhart^{1*}, Venugopal Gudipati^{1*}, Michael K. Uhl², Alexandra Binter¹, Sergio A. Pulido³, Robert Saf⁴, Klaus Zangger³, Karl Gruber² and Peter Macheroux¹

¹ Institute of Biochemistry, Graz University of Technology, Austria

² Institute of Molecular Biosciences, University of Graz, Austria

³ Institute of Chemistry, University of Graz, Austria

⁴ Institute of Chemistry and Technology of Materials, Graz University of Technology, Austria

Keywords

antioxidant defense; cancer; flavin; quinones; single-nucleotide polymorphism

Correspondence

P. Macheroux, Institute of Biochemistry, Graz University of Technology, Petersgasse 12, A-8010 Graz, Austria
Fax: +43 316 873 6952
Tel: +43 316 873 6450
E-mail: peter.macheroux@tugraz.at

*These authors contributed equally to this work.

(Received 7 June 2014, revised 22 July 2014, accepted 14 August 2014)

doi:10.1111/febs.12975

Human NAD(P)H:quinone oxidoreductase 1 (NQO1) is essential for the antioxidant defense system, stabilization of tumor suppressors (e.g. p53, p33, and p73), and activation of quinone-based chemotherapeutics. Overexpression of NQO1 in many solid tumors, coupled with its ability to convert quinone-based chemotherapeutics into potent cytotoxic compounds, have made it a very attractive target for anticancer drugs. A naturally occurring single-nucleotide polymorphism (C609T) leading to an amino acid exchange (P187S) has been implicated in the development of various cancers and poor survival rates following anthracyclin-based adjuvant chemotherapy. Despite its importance for cancer prediction and therapy, the exact molecular basis for the loss of function in NQO1 P187S is currently unknown. Therefore, we solved the crystal structure of NQO1 P187S. Surprisingly, this structure is almost identical to NQO1. Employing a combination of NMR spectroscopy and limited proteolysis experiments, we demonstrated that the single amino acid exchange destabilized interactions between the core and C-terminus, leading to depopulation of the native structure in solution. This collapse of the native structure diminished cofactor affinity and led to a less competent FAD-binding pocket, thus severely compromising the catalytic capacity of the variant protein. Hence, our findings provide a rationale for the loss of function in NQO1 P187S with a frequently occurring single-nucleotide polymorphism.

Database

Structural data are available in the Protein Data Bank under the accession numbers [4cet](#) (P187S variant with dicoumarol) and [4cf6](#) (P187S variant with Cibacron blue).

Structured digital abstract

- [NQO1 P187S](#) and [NQO1 P187S](#) bind by [nuclear magnetic resonance](#) ([View interaction](#))
- [NQO1 P187S](#) and [NQO1 P187S](#) bind by [x-ray crystallography](#) ([1](#), [2](#))
- [NQO1](#) and [NQO1](#) bind by [molecular sieving](#) ([1](#), [2](#))

Abbreviations

ITC, isothermal titration microcalorimetry; NQO1, NAD(P)H:quinone oxidoreductase 1; PDB, Protein Data Bank; SNP, single-nucleotide polymorphism; WT, wild type.

Introduction

NAD(P)H:quinone oxidoreductase 1 (NQO1; EC 1.6.99.2) is a dimeric (61.7 kDa) human cytosolic FAD-dependent enzyme catalyzing the two-electron reduction of intracellular quinones to hydroquinones. NQO1 is an essential component of the antioxidant defense system, preventing the formation of potentially harmful semiquinone radicals [1]. Additionally, NQO1 stabilizes several tumor suppressors (p33^{ING1b}, p53, and p73), thereby exerting an antineoplastic effect [2–5], and also activates quinone-based chemotherapeutics by reducing the quinone pharmacophore to a cytotoxic hydroquinone form [6]. It was recently shown that NQO1 maintains mitochondrial integrity as a part of the p62–Keap1–Nrf2–Nqo1 cascade that has evolved to prevent mitochondrial dysfunction, thus attenuating the rate of aging in vertebrates [7].

A frequent single-nucleotide polymorphism (SNP) in the *NQO1* gene (on human chromosome 16q22.1), whereby C609 is changed to T, results in the replacement of Pro187 by serine in the protein [8]. The frequency of the *NQO1*2* homozygous genotype was estimated to be between 4% and 20%, depending on the ethnic group, with the highest prevalence being seen in Asian populations [9]. The *NQO1*2* genotype is prevalent in individuals (> 25%) who are susceptible to increased benzene hematotoxicity and acute myelogenous leukemia. In addition, it appears to be linked to poor survival rates of women with breast cancer after anthracycline-based adjuvant chemotherapy [10–12]. It was proposed that the occurrence of the *NQO1*2* genotype is a prognostic and predictive marker for breast cancer [10].

Despite its importance for cancer prediction and therapy, the exact structural and molecular basis for the loss of function in NQO1 P187S is currently unknown. The site of amino acid exchange (P187S) is neither near the FAD-binding active site of the enzyme nor near the NAD(P)H-binding site. Therefore, it was speculated that the proline to serine replacement leads to local perturbation of a central β -sheet, reducing the affinity of FAD, and thus lowering catalytic activity [13]. It was also proposed that FAD acts as a chemical chaperone, maintaining the properly folded state of NQO1 [14]. Our findings establish that the amino acid replacement destabilizes the native fold of the enzyme, thus contradicting previous assumptions proposed to rationalize the loss of function in NQO1 P187S.

Results and Discussion

In view of the important cellular functions of NQO1 and the high frequency of the *NQO1*2* genotype, we

studied the biochemical and structural properties of NQO1 P187S in comparison with NQO1. During purification of the recombinant NQO1 proteins by Ni²⁺-nitrilotriacetic acid affinity and size exclusion chromatography, we noticed that NQO1 P187S showed partial depletion of the FAD cofactor, indicating that it had lower cofactor-binding affinity than NQO1. Therefore, we prepared the apo-forms of NQO1 and NQO1 P187S, and studied binding of the FAD cofactor to the apo-forms by monitoring difference absorption changes. As shown in Fig. 1 (left diagrams), the spectral perturbations observed for NQO1 and NQO1 P187S showed clear differences in their absorption minima and maxima, as well as their isosbestic points. However, both titrations produced sharp endpoints (Fig. 1, insets), indicating that the dissociation constants of FAD binding are below the micromolar range for both NQO1 and NQO1 P187S. As the dissociation constants for both proteins are in the same range, we assumed that reduced activity of NQO1 P187S cannot be explained solely by the loss of FAD, as suggested in previous studies [14]. For the accurate determination of dissociation constants, FAD was titrated with apo-NQO1 and apo-NQO1 P187S in a microcalorimeter. These isothermal titration microcalorimetry (ITC) measurements showed that each protomer of the dimeric protein has a single FAD-binding site, albeit NQO1 P187S showed an increase in the dissociation constant (K_d) by a factor of 7 as compared with NQO1 ($K_d = 64 \pm 23$ nM and $K_d = 428 \pm 90$ nM for NQO1 and NQO1 P187S, respectively; Fig. 1, right diagrams). Thus, our experiments show that FAD binding is affected not only qualitatively in terms of the mode of physical interactions, but also quantitatively (i.e. lower affinity).

Furthermore, rapid reaction measurements demonstrated that the reductive half-reaction of the catalytic cycle is severely affected in NQO1 P187S. The bimolecular rate constants of NQO1 P187S were decreased by factors of 300 and 70 for NADH and NADPH, respectively (Table 1). On the other hand, the oxidative half-reaction, i.e. reduction of a quinone substrate (e.g. benzoquinone or menadione) by the reduced FAD cofactor, was still very rapid in NQO1 P187S and was complete within the dead time of the stopped-flow instrument (~ 5 ms). As the reductive half-reaction is the rate-limiting step in the catalytic cycle, the lower rate of reduction leads directly to a decrease in catalytic turnover in NQO1 P187S. Hence, it is highly probable that NQO1 P187S will metabolize cellular quinones, radical oxygen species and prodrugs at a much lower rate than that of NQO1. In this context it should be noted that the much lower rate of

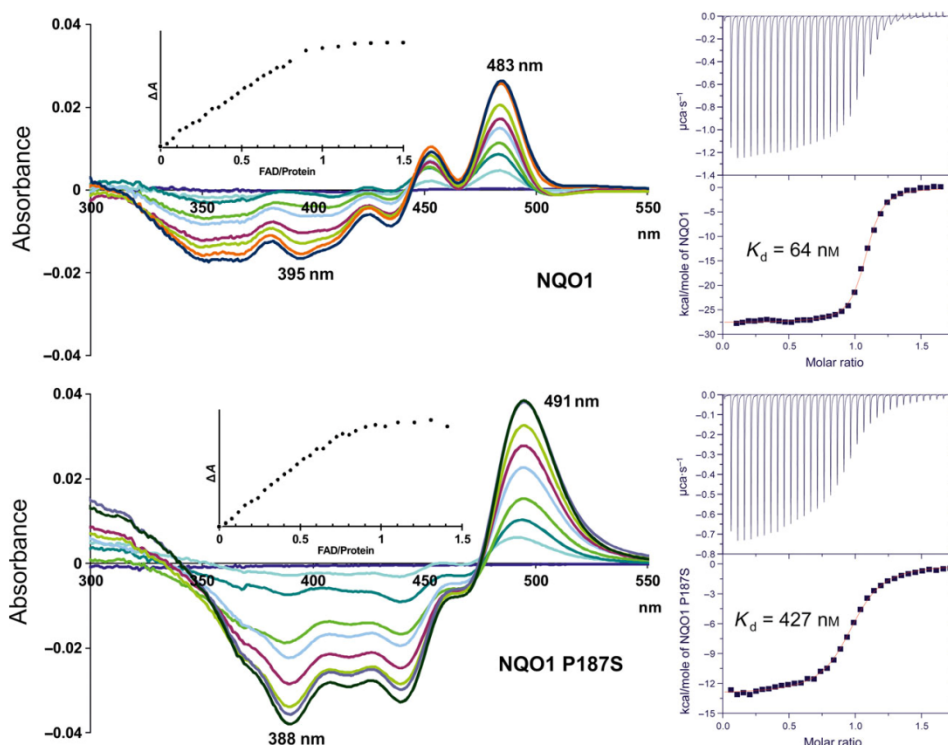


Fig. 1. The binding mode and affinity of FAD for NQO1 P187S are different from those for NQO1. Left diagrams: UV-visible difference absorption spectra. Representative difference absorption spectra obtained from the difference titration of apo-NQO1 and apo-NQO1 P187S with the FAD cofactor in the spectral range of 300–550 nm are shown. The spectra were recorded after the addition of 0 μL (black), 6 μL (red), 12 μL (light green), 18 μL (orange), 24 μL (light blue), 30 μL (magenta), 36 μL (blue), 45 μL (green) and 60 μL (light brown) of FAD stock solution (1 mM). Insets: the spectral changes were monitored by plotting the sum of the absolute value of the spectra against the FAD/protein ratio. The data indicate a binding ratio of one FAD per subunit for both NQO1 and NQO1 P187S. Right diagrams: ITC. NQO1 (top right) and NQO1 P187S (bottom right) were titrated into an FAD solution. The upper panel in each diagram shows the time-dependent release of heat during the titration (exothermic). Peak integrals as a function of the FAD/protein molar ratio are shown in the bottom panel of each diagram.

Table 1. The reductive half-reaction of NQO1 P187S is compromised, thereby affecting its ability to accept electrons from NAD(P)H. Bimolecular rate constants ($\text{M}^{-1}\cdot\text{s}^{-1}$) were determined for NQO1 proteins with NADH or NADPH as reducing agent. The absorption change of protein-bound FAD at 445 nm was monitored in a stopped-flow instrument at 4 $^{\circ}\text{C}$.

Protein	NADH k_{red} ($\text{M}^{-1}\cdot\text{s}^{-1}$)	NADPH k_{red} ($\text{M}^{-1}\cdot\text{s}^{-1}$)
NQO1	$(3.5 \times 10^5) \pm (1.0 \times 10^6)$	$(5.7 \times 10^5) \pm (2.7 \times 10^6)$
NQO1 P187S	$(1.2 \times 10^4) \pm (1.7 \times 10^3)$	$(8.5 \times 10^4) \pm (1.8 \times 10^5)$
NQO1 $\Delta 50$	$(4.7 \times 10^3) \pm (0.7 \times 10^3)$	$(1.3 \times 10^4) \pm (0.1 \times 10^4)$
NQO1 P187S $\Delta 50$	$(3.2 \times 10^3) \pm (0.2 \times 10^3)$	$(8.2 \times 10^4) \pm (0.2 \times 10^4)$

reduction strongly indicates that the FAD-binding site is catalytically less competent, corroborating the conclusion that the mode of FAD binding is different in NQO1 P187S.

The observed qualitative and quantitative differences in the physical properties of FAD binding and catalysis suggested structural perturbations in the FAD-binding pocket of NQO1 P187S. To analyze these putative structural differences, we solved the X-ray crystal structure of NQO1 P187S (Fig. 2B) (for data collection and refinement statistics, see Table 2). Initial crystallization attempts were successful in the presence

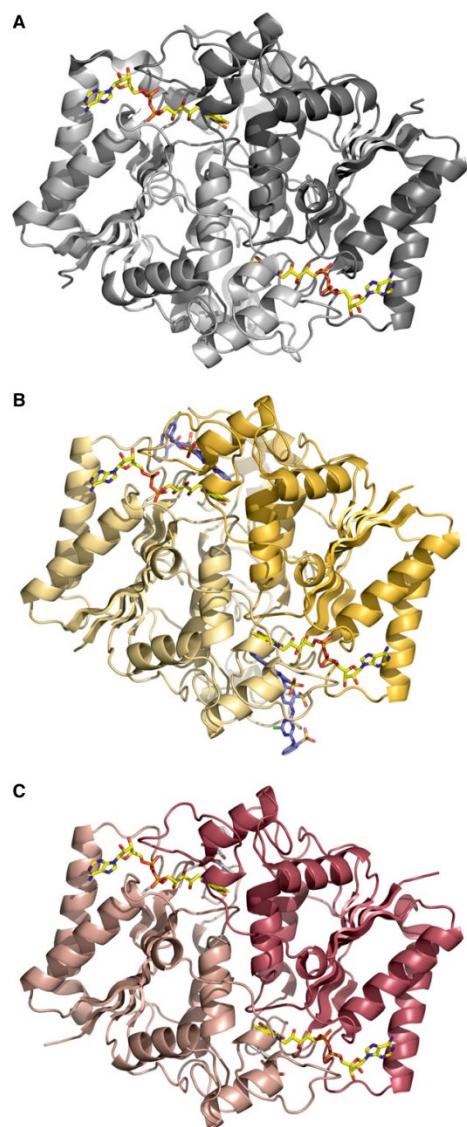


Fig. 2. Comparison of the X-ray crystallographic dimeric structures of NQO1, NQO1 P187S, and the truncated form of NQO1 P187S. (A) X-ray crystal structure of NQO1 (PDB code: [1d4a](#)). (B, C) X-ray crystal structures of NQO1 P187S and the truncated form of NQO1 P187S (50 amino acids at the C-terminus), respectively. FAD cofactor (A–C) and Cibacron blue (B) are shown as stick models.

Table 2. Crystallographic data and refinement statistics for the NQO1 P187S and NQO1 P187S Δ 50 crystal structures (50 amino acids truncated at the C-terminus).

	NQO1 P187S	NQO1 P187S Δ 50
Data collection		
X-ray source	ESRF ID-29	ELETTRA XRD1
Wavelength (Å)	0.9724	1.1354
Temperature (K)	100	100
Space group	I222	P4 ₁ 2 ₁ 2
Cell dimensions		
<i>a</i> , <i>b</i> , <i>c</i> (Å)	104.17, 104.56, 118.57	51.05, 51.05, 169.04
Resolution (Å)	26.74–2.69	33.81–2.20
High-resolution shell	2.84–2.69	2.26–2.20
Total no. of reflections	114 922 (16 147)	144 289 (7592)
Unique no. of reflections	18 149 (2523)	12 127 (843)
Multiplicity	6.3 (6.4)	11.9 (9.0)
Completeness (%)	99.5 (97.0)	99.8 (98.0)
$R_{p.i.m.}$ (%)	6.4 (31.4)	3.5 (21.0)
R_{meas} (%)	16.0 (80.7)	12.4 (65.5)
$\ \sigma \ $ average	9.3 (2.4)	18.3 (3.2)
Refinement		
Resolution (Å)	46.22–2.69	33.20–2.20
High-resolution shell	2.83–2.69	2.42–2.20
R_{work}	0.1847 (0.3102)	0.1755 (0.2292)
R_{free}	0.2074 (0.3448)	0.2239 (0.2955)
No. of atoms	4531	2004
Protein	4316	1787
Cofactor/substrate	208	78
Water	7	139
Protein residues	541	222
<i>B</i> -factors (total)		
Protein (Å ²)	41.9	34.1
Cofactor/substrate (Å ²)	44.2	30.3
Water (Å ²)	38.0	37.8
All atoms (Å ²)	42.0	34.2
Rmsds		
Bond lengths (Å)	0.003	0.004
Bond angles (°)	0.719	0.895
Ramachandran	0	0
outliers (%)		

Values in parentheses are for the highest-resolution shell.

of an equimolar concentration of Cibacron blue and excess dicoumarol. These crystals diffracted to 2.7 Å and showed a structural topology (Fig. 3A) that was almost identical to that of the NQO1 crystal structure [15,16], with an rmsd of 0.33 Å for 249 C α atoms. The FAD-binding site of NQO1 P187S showed no discernible differences, with both the flavin isoalloxazine ring and the AMP moiety engaging in the same interactions as in NQO1 (Fig. 3B). The same was true for the region around the amino acid exchange site, where no significant structural differences between NQO1 and NQO1 P187S were observed (Fig. 3C). Although our spectroscopic and kinetic measurements have

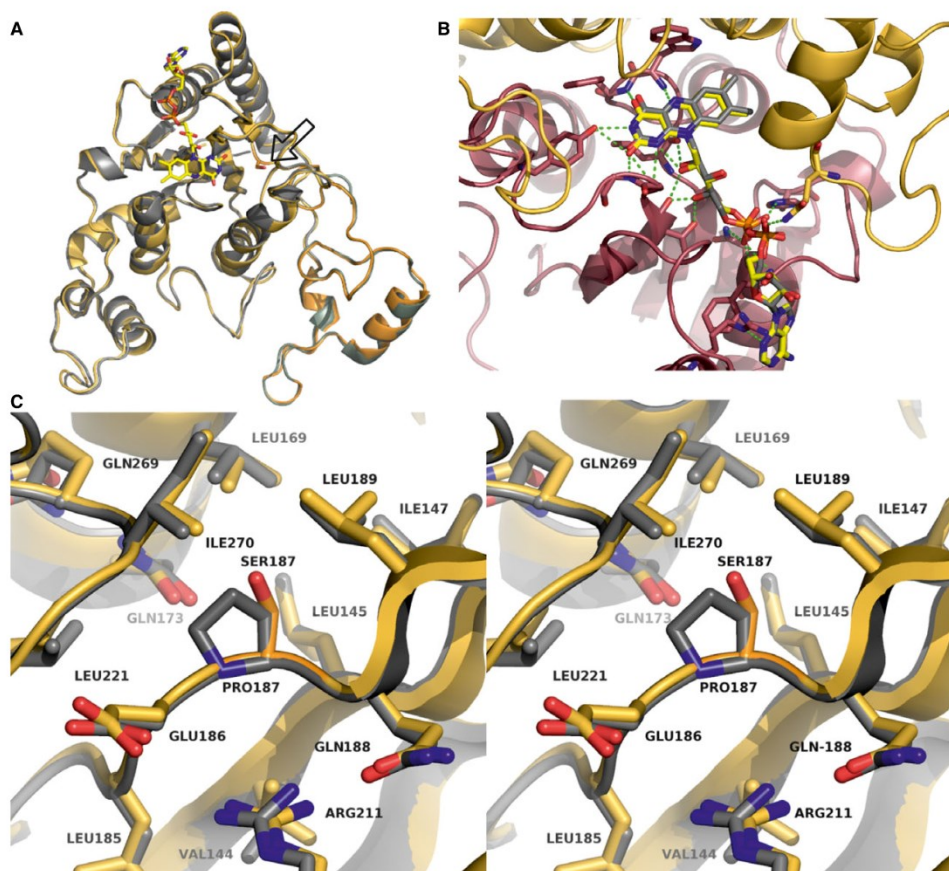


Fig. 3. The crystal structures of NQO1 P187S and NQO1 are almost identical. (A) Crystal structure of an NQO1 P187S (gold) subunit superimposed on NQO1 (gray) (PDB: [1d4a](#)); the amino acid exchange site is represented as a stick model (located on the right side of the FAD cofactor isoalloxazine ring). (B) Close-up view of the FAD-binding site in NQO1 P187S. The FAD molecule is represented as sticks model, and the two subunits of NQO1 are represented as cartoons and shown in red and gold. Hydrogen bonds between FAD and the protein backbone are depicted as green dashed lines. (C) Stereo representation showing the site of the amino acid replacement; NQO1 P187S (gold) is superimposed on NQO1 (gray).

documented the effects of the proline to serine exchange on catalytic function, the determined crystal structure of NQO1 P187S is almost identical to NQO1, and hence does not provide a structure-based explanation for the lower enzymatic activity. However, we noticed that crystallization of NQO1 P187S was much slower than that of NQO1 (weeks rather than days), suggesting that NQO1 P187S might be present in a less ordered state in solution. This prompted us to

employ NMR spectroscopy to characterize the structural properties of NQO1 and NQO1 P187S in solution.

Both 1D proton spectra (Fig. 4) and 2D $^1\text{H}/^{15}\text{N}$ -HSQC measurements (Fig. 5A,C) obtained with uniformly ^{15}N -labeled proteins revealed significant structural differences between NQO1 and NQO1 P187S. Signals indicative of a well-folded protein (e.g. peaks below 0 ppm in the ^1H -NMR spectrum) and well-dispersed

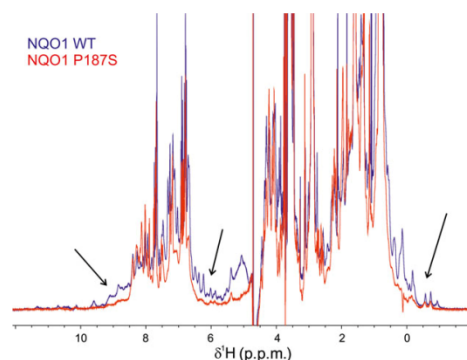


Fig. 4. NQO1 P187S shows different structural topology in solution to that of NQO1. Intensities of ^1H -NMR spectra for NQO1 (blue) and NQO1 P187S (red) were normalized on the methyl region (0.9 ppm) and superimposed. Signals outside the random coil regions (arrows), which reflect tertiary structure, are much more pronounced for NQO1 than for NQO1 P187S, indicating its loss of structure in solution.

signals beyond ~ 8.5 ppm in $^1\text{H}/^{15}\text{N}$ -HSQC spectra were significantly more pronounced for NQO1 than for NQO1 P187S (Fig. 4). To gain further insights into the dynamic behavior, we carried out ^{15}N relaxation measurements. Histograms showing the distribution of the rotational correlation time are presented in Fig. 5B,D. Short correlation times (< 20 ns) are indicative of highly flexible residues, whereas the well-structured regions of a protein in the molecular mass range of NQO1 should give rise to values of ~ 30 – 40 ns. In

the case of NQO1 P187S, more signals with very short correlation times were observed. For example, 50 peaks with a rotational correlation time below 10 ns were found for NQO1 P187S, and only 32 for NQO1, indicating that, overall, the very flexible regions of NQO1 P187S encompass a larger proportion than in NQO1. On the other hand, much longer correlation times of up to 58 ns were observed for NQO1 (compare Fig. 5B and Fig. 5D). Peaks missing in the $^1\text{H}/^{15}\text{N}$ -HSQC spectrum of NQO1 P187S (Fig. 5C) are probably in the intermediate-fast motional regime ($k_{\text{ex}} \sim \text{ms}$), leaving only the very flexible residues observable. In order to confirm that the reduced number of signals in the $^1\text{H}/^{15}\text{N}$ -HSQC spectrum of NQO1 P187S (Fig. 5C) was not attributable to the formation of protein aggregates, we performed analytical size exclusion chromatography (Fig. 6). The calculated size of NQO1 (61 kDa) agrees well with the theoretical size of NQO1 dimers (62 kDa); on the other hand, the calculated size of NQO1 P187S (78.33 kDa) suggests that the hydrodynamic radius is larger than that of NQO1. In addition, dynamic light scattering experiments failed to detect protein aggregation even with extended periods of time (up to 8 h). Thus, size exclusion chromatography and dynamic light scattering data concur with the NMR data that NQO1 P187S has a larger disordered portion than is present in the globular structure of NQO1. As signals indicative of a native structure are present in both 1D (Fig. 4) and 2D (Fig. 5A,C) spectra, but with significantly reduced intensity, we assume that, in addition to there being more extended highly mobile regions in NQO1 P187S, the percentage of fully structured pro-

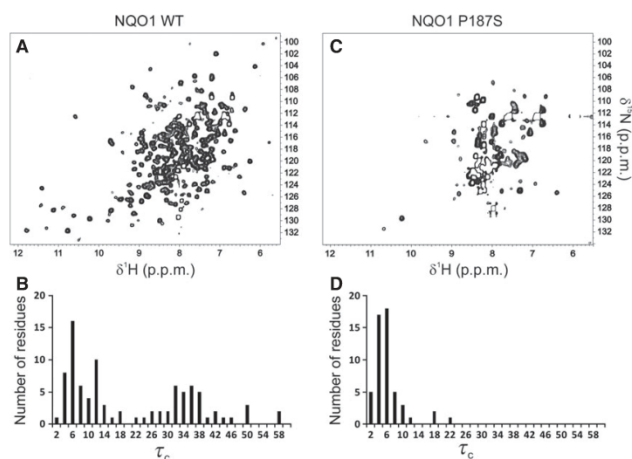
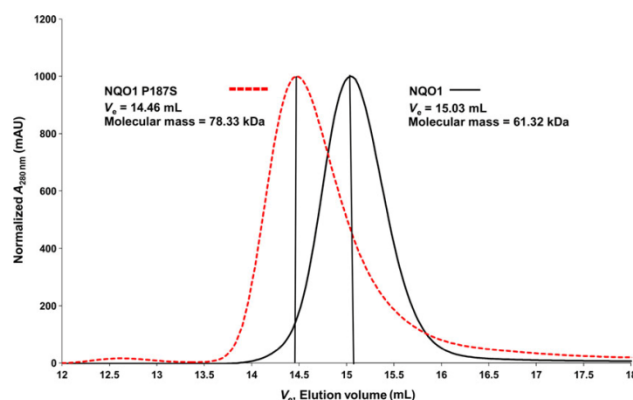


Fig. 5. Destabilization of the NQO1 P187S structure in solution. Two-dimensional $^1\text{H}/^{15}\text{N}$ -HSQC spectra of NQO1 and NQO1 P187S are shown in (A) and (C), respectively. The distribution of rotational correlation times (τ_c in ns) for NQO1 and NQO1 P187S are shown in (B) and (D), respectively. The almost complete absence of well-dispersed signals in the HSQC spectrum and of high τ_c values are indicative of the increased mobility in NQO1 P187S.

Fig. 6. Analytical size exclusion chromatography of NQO1 and NQO1 P187S. Analytical size exclusion chromatograms of purified NQO1 (continuous line) and NQO1 P187S (dashed line) obtained with a Superdex 200 (10/300) analytical column are shown. The calculated molecular masses of NQO1 (61.3 kDa) and NQO1 P187S (78.33 kDa) indicate that both proteins exist in dimeric forms. The lower elution volume observed for NQO1 P187S indicates deviation from the globular structure adopted by NQO1, thus supporting our NMR data showing that NQO1 P187S has a more disordered structure than NQO1.

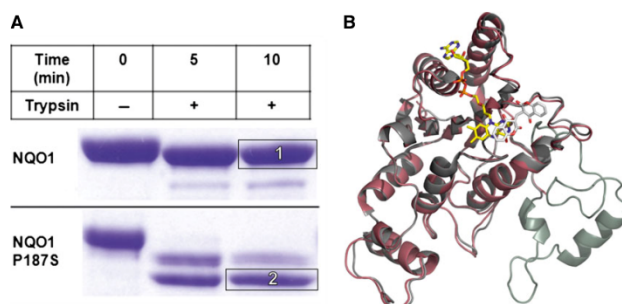


tein is lower, in line with the substantially slower crystallization of the variant. Overall, contrasting structural evidence from X-ray crystallography and NMR spectroscopy led us to assume that both disordered and structured conformations of NQO1 P187S exist simultaneously. However, it is apparent that the percentage of NQO1 P187S showing a native conformation is significantly reduced, as rapid reaction experiments (Table 1) showed that the catalytic activity of NQO1 P187S is severely compromised.

In a different batch of crystallization trials, crystals were obtained for NQO1 P187S in the absence of Cibacron blue; these diffracted to 2.2 Å (Fig. 2C) (for data collection and refinement statistics, see Table 2). With these crystals, electron density was not obtained for the last 50 C-terminal amino acids (Fig. 7B). Cibacron blue and dicoumarol are both competitive inhibitors of NADH [17,18], indicating that occupation of the NADH-binding pocket stabilizes the C-terminus and thus prevents proteolysis during crystallization. Apart from the missing C-terminus, this crystal structure showed no difference from NQO1 in the overall

topology of the structure or the active site. ESI-MS analysis of a protein crystal taken from the same crystallization drop confirmed that the protein was truncated, indicating that the C-terminus was lost because of proteolytic cleavage. Closer inspection of the missing C-terminal amino acids revealed that the cleavage of NQO1 P187S had occurred at amino acid 224. To gain further insights into the loss of the C-terminus during the crystallization procedure, we performed limited proteolysis experiments (Fig. 7A). NQO1 P187S was rapidly cleaved by trypsin, whereas NQO1 was less susceptible to tryptic cleavage. Complete in-gel tryptic digestion of the protein bands (insets 1 and 2 in Fig. 7A) and subsequent peptide mass fingerprinting by MALDI-TOF MS confirmed that the C-terminus was cleaved within 5 min in NQO1 P187S but was still present in NQO1 (Fig. 8). The C-terminus of NQO1 was cleaved much more slowly than in NQO1 P187S; that is, more than half of the protein retained the C-terminus even after 160 min of incubation. To assess the role of the C-terminus in catalysis, we generated C-terminally truncated

Fig. 7. The C-terminus of NQO1 P187S is flexible. (A) Limited proteolysis of NQO1 and NQO1 P187S by trypsin analyzed with SDS/PAGE. The C-terminus of NQO1 P187S was proteolysed within 5 min, indicating that it is flexible. (B) Superimposed X-ray crystal structures of NQO1 (gray) and NQO1 P187S (C-terminal truncation) (magenta). The C-terminus of NQO1 P187S was cleaved by an unknown protease during the crystallization procedure, confirming our hypothesis that the C-terminus is flexible.



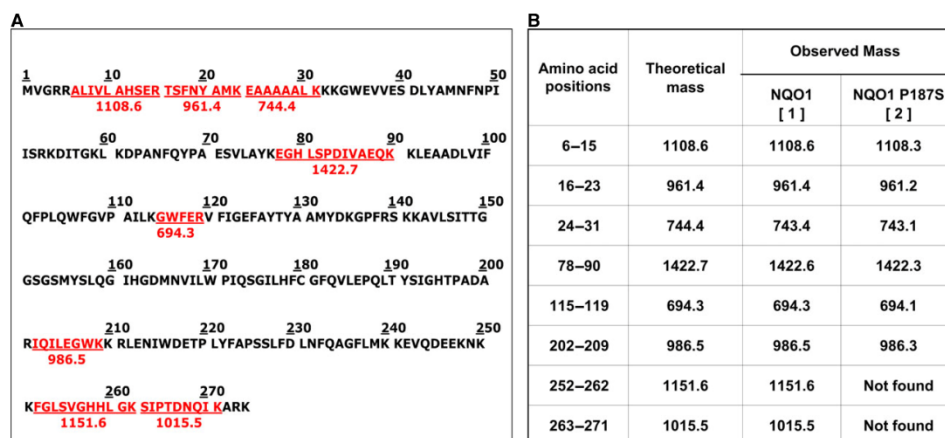


Fig. 8. MALDI-TOF MS analysis of NQO1 proteins after limited proteolysis. The C-terminus of NQO1 P187S is more rapidly proteolysed than that of NQO1. (A) Theoretical tryptic digest of NQO1 generated by the EXPASY PEPTIDECUTTER tool; peptide sequences colored in red were used as a peptide fingerprint for analysis of the MALDI-TOF MS data. (B) Table listing the peptides from SDS/PAGE bands after MALDI-TOF MS of NQO1 and NQO1 P187S (insets 1 and 2 in Fig. 7A).

proteins (NQO1 Δ 50 and NQO1 P187S Δ 50) and determined the rates of reduction. In the case of NQO1 P187S Δ 50, the bimolecular rate constants for NADH and NADPH were only marginally affected by the C-terminal truncation (Table 1). In contrast, the bimolecular rate constants for NQO1 Δ 50 (with either NADH or NADPH as reducing agent) were decreased 1000-fold compared with that of NQO1 (Table 1), proving that the C-terminus is important for enzymatic activity. Thus the P187S amino acid exchange affects the kinetics of FAD reduction to a similar extent as the complete removal of the C-terminus in NQO1 Δ 50. This finding supports our conclusion that the C-terminus is not properly associated with the core domain in NQO1 P187S. This perturbation of the interdomain contact leads to a higher degree of flexibility of the C-terminus, compromising the catalytic efficiency of the variant.

Overall, our structural and biochemical experiments reveal that the proline to serine replacement disrupts the interaction of the core with the C-terminus, resulting in a disordered tertiary structure that ultimately leads to greatly diminished enzymatic activity. A plausible explanation for the disruption of the interaction between the core and the C-terminus in NQO1 P187S is the replacement of the hydrophobic proline with a hydrophilic serine, leading to unfavorable contacts with hydrophobic residues surrounding position 187 (Leu145, Ile147, Leu169, Leu189, and Ile170; Fig. 2C),

and thus destabilizing the contact area between the C-terminus and the hydrophobic core domain.

The evidence presented so far in this article provides a rationale for the decrease in enzymatic activity of a crucial metabolic enzyme NQO1 with a point mutation. However, information is scarce as to how the single amino acid exchange affects the protein interaction properties of NQO1 P187S. NQO1 physically interacts with the tumor suppressor proteins p53 and p73 in an NADH-dependent manner, and protects them from 20S proteasomal degradation, whereas NQO1 P187S is unable to prevent the degradation of p53 and p73 [3,14]. Moscovitz *et al.* showed that supplementing *NQO1*2* cell lines with increasing concentrations of riboflavin, the precursor of FAD, stabilizes the intracellular levels of NQO1 P187S [14]. The authors of this study proposed that riboflavin or FAD analogs may offer a potential therapeutic avenue for *NQO1*2* homozygous individuals, who are sensitive to benzene hematotoxicity and are at increased risk of developing various cancers. In order to determine whether the evidence provided by the authors also holds true *in vitro*, we repeated the limited proteolysis experiments (Fig. 7A) in the presence of a 10-fold molar excess of FAD (Fig. S9). In contrast to the *in vivo* results, addition of FAD to NQO1 P187S did not prevent the cleavage of the C-terminus by trypsin (Fig. 9), suggesting that the intracellular levels of this protein variant might not be dependent on FAD levels.

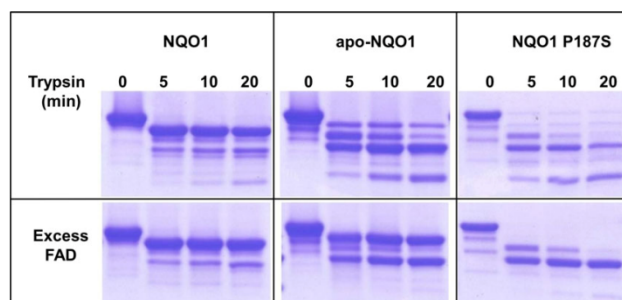


Fig. 9. Interdomain association between the C-terminus and core domain of NQO1 P187S is not stabilized by the presence of FAD. NQO1, apo-NQO1 and NQO1 P187S were subjected to limited tryptic digestion, in the presence (bottom panel) or absence (top panels) of excess FAD. Protein solution (30 μM) was digested with 2 $\text{ng}\cdot\mu\text{L}^{-1}$ sequencing-grade modified trypsin in the presence or absence of 300 μM FAD, and analyzed with SDS-PAGE. In the presence of FAD, apo-NQO1 was stabilized, whereas the C-terminus of NQO1 P187S was completely cleaved within 5 min. NQO1 P187S was stabilized after proteolysis of the C-terminus, indicating that FAD does not stabilize the interaction between the C-terminus and the core domain. However, the core domain appears to be more stable in the presence of FAD in NQO1 P187S.

The overexpression of NQO1 in various solid tumors and its ability to activate quinone-based chemotherapeutics have made it a subject of numerous investigations, leading to proposals that NQO1 is an attractive target for anticancer treatment [6]. The ability of NQO1 to bioactivate quinone pharmacophores to cytotoxic two-electron-reduced hydroquinones is of paramount importance for the proposed anticancer treatment. However, it has always been a matter of debate as to whether it is a single-electron reductase, such as NADPH:cytochrome P450 reductase, or a two-electron reductase, such as NQO1, which bioactivates quinone pharmacophores. A recent study reported the association of the *NQO1*2* homozygous genotype with adverse breast cancer outcomes and poor survival rates after anthracycline-based chemotherapy (17% for *NQO1*2* versus 75% for other genotypes) [10]. The authors proposed that NQO1 influences the outcome of epirubicin treatment through at least three mechanisms: the p53 pathway; the tumor necrosis factor–nuclear factor- κB pathway; and direct detoxification of reactive oxygen species. The wealth of information available on the involvement of the *NQO1*2*/NQO1 P187S homozygous genotype/variant in cancer development and the failure to activate chemotherapeutics stands in contrast to the lack of knowledge on the loss of function at the molecular and structural levels. The results of our study further underline the importance of the *NQO1* genotype in cancer patients, and indicate that *NQO1*2* homozygous patients will respond poorly to quinone-based chemotherapy [9,10]. Equally, the quinone-based drug

EPI-743, which specifically targets NQO1, was granted an orphan designation for treating mitochondrial diseases. However, no information is currently available on how patients with the homozygous *NQO1*2* genotype respond to this drug [19].

In conclusion, our study provides sufficient biochemical, structural and spectroscopic evidence to rationalize the loss of function in the common human NQO1 P187S variant. In addition, the results of our study explain the resistance to treatment with anthracycline-based cancer chemotherapeutics, e.g. epirubicin. Equally, our study emphasizes the importance of combining structural methods to enhance our understanding of the effects that SNPs have on protein properties, in particular folding dynamics. On the basis of our results, we suggest that it is greatly beneficial to analyze *NQO1* allelic status prior to treatment with quinone-based chemotherapeutics. In the case of NQO1, it is conceivable that efforts to reinforce interdomain contacts, e.g. with small-molecular chaperones, may lead to repopulation of the catalytically competent native structure, thus paving the way for more efficient treatment with quinone-based anticancer drugs.

Experimental procedures

Molecular cloning of *NQO1*

The *NQO1* gene sequence (UniProtKB/Swiss-Prot: [P15559](#)) was codon-optimized for *Escherichia coli* expression and chemically synthesized (GeneArt, Carlsbad, CA, USA). The *NQO1* genes were cloned into the pET28a

(Merck, Darmstadt, Germany) vector with *Nde*I and *Xho*I restriction sites to encode for an N-terminal histidine-tagged fusion protein by the use of gene-specific primers (Eurofins, Luxembourg). *NQO1 P187S*, *NQO1 Δ50* and *NQO1 P187S Δ50* were generated with the Quik-Change II XL Site-Directed Mutagenesis Kit (Santa Clara, CA, USA).

Protein expression and purification

Protein expression was carried out in LB broth (5 g·L⁻¹ sodium chloride) containing 50 μg·L⁻¹ kanamycin. Fresh medium was inoculated with 40 mL·L⁻¹ of an overnight culture and grown to a $D_{600\text{ nm}}$ of 0.95 before induction with 0.4 mM isopropyl thio-β-D-galactoside. Cells were harvested at 17 600 g for 5 min, resuspended in 1% saline solution, and pelleted at 3700 g at 4 °C for 45 min. Cell pellets were resuspended in lysis buffer (50 mM Hepes, 150 mM NaCl, 10 mM imidazole, pH 7.0) with 2 mL of buffer per 1 g of pellet. One milligram of FAD (disodium salt hydrate; Sigma Aldrich, St Louis, MO, USA) and 10 μL of protease inhibitor cocktail for use in the purification of histidine-tagged proteins in dimethylsulfoxide solution (Sigma Aldrich, St Louis, MO, USA) were added per 25 mL of slurry. Cell disruption was achieved by sonication with a Labsonic P instrument (Sartorius, Göttingen, Germany) with 70% intensity and 0.5 pulse for 10 min on ice. The cell lysate was centrifuged at 38 759 g for 30 min, and the supernatant was loaded onto a 5-mL HisTrap FF (GE Healthcare, Little Chalfont, UK) column previously equilibrated with 50 mM Hepes, 150 mM NaCl, and 20 mM imidazole (pH 7.0). The column was washed with 50 mL of 50 mM Hepes, 150 mM NaCl, and 50 mM imidazole (pH 7.0), after which proteins were eluted with 50 mM Hepes, 150 mM NaCl, and 300 mM imidazole (pH 7.0). Fractions containing target proteins were pooled and concentrated with centrifugal filter units (Amicon Ultra-15, 30 k; Millipore, Billerica, MA, USA). Concentrated protein was applied to a HiLoad 16/60 Superdex 200 prep grade column (GE Healthcare, Little Chalfont, UK) equilibrated with 50 mM sodium phosphate and 150 mM NaCl (pH 7.0) for further purification. The fractions containing target proteins were collected, and this was followed by rebuffing with a PD-10 desalting column (GE Healthcare, Little Chalfont, UK) in 50 mM Hepes (pH 7.0). The protein solutions were shock frozen and stored at -80 °C if not used immediately.

Apoprotein preparation

Apoproteins were prepared according to the method described by Hefti *et al.* [20]; any exceptions to the protocol are mentioned below. NQO1 or NQO1 P187S was applied to a 5-mL HisTrap FF (GE Healthcare, Little Chalfont, UK) column previously equilibrated with 50 mM

Hepes, 150 mM NaCl, and 20 mM imidazole (pH 7.0). The column was washed with 50 mL of buffer containing 50 mM Hepes, 150 mM NaCl, 2 M urea, and 2 M KBr (pH 7.0), and then re-equilibrated with 50 mM Hepes, 150 mM NaCl, and 20 mM imidazole (pH 7.0) (~25 mL). Apo-protein was then eluted with 50 mM Hepes, 150 mM NaCl, and 300 mM imidazole (pH 7.0). Removal of FAD was verified spectrophotometrically after rebuffing of the protein into 50 mM Hepes (pH 7.0), by the use of PD-10 desalting columns (GE Healthcare, Little Chalfont, UK).

UV-visible absorption difference titration

Difference titrations were carried out in tandem cuvettes (two separated chambers in the sample and reference cuvettes) with a Specord 200 plus spectrophotometer (Analytik Jena, Jena, Germany) at 25 °C. The cuvettes were filled with 800 μL of 50 μM apo-protein solution in buffer (50 mM Tris, 150 mM NaCl, pH 7.5) in one chamber, and 800 μL of buffer in the other chamber. The titration experiment was performed by addition of FAD (1 mM stock solution) to the apo-protein in the sample cuvette and to the buffer in the reference cuvette. The same volume of buffer was added to the apo-protein solution in the reference cell in order to obtain the same protein concentrations in the sample and reference cuvette. After completion of the additions and careful mixing with a Pasteur pipette (one for each chamber being used throughout the titration experiment), an absorption spectrum was recorded (250–600 nm).

ITC

A VP-ITC system (MicroCal; GE Healthcare, Little Chalfont, UK) was used for calorimetric determination of the dissociation constants for FAD. All experiments were performed at 25 °C in 50 mM Hepes (pH 7.0), and solutions were degassed before measurements. The titration experiments were performed with (290 ± 10) μM apo-protein solution in the syringe and (27 ± 1) μM FAD solution in the measurement cell. The concentrations of FAD and the apo-protein were determined spectrophotometrically. All experiments comprised 35 injections (initial injection of 2 μL, with an injection duration time of 4 s, and a spacing time of 300 s, followed by 34 injections of 6 μL, with an injection duration time of 5.4 s, and a spacing time of 300 s). Standard measurements without FAD were subtracted and the first measurement point was rejected; the remaining data points were analyzed on the assumption of a single-site binding model with ORIGIN version 7.0 (MicroCal) for ITC data analysis.

Rapid reaction studies

Stopped-flow measurements were carried out with a Hi-Tech (SF-61DX2) stopped-flow device (TgK Scientific

Limited, Bradford-on-Avon, UK), positioned in a glove box from Belle Technology (Weymouth, UK), at 4 °C. Buffers were flushed with nitrogen, and this was followed by incubation in the glove box environment. The enzyme and substrate solutions were deoxygenated by incubation in the glove box environment, and then diluted with buffer to the required concentrations. Enzyme and substrate were rapidly mixed in the stopped-flow device, and FAD oxidation and reduction were measured by monitoring changes at $A_{455\text{ nm}}$ with a KinetaScanT diode array detector (MG-6560; TgK Scientific Limited). Initial rates were calculated by fitting the curves with a two-exponential function.

The reductive half-reaction was investigated by mixing proteins (40 μM) in 50 mM Hepes (pH 7.0) with NADPH or NADH in the stopped-flow device. In the case of NQO1, the NAD(P)H concentrations were in the range of 50–200 μM , and in the case of NQO1 P187S, NQO1 $\Delta 50$ and NQO1 P187S $\Delta 50$, the NAD(P)H concentrations were between 50 μM and 5 mM. The absorption decrease was monitored at 455 nm. To study the oxidative half-reaction, proteins (40 μM) in 50 mM Hepes (pH 7.0) were first reduced by the addition of equimolar amounts of NADH. The reduced enzymes were then mixed with either benzoquinone or menadione (30–100 μM), and the reoxidation of the reduced FAD cofactor was monitored at 455 nm.

Crystallization conditions used for obtaining the NQO1 P187S structure

NQO1 P187S at 11 $\text{mg}\cdot\text{mL}^{-1}$ in 50 mM Hepes (pH 7.0) saturated with dicoumarol and equimolar Cibacron blue was crystallized by the microbatch method in a precipitating solution containing 60% Tacsimate (pH 7.0) (Hampton Research Index Screen, condition 29), and incubated at 289 K. The total drop volume was 1 μL , with equal amounts of protein and precipitant solution. The bluish crystal grew to full size (~85 μm) within 30 days. Crystals were harvested from their mother liquor with CryoLoops (Hampton Research), and flash-cooled in liquid nitrogen.

Crystallization conditions used for obtaining the NQO1 P187S structure (C-terminal truncation)

NQO1 P187S at 11 $\text{mg}\cdot\text{mL}^{-1}$ in 50 mM Hepes (pH 7.0) saturated with dicoumarol was crystallized by the vapour batch method in a precipitating solution containing 5 mM cobalt(II) chloride hexahydrate, 5 mM nickel(II) chloride hexahydrate, 5 mM cadmium chloride hydrate, 5 mM magnesium chloride hexahydrate, 100 mM Hepes (pH 7.5), and 12% (w/v) poly(ethylene glycol) 3350 (Hampton Research Index Screen, condition 64), and incubated at 289 K. The total drop volume was 1 μL , with equal amounts of protein and precipitant solution. The yellow crystals grew to full size (~80 μm) within 2 months. Crystals were harvested

from their mother liquor with CryoLoops (Hampton Research), and flash-cooled in liquid nitrogen.

Structure determination and refinement of NQO1 P187S

A complete dataset was collected from a single crystal at beamline ID-29 ($\lambda = 1.0\text{ \AA}$) at the European Synchrotron Radiation Facility. The dataset was collected to 2.69- \AA resolution from an orthorhombic crystal (space group $I222$). Data were processed with XDS [21]. Analysis of the dataset with PHENIX [22] showed a pseudomerohedral twin operator with a twin law $[-k, -h, -l]$ and a twin fraction of 39% according to Yeates' L -test [23]. Patterson analysis revealed a significant off-origin peak of 49.5% of the origin peak, indicating pseudotranslational symmetry. The calculated Matthews coefficient [24] indicated the presence of two molecules per asymmetric unit. The structure was solved by molecular replacement with PHASER [25], and the detwinned dataset was produced with DETWIN [3]. The partially refined structure of NQO1 P187S (C-terminal truncation) was used as search template. The best PHASER result (based on log-likelihood statistics) was further used as the input model for the automated chain-tracing/rebuilding program BUCCANEER [26]. R_{free} values were computed from 5% randomly chosen reflections that were not used during refinement [27]. Structure refinement and model rebuilding were carried out with PHENIX [22] and COOT [28,29] by alternating real-space fitting against σ_A -weighted $2F_o - F_c$ and $F_o - F_c$ electron density maps and least-square optimizations. Seven water molecules were manually placed into strong peaks of the difference electron density map. The final model was refined to $R = 18.5\%$ and $R_{\text{free}} = 20.7\%$. Details of the data reduction and structure refinement are shown in Table 2.

Electron density could not be observed for residues 1–3 and residue 274 in one protomer, and for residues 1–3 in the other protomer. The cofactor FAD and the ligand Cibacron blue were placed manually into the difference electron density map. Electron density for dicoumarol could not be identified. Validation of the structure was carried out with MOLPROBITY [30], yielding a Ramachandran plot with 93.5% of the residues in favored regions, 6.5% in allowed regions, and none in disallowed regions. Prediction of the biologically active form of NQO1 P187S was performed with the PISA server [31]. Figures were created with PYMOL [32].

Structure determination and refinement of NQO1 P187S (C-terminal truncation)

A complete dataset for NQO1 P187S with a C-terminal truncation was collected from a single crystal at beamline XRD1 ($\lambda = 1.1\text{ \AA}$) at ELETTRA (Trieste, Italy). The dataset was collected to 2.2- \AA resolution from a tetragonal

crystal (space group $P4_12_12$). The data were processed with XIA2 [33]. The calculated Matthews coefficient [24] indicated the presence of one molecule per asymmetric unit. The structure was solved by molecular replacement with PHENIX AUTOMR [22] and PHASER [25], with the structure of the NQO1 protomer [Protein Data Bank (PDB) entry [1qbg](#)] as the search template. The best PHASER result (based on log-likelihood statistics) was further used as the input model for the automated chain-tracing/rebuilding program BUCCANEER [26]. R_{free} values were computed from 5% randomly chosen reflections that were not used during refinement [27]. Structure refinement and model rebuilding were carried out with PHENIX [22] and COOT [28,29] by alternating real-space fitting against σ_A -weighted $2F_o - F_c$ and $F_o - F_c$ electron density maps and least-square optimizations. Water molecules were placed into the difference electron density map, and accepted or rejected according to geometry criteria and refined B -factors. The final model was refined to $R = 17.6\%$ and $R_{\text{free}} = 22.4\%$. Details of the data reduction and structure refinement are shown in Table 2.

Electron density could not be observed for the first two residues and the last 51 residues (missing C-terminus). Additional electron density in the active site was assigned to the cofactor FAD and dicoumarol. Validation of the structure was carried out with MOLPROBITY [30], yielding a Ramachandran plot with 97.3% of the residues in favored regions, 2.7% in allowed regions, and none in disallowed regions. Prediction of the biologically active form of NQO1 P187S (C-terminal truncation) was performed with the PISA server [31].

Labeling of NQO1 and NQO1 P187S with ^{15}N

Instead of LB broth (Lennox), a minimal medium containing $6.8 \text{ g}\cdot\text{L}^{-1} \text{Na}_2\text{HPO}_4$, $3 \text{ g}\cdot\text{L}^{-1} \text{KH}_2\text{PO}_4$, $0.5 \text{ g}\cdot\text{L}^{-1} \text{NaCl}$, $1 \text{ g}\cdot\text{L}^{-1} ^{15}\text{NH}_4\text{Cl}$, $3 \text{ g}\cdot\text{L}^{-1}$ glucose, $1 \mu\text{g}\cdot\text{L}^{-1}$ biotin, $1 \mu\text{g}\cdot\text{L}^{-1}$ thiamin, $50 \mu\text{g}\cdot\text{mL}^{-1}$ kanamycin and 1 mL of $\times 1000$ microsalts [150 mM CaCl_2 , 20 mM FeCl_3 , $50 \text{ mM H}_3\text{BO}_3$, $150 \mu\text{M CoCl}_2$, $800 \mu\text{M CuCl}_2$, 1.5 mM ZnCl_2 , $15 \mu\text{M (NH}_4)_6\text{Mo}_7\text{O}_{24}\cdot 4\text{H}_2\text{O}$] was used for protein expression as described above.

NMR spectroscopy

One-dimensional ^1H -NMR spectra were recorded with a Bruker Avance III 500-MHz NMR spectrometer at 298 K (Bruker, Rheinstetten, Germany). All other NMR experiments were carried out with a Bruker Avance III 700-MHz NMR spectrometer, equipped with a cryogenically cooled, 5-mm TCI probe at 298 K. Samples containing 20–40 $\text{mg}\cdot\text{mL}^{-1}$ NQO1 or NQO1 P187S in 50 mM Hepes (pH 6.5) in 90% H_2O and 10% D_2O were used for NMR measurements. For ^{15}N relaxation measurements, series of

10 interleaved, relaxation-edited, $^1\text{H}/^{15}\text{N}$ -HSQC spectra were recorded. The spectra were processed with NMRPIPE [34] and analyzed with CCPNMR [35]. Rotational correlation times were calculated from the ^{15}N T_1/T_2 ratios as previously described [36].

Analytical size exclusion chromatography

Size exclusion chromatography was performed with a pre-packed Superdex-200 10/300 GL column (Pharmacia) equilibrated with a 50 mM Hepes (pH 7) and 150 mM NaCl buffer solution. Purified NQO1 and NQO1 P187S (100 μL of $\sim 300 \mu\text{M}$) were injected separately and eluted with a $0.5 \text{ mL}\cdot\text{min}^{-1}$ flow rate. Protein elution was monitored by following the absorption at 280 nm and 455 nm. The $A_{280 \text{ nm}}$ (mAU) values were normalized to 1 by dividing all the values by the maximum absorption value in the elution profile; all of the normalized values were further multiplied by a factor of 1000. The Superdex-200 column was calibrated with molecular mass standards according to the manufacturer's instructions.

Limited proteolysis

NQO1, apo-NQO1 and NQO1 P187S at 30 μM in 50 mM Hepes and 150 mM NaCl (pH 7.5) buffer were subjected to limited proteolysis at 37 °C by the addition of trypsin (Promega, Madison, WI, USA) to a final concentration of $2 \mu\text{g}\cdot\text{mL}^{-1}$. The reaction was stopped after 5, 10, 20 and 40 min by adding SDS sample buffer to aliquots of the reaction mixture and immediately boiling at 95 °C for 10 min. FAD at 300 μM was added to the protein solution prior to the addition of trypsin (Fig. 9). The samples were analyzed by performing SDS-PAGE with precast gradient gels (Thermo Scientific, Waltham, MA, USA) (Fig. 7A) or with linear 12.5% polyacrylamide gels (Fig. 9).

Maldi-TOF MS

Coomassie-stained protein gel bands (1 and 2 in Fig. 7A) were excised and destained by following standard in-gel digestion protocols. The cysteines were in-gel-alkylated and reduced with iodoacetamide and dithiothreitol, respectively. The proteins were in-gel-digested with trypsin at 37 °C. Peptide mixtures were extracted after trypsin digestion, and the mixture was desalted with ZipTip (Millipore, Darmstadt, Germany). The purified peptides were spotted onto a MALDI target plate together with matrix α -cyano-4-hydroxycinnamic acid, and the spectra were recorded on a Micromass ToFSpec 2E in reflectron mode at an accelerating voltage of +20 kV. The instrument was calibrated with a poly(ethylene glycol) mixture (Sigma-Aldrich, St Louis, MO, USA). ProteoMasS ACTH Fragment 18–39 (Sigma-Aldrich, St Louis, MO, USA) was used as the peptide calibration

standard for the instrument. The spectra were analyzed with MASSLYNX 4.1, and peptide mass profiles were assigned.

Acknowledgements

This work was supported by the Austrian Fonds zur Förderung der wissenschaftlichen Forschung (FWF) through project P22361 to P. Macheroux and K. Gruber, and the PhD program 'Molecular Enzymology' (W901) to K. Zangger, K. Gruber, and P. Macheroux. We also thank the interuniversity program in natural sciences, NAWI Graz, for financial support. We would also like to acknowledge M. Haindl for helping with the crystallization experiments.

Author contributions

K.G. and P.M. initiated the project; W.-D.L., V.G., K.Z., M.K.U., K.G. and P.M. designed experiments, and analysed data; W.-D.L. and V.G. expressed and purified proteins; M.K.U. and K.G. crystallized proteins and determined the crystal structures. W.-D.L., V.G. and A.B. performed biochemical experiments, determined binding constants as well as kinetic parameters; V.G. and R.S. performed mass spectrometry; K.Z. and S.P. performed NMR-experiments; K.Z., K.G. and P.M. wrote the manuscript.

References

- Dinkova-Kostova AT & Talalay P (2010) NAD(P)H: quinone acceptor oxidoreductase 1 (NQO1), a multifunctional antioxidant enzyme and exceptionally versatile cytoprotector. *Arch Biochem Biophys* **501**, 116–123.
- Asher G, Lotem J, Cohen B, Sachs L & Shaul Y (2001) Regulation of p53 stability and p53-dependent apoptosis by NADH quinone oxidoreductase 1. *Proc Natl Acad Sci USA* **98**, 1188–1193.
- Asher G, Tsvetkov P, Kahana C & Shaul Y (2005) A mechanism of ubiquitin-independent proteasomal degradation of the tumor suppressors p53 and p73. *Genes Dev* **19**, 316–321.
- Garate M, Wong RP, Campos EI, Wang Y & Li G (2008) NAD(P)H quinone oxidoreductase 1 inhibits the proteasomal degradation of the tumour suppressor p33 (ING1b). *EMBO Rep* **9**, 576–581.
- Gong X, Kole L, Iskander K & Jaiswal AK (2007) NRH:quinone oxidoreductase 2 and NAD(P)H:quinone oxidoreductase 1 protect tumor suppressor p53 against 20S proteasomal degradation leading to stabilization and activation of p53. *Cancer Res* **67**, 5380–5388.
- Siegel D, Yan C & Ross D (2012) NAD(P)H: quinone oxidoreductase 1 (NQO1) in the sensitivity and resistance to antitumour quinones. *Biochem Pharmacol* **83**, 1033–1040.
- Kwon J, Han E, Bui CB, Shin W, Lee J, Lee S, Choi YB, Lee AH, Lee KH, Park C *et al.* (2012) Assurance of mitochondrial integrity and mammalian longevity by the p62–Keap1–Nrf2–Nqo1 cascade. *EMBO Rep* **13**, 150–156.
- Traver RD, Horikoshi T, Danenberg KD, Stadlbauer TH, Danenberg PV, Ross D & Gibson NW (1992) NAD(P)H:quinone oxidoreductase gene expression in human colon carcinoma cells: characterization of a mutation which modulates DT-diaphorase activity and mitomycin sensitivity. *Cancer Res* **52**, 797–802.
- Kelsey KT, Ross D, Traver RD, Christiani DC, Zuo ZF, Spitz MR, Wang M, Xu X, Lee BK, Schwartz BS *et al.* (1997) Ethnic variation in the prevalence of a common NAD(P)H quinone oxidoreductase polymorphism and its implications for anti-cancer chemotherapy. *Br J Cancer* **76**, 852–854.
- Fagerholm R, Hofstetter B, Tommiska J, Aaltonen K, Vrtel R, Syrjakoski K, Kallioniemi A, Kilpivaara O, Mannermaa A, Kosma VM *et al.* (2008) NAD(P)H:quinone oxidoreductase 1 NQO1*2 genotype (P187S) is a strong prognostic and predictive factor in breast cancer. *Nat Genet* **40**, 844–853.
- Lan Q, Zhang L, Li G, Vermeulen R, Weinberg RS, Dosemeci M, Rappaport SM, Shen M, Alter BP, Wu Y *et al.* (2004) Hematotoxicity in workers exposed to low levels of benzene. *Science* **306**, 1774–1776.
- Smith MT, Wang Y, Kane E, Rollinson S, Wiemels JL, Roman E, Roddam P, Cartwright R & Morgan G (2001) Low NAD(P)H:quinone oxidoreductase 1 activity is associated with increased risk of acute leukemia in adults. *Blood* **97**, 1422–1426.
- Chen S, Wu K & Knox R (2000) Structure–function studies of DT-diaphorase (NQO1) and NRH:quinone oxidoreductase (NQO2). *Free Radic Biol Med* **29**, 276–284.
- Moscovitz O, Tsvetkov P, Hazan N, Michaelevski I, Keisar H, Ben-Nissan G, Shaul Y & Sharon M (2012) A mutually inhibitory feedback loop between the 20S proteasome and its regulator, NQO1. *Mol Cell* **47**, 76–86.
- Asher G, Dym O, Tsvetkov P, Adler J & Shaul Y (2006) The crystal structure of NAD(P)H quinone oxidoreductase 1 in complex with its potent inhibitor dicoumarol. *Biochemistry* **45**, 6372–6378.
- Faig M, Bianchet MA, Talalay P, Chen S, Winski S, Ross D & Amzel LM (2000) Structures of recombinant human and mouse NAD(P)H:quinone oxidoreductases: species comparison and structural changes with substrate binding and release. *Proc Natl Acad Sci USA* **97**, 3177–3182.

- 17 Hosoda S, Nakamura W & Hayashi K (1974) Properties and reaction mechanism of DT diaphorase from rat liver. *J Biol Chem* **249**, 6416–6423.
- 18 Prochaska HJ (1988) Purification and crystallization of rat liver NAD(P)H:(quinone-acceptor) oxidoreductase by cibacron blue affinity chromatography: identification of a new and potent inhibitor. *Arch Biochem Biophys* **267**, 529–538.
- 19 Martinelli D, Catteruccia M, Piemonte F, Pastore A, Tozzi G, Dionisi-Vici C, Pontrelli G, Corsetti T, Livadiotti S, Kheifets V *et al.* (2012) EPI-743 reverses the progression of the pediatric mitochondrial disease – genetically defined Leigh syndrome. *Mol Genet Metab* **107**, 383–388.
- 20 Hefti MH, Milder FJ, Boeren S, Vervoort J & van Berkel WJ (2003) A His-tag based immobilization method for the preparation and reconstitution of apo flavoproteins. *Biochim Biophys Acta* **1619**, 139–143.
- 21 Kabsch W (2010) XDS. *Acta Crystallogr*, **D66**, 125–132.
- 22 Adams PD, Afonine PV, Bunkoczi G, Chen VB, Davis IW, Echols N, Headd JJ, Hung L-W, Kapral GJ, Grosse-Kunstleve RW *et al.* (2010) PHENIX: a comprehensive Python-based system for macromolecular structure solution. *Acta Crystallogr* **D66**, 213–221.
- 23 Padilla JE & Yeates TO (2003) A statistic for local intensity differences: robustness to anisotropy and pseudo-centering and utility for detecting twinning. *Acta Crystallogr* **D59**, 1124–1130.
- 24 CCP4 (1994) The CCP4 suite – programs for protein crystallography. *Acta Crystallogr.*, **D50** 760–763.
- 25 McCoy AJ, Grosse-Kunstleve RW, Adams PD, Winn MD, Storoni LC & Read RJ (2007) Phaser crystallographic software. *J Appl Crystallogr* **40**, 658–674.
- 26 Cowtan K (2006) The Buccaneer software for automated model building. 1. Tracing protein chains. *Acta Crystallogr* **D62**, 1002–1011.
- 27 Kleywegt GJ & Brunger AT (1996) Checking your imagination: applications of the free R value. *Structure* **4**, 897–904.
- 28 Emsley P & Cowtan K (2004) Coot: model-building tools for molecular graphics. *Acta Crystallogr* **D60**, 2126–2132.
- 29 Emsley P, Lohkamp B, Scott WG & Cowtan K (2010) Features and development of Coot. *Acta Crystallogr* **D66**, 486–501.
- 30 Chen VB, Arendall WB 3rd, Headd JJ, Keedy DA, Immormino RM, Kapral GJ, Murray LW, Richardson JS & Richardson DC (2010) MolProbity: all-atom structure validation for macromolecular crystallography. *Acta Crystallogr* **D66**, 12–21.
- 31 Krissinel E & Henrick K (2007) Inference of macromolecular assemblies from crystalline state. *J Mol Biol* **372**, 774–797.
- 32 Delano WL (2002) The PyMOL Molecular Graphics System. DeLano Scientific, San Carlos, CA.
- 33 Winter G (2010) xia2: an expert system for macromolecular crystallography data reduction. *J Appl Crystallogr* **43**, 186–190.
- 34 Delaglio F, Grzesiek S, Vuister GW, Zhu G, Pfeifer J & Bax A (1995) NMRPipe: a multidimensional spectral processing system based on UNIX pipes. *J Biomol NMR* **6**, 277–293.
- 35 Vranken WF, Boucher W, Stevens TJ, Fogh RH, Pajon A, Llinas M, Ulrich EL, Markley JL, Ionides J & Laue ED (2005) The CCPN data model for NMR spectroscopy: development of a software pipeline. *Proteins* **59**, 687–696.
- 36 Farrow NA, Muhandiram R, Singer AU, Pascal SM, Kay CM, Gish G, Shoelson SE, Pawson T, Forman-Kay JD & Kay LE (1994) Backbone dynamics of a free and phosphopeptide-complexed Src homology 2 domain studied by ¹⁵N NMR relaxation. *Biochemistry* **33**, 5984–6003.

The impact of human *NQO13, coding for NAD(P)H:quinone oxidoreductase 1 R139W, on the catalytic competence, structure and stability of the cancer associated flavoenzyme**

Author Contributions

The manuscript has been submitted to BBA MOLECULAR BASIS OF DISEASE on the 15th of June. The research was carried out in cooperation with the Institute of Molecular Biosciences (University of Graz, Austria) and the Institute of Chemistry (University of Graz, Austria). Emilia Strandback (Institute of Biochemistry, Graz University of Technology, Austria) performed ITC measurements and expressed proteins. Venugopal Gudipati and David M. Rantasa (Institute of Biochemistry, Graz University of Technology, Austria) cloned and expressed proteins for the kinetic measurements. Michael Karl Uhl (Institute of Molecular Biosciences, University of Graz, Austria) performed the crystallisation experiments and structure determination and refinement of the crystallisation data. Klaus Zangger (Institute of Chemistry, University of Graz, Austria) performed NMR and HSQC measurements and assisted in writing this paper. Karl Gruber (Institute of Molecular Biosciences, University of Graz, Austria) helped with data interpretation and assisted in writing this paper. Peter Macheroux (Institute of Biochemistry, Graz University of Technology, Austria) managed the project and is responsible for the most part of the writing and correcting of the paper. My contribution consisted in cloning of proteins and expression of the unlabelled and isotopically labelled proteins as well as doing measurements with ITC, spectrophotometer and thermostability measurements.

The impact of human *NQO13, coding for NAD(P)H:quinone oxidoreductase 1 R139W, on the catalytic competence, structure and stability of the cancer associated flavoenzyme**

Wolf-Dieter Lienhart^{1‡}, Emilia Strandback^{1‡}, Venugopal Gudipati¹, Michael K. Uhl², David M. Rantasa¹, Klaus Zangger³, Karl Gruber² and Peter Macheroux¹

¹Institute of Biochemistry, Graz University of Technology, Petersgasse 12/2, A-8010 Graz, Austria

²Institute of Molecular Biosciences, University of Graz, Humboldtstraße 50/3, A-8010 Graz, Austria

³ Institute of Chemistry, University of Graz, Heinrichstrasse 28, A-8010 Graz, Austria

*to whom correspondence should be addressed:

Prof. Dr. Peter Macheroux

Graz University of Technology

Institute of Biochemistry

Petersgasse 12/2

A-8010 Graz, Austria

Tel.: +43-316-873 6450

Fax: +43-316-873 6952

Email: peter.macheroux@tugraz.at

[‡]The first two authors have contributed equally to this work.

Abstract

The human NAD(P)H:quinone oxidoreductase 1 (NQO1; EC 1.6.99.2) is an essential enzyme in the antioxidant defence system. Furthermore, NQO1 protects tumour suppressors like p53, p33 and p73 from proteasomal degradation. The activity of NQO1 is also exploited in chemotherapy for the activation of quinone-based treatments. Various single nucleotide polymorphisms are known, such as *NQO1*2* and *NQO1*3* yielding protein variants of NQO1 with single amino acid replacements, *i.e.* P187S and R139W, respectively. While the former NQO1 variant is linked to a higher risk for specific kinds of cancer, the role, of the arginine 139 to tryptophan exchange in disease development remains obscure. Interestingly, mitomycin C resistant human colon cancer cells were shown to harbour the *NQO1*3* variant resulting in substantially reduced enzymatic activity. However, the molecular cause for this decrease remains unclear. In order to resolve this issue, we have characterized recombinant NQO1 R139W biochemically and structurally. In this report we show by X-ray crystallography and 2D-NMR spectroscopy that this variant adopts the same structure as the wild-type protein. Furthermore, the kinetic parameters obtained for the variant are similar to those reported for the wild-type enzyme. Similarly, thermostability of the variant was only slightly affected by the amino acid replacement. Therefore we conclude that the previously reported effects in human cancer cells cannot be attributed to protein stability or enzyme activity. Therefore we conclude that loss of exon 4 during maturation of *pre*-mRNA is the major cause of the observed lack of enzyme activity and hence reduced activation of quinone-based chemotherapeutics.

Keywords: Cancer; FAD; isothermal titration calorimetry; NMR-spectroscopy; single nucleotide polymorphism (SNP); X-ray crystallography.

1. Introduction

NAD(P)H:quinone oxidoreductase 1 (NQO1; EC 1.6.99.2)¹ is an important enzyme in the human antioxidant defence system. Among other functions the dimeric flavoprotein is converting quinones to hydroquinones preventing the formation of semiquinone radicals.² One further important role is the regulation and stabilisation of various tumour suppressors like p33^{ING1b}, p53 and p73. Thereby NQO1 is managing the degradation of the tumour suppressors by the 20S proteasome in a NADH dependent manner.^{3,4} Single nucleotide polymorphisms result in the expression of different protein variants of NQO1. The two most prevalent variants in the human population are *NQO1*2* (*NQO1 609C>T*; NQO1 P187S) and *NQO1*3* (*NQO1 465C>T*; NQO1 R139W), which are connected to a higher risk for specific cancers⁵⁻⁹. Several studies have focused on *NQO1*2* and have shown a reduction or even a loss of the enzymatic activity of NQO1 P187S^{10,11}. Furthermore, this single nucleotide polymorphism (SNP) gives rise to reduced stability of the protein and to a loss of the FAD cofactor. However, the involvement of *NQO1*3* in the development of cancer is currently unclear. Initial observations

indicated that splicing of the transcript of *NQO1**3 yields mature mRNA lacking, which consequently leads to the loss of the FAD binding domain.¹² In the mitomycin C resistant tumour cell lines HCT 116-R30A solely the mRNA of *NQO1**3 could be detected while in the mitomycin C sensitive HCT 116 cell line mRNAs of *NQO1**1 and *NQO1**3 were detectable.¹³ These findings led to the assumption that the higher cancer risk for the *NQO1**3 polymorphism might be caused by erroneous splicing of the pre-mRNA derived from *NQO1**3. As a matter of fact, the nucleotide transition found in *NQO1**3 disrupts the consensus sequence of the 5' splicing site required for the correct splicing by the spliceosomes and thus rationalizes the observations mentioned above.⁹ Since the full length mRNA of *NQO1**3 is still representing one to two thirds of the whole mRNA⁹, it is unclear, if the higher risk for specific cancers can be explained solely by erroneous splicing. Until now no structural information is available to evaluate inasmuch the amino acid exchange affects the structural properties of the NQO1 R139W variant as was previously shown in our laboratory for the NQO1 P187S variant.¹⁴ A loss of enzymatic activity is increasing the toxicity of benzene as well as aggravating the cancer treatment of patients.¹⁵ The broad substrate specificity of NQO1 allows the activation of chemotherapeutic prodrugs, like mitomycin C or β -lapachone. Since various tumours are upregulating the NQO1 levels, these chemotherapeutics are acting more specific on cancer than healthy cells.¹⁶⁻¹⁸ Also the success of the prevalent cancer treatment with cisplatin is affected by the NQO1 activity. One limitation for the use of cisplatin is the induced nephrotoxicity. Activation of NQO1 can improve the negative effects of the treatment to the kidneys while a loss of enzyme activity is causing an accelerated damage of the renal system.¹⁹ Taken together the status of NQO1 expression and activity is essential for the success of quinone-based chemotherapies and therefore detailed biochemical and structural studies are paramount to generate a sound basis for the development and design of cancer intervention strategies.

2. Materials and Methods

*2.1. Molecular cloning of *nqo1*, protein expression and purification*

The cloning of NQO1 and the generation of the NQO1 R139W variant as well as the expression and purification was carried out according to the procedure described by Lienhart and Gudipati *et al.*¹⁴.

2.2. Apoprotein preparation and UV/Vis absorption difference titration

Apoprotein preparation and difference titration spectra were conducted according to the protocol described by Lienhart and Gudipati *et al.*¹⁴.

2.3. Isothermal titration microcalorimetry (ITC)

A VP-ITC system (MicroCal, GE Healthcare, Little Chalfont, UK) was used for calorimetric determination of the dissociation constants for FAD. The experiments were performed at 10 °C or 25 °C in 50 mM HEPES, pH 7.0 buffer or 50 mM NaPi buffer containing 150 mM NaCl, pH 7.0. The solutions were degassed before measurements. The titration experiments were performed with either apo-protein solution or FAD solution in the syringe and in each case the other solution in the sample cell. The concentrations of FAD and the apo-protein were determined spectrophotometrically. The first injection was rejected while the remaining data points were analysed assuming a single site or a two site binding model with Origin version 7.0 (MicroCal) for ITC data analysis¹⁴.

2.4. Steady state measurements

Measurements with 1 ml of 0.5 µM NQO1 and 14 mM napthoquinone in 50 mM HEPES (pH 7.0) in the reference and sample cell were started by the addition of NADH concentrations in the range of 0.05 and 0.3 mM in the sample cell. The oxidation of NADH was monitored at 340 nm with a Specord 200 plus spectrophotometer (Analytik Jena AG, Jena, Germany).

2.5. Rapid reaction studies

Stopped flow measurements were carried out with a Hi-Tech (SF-61DX2) stopped flow device (TgK Scientific Limited, Bradford-on-Avon, UK), positioned in a nitrogen-filled glove box from Belle Technology (Weymouth, UK) at 4 °C. Buffers were flushed with nitrogen, followed by incubation in the glove box environment. The enzyme and substrate solutions were deoxygenated by incubation in the glove box environment and then diluted with buffer to the required concentrations. Enzyme and substrate were rapidly mixed in the stopped-flow device and FAD oxidation and reduction were measured by monitoring changes at 455 nm with a KinetaScanT diode array detector (MG-6560, TgK Scientific Limited). Initial rates were calculated by fitting the curves with Specfit 32, a multivariate data analysis program (Spectrum Software Associates, Chapel Hill, North Carolina, USA), using a two exponential function.

The reductive half reaction was investigated by mixing proteins (40 µM) in 50 mM HEPES (pH 7.0) with NADPH or NADH in the stopped flow device. The NAD(P)H concentrations were in the range of 50–200 µM. The absorption decrease was monitored at 455 nm¹⁴. The oxidative half reaction was investigated by mixing reduced proteins (40 µM and equimolar NADH) in 50 mM HEPES (pH 7.0) with either benzoquinone or menadione (30-100 µM) in the stopped flow device. The reoxidation of the FAD cofactor was monitored at 455 nm.

2.6. Crystallization and structure determination of NQO1 R139W

NQO1 R139W at 6.1 mg/ml in 50 mM HEPES (pH 7.5) was crystallized by the microbatch method in a precipitating solution containing 200 mM Li₂SO₄, 100 mM BisTris (pH 6.5), 25% w/v PEG 3350 (Hampton Research Index Screen, condition 75), and incubated at 289 K. The total drop volume was 1 μ L, with equal amounts of protein and precipitant solution. Yellow crystals grew to full size (\sim 100 μ m) within 2 months. Crystals were harvested from their mother liquor with CryoLoops™ (Hampton Research), and flash-cooled in liquid nitrogen.

A complete diffraction dataset was collected up to 2.1 Å resolution from a single triclinic crystal (space group *P*1) at the Swiss Light Source (SLS) of the Paul Scherrer Institute in Villingen, Switzerland (beamline X06DA). The data were processed using the program XDS²⁰. The calculated Matthews coefficient²¹ indicated the presence of 4 molecules per asymmetric unit. The structure was determined by molecular replacement using the program PHASER²² and the wild type structure of NQO1 (PDB code: 1QBG) as search template.

R_{free} values were computed from 5% randomly chosen reflections which were not used during refinement²³. Structure refinement and model rebuilding were carried out with the programs PHENIX²⁴ and COOT^{25,26} by alternating real-space fitting against σ_A -weighted 2Fo – Fc and Fo – Fc electron density maps and least square optimizations. Validation of the structure was carried out with the program MOLPROBITY²⁷ yielding a Ramachandran plot with 97.0% of the residues in favoured regions, 3.0% in allowed and none in disallowed regions. Prediction of the biologically active form of NQO1 R137W was done using the PISA server²⁸. Figures were created using the program PyMOL (DeLano Scientific, San Carlos, CA, USA).

The final model was refined to $R = 16.9\%$ and $R_{\text{free}} = 20.1\%$. Details of the data reduction and structure refinement are listed in Table 1:

Table 1: Data collection and refinement statistics.

NQO1 R139W	
Data collection	
X-ray source	SLS-X06DA
Wavelength (Å)	1.0
Temperature	100 K
Space group	<i>P</i> 1
Cell dimensions	
<i>a</i> , <i>b</i> , <i>c</i> (Å)	54.61, 59.93, 99.83
α , β , γ (Å)	100.37, 92.85, 90.22
Resolution (Å)*	49.03-2.09 (2.17-2.09)
Reflections	194450 (16603)
Unique reflections	67587 (5937)
Multiplicity*	2.9 (2.8)

Completeness (%)*	97.1 (86.89)
R_{meas}	0.093 (0.339)
R_{merge}	0.076 (0.296)
$\langle I/\sigma I \rangle^*$	12.27 (4.1)
$CC_{1/2}^*$	0.995 (0.906)
CC^*	0.999 (0.975)
Refinement	
Resolution (Å)	49.03-2.09
$R_{\text{work}} / R_{\text{free}}$	0.1693 / 0.2013
No. of atoms	
Protein	8659
Cofactor/ligands	240
Water	1052
Mean B-factors (Å ²)	
Protein	23.40
Cofactor/ligands	26.60
Water	32.30
All atoms	24.40
R.m.s. deviations	
Bond lengths (Å)	0.004
Bond angles (°)	0.95
Ramachandran outliers (%)	0
PDB-entry	5A4K

*Values in parentheses are for highest-resolution shell.

2.7. ¹⁵N-Labeling of NQO1 and NQO1 R139W

Minimal medium containing 6.8 g/l Na₂HPO₄, 3 g/l KH₂PO₄, 0.5 g/l NaCl, 1 g/l ¹⁵NH₄Cl, 3 g/l glucose, 1 µg/l biotin, 1 µg/l thiamin, 50 µg/ml kanamycin and 1 ml 1000x microsalts [150 mM CaCl₂, 20 mM, FeCl₃, 50 mM H₃BO₃, 150 µM CoCl₂, 800 µM CuCl₂, 1.5 mM ZnCl₂, 15 µM (NH₄)₆Mo₇O₂₄·4H₂O] was used for protein expression as described in Lienhart and Gudipati *et al.*¹⁴.

2.8. NMR spectroscopy

All NMR experiments were carried out with a Bruker Avance III 700 MHz spectrometer using a cryogenically cooled 5 mm TXI probe with z-axis gradients at 298 K. Samples containing between 20-40 mg/ml NQO1 or NQO1 R139W in 50 mM HEPES, pH 6.5 in 90% H₂O and 10% D₂O were used. For the ¹H-¹⁵N HSQC spectra, data matrices of 2048 x 160 points were acquired and zero filled to 4k x 256 points prior to Fourier transformation. Sixty degree phase shifted squared sine bell window functions were applied in both dimensions¹⁴.

2.9. Thermostability

The melting points were determined with a CFX Connect™ Real-Time PCR Detection System (Bio-Rad Laboratories, Inc.; Hercules; California; USA) by detecting the release of the cofactor during heating. The tested proteins have been dialysed in water over night and mixed with concentrated buffer and salt solutions to obtain all tested conditions.

3. Results

3.1. UV-visible absorption spectrometry

Heterologous expression of the NQO1 R139W variant in *E. coli* BL21 yielded similar amounts of soluble protein as previously reported for wild-type NQO1.¹⁴ Preparations of the R139W variant showed the typical yellow color indicating that the protein tightly binds the FAD cofactor in stark contrast to the P187S variant that was isolated largely as an apo-protein.¹⁴ Further analysis by absorption spectrophotometry showed that the UV-visible absorption spectrum of wild-type NQO1 and the R139W variant are nearly identical with absorption maxima at 375 and 455 nm (Figure 1, bottom panel). Similarly, titration of apo-proteins with FAD gave rise to nearly identical differences in the absorption spectrum indicating that the FAD binding pocket provided by wild-type NQO1 and the R139W variant are not affected by the amino acid replacement (Figure 1, top panel).

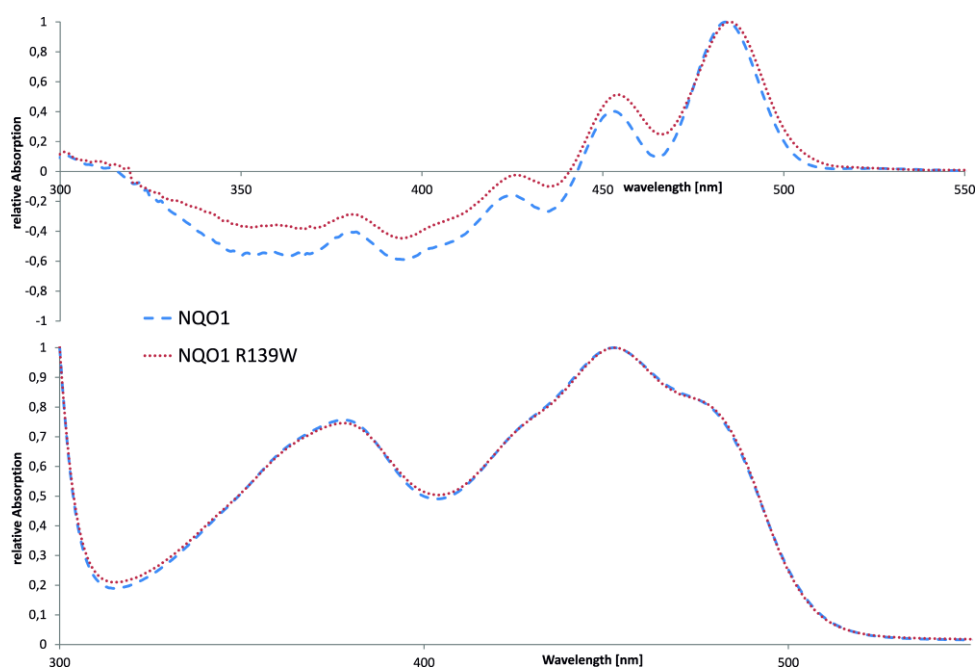


Fig. 1. UV-visible and difference titration absorption spectra of NQO1 and NQO1 R139W. Difference titration spectra with protein/FAD ratio of 1 normalised to the maximum at 480 nm (top panel) and absorption spectra of NQO1 and NQO1 R139W normalised at the maximum at 455 nm (bottom panel).

3. 2. Isothermal titration calorimetry

To obtain quantitative information on the binding affinity of the FAD cofactor to the R139W variant we conducted isothermal titration calorimetry experiments. Initially, we titrated the wild-type apo-protein with FAD resulting in raw data that could best be fitted to a two binding site model (Figure 2). This result was unexpected because the two FAD binding pockets in the homodimeric protein are structurally identical. We noticed that some of the protein (not quantified) used in the titration experiment had precipitated in the course of the experiment (ca. 1 hour). To further investigate the cause of protein precipitation and its implications for the experimental results, we repeated the measurement at a lower temperature, *i.e.* at 10 °C instead of 25 °C. As shown in Figure 2 (compare left and right panel) this did not fundamentally change the experimental result, *i.e.* a two binding site model was still required to fit the raw data (top panels in Figure 2). As before, protein precipitation was observed although an identical protein preparation kept at the same temperature showed no precipitation indicating that the protein was unstable under the experimental conditions.

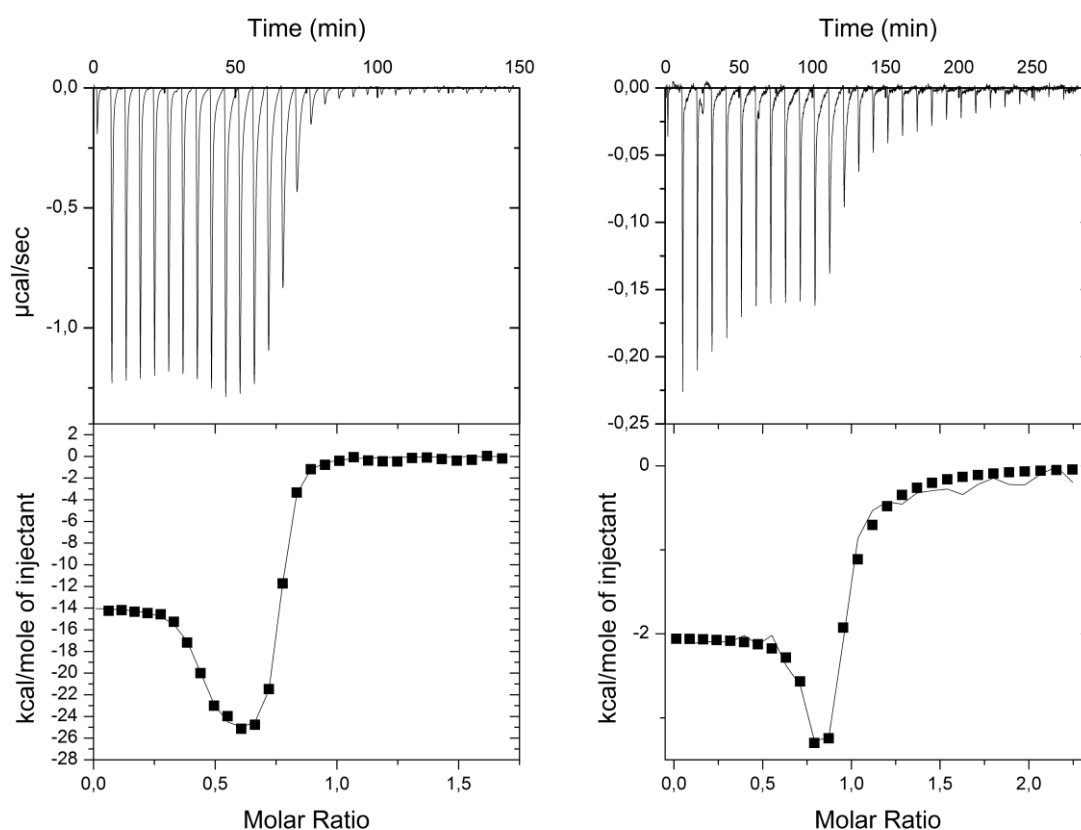


Fig. 2. ITC measurements of NQO1 wild-type in phosphate buffer. The measurements were conducted by titrating apo NQO1 in the sample cell of the microcalorimeter and FAD in the injection syringe. Data was fitted using the two binding site model. Left panels: First injection with 2 μl and 27 injections with 11 μl of 415 μM FAD solution in 43 μM NQO1 apoprotein solution and 300 seconds spacing at 25 °C. The determined K_D and N values are: $K_{D1} = 3$ nM; $K_{D2} = 122$ nM; $N_1 = 0,48$; $N_2 = 0,49$. Right: First injection with 2 μl and 28 injections with 11 μl of 415 μM FAD solution in 43 μM NQO1 apoprotein solution and 600 seconds spacing at 10 °C. The determined K_D and N values are: $K_{D1} = 78$ nM; $K_{D2} = 4730$ nM; $N_1 = 0,79$; $N_2 = 0,0002$.

Therefore, we sought to improve the stability of the apo-protein and determined the thermostability in different buffers (Table 2). This revealed that HEPES buffer (pH 7) provided some thermal stabilisation and therefore ITC measurements were repeated in the best buffer identified (see Table 2). Nevertheless ITC measurements in HEPES buffer, pH 7 under various regimes (for details see figure captions) generated raw data that could best be fitted to a two binding site model with variable stoichiometry and dissociation constants.

Table 2: Thermostability measurements. Melting points were determined with a CFX Connect™ Real-Time PCR Detection System under different buffer and salt conditions of NQO1 and NQO1 R139W. Melting points are given in °C.

buffer	NQO1	NQO1 R139W
50 mM potassium phosphate, pH 7	54.0	52.0
50 mM sodium phosphate, pH 7	54.0	52.0
50 mM Tris/Cl, pH 7	54.5	52.5
50 mM HEPES, pH 7	56.0	54.0
125 mM potassium chloride	53.5	51.5
125 mM sodium chloride	53.5	51.5
Water, distilled	59.8	59.0

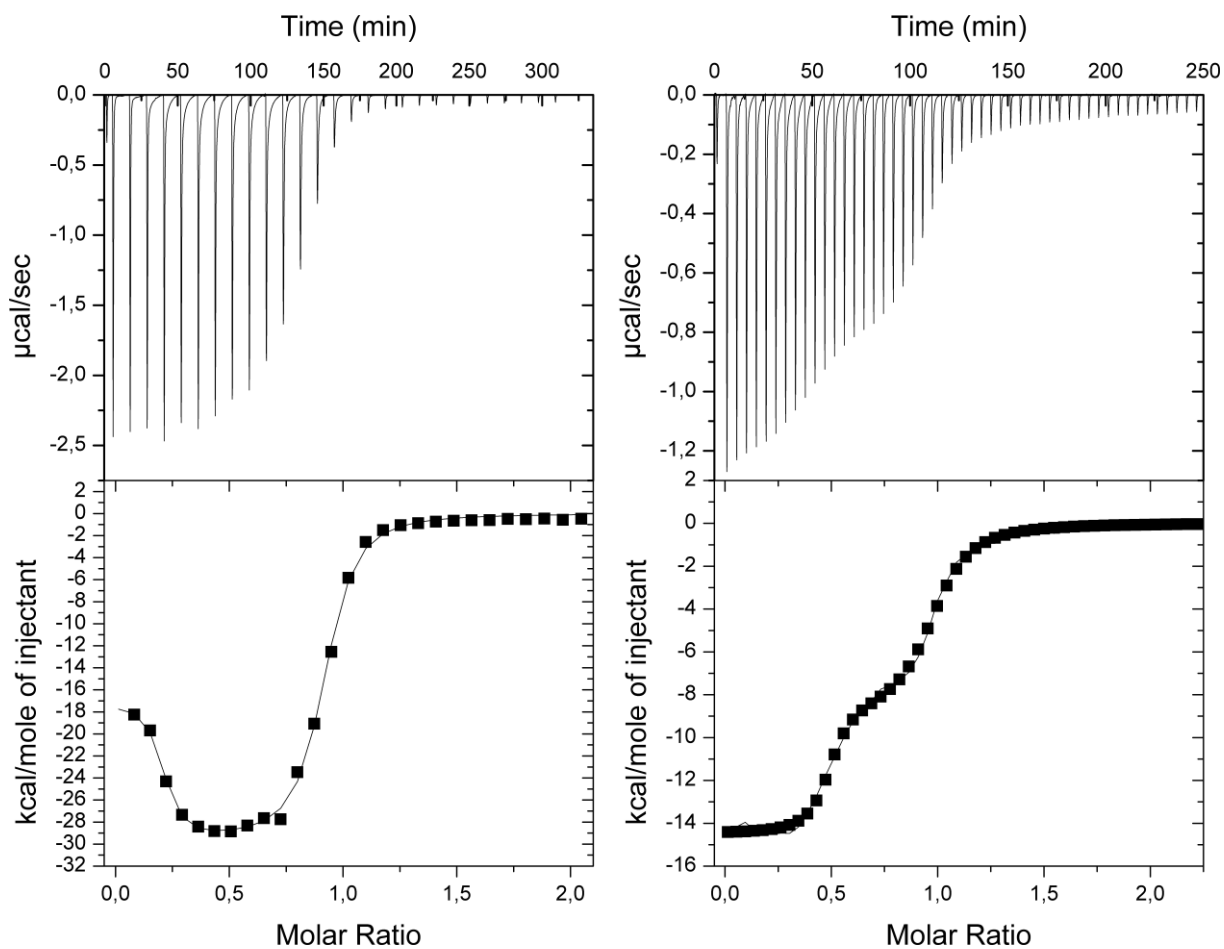


Fig. 3. ITC measurements of NQO1 wild-type in HEPES buffer. The measurements were conducted with apo-NQO1 in the sample cell of the microcalorimeter and FAD in the injection syringe. Data was fitted using the two binding site model. Left: First injection with 2 μl and 27 injections with 10 μl of 457 μM FAD solution in 46.8 μM NQO1 apo-protein solution and 600 seconds spacing at 25 $^{\circ}\text{C}$. The determined K_D and N values are: $K_{D1} = 4$ nM; $K_{D2} = 295$ nM; $N1 = 0,18$; $N2 = 0,71$. Right: First injection with 2 μl and 49 injections with 6 μl of 477 μM FAD solution in 49.4 μM NQO1 apo-protein solution and 300 seconds spacing at 25 $^{\circ}\text{C}$. The determined K_D and N values are: $K_{D1} = 9,2$ nM; $K_{D2} = 780$ nM; $N1 = 0,47$; $N2 = 0,5$.

Finally, the set-up of the ITC experiment was altered such that FAD was placed in the sample cuvette and titrated with apo-protein. This led to reproducible measurements and the obtained raw data could be fitted to a one binding site model (Figure 4).¹⁴ The average of the determined K_D values for wild-type NQO1 and the NQO1 R139W variant were 64 ± 23 and 155 ± 27 nM, respectively. Thus it can be concluded that the arginine to tryptophan replacement has only a marginal effect on the binding affinity of the FAD cofactor.

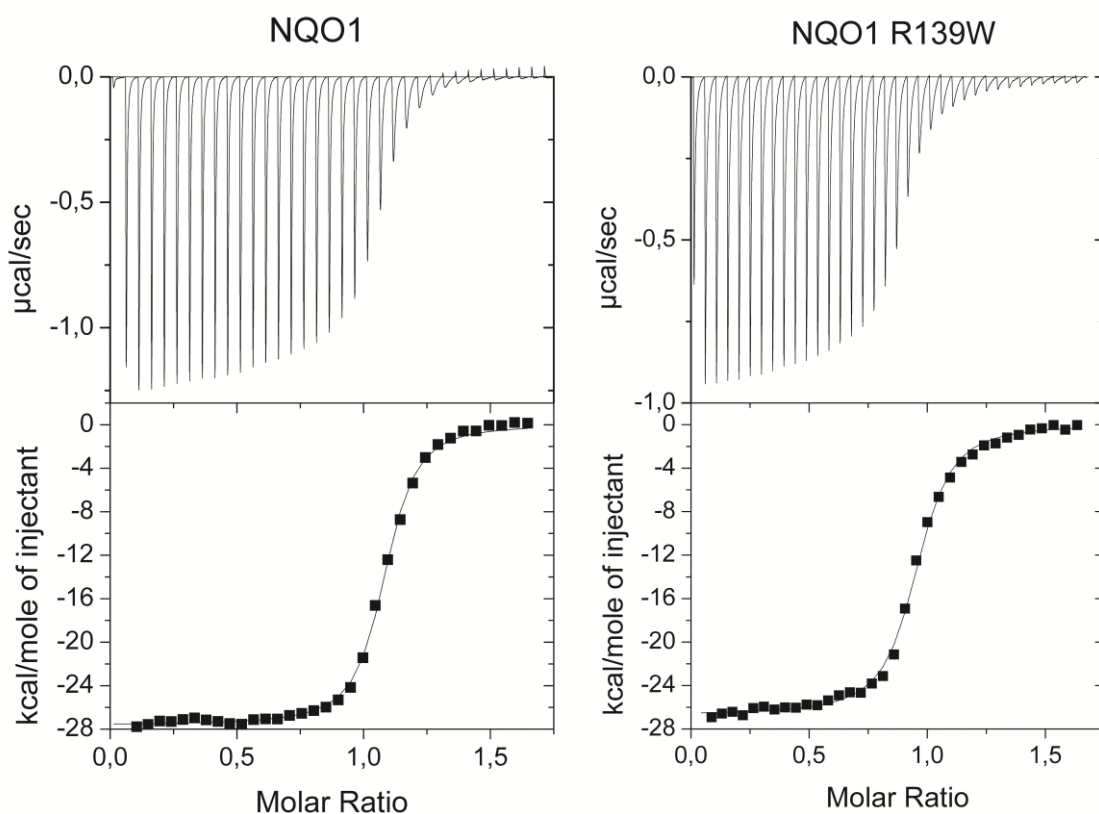


Fig. 4. ITC measurement of wild-type NQO1 and NQO1 R139W. NQO1 wild-type (left panels): First injection with 2 μl and 34 injections with 6 μl of 284 μM FAD solution in 29 μM NQO1 apoprotein solution and 300 seconds spacing (top). From three independent measurements under the same conditions the dissociation constant was calculated to $K_D = 64 \pm 23$ nM. NQO1 R139W (right panels): 35 injections with 6 μl of 298 μM FAD solution in 29 μM NQO1 apoprotein solution and 300 seconds spacing (top). From three independent measurements under the same conditions the dissociation constant was calculated to $K_D = 155 \pm 27$ nM.

3. 3. Kinetic measurements

Next, we determined the reductive rates for the R139W variant with NADH and NADPH as reducing co-substrates. As shown in Table 3, the limiting values for reduction are comparable to those determined earlier for wild-type NQO1. The oxidative half reaction of the NQO1 R139W variant was completed within the dead time of the stopped flow device as was reported previously for the wild-type and the NQO1 P187S variant.¹⁴ The steady state kinetics showed a linear initial phase with an identical slope compared to wild-type NQO1 (data not shown) again indicating that the NQO1 R139W variant has similar catalytic properties than wild-type enzyme.

Table 3: Reductive rates

Reductive rates of NQO1 and NQO1 R139W with NADH and NADPH.

	$k_{\text{red}}(\text{NADH}) \text{ M}^{-1} \text{ min}^{-1}$	$k_{\text{red}}(\text{NADPH}) \text{ M}^{-1} \text{ min}^{-1}$
NQO1	$2.1 \times 10^8 \pm 0.6 \times 10^8$	$3.4 \times 10^8 \pm 1.6 \times 10^8$
NQO1 R139W	$3.6 \times 10^8 \pm 0.7 \times 10^8$	$3.2 \times 10^8 \pm 0.8 \times 10^8$

3. 4. Structural studies: X-ray crystallography and NMR-spectroscopy

To gain further insight into the structural properties of the R139W variant we determined the crystal structure (see Materials & Methods and Table 1). The structure was determined to 2.1 Å and is virtually identical to the wild-type structure with the exception of the amino acid replacement in position 139 (Figure 5).

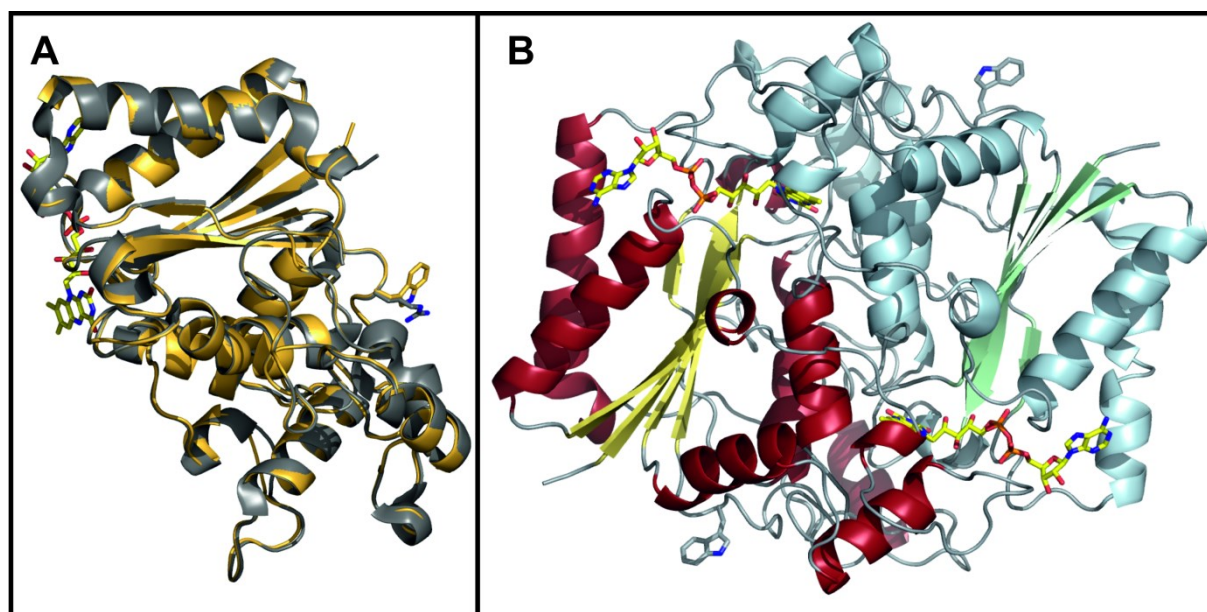


Fig. 5. Crystal structure of NQO1 R139W. Panel A: Cartoon model of the superposition of NQO1 and NQO1 R139W with the arginine and tryptophan residue (right) and the FAD (left) shown as a stick model. Panel B: Cartoon model of the NQO1 R139W homodimer with the tryptophan residue and the FAD shown as a stick model.

Recently, we showed for the NQO1 P187S variant that despite adopting the same structure in the crystal it behaved very differently in solution as evidenced by 2D HSQC NMR-spectroscopy.¹⁴ Thus the R139W variant was also analysed using this technique. As shown in Figure 6, the 2D HSQC spectra of NQO1 (red) and NQO1 R139W (black) are again nearly identical with the exception of an additional signal found in the region typical for tryptophan side chain indole nitrogen (marked by an arrow in Figure 6). Minor shifts observed for a few signals are typical for a single amino acid exchange. Identical line-widths also indicate that the flexibilities of the two proteins are essentially unchanged.

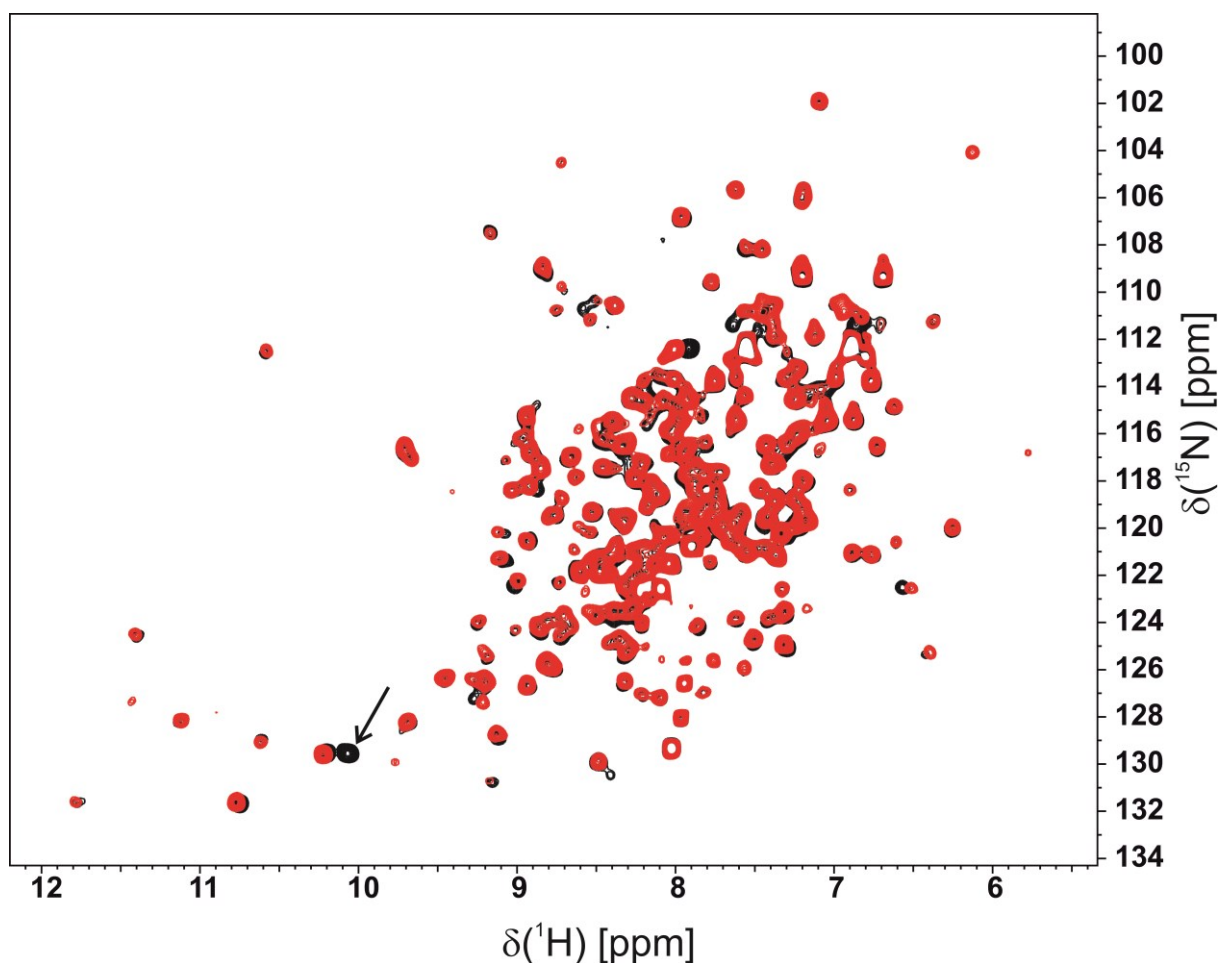


Fig. 6. 2D ^1H - ^{15}N HSQC spectra. Overlay of the 2D ^1H - ^{15}N HSQC spectrum of NQO1 R139W (black) and wild-type (red). An additional tryptophan side chain NH signal is visible in the R139W variant and indicated by an arrow. All other signals are almost identical in the HSQC spectrum of the R139W variant and wild-type, respectively, indicative of a very similar structure. A few minor shift differences result from residues close to residue 139.

Taken together our findings show that the NQO1 R139W variant has very similar biochemical, kinetic and structural properties as the wild-type enzyme. Small differences were found in the affinity of the FAD-cofactor (Figure 4) and the thermostability (Table 2).

4. Discussion

NQO1 constitutes an important enzyme of the cellular defence system and plays a central role in the activation of quinone-based chemotherapeutics. The occurrence of genetic variants in the human population necessitates the proper evaluation of the biochemical properties of the resulting protein variants. Previous studies on the P187S protein variant (encoded by *NQO1*2*) demonstrated that this single amino acid exchange causes strong destabilization of the tertiary structure leading to a substantial loss of function.^{14,29} Astonishingly, we could demonstrate that the variant adopts a very similar crystal structure, while in solution the protein is present largely in an unfolded state.¹⁴ This

very unusual and unexpected behaviour of the P187S variant prompted us to initiate a parallel study on the R139W variant caused by a single nucleotide transition in the *nqo1* gene (*NQO1**3). Initial analysis of the recombinant R139W variant by UV-visible absorption spectroscopy indicated that the affinity of the FAD cofactor as well as the nature of the cofactor binding site were not affected by the arginine to tryptophan replacement (Figure 1). Further studies by ITC intended to obtain dissociation constants for FAD binding revealed that the apo-proteins of both wild-type and the R139W variant precipitated during the experiment, probably due to the damaging effect of shearing forces exerted by constant mixing in the sample cell. As a consequence this particular experimental set-up resulted in non-reproducible and erroneous results leading to artefacts for the stoichiometry as well as binding affinities. Similar experiments were recently reported for wild-type NQO1 as well as the P187S and R139W variants.²⁹ In this study a sequential two site binding model was assumed to fit the data despite the fact that there is neither biochemical nor structural evidence that the two observed binding sites in the homodimeric protein are interdependent. Importantly, our ITC studies clearly demonstrate that these experimental artefacts can be avoided by simply reversing the order of the titration leading in reproducible data that is in accordance to the biochemical and structural findings. We believe that this observation may also have implications for other biochemical systems investigated by ITC where one binding partner (in most cases this will be the macromolecule rather than the small ligand) is unstable under the experimental conditions. In the case of flavoproteins it is well-known that apo-proteins are much less stable than the holoproteins in part due to the damaging effects required to prepare the apo-protein as well as the intrinsic destabilisation of the overall protein structure due to depletion of the flavin prosthetic group (mostly FMN or FAD).

The detailed biochemical and structural analysis of the R139W variant revealed only minor differences in comparison to wild-type NQO1. These concern FAD affinity (ca. 2.5 weaker binding) and thermostability, *i.e.* by ca. 2 °C. Thus it can be safely concluded that the expression of this variant in humans has no adverse effect on the level of NQO1 activity. Therefore, the observed effects are most probably caused by erroneous splicing of the premature mRNA, leading to the loss of exon 4 and thus giving rise to an elevated number on inactive protein in the cell.

Acknowledgements

This work was supported by the Austrian Fonds zur Förderung der wissenschaftlichen Forschung (FWF) through project P22361 to P.M and K.G. and the PhD program “Molecular Enzymology” (W901) to K.Z., K.G. and P.M. We also thank the interuniversity program in natural sciences, NAWI Graz, for financial support.

References

1. Lienhart WD, Gudipati V, Macheroux P. The human flavoproteome. *Arch.Biochem.Biophys.* 2013;**535**:150-62.
2. Ross D, Siegel D. NAD(P)H:quinone oxidoreductase 1 (NQO1, DT-diaphorase), functions and pharmacogenetics. *Methods Enzymol.* 2004;**382**:115-44.
3. Garate M, Wong RP, Campos EI, Wang Y, Li G. NAD(P)H quinone oxidoreductase 1 inhibits the proteasomal degradation of the tumour suppressor p33(ING1b). *EMBO Rep.* 2008;**9**:576-81.
4. Asher G, Tsvetkov P, Kahana C, Shaul Y. A mechanism of ubiquitin-independent proteasomal degradation of the tumor suppressors p53 and p73. *Genes Dev.* 2005;**19**:316-21.
5. Eguchi-Ishimae M, Eguchi M, Ishii E, Knight D, Sadakane Y, Isoyama K, et al. The association of a distinctive allele of NAD(P)H:quinone oxidoreductase with pediatric acute lymphoblastic leukemias with MLL fusion genes in Japan. *Haematologica* 2005;**90**:1511-5.
6. Krajcinovic M, Sinnott H, Richer C, Labuda D, Sinnott D. Role of NQO1, MPO and CYP2E1 genetic polymorphisms in the susceptibility to childhood acute lymphoblastic leukemia. *International Journal of Cancer* 2002;**97**:230-6.
7. Mandal RK, Nissar K, Mittal RD. Genetic variants in metabolizing genes NQO1, NQO2, MTHFR and risk of prostate cancer: a study from North India. *Mol.Biol.Rep.* 2012;**39**:11145-52.
8. Freriksen JJ, Salomon J, Roelofs HM, Te Morsche RH, van der Stappen JW, Dura P, et al. Genetic polymorphism 609C>T in NAD(P)H:quinone oxidoreductase 1 enhances the risk of proximal colon cancer. *J.Hum.Genet.* 2014;**59**:381-6.
9. Pan SS, Han Y, Farabaugh P, Xia H. Implication of alternative splicing for expression of a variant NAD(P)H:quinone oxidoreductase-1 with a single nucleotide polymorphism at 465C>T. *Pharmacogenetics* 2002;**12**:479-88.
10. Siegel D, Anwar A, Winski S, Kepa J, Zolman K, Ross D. Rapid polyubiquitination and proteasomal degradation of a mutant form of NAD(P)H : Quinone oxidoreductase 1. *Mol.Pharmacol.* 2001;**59**:263-8.
11. Traver RD, Siegel D, Beall HD, Phillips RM, Gibson NW, Franklin WA, et al. Characterization of a polymorphism in NAD(P)H: Quinone oxidoreductase (DT-diaphorase). *Br.J.Cancer* 1997;**75**:69-75.
12. Gasdaska PY, Fisher H, Powis G. An alternatively spliced form of NQO1 (DT-diaphorase) messenger RNA lacking the putative quinone substrate binding site is present in human normal and tumor tissues. *Cancer Res.* 1995;**55**:2542-7.
13. Hu LT, Stamberg J, Pan S. The NAD(P)H:quinone oxidoreductase locus in human colon carcinoma HCT 116 cells resistant to mitomycin C. *Cancer Res.* 1996;**56**:5253-9.
14. Lienhart W, Gudipati V, Uhl MK, Binter A, Pulido SA, Saf R, et al. Collapse of the native structure caused by a single amino acid exchange in human NAD(P)H:quinone oxidoreductase 1. *FEBS Journal* 2014;**281**:4691-704.
15. Nebert DW, Roe AL, Vandale SE, Bingham E, Oakley GG. NAD(P)H:quinone oxidoreductase (NQO1) polymorphism, exposure to benzene, and predisposition to disease: a HuGE review. *Genet.Med.* 2002;**4**:62-70.

16. Begleiter A, El-Gabalawy N, Lange L, Leith MK, Guziec LJ, Guziec FS, Jr. A Model for NAD(P)H:Quinoneoxidoreductase 1 (NQO1) Targeted Individualized Cancer Chemotherapy. *Drug Target Insights* 2009;**4**:1-8.
17. Siegel D, Yan C, Ross D. NAD(P)H:quinone oxidoreductase 1 (NQO1) in the sensitivity and resistance to antitumor quinones. *Biochem.Pharmacol.* 2012;**83**:1033-40.
18. Dai Z, Papp AC, Wang D, Hampel H, Sadee W. Genotyping panel for assessing response to cancer chemotherapy. *BMC Med.Genomics* 2008;**1**:24,8794-1-24.
19. Gang GT, Kim YH, Noh JR, Kim KS, Jung JY, Shong M, et al. Protective role of NAD(P)H:quinone oxidoreductase 1 (NQO1) in cisplatin-induced nephrotoxicity. *Toxicol.Lett.* 2013;**221**:165-75.
20. Kabsch W. XDS. *Acta Crystallogr.D Biol.Crystallogr.* 2010;**66**:125-32.
21. Collaborative Computational Project N4. The CCP4 suite: programs for protein crystallography. *Acta Crystallogr.D Biol.Crystallogr.* 1994;**50**:760-3.
22. McCoy AJ, Grosse-Kunstleve RW, Adams PD, Winn MD, Storoni LC, Read RJ. Phaser crystallographic software. *J.Appl.Crystallogr.* 2007;**40**:658-74.
23. Kleywegt GJ, Brunger AT. Checking your imagination: applications of the free R value. *Structure* 1996;**4**:897-904.
24. Adams PD, Afonine PV, Bunkoczi G, Chen VB, Davis IW, Echols N, et al. PHENIX: a comprehensive Python-based system for macromolecular structure solution. *Acta Crystallogr.D Biol.Crystallogr.* 2010;**66**:213-21.
25. Emsley P, Cowtan K. Coot: model-building tools for molecular graphics. *Acta Crystallogr.D Biol.Crystallogr.* 2004;**60**:2126-32.
26. Emsley P, Lohkamp B, Scott WG, Cowtan K. Features and development of Coot. *Acta Crystallogr.D Biol.Crystallogr.* 2010;**66**:486-501.
27. Chen VB, Arendall WB, 3rd, Headd JJ, Keedy DA, Immormino RM, Kapral GJ, et al. MolProbity: all-atom structure validation for macromolecular crystallography. *Acta Crystallogr.D Biol.Crystallogr.* 2010;**66**:12-21.
28. Krissinel E, Henrick K. Inference of macromolecular assemblies from crystalline state. *J.Mol.Biol.* 2007;**372**:774-97.
29. Pey AL, Megarity CF, Timson DJ. FAD binding overcomes defects in activity and stability displayed by cancer-associated variants of human NQO1. *Biochim.Biophys.Acta* 2014;**1842**:2163-73.

Chapter 3: Additional publications

Biocatalytic Enantioselective Oxidative C-C Coupling by Aerobic C-H Activation

Author Contributions

The manuscript has been published in ANGEWANDTE CHEMIE INTERNATIONAL EDITION (2011), Volume 50, Number 5, Pages 1068-1071. The title page of ANGEWANDTE CHEMIE INTERNATIONAL EDITION (2011), Volume 50, Number 5 is as well corresponding to the published paper. The main work was part of the PhD theses of Joerg H. Schrittwieser and Verena Resch (Institute of Chemistry, University of Graz, Austria) who performed most of the experiments. My contribution consisted in the synthesis, purification and of individual compounds and their validation.

Detailed supplementary Information is available online on the homepage of the journal.

A German version of the article was published in ANGEWANDTE CHEMIE (2011), Volume 123, Number 5, Pages 1100-1103. The title page of ANGEWANDTE CHEMIE (2011), Volume 123, Number 5 is as well corresponding to the published paper. This version is available online under: <https://doi.org/10.1002/ange.201006268>

A Journal of the Gesellschaft Deutscher Chemiker

D 3461

50
YEARS

Angewandte

International Edition

Chemie

www.angewandte.org

2011–50/5



Photochemical Reactions

T. Bach and J. P. Hehn

Shape Control

Y. Wang and J. Fang

Asymmetric Catalysis

M. Bandini

Porous Molecules

A. I. Cooper

ACIEFS 50 (5) 967–1200 (2011) · ISSN 1433–7851 · Vol. 50 · No. 5

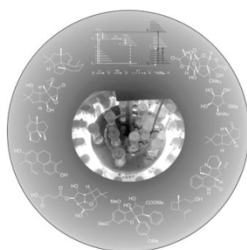


 WILEY-VCH

Cover Picture

Joerg H. Schrittwieser, Verena Resch, Johann H. Sattler, Wolf-Dieter Lienhart, Katharina Durchschein, Andreas Winkler, Karl Gruber, Peter Macheroux, and Wolfgang Kroutil*

Berberine bridge enzyme (BBE) from the California poppy enantioselectively converts benzyloquinolines into berbines by oxidative C–C coupling that consumes O₂ as a stoichiometric oxidant. In their Communication on page 1068 ff., W. Kroutil and co-workers describe the first biocatalytic application of BBE on a preparative scale. Novel optically pure benzyloquinolines and berbines were prepared by BBE-catalyzed oxidative kinetic resolution of racemic substrates. Cover picture by V. Resch.

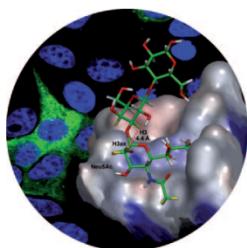
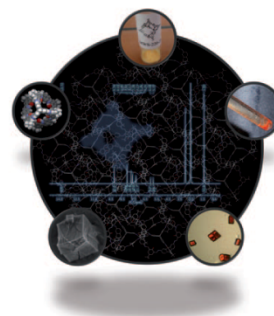


Photochemical Reactions

Synthetic chemists have often been reluctant to use photochemical reactions in organic synthesis. T. Bach and J. P. Hehn show in their Review on page 1000 ff. that this reserve is unfounded by highlighting the most important photochemical transformations that have been employed in natural product synthesis.

Cage Compounds

In their Communication on page 1046 ff., M. Mastalerz and co-workers describe a functionalized cage compound with exceptionally high surface area and remarkable gas-adsorption properties.



Rotaviruses

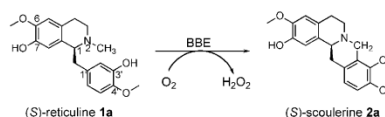
M. von Itzstein and co-workers describe in their Communication on page 1055 ff. how α -GM3 (α -2,3-sialyllactose) binds to the rotavirus surface protein VP8* with both the sialic acid and galactose moieties contributing to the binding event.

Biocatalytic Enantioselective Oxidative C–C Coupling by Aerobic C–H Activation**

Joerg H. Schrittwieser, Verena Resch, Johann H. Sattler, Wolf-Dieter Lienhart, Katharina Durchschein, Andreas Winkler, Karl Gruber, Peter Macheroux, and Wolfgang Kroutil*

Reactions that form carbon–carbon bonds are the basis for organic chemistry, setting up the carbon framework of organic molecules. In particular, the formation of C–C bonds by organo- or metal-catalyzed activation of C–H bonds^[1] has recently obtained increased attention.^[2] However, to the best of our knowledge, no biocatalytic oxidative C–C bond-forming reaction has yet been exploited for synthetic purposes. To date, biocatalysis only offers a limited number of enzymes for synthetic C–C bond formation,^[3] such as aldolases^[4] transketolases^[4d,5] and hydroxynitrile lyases.^[3,6] Other enzymatic C–C bond-forming reactions have just started to be investigated.^[8] All of these enzymes are either lyases or transferases, but not redox enzymes.^[9]

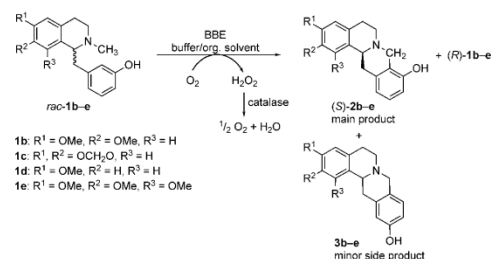
In contrast, the berberine bridge enzyme (BBE) [EC 1.21.3.3] is a redox enzyme that converts (*S*)-reticuline **1a** as the natural substrate with a 1-benzyl-1,2,3,4-tetrahydroisoquinoline backbone to (*S*)-scoulerine **2a**, a berbine derivative. The transformation occurs through an intramolecular C–C coupling by activation of the methyl group attached to the tertiary nitrogen atom at the expense of molecular oxygen (Scheme 1).^[10] The enzyme is found in plants, mainly from the poppy family, where it plays a central role in the biosynthesis of benzophenanthridine alkaloids.^[11,12] Only recently, BBE from *Eschscholzia californica* (California poppy) could be expressed efficiently in *Pichia pastoris*^[13] to give a sufficient quantity of the enzyme for crystallization and investigation of



Scheme 1. Natural reaction of BBE. Formation of the “berberine bridge” by oxidative C–C coupling at the expense of molecular oxygen.

the mechanism.^[10,14] Thus, BBE has been thoroughly investigated regarding its biochemical properties and catalytic mechanism, while its potential as a biocatalyst for preparative transformation of non-natural substrates has not been explored yet. A major concern referred to the question whether non-natural substrates could be transformed at all, since plant enzymes may have strict substrate specificity. Furthermore, no information on the enantioselectivity of the catalyst for non-natural substrates was available. The biochemical investigations of BBE were all performed on a microgram^[10] scale and at low substrate concentration (0.5 mM),^[15] both of which have to be significantly increased for preparative applications.

To gain sufficient quantities of a non-natural model substrate that can easily be prepared, racemic tetrahydroisoquinoline *rac*-**1b** (Scheme 2), which lacks the methoxy group of reticuline in the 4'-position and possesses a methoxy instead of the hydroxy group in position 7 of the benzylisoquinoline backbone, was prepared in five steps with 40% overall yield (see the Supporting Information). As a first test, reductive rate measurements were performed, which clearly indicated that the non-natural substrate *rac*-**1b** was accepted



Scheme 2. Biocatalytic enantioselective oxidative C–C coupling of non-natural substrates by BBE led to optically pure (*R*)-**2b–e** and (*S*)-**2b–e** as the main products by kinetic resolution.

[*] J. H. Schrittwieser,^[1] V. Resch,^[1] J. H. Sattler, W.-D. Lienhart, K. Durchschein, Prof. Dr. W. Kroutil
Department of Chemistry, Organic and Bioorganic Chemistry
University of Graz, Heinrichstrasse 28, 8010 Graz (Austria)
Fax: (+43) 316-380-9840
E-mail: wolfgang.kroutil@uni-graz.at
Dr. A. Winkler, Prof. Dr. P. Macheroux
Institute of Biochemistry, Graz University of Technology
Petersgasse 12, 8010 Graz (Austria)
Prof. Dr. K. Gruber
Institute of Molecular Biosciences, University of Graz
Humboldtstraße 50/III, 8010 Graz (Austria)

[†] These authors contributed equally to this work.

[**] This study was financed by the Austrian Science Fund (FWF Project P20903-N17 and P22115-N17). We thank the European Commission (MC-ITN Biotrains, grant agreement no.: 238531) for financial support. We thank Christoph Göbl for measuring CD spectra and Bernd Werner for NMR measurements.

Supporting information for this article is available on the WWW under <http://dx.doi.org/10.1002/anie.201006268>.

by purified BBE at a promising rate of $k_{\text{red}} = 2 \text{ s}^{-1}$. A first preparative transformation (8 mg) under nonoptimized conditions allowed to identify the product of the transformation as **2b** by comparison of the MS spectrum with literature values.^[16]

Subsequently, substrate *rac-1b* was used for further optimization studies. It quickly became clear that as soon as a higher substrate concentration was used and higher conversions were achieved, the hydrogen peroxide formed as byproduct inhibited or degraded the enzyme; therefore it was necessary to add catalase to disproportionate the formed hydrogen peroxide to water and molecular oxygen.^[17]

Since substrate *rac-1b* was barely soluble in buffer, various water-miscible as well as water-immiscible organic solvents were tested for substrate solubilization. A substrate concentration of 2 g L^{-1} (7 mM) was chosen for the studies of organic cosolvents as a first step to increase the substrate concentration compared to the biochemical studies. Testing the solvents at 10% v/v, BBE showed an unexpectedly high tolerance toward a broad range of organic solvents (Figure 1).

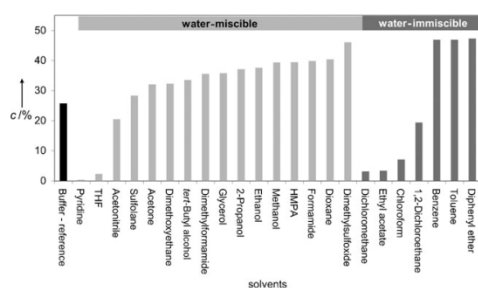


Figure 1. Conversion c of substrate *rac-1b* by BBE in the presence of organic solvents (10% v/v) in buffer.

For instance, dimethyl sulfoxide (DMSO) led to almost 50% conversion, which was the best value obtained for all water-miscible organic solvents tested. Nevertheless, also dioxane, formamide, methanol, ethanol, and even hexamethyl phosphoric triamide (HMPA) were accepted; methanol was already used in previous biochemical studies to solubilize the natural substrate (*S*)-reticuline. On the other hand, tetrahydrofuran (THF) led to low conversion. Similar low conversions were achieved by employing some water-immiscible solvents like dichloromethane or ethyl acetate. Best results were obtained by employing toluene, benzene, or diphenyl ether in a two-phase system. Toluene was chosen for further studies because of its lower toxicity compared to benzene and because of an easier work-up procedure compared to the water-miscible organic solvents. Testing the tolerance of BBE toward increasing concentrations of toluene showed that employing 80% v/v of toluene still led to 50% conversion within 24 h at 4 g L^{-1} substrate concentration and 0.1 g L^{-1} BBE (Figure 2). Even at 99% v/v toluene the enzyme was still remarkably active; however, in dry toluene no conversion could be detected. The latter experiment was

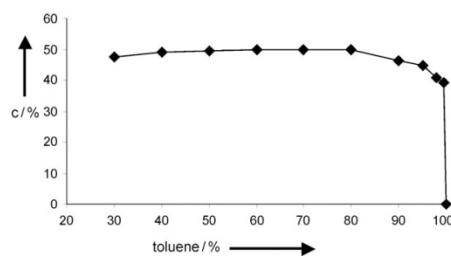


Figure 2. Enzymatic transformation of substrate *rac-1b* in the presence of increasing amounts of toluene (% v/v).

performed by suspending freeze-dried BBE in toluene; it was ensured that the enzyme was not damaged by freeze-drying: reactions with rehydrated enzyme showed full activity.

Experiments to chemically synthesize **2b** as reference material by Pictet–Spengler^[18] reaction from *N*-demethylated **1b** and formaldehyde gave a mixture of the racemic regioisomers **2b/3b** in a 40:60 ratio according to GC–MS analysis. The products were isolated in low yields of 30% and 15%, respectively. Obviously, the enzymatic reaction is unique not only concerning the catalyzed transformation, but also with respect to regioselectivity. Nevertheless, the regioisomer **3b** was also found as a minor side-product of the enzymatic transformation in the solvent study. The formation of **3b** varied depending on 1) the type of solvent used and 2) solvent concentration. For instance, product **2b** and regioisomer **3b** were formed in a ratio of 96:4 when employing toluene (99.4% v/v), while when using acetonitrile (10% v/v) a ratio of 1:1 was obtained.^[17]

In addition to the identification of a suitable cosolvent, other reaction parameters were optimized such as buffer salt and buffer concentration, pH value, temperature, shaking celerity, and the amount of catalase. The most suitable buffer was found to be 10 mM tris(hydroxymethyl)aminomethane hydrochloride (Tris-HCl) at pH 9 containing 10 mM MgCl_2 . Reactions were ideally performed in the dark^[19] by employing catalase, purified BBE (1 g L^{-1}), and a two-phase toluene/buffer mixture 70:30 v/v for a substrate concentration of 20 g L^{-1} . Employing these conditions, the transformation of *rac-1b* stops at 50% conversion after 12 h as shown in a time study. This corresponds to a space–time yield of $20 \text{ g L}^{-1} \text{ d}^{-1}$ and an apparent turnover number of 1850.

The conversions obtained for the transformation of the racemic substrate *rac-1b* never exceeded 50%, which already indicated that the enzyme might possess excellent enantioselectivity. Indeed, the analysis of the reactions by HPLC on a chiral phase showed that only one single enantiomer was transformed while the other one remained untouched, consequently leading to an optically pure product. Thus, BBE catalyzed the kinetic resolution of *rac-1b* to give optically pure products (*S*)-**2b** and (*R*)-**1b** both in $>97\%$ ee as determined by HPLC, which corresponds to an enantioselectivity $E > 200$.

To test whether other racemic benzyloquinoline derivatives would be transformed as well, substrates **1c–e** were

synthesized and subjected to BBE-catalyzed ring closure. Substrate *rac*-**1c** bears a methylene bridge between the two oxygen atoms at the isoquinoline part, *rac*-**1d** possesses only one methoxy and *rac*-**1e** three methoxy groups. All three benzyloquinolines turned out to be good substrates that were enantioselectively transformed into the corresponding berbine derivative by oxidative C–C coupling. Most of the obtained products have never been described before, neither in optically pure nor racemic form. Compounds **1c** and **2c** have been described in racemic form only, and product **2b** has previously been described only after isolation of 5 mg of this compound (common name: manibacanine) from the stem bark of *Anila canelilla*.^[16] Thus, the biocatalytic C–C coupling using BBE allowed to access novel optically pure alkaloids.

To demonstrate the applicability of the enzyme on a preparative scale, all four non-natural substrates (**1b–e**) were transformed on a 500 mg scale. All substrates could be fully resolved within 24 h and the products of the kinetic resolution (*R*)-**1b–e** and (*S*)-**2b–e** could be isolated with good to excellent yield and excellent optical purity (Table 1).

Table 1: Preparative oxidative C–C coupling employing BBE.^[a]

Subst.	<i>c</i> ^[b] [%]	(<i>R</i>)- 1 [mg (%)]	<i>ee</i> (1) ^[c] [%]	(<i>S</i>)- 2 [mg (%)]	<i>ee</i> (2) ^[c] [%]	<i>E</i> ^[d]
1b	50	249 (50)	>97	207 (42)	>97	>200
1c	50	231 (46)	>97	155 (31)	>97	>200
1d	50	181 (36)	>97	177 (36)	>97	>200
1e	50	237 (47)	>97	194 (39)	>97	>200

[a] Reactions were performed in the dark in toluene/buffer 70:30, pH 9, at a substrate concentration of 20 g L⁻¹, 1 g L⁻¹ BBE, 0.05 g L⁻¹ catalase, 40 °C, 24 h. [b] Conversion was measured by HPLC on an achiral C18 phase. Depending on the substrate converted, 4–10% of the regioisomer **3b–e** were formed: **1b**: 8%, **1c**: 7%, **1d**: 4%, **1e**: 10%. [c] Enantiomeric excess was measured by HPLC on a chiral phase. [d] *E* value determined from the *ee* of the substrate and product.^[20]

Benzyloquinolines and berbines are two closely related families of alkaloids^[21] that show a broad range of biological activities. For instance, 1-benzyl-1,2,3,4-tetrahydroisoquinolines have been found to act antispasmodic^[22] or hypotensive.^[23] Berbines possess many biological effects such as analgesic, sedative, tranquilizing, hypnotic, antihypertensive, hypo-locomotion, and muscle relaxation activity.^[24] 1-chloroscoulerine is expected to enable a novel treatment of schizophrenia.^[25]

Chemical asymmetric synthesis of benzyloquinoline and berbine alkaloids by various different strategies has been reported, in general requiring many steps and therefore resulting in limited overall yields.^[26] Amongst the published procedures only few catalytic processes are found that involve metal-catalyzed asymmetric hydrogenation,^[27] intramolecular allylic amination,^[28] and metal- or organocatalyzed asymmetric alkylation reactions.^[29] Despite the impressive progress in these areas, optically pure compounds (*ee* > 99%) were rarely obtained. The concept presented herein allows a novel approach and provides access to optically pure benzyloquinoline and berbine alkaloids.

In summary, the berberine bridge enzyme from California poppy was employed for a highly enantioselective biocatalytic oxidative C–C coupling reaction to prepare optically pure berbine derivatives as well as optically pure tetrahydrobenzyloquinolines. The described reaction was successfully performed on a 500 mg scale only requiring molecular oxygen as oxidant and mild reaction conditions, thus it represents a step towards cleaner and more selective organic transformations that expand the scope of C–C bond formation.^[30]

Experimental Section

Representative preparative C–C coupling: Substrate **1b** (500 mg, 1.6 mmol, final concentration: 20 g L⁻¹ = 65 mM) was dissolved in toluene (17.5 mL) and buffer (7.5 mL, Tris-HCl, 10 mM, pH 9, 10 mM MgCl₂) containing BBE (1.5 mL enzyme solution, final concentration: 1 g L⁻¹ = 0.017 mM) and catalase (125 mg crude preparation). The mixture was shaken in a light-shielded round bottom flask (50 mL) in an Incubator Mini Shaker (VWR, rotary, orbit 3 mm) at 200 rpm and 40 °C for 24 h. The reaction was stopped by phase separation followed by extraction of the aqueous phase with ethyl acetate (3 × 10 mL). The combined organic phases were dried (Na₂SO₄) and the organic solvents were removed under reduced pressure. The crude product was purified by silica gel chromatography (silica gel 60, 0.040–0.063 mm, Merck, Lot.: 1.09385.9025; eluent: CH₂Cl₂/MeOH/NH₄OH 97:2:1) to give 207 mg of (*S*)-**1b** (42% yield, >97% *ee*) and 249 mg (*S*)-**2b** (49% yield, >97% *ee*) (for full characterization (NMR spectra, HPLC data, optical rotation, HRMS, and CD spectra) see the Supporting Information).

Received: October 6, 2010

Published online: January 18, 2011

Keywords: alkaloids · asymmetric synthesis · C–C coupling · C–H activation · enzyme catalysis

- [1] a) W. Liu, H. Cao, A. Lei, *Angew. Chem.* **2010**, *122*, 2048–2052; *Angew. Chem. Int. Ed.* **2010**, *49*, 2004–2008; b) K. Godula, D. Sames, *Science* **2006**, *312*, 67–72.
- [2] a) Y. Wei, H. Zhao, J. Kan, W. Su, M. Hong, *J. Am. Chem. Soc.* **2010**, *132*, 2522–2523; b) Z.-H. Guan, Z.-Y. Yan, Z.-H. Ren, X.-Y. Liu, Y.-M. Liang, *Chem. Commun.* **2010**, *46*, 2823–2825; c) M. Chen, X. Zheng, W. Li, J. He, A. Lei, *J. Am. Chem. Soc.* **2010**, *132*, 4101–4103; d) F. Benfatti, M. G. Capdevila, L. Zoli, E. Benedetto, P. G. Cozzi, *Chem. Commun.* **2009**, 5919–5921; e) Z. Li, L. Cao, C.-J. Li, *Angew. Chem.* **2007**, *119*, 6625–6627; *Angew. Chem. Int. Ed.* **2007**, *46*, 6505–6507.
- [3] M. Pohl, A. Liese in *Biocatalysis in the Pharmaceutical and Biotechnology Industry* (Ed.: R. N. Patel), CRC Press, Boca Raton, **2007**, pp. 661–676.
- [4] a) P. Clapés, W.-D. Fessner, G. A. Sprenger, A. K. Samland, *Curr. Opin. Chem. Biol.* **2010**, *14*, 154–167; b) D. G. Gillingham, P. Stallforth, A. Adibekian, P. H. Seeberger, D. Hilvert, *Nat. Chem.* **2010**, *2*, 102–105; c) S. M. Dean, W. A. Greenberg, C.-H. Wong, *Adv. Synth. Catal.* **2007**, *349*, 1308–1320; d) W.-D. Fessner, S. Jennwein in *Biocatalysis in the Pharmaceutical and Biotechnology Industry* (Ed.: R. N. Patel), CRC Press, Boca Raton, **2007**, pp. 363–400.
- [5] R. Wohlgenuth, *J. Mol. Catal. B* **2009**, *61*, 23–29.
- [6] a) J. Holt, U. Hanefeld, *Curr. Org. Synth.* **2009**, *6*, 15–37; b) F. Effenberger, S. Förster, C. Kobler in *Biocatalysis in the Pharmaceutical and Biotechnology Industry* (Ed.: R. N. Patel), CRC Press, Boca Raton, **2007**, pp. 677–698; c) T. Purkharthofer,

- W. Skranc, C. Schuster, H. Griengl, *Appl. Microbiol. Biotechnol.* **2007**, *76*, 309–320.
- [7] Selected examples: a) C. Dresen, M. Richter, M. Pohl, S. Lüdeke, M. Müller, *Angew. Chem.* **2010**, *122*, 6750–6753; *Angew. Chem. Int. Ed.* **2010**, *49*, 6600–6603; b) P. Lehwald, M. Richter, C. Röhr, H.-w. Liu, M. Müller, *Angew. Chem.* **2010**, *122*, 2439–2442; *Angew. Chem. Int. Ed.* **2010**, *49*, 2389–2392; c) M. Müller, D. Gocke, M. Pohl, *FEBS J.* **2009**, *276*, 2894–2904.
- [8] For use of methyl transferases, see: a) H. Stecher, M. Tengg, B. J. Ueberbacher, P. Remler, H. Schwab, H. Griengl, M. Gruber-Khadjawi, *Angew. Chem.* **2009**, *121*, 9710–9712; *Angew. Chem. Int. Ed.* **2009**, *48*, 9546–9548; b) for hydroxynitrile lyase catalyzed Henry reaction, see: T. Purkarthofer, K. Gruber, M. Gruber-Khadjawi, K. Waich, W. Skranc, D. Mink, H. Griengl, *Angew. Chem.* **2006**, *118*, 3532–3535; *Angew. Chem. Int. Ed.* **2006**, *45*, 3454–3456; c) for opening of epoxides with cyanide catalyzed by halohydrin dehalogenases, see: M. M. Elenkov, B. Hauer, D. B. Janssen, *Adv. Synth. Catal.* **2006**, *348*, 579–585; d) for peroxidase-catalyzed coupling of solid-supported *ortho*-methoxyphenols, see: S. Antonioti, J. S. Dordick, *Adv. Synth. Catal.* **2005**, *347*, 1119–1124; e) for enzymatic aromatic prenylation, see: L. A. Wessjohan, B. Sontag, M.-A. Desoy in *Bioorganic Chemistry* (Eds.: U. Diederichsen, T. K. Lindhorst, B. Westermann, L. A. Wessjohan), Wiley-VCH, Weinheim, **1999**, pp. 79–88.
- [9] Only laccases have been employed to activate mainly phenolic compounds for radical C–C bond formation. For recent reviews, see: a) S. Riva, *Trends Biotechnol.* **2006**, *24*, 219–226; b) S. Witayakran, A. J. Ragauskas, *Adv. Synth. Catal.* **2009**, *351*, 1187–1209.
- [10] A. Winkler, A. Lyskowski, S. Riedl, M. Puhl, T. M. Kutchan, P. Macheroux, K. Gruber, *Nat. Chem. Biol.* **2008**, *4*, 739–741.
- [11] S. Paul, N. Naotaka, M. H. Zenk, *Phytochemistry* **1985**, *24*, 2577–2583.
- [12] E. Rink, H. Boehn, *FEBS Lett.* **1975**, *49*, 396–399.
- [13] A. Winkler, F. Hartner, T. M. Kutchan, A. Glieder, P. Macheroux, *J. Biol. Chem.* **2006**, *281*, 21276–21285.
- [14] A. Winkler, K. Motz, S. Riedl, M. Puhl, P. Macheroux, K. Gruber, *J. Biol. Chem.* **2009**, *284*, 19993–20001.
- [15] A. Winkler, M. Puhl, H. Weber, T. M. Kutchan, K. Gruber, P. Macheroux, *Phytochemistry* **2009**, *70*, 1092–1097.
- [16] J.-M. Oger, A. Fardeau, P. Richomme, H. Guinaudeau, A. Fournet, *Can. J. Chem.* **1993**, *71*, 1128–1135.
- [17] Full details about optimization of the reaction and solvent study will be published in due course.
- [18] E. D. Cox, J. M. Cook, *Chem. Rev.* **1995**, *95*, 1797–1842.
- [19] Reactions were performed in the dark to minimize photo-induced degradation: a) W. Holzer, J. Shirdel, P. Zirak, A. Penzkofer, P. Hegemann, R. Deutzmann, E. Hochmuth, *Chem. Phys.* **2005**, *308*, 69–78; as well as other photo-induced side-reactions, for example, reduction of flavin: b) M. Mifsud Grau, J. C. van der Toorn, L. G. Otten, P. Macheroux, A. Taglieber, F. E. Zilly, I. W. C. E. Arends, F. Hollmann, *Adv. Synth. Catal.* **2009**, *351*, 3279–3286.
- [20] J. L. L. Rakels, A. J. J. Straathof, J. J. Heijnen, *Enzyme Microb. Technol.* **1993**, *15*, 1051–1056.
- [21] a) M. W. Fraaije, A. Mattevi, *Nat. Chem. Biol.* **2008**, *4*, 719–721; b) J. Keasling, *Nat. Chem. Biol.* **2008**, *4*, 524–525; c) K. W. Bentley, *The Isoquinoline Alkaloids*, Harwood, Amsterdam, **1998**.
- [22] M. L. Martin, M. T. Diaz, M. J. Montero, P. Prieto, L. S. Roman, D. Cortes, *Planta Med.* **1993**, *59*, 63–67.
- [23] S. Chulia, M. D. Ivorra, C. Lugnier, E. Vila, M. A. Noguera, P. D'Ocon, *Br. J. Pharmacol.* **1994**, *113*, 1377–1385.
- [24] a) J.-M. Gao, W.-T. Liu, M.-L. Li, H.-W. Liu, X.-C. Zhang, Z.-X. Li, *J. Mol. Struct.* **2008**, *892*, 466–469, and references cited therein; b) W. J. Eisenreich, G. Hofner, F. Bracher, *Nat. Prod. Res.* **2003**, *17*, 437–440; c) Y. Kashiwada, A. Aoshima, Y. Ikeshiro, Y.-P. Chen, H. Furukawa, M. Itoigawa, T. Fujioka, K. Mihashi, L. M. Cosentino, S. L. Morris-Natschke, K.-H. Lee, *Bioorg. Med. Chem.* **2005**, *13*, 443–448; d) F. N. Ko, J. H. Guh, S. M. Yu, Y. S. Hou, Y. C. Wu, C. M. Teng, *Br. J. Pharmacol.* **1994**, *112*, 1174–1180.
- [25] J. Li, G. Jin, J. Shen, R. Ji, *Drugs Future* **2006**, *31*, 379–384.
- [26] M. Chrzanowska, M. D. Rozwadowska, *Chem. Rev.* **2004**, *104*, 3341–3370.
- [27] a) P.-C. Yan, J.-H. Xie, G.-H. Hou, L.-X. Wang, Q.-L. Zhou, *Adv. Synth. Catal.* **2009**, *351*, 3243–3250; b) S.-M. Lu, Y.-Q. Wang, X.-W. Han, Y.-G. Zhou, *Angew. Chem.* **2006**, *118*, 2318–2321; *Angew. Chem. Int. Ed.* **2006**, *45*, 2260–2263; c) M. Kitamura, Y. Hsiao, M. Ohta, M. Tsukamoto, T. Ohta, H. Takaya, R. Noyori, *J. Org. Chem.* **1994**, *59*, 297–310.
- [28] C. Shi, I. Ojima, *Tetrahedron* **2007**, *63*, 8563–8570.
- [29] a) C. Dubs, Y. Hamashima, N. Sasamoto, T. M. Seidel, S. Suzuki, D. Hashizume, M. Sodeoka, *J. Org. Chem.* **2008**, *73*, 5859–5871; b) N. Sasamoto, C. Dubs, Y. Hamashima, M. Sodeoka, *J. Am. Chem. Soc.* **2006**, *128*, 14010–14011; c) A. M. Taylor, S. L. Schreiber, *Org. Lett.* **2006**, *8*, 143–146; d) S. Wang, C. T. Seto, *Org. Lett.* **2006**, *8*, 3979–3982; e) T. Itoh, M. Miyazaki, H. Fukuoka, K. Nagata, A. Ohsawa, *Org. Lett.* **2006**, *8*, 1295–1297.
- [30] a) J. M. Woodley, *Trends Biotechnol.* **2008**, *26*, 321–327; b) D. J. Pollard, J. M. Woodley, *Trends Biotechnol.* **2007**, *25*, 66–73; c) H. E. Schoemaker, D. Mink, M. G. Wubbolts, *Science* **2003**, *299*, 1694–1697.

Biocatalytic Organic Synthesis of optically pure (*S*)-Scoulerine and Berbine and Benzylisoquinoline Alkaloids

Author Contributions

The manuscript has been published in THE JOURNAL OF ORGANIC CHEMISTRY (2011), Volume 76, Number 16, Pages 6703-6714. The main work was part of the PhD theses of Joerg H. Schrittwieser and Verena Resch (Institute of Chemistry, University of Graz, Austria) who performed most of the experiments. My contribution consisted in the synthesis, purification and of individual compounds and their validation.

Detailed supplementary Information is available online on the homepage of the journal.

Biocatalytic Organic Synthesis of Optically Pure (*S*)-Scoulerine and Berbine and Benzylisoquinoline Alkaloids

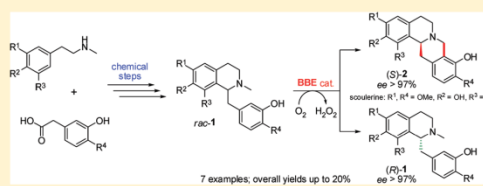
Joerg H. Schrittwieser,[†] Verena Resch,[†] Silvia Wallner,[‡] Wolf-Dieter Lienhart,[†] Johann H. Sattler,[†] Jasmin Resch,[†] Peter Macheroux,[‡] and Wolfgang Kroutil^{*,†}

[†]Department of Chemistry, Organic & Bioorganic Chemistry, University of Graz, Heinrichstrasse 28, 8010 Graz, Austria

[‡]Institute of Biochemistry, Graz University of Technology, Petersgasse 12, 8010 Graz, Austria

S Supporting Information

ABSTRACT: A chemoenzymatic approach for the asymmetric total synthesis of the title compounds is described that employs an enantioselective oxidative C–C bond formation catalyzed by berberine bridge enzyme (BBE) in the asymmetric key step. This unique reaction yielded enantiomerically pure (*R*)-benzylisoquinoline derivatives and (*S*)-berbines such as the natural product (*S*)-scoulerine, a sedative and muscle relaxing agent. The racemic substrates *rac*-1 required for the biotransformation were prepared in 4–8 linear steps using either a Bischler–Napieralski cyclization or a C1–C α alkylation approach. The chemoenzymatic synthesis was applied to the preparation of fourteen enantiomerically pure alkaloids, including the natural products (*S*)-scoulerine and (*R*)-reticuline, and gave overall yields of up to 20% over 5–9 linear steps.



INTRODUCTION

Benzylisoquinolines and berbines¹ are two closely related classes of alkaloids encompassing more than 100 known structures. Both alkaloid families are associated with a broad range of biological activities: Many 1-benzyl-1,2,3,4-tetrahydroisoquinolines act as antispasmodic or hypotensive and some, such as norcoclaurine, coclaurine, and *N*-methylcoclaurine, possess anti-HIV activity *in vitro*.² Berbines show diverse biological activities such as analgesic, sedative, hypnotic, or anti-inflammatory effects,³ and the non-natural derivative *l*-chloroscoulerine is currently investigated as a novel treatment of schizophrenia.⁴ In addition, tetrahydroisoquinolines have recently been employed as chiral ligands for metal-catalyzed transfer-hydrogenation.⁵

Because of their biological significance, benzylisoquinolines and berbines have been targets for organic synthesis for a long time, and their asymmetric synthesis has been achieved by many different strategies.^{6,7} However, a large number of steps and harsh reaction conditions are often required, resulting in limited overall yields and ee values. Furthermore, among the published procedures only few catalytic processes are found, with metal-catalyzed asymmetric hydrogenation,⁸ intramolecular allylic amination or amidation,⁹ and various metal- or organocatalyzed asymmetric alkylation reactions¹⁰ representing the most notable exceptions. Despite the impressive progress in these areas, enantiomerically pure (ee > 99%) substances are rarely obtained. On the other hand, optically pure benzylisoquinoline¹¹ and berbine alkaloids are produced by a number of plants belonging mainly to the Berberidaceae and Papaveraceae families. However, isolation of the natural products is cumbersome, and biotransformations using

plant cell cultures¹² afford minute amounts only. The production of benzylisoquinolines and related alkaloids from the morphine and sanguinarine pathways using recombinant enzymes in *Escherichia coli* and *Saccharomyces cerevisiae* has recently been reported,¹³ but conversions were rather low (<15%) in these fermentative processes and product isolation was not reported. In addition, this approach is limited to a small number of target molecules and is therefore not as flexible as chemical and biocatalytic synthetic methods.

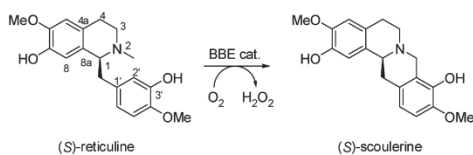
Biocatalytic steps in organic synthesis have already proven to be an efficient, highly stereoselective and flexible option in the preparation of many target compounds.¹⁴ Of special interest are C–C bond-forming enzymes to set up the carbon framework of the organic molecules.¹⁵ Berberine bridge enzyme (BBE) represents an outstanding biocatalyst enabling an aerobic oxidative C–C bond formation transforming benzylisoquinolines to berbines. BBE catalyzes the first committed step in the benzophenanthridine, protoberberine, and protopine biosynthesis pathways¹⁶ in plants as it converts (*S*)-reticuline to (*S*)-scoulerine by intramolecular C–C coupling, forming the so-called “berberine bridge” (Scheme 1).

This transformation takes place via oxidative C–H activation of the substrate’s *N*-methyl group at the expense of molecular oxygen, a reaction unparalleled in organic synthesis.¹⁷ BBE from *Eschscholzia californica* (California poppy) has been heterologously expressed in *Pichia pastoris*, and its X-ray crystal structure and molecular mechanism have been solved.^{17,18}

Received: May 24, 2011

Published: July 08, 2011

Scheme 1. C–C Bond Formation Leading to (S)-Scoulerine Catalyzed by Berberine Bridge Enzyme (BBE)



Recently, it has been shown that BBE accepts also non-natural substrates, whereby it transforms exclusively the (S)-enantiomer of racemic benzyloisoquinolines to optically pure (S)-berbines. Since this reaction represents a highly enantioselective kinetic resolution, it provides access to the remaining optically pure (R)-substrates as well.¹⁹

In the present paper, we demonstrate the broad applicability of the enzyme to establish a novel synthetic route to optically pure (S)-berbines and (R)-benzyloisoquinolines, including the first asymmetric total synthesis of naturally occurring (S)-scoulerine.

RESULTS AND DISCUSSION

The synthesis of racemic 1-substituted tetrahydroisoquinolines **1** usually relies on one out of three different strategies: (i) formation of the C1–C8a bond of the isoquinoline core employing either the Pictet–Spengler²⁰ or the Bischler–Napieralski²¹ cyclization, (ii) alkylation at position C1 of the isoquinoline via nucleophilic or electrophilic activation,²² and (iii) formation of the C4–C4a bond by a Pomeranz–Fritsch reaction (Scheme 2).²³ The first two approaches are particularly appealing since the target molecule is disconnected at central bonds leading to simple starting materials. We focused first on the Bischler–Napieralski cyclization of amides **3a–g**, since it offers a broad scope and mild reaction conditions. Therefore, the *N*-methylphenethylamines **4a–g** and phenylacetic acid derivatives **5a** and

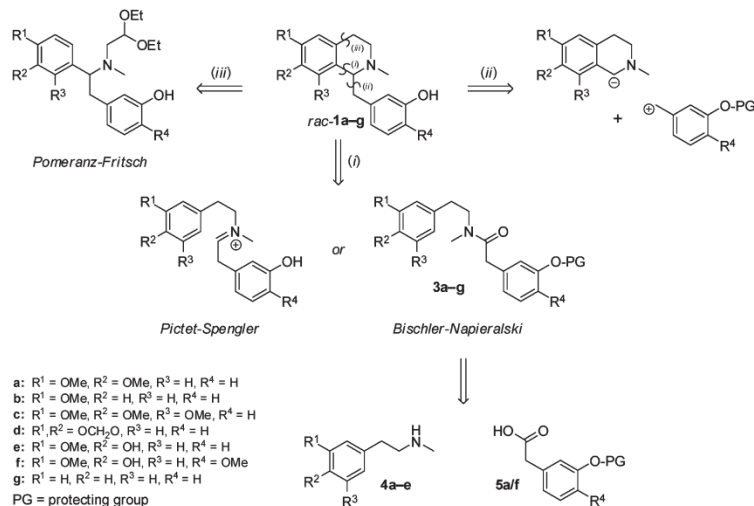
5f were needed for synthesis of the amides **3a–g** used as educts in the cyclization reaction.

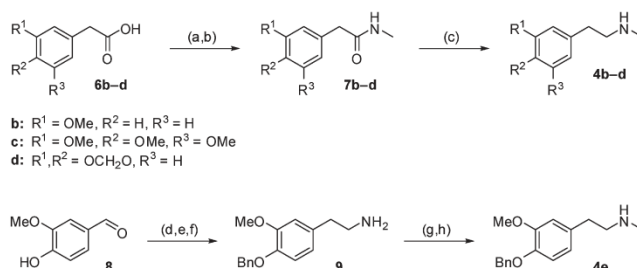
Although *N*-methyl-(3,4-dimethoxyphenyl)ethylamine (*N*-methylhomoveratrylamine) **4a** as well as *N*-methylphenethylamine **4g** were commercially available, all other phenethylamines had to be synthesized. Compounds **4b–d** were prepared from the corresponding phenylacetic acid derivatives **6b–d** via conversion into the *N*-methylamides **7b–d** followed by reduction (Scheme 3). The latter transformation was first attempted employing LiAlH₄ as reducing agent; however, only incomplete conversion was achieved even with a 3-fold excess of LiAlH₄ and prolonged reaction time under reflux heating (48 h). Fortunately, borane proved to be more efficient: the reduction of **7b** with BH₃·THF led to full conversion as judged by TLC and GC–MS, giving **4b** in 72% isolated yield.

Compound **4e** was obtained starting from cheap and readily available vanillin **8**.²⁴ Benzoylation followed by Henry-reaction with nitromethane and LiAlH₄-reduction afforded the primary amine derivative **9** in 47% overall yield (Scheme 3). In a first trial, the amine **9** was reacted with acid chloride **5a** to give the corresponding amide. *N*-Methylation of this compound was attempted following a published procedure,²⁵ but unfortunately alkylation occurred not only at the nitrogen but also on the α -carbon of the amide, giving an undesired dimethylated product in 72% yield. In a second trial, cyclization of the secondary amide formed from **9** and **5a** led to the desired tetrahydroisoquinoline; however, *N*-methylation employing methyl iodide in the presence of sodium hydride and triethylamine²⁶ did not lead to any conversion. Finally, the third attempt was successful: the monomethylation of **9** was performed prior to amide formation via conversion into a carbamate and LiAlH₄ reduction, giving the desired *N*-methylphenethylamine derivative **4e** in 66% yield.

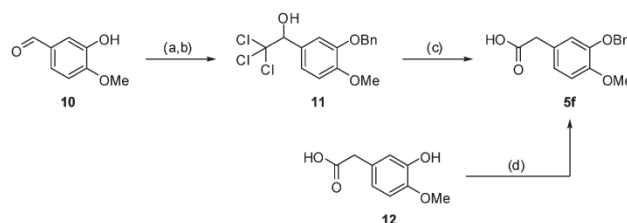
For the preparation of the phenylacetic acid building blocks two different approaches were investigated. Compound **5a** was obtained from 3-hydroxyphenylacetic acid by selective monobenzoylation

Scheme 2. Strategies for the Construction of 1-Substituted 1,2,3,4-Tetrahydroisoquinolines

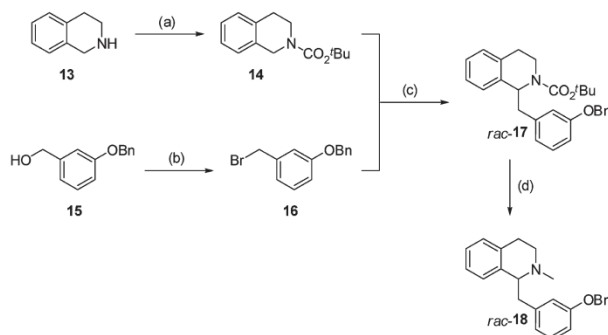


Scheme 3. Synthesis of Phenethylamine Derivatives 4b–e^a

^a Reagents and conditions: (a) (COCl)₂ (1.2 equiv), DMF cat., toluene, room temperature, 2 h, quant. (b) MeNH₂, aq NaOH, CH₂Cl₂, 0 °C to room temperature, 16 h, 78–95%. (c) BH₃·THF (5 equiv), THF, reflux, 16 h, 58–78%. (d) BnBr (1.0 equiv), K₂CO₃, argon, room temperature, 20 h, 89%. (e) MeNO₂ (3.2 equiv), NH₄OAc, HOAc, reflux, 5 h, 68%. (f) LiAlH₄ (5 equiv), THF, reflux, 20 h, 77%. (g) ClCO₂Et (1.2 equiv), Et₃N, CH₂Cl₂, 0 °C to room temperature, 3 h, 99%. (h) LiAlH₄ (5 equiv), THF, 0 °C to reflux, 4 h, 67%.

Scheme 4. Synthesis of Phenylacetic Acid Derivative 5f^a

^a Reagents and conditions: (a) BnBr (1.0 equiv), K₂CO₃ (1.1 equiv), EtOH, argon, room temperature, 20 h, 91%. (b) CHCl₃ (3.6 equiv), KOH (1.3 equiv), DMF, argon, –10 °C, 2.5 h, 97%. (c) (PhSe)₂ (1.05 equiv), NaBH₄ (2.1 equiv), NaOH (6.0 equiv), ethanol, room temperature, 30 min, 40 °C, 18 h, 31%. (d) BnBr (1.1 equiv), KOH, NaI cat., EtOH, 100 °C, 16 h, 67%.

Scheme 5. Synthesis of 1-(3-Benzyloxybenzyl)-2-methyl-1,2,3,4-tetrahydroisoquinoline 18^a

^a Reagents and conditions: (a) Boc₂O (1.02 equiv), CH₂Cl₂, room temperature, 2 h, quant. (b) CBr₄ (1.05 equiv), PPh₃ (1.04 equiv), CH₂Cl₂, 0 °C to room temperature, 3 h, 94%. (c) *t*-BuLi (1.05 equiv), TMEDA (1.05 equiv), THF, –78 to –50 °C, 4 h, 51%. (d) LiAlH₄ (5 equiv), THF, 0 °C to reflux, 16 h, 74%.

of the dianion.²⁷ 3-Benzyloxy-4-methoxyphenylacetic acid **5f** was also obtained by this method, requiring the commercially accessible acid **12** as starting material. Alternatively, **5f** was synthesized from isovanillin **10** in a three-step sequence

involving one-carbon homologation via the α -trichloromethylcarbinol **11** (Scheme 4).²⁸

With the required building blocks (**4** and **5**) in hand, amide coupling was performed. The carboxylic acids **5** were converted

into the corresponding acyl chlorides using oxalyl dichloride in toluene and connected with the amines under Schotten–Baumann conditions. Amides **3a–g** were obtained in yields ranging from 63% to 97%. The best results were generally obtained when the acyl chloride was applied in slight excess.

Next, the Bischler–Napieralski cyclization of these amides was investigated to obtain the corresponding racemic tetrahydroisoquinolines **1**. A broad range of reagents, employed in a wide variety of solvents, has been reported to effect this transformation.^{21a}

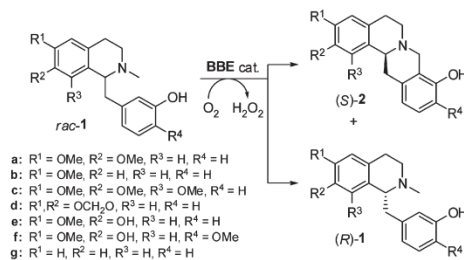
Table 1. Overall Yields of Chemical Route to Racemic Tetrahydroisoquinolines *rac-1a–g*

Product	Structure	Steps (linear)	Overall Yield [%]
<i>rac-1a</i>		5 (5)	40
<i>rac-1b</i>		8 (6)	42
<i>rac-1c</i>		8 (6)	28
<i>rac-1d</i>		8 (6)	43
<i>rac-1e</i>		10 (8)	21
<i>rac-1f</i>		10 (8)	16
<i>rac-1g</i>		5 (4)	33

Cyclization of **3a** employing PCl_5 in chloroform at room temperature followed by NaBH_4 -reduction afforded the desired tetrahydroisoquinoline, albeit only in 13% yield. The best results were obtained using phosphorus oxychloride in refluxing acetonitrile, followed by NaBH_4 -reduction in methanol. This sequence gave the tetrahydroisoquinolines in yields of 85–97%. Only the cyclization of **3g** failed under these conditions, most likely owing to the lack of electron-donating substituents on the aromatic ring of the original amine building block. Although the Bischler–Napieralski reaction of nonactivated arenes is described in literature,^{21a,29} no conversion was achieved in our case even under the most forcing reaction conditions employed (P_2O_5 in tetralin at 206 °C). Consequently, we had to change our strategy for the synthesis of **1g**. Alkylation of a C1-lithiated tetrahydroisoquinoline derivative appeared promising and lithiation of tetrahydroisoquinoline carbamates employing *t*-BuLi has previously been described.^{22a} Carbamate **14** and 3-benzyloxybenzyl bromide **16** were prepared and reacted following the published procedure to give the desired C–C coupling product in 29% yield (Scheme 5). By slightly changing the reaction conditions, i.e., higher temperature during the alkylation stage (see Experimental Section), this value could be improved to 51%, which approaches the reported yields obtained with less hindered nucleophiles.^{22a} The alkylated carbamate was converted into the *N*-methyltetrahydroisoquinoline by LiAlH_4 reduction. This represents an improvement on the original report, where this transformation was achieved in a two-step deprotection/reductive amination sequence. In our case the carbamate moiety serves a triple purpose: it protects the nitrogen atom, directs the lithiation, and serves as precursor of the *N*-methyl group.

The synthesis of racemic tetrahydroisoquinolines **1a–g** (summarized in Table 1) was completed by hydrogenolytic cleavage of the benzyl ether protective groups, which proceeded quantitatively and generally gave the target compounds without the need for chromatographic purification. For instance, racemic

Table 2. Yields of BBE-Catalyzed Oxidative Kinetic Resolution via C–C Bond Formation



entry	substrate	c [%] ^a	yield (S)-2 [%] ^b	ee (S)-2 [%] ^c	yield (R)-1 [%] ^b	ee (R)-1 [%] ^c	E ^d
1	<i>rac-1a</i> ^e	50	42	>97	50	>97	>200
2	<i>rac-1b</i> ^e	50	36	>97	36	>97	>200
3	<i>rac-1c</i> ^e	50	39	>97	47	>97	>200
4	<i>rac-1d</i> ^e	50	31	>97	46	>97	>200
5	<i>rac-1e</i>	50	22	>97	49	>97	>200
6	<i>rac-1f</i>	50	47	>97	37	>97	>200
7	<i>rac-1g</i>	50	46	>97	49	>97	>200

^a Determined by HPLC on an achiral stationary phase. ^b Isolated yield (maximum theoretical yield = 50%). ^c Determined by HPLC on a chiral stationary phase. ^d Determined from the ee of substrate and product. ^e Kinetic resolution from ref 19.

reticuline **rac-1f**, as the most complex structure, was obtained with 16% overall yield, while the most efficient synthesis in terms of yield was achieved for **rac-1d** and **rac-1b** with 43% and 42% isolated overall yield, respectively.

Finally, the racemic tetrahydroisoquinolines **rac-1a–g** were subjected to enantioselective oxidative ring closure catalyzed by BBE, leading to the untouched optically pure (*R*)-substrates and the optically pure (*S*)-berbine products **2a–g** via kinetic resolution (Table 2). The reaction was performed employing 1 g/L BBE, 5 g/L catalase, and 20 g/L substrate in a toluene/buffer (70:30) biphasic mixture.¹⁹ Under these conditions, substrate solubility is not an issue. Maximum conversion (50%) was achieved within 24 h in all cases, and the enantiomerically pure products (*ee* > 97%, HPLC) were obtained in good to excellent yields (Table 2). For instance, the kinetic resolution of racemic reticuline **rac-1f** yielded optically pure (*R*)-reticuline (**R-1f**) and optically pure (*S*)-scoulerine (**S-2f**) in 37% and 47% isolated yield.

CONCLUSION

The combination of chemical synthesis of racemic 1-benzyl-1,2,3,4-tetrahydroisoquinolines with biocatalytic enantioselective intramolecular oxidative C–C coupling by BBE provided a new and efficient synthetic route to enantiomerically pure benzyloisoquinoline and berbine alkaloids. The racemic substrates for BBE were prepared by two different pathways: either via Bischler–Napieralski cyclization or by alkylation of Boc-protected tetrahydroisoquinoline. BBE-catalyzed kinetic resolution proceeded with excellent enantioselectivity (*E* > 200), affording optically pure products in all cases. The overall chemoenzymatic synthesis resulted in yields of up to 20% for the benzyloisoquinolines and 17% for the berbines, which represents a competitive alternative to the conventional asymmetric syntheses of these compounds.^{21,4,6,24,50} In particular, this novel synthetic route enabled the first asymmetric total synthesis of naturally occurring (*S*)-scoulerine, a sedative and muscle-relaxing agent,^{3b,31} yielding 230 mg (7.4%) of the enantiomerically pure alkaloid over 9 linear steps.

EXPERIMENTAL SECTION

Synthesis of Amides 7b–d. A literature procedure³² was adapted for our purpose: A solution of phenylacetic acid derivative **6b–d** (20.0 mmol), oxalyl chloride (2.89 g, 22.8 mmol) and one drop of DMF in dry toluene (50 mL) was stirred at room temperature for 1 h. The solvent was evaporated under reduced pressure to give the acyl chloride (quant), which was used without further purification. A solution of the crude acyl chloride (20.0 mmol) in CH₂Cl₂ (40 mL) was cooled to 0 °C on an ice bath. A solution of amino methane (40% in H₂O; 4.11 g, 52.9 mmol) in 2 M aqueous NaOH (20 mL) was added dropwise over 1 h. The ice bath was removed and stirring was continued overnight. The phases were separated and the aqueous phase was extracted with CH₂Cl₂ (2 × 20 mL). The combined organic phases were washed with 2 N HCl solution (100 mL), saturated NaHCO₃ solution (100 mL), and water (100 mL) and dried over Na₂SO₄. Evaporation of the solvent under reduced pressure yielded the amides **7b–d**, which were used in the following transformation without further purification.

3-Methoxyphenyl-*N*-methylacetamide (7b). Yield: 3.40 g (95%) as a pale yellowish solid. Mp: 41–44 °C. TLC (petroleum ether/EtOAc = 1/1); *R_f* = 0.22. The ¹H and ¹³C NMR as well as MS data are in accordance with literature.^{19,33}

***N*-Methyl-3,4,5-trimethoxyphenylacetamide (7c).** Yield: 3.74 g (78%) as a pale yellowish solid. Mp: 87–89 °C (lit.³⁴ 90.5–91.5 °C).

TLC (petroleum ether/EtOAc = 1/1); *R_f* = 0.12. The ¹H and ¹³C NMR as well as MS data are in accordance with literature.¹⁹

(3,4-Methylenedioxy)phenyl-*N*-methylacetamide (7d). Yield: 3.68 g (95%) as a pale yellowish solid. Mp: 100–101 °C (lit.³⁵ 99–101 °C). TLC (petroleum ether/EtOAc = 1/1); *R_f* = 0.20. The ¹H and ¹³C NMR as well as MS data are in accordance with literature.^{19,32}

Reduction of Amides 7b–d Giving Amines 4b–d. A literature procedure³² was adapted for our purpose: BH₃·THF (1.0 M in THF; 100 mL, 100 mmol) was added to a solution of amide **7b–d** (17.4–20.0 mmol) in anhydrous THF (100 mL) and the mixture was gently refluxed for 18 h under an argon atmosphere. The solution was allowed to cool to room temperature, and 6 N HCl solution (20 mL) was cautiously added. After stirring for 30 min, the resulting solution was concentrated under reduced pressure, basified by addition of 2 M NaOH solution (100 mL), and saturated with NaCl. The product was extracted into EtOAc (3 × 30 mL), and the combined organic phases were washed with brine, dried over Na₂SO₄, and evaporated under reduced pressure to give the crude product as a yellowish liquid. Flash chromatography (silica; CH₂Cl₂/MeOH/NH₃(aq) = 90/9/1) afforded the pure amine **4b–d**.

***N*-Methyl-3-methoxyphenethylamine (4b).** Yield: 2.23 g (72%) as a pale yellowish liquid. TLC (CH₂Cl₂/MeOH/NH₃(aq) = 90/9/1); *R_f* = 0.21. The ¹H and ¹³C NMR as well as MS data are in accordance with literature.^{19,33}

***N*-Methyl-3,4,5-trimethoxyphenethylamine (4c).** Yield: 3.54 g (78%) as a pale yellowish liquid, which crystallized upon standing to a pale yellowish solid. Mp: 175–177 °C (lit.³⁴ 178 °C). TLC (CH₂Cl₂/MeOH/NH₃(aq) = 90/9/1); *R_f* = 0.37. The ¹H and ¹³C NMR as well as MS data are in accordance with literature.¹⁹

***N*-Methyl-(3,4-methylenedioxy)phenethylamine (4d).** Yield: 1.81 g (58%) as a pale yellowish liquid. TLC (CH₂Cl₂/MeOH/NH₃(aq) = 90/9/1); *R_f* = 0.20. The ¹H and ¹³C NMR as well as MS data are in accordance with literature.^{19,35}

4-Benzyloxy-3-methoxybenzaldehyde³⁶. K₂CO₃ (20.1 g, 0.146 mol) and benzyl bromide (22.5 g, 0.132 mol) were added to a solution of vanillin **8** (20.0 g, 0.131 mol) in ethanol (120 mL). The mixture was stirred for 20 h at room temperature under argon atmosphere. The solution was filtered through Celite and washed with CH₂Cl₂ (3 × 100 mL), and the solvent was evaporated under reduced pressure. The residue was taken up in CH₂Cl₂ (200 mL), washed with 5% NaOH solution (100 mL) and dried over K₂CO₃. Evaporation of the solvent under reduced pressure yielded 30.5 g of a yellow solid. Recrystallization from ethanol gave 4-benzyloxy-3-methoxybenzaldehyde (28.1 g, 89%) as a white solid. Mp: 61–63 °C (lit.³⁶ 61–62 °C). TLC (petroleum ether/EtOAc = 3/1); *R_f* = 0.62. The ¹H and ¹³C NMR as well as MS data are in accordance with literature.³⁶

4-Benzyloxy-3-methoxy-β-nitrostyrene³⁷. A solution of 4-benzyloxy-3-methoxybenzaldehyde (22.7 g, 0.094 mol), nitromethane (18.4 g, 0.301 mol), and NH₄OAc (18.4 g, 0.239 mol) in AcOH (220 mL) was refluxed for 5 h. The mixture was poured into ice–water (300 mL), followed by addition of CH₂Cl₂ (150 mL) to dissolve the formed precipitate. The phases were separated, and the aqueous phase was extracted with CH₂Cl₂ (3 × 50 mL). The combined organic phases were washed with water (100 mL), half-saturated Na₂CO₃ solution (50 mL), and brine (50 mL), dried over Na₂SO₄, and evaporated under reduced pressure to give 21.4 g of a brown solid. Recrystallization from ethanol gave 4-benzyloxy-3-methoxy-β-nitrostyrene (18.1 g, 68%) as a yellow solid. Mp: 119–121 °C (lit.³⁶ 124–125 °C). TLC (petroleum ether/EtOAc = 3/1); *R_f* = 0.47. The ¹H and ¹³C NMR as well as MS data are in accordance with literature.³⁶

4-Benzyloxy-3-methoxyphenethylamine (9)³⁶. To a suspension of LiAlH₄ (8.05 g, 212 mmol) in dry THF (120 mL) under argon was added dropwise a solution of 4-benzyloxy-3-methoxy-β-nitrostyrene (12.0 g, 42.0 mmol) in dry THF (80 mL) over 1 h. The reaction

mixture was refluxed for 16 h, then diluted with THF (100 mL), and cooled to 0 °C on an ice bath. To the vigorously stirred mixture were added water (8 mL), 15% NaOH solution (8 mL), and water (24 mL), the ice bath was removed, and stirring was continued for 1 h at room temperature. The resulting suspension was filtered through Celite, washed with THF, and evaporated under reduced pressure. The residue was dissolved in 10% HCl solution (20 mL) and washed with ether; afterward the aqueous layer was made basic and extracted with ether (3 × 50 mL). The combined organic phases were washed with water (20 mL) and brine (20 mL), dried over K₂CO₃, and evaporated under reduced pressure to give 8.28 g (77%) of 4-benzyloxy-3-methoxyphenethylamine as a yellowish liquid that crystallized upon standing to a yellowish solid. Mp: 63–65 °C (lit.³⁸ 59–61 °C). TLC (CH₂Cl₂/MeOH/NH₃(aq) = 90/9/1): R_f = 0.27. The ¹H and ¹³C NMR as well as MS data are in accordance with literature.³⁶

Ethyl 4-Benzyloxy-3-methoxyphenethylcarbamate. A literature procedure³⁹ was adapted for our purpose: To a solution of 4-benzyloxy-3-methoxyphenethylamine **9** (4.00 g, 15.5 mmol) in dichloromethane (120 mL) were added triethylamine (1.75 g, 17.3 mmol) and ethyl chloroformate (2.01 g, 18.4 mmol), and the mixture was stirred for 3 h at room temperature. Water (100 mL) was added, the phases were separated, and the aqueous phase was extracted with CH₂Cl₂ (2 × 30 mL). The combined organic phases were dried over Na₂SO₄ and evaporated under reduced pressure to give 5.06 g (99%) of ethyl 4-benzyloxy-3-methoxyphenethylcarbamate as a yellow liquid that crystallized upon standing to a yellowish solid. Mp: 80–81 °C. TLC (petroleum ether/EtOAc = 3/1): R_f = 0.23. ¹H NMR (CDCl₃, 300 MHz): δ 1.24 (3H, t, J = 7.1 Hz, OCH₂CH₃), 2.75 (2H, t, J = 7.1 Hz, Ar-CH₂CH₂-N), 3.41 (2H, dt, J₁ = 6.6 Hz, J₂ = 6.5 Hz, Ar-CH₂CH₂-N), 3.89 (3H, s, OCH₃), 4.12 (2H, q, J = 7.2 Hz, OCH₂CH₃), 4.71 (1H, br s, NH), 5.15 (2H, s, PhCH₂O), 6.66–6.86 (3H, m, Ar), 7.31–7.47 (5H, m, Ar). ¹³C NMR (CDCl₃, 75 MHz): δ 14.7, 30.3, 35.8, 42.2, 56.0, 60.7, 71.1, 112.5, 114.3, 120.7, 127.3, 127.8, 128.5, 132.0, 137.3, 146.8, 149.7, 156.6. MS (EI, 70 eV): m/z = 329 (M⁺, 13), 240 (27), 137 (59), 91 (100).

4-Benzyloxy-3-methoxy-N-methylphenethylamine (4e). A literature procedure³⁹ was adapted for our purpose: A solution of 4-benzyloxy-3-methoxyphenethylcarbamate (7.43 g, 22.6 mmol) in anhydrous THF (160 mL) under argon atmosphere was cooled to 0 °C on an ice bath. LiAlH₄ (4.33 g, 114 mmol) was added in portions to the stirred solution; afterward the ice bath was removed and the mixture was refluxed for 4 h. The suspension was diluted with THF (50 mL) and cooled to 0 °C on an ice bath. To the vigorously stirred mixture were added water (4.3 mL), 15% NaOH solution (4.3 mL) and water (12.9 mL), the ice bath was removed, and stirring was continued for 1 h at room temperature. The resulting suspension was filtered through Celite, washed with THF, dried over Na₂SO₄, and evaporated under reduced pressure to give 6.44 g of a brownish liquid. Flash chromatography (silica; CH₂Cl₂/MeOH/NH₃(aq) = 90/9/1) afforded 4-benzyloxy-3-methoxy-N-methylphenethylamine (4.16 g, 67%) as an orange liquid. TLC (CH₂Cl₂/MeOH/NH₃(aq) = 90/9/1): R_f = 0.22. ¹H NMR (CDCl₃, 300 MHz): δ 1.73 (1H, br s, NH), 2.44 (3H, s, NCH₃), 2.73–2.86 (4H, m, CH₂-CH₂-N), 3.90 (3H, s, OCH₃), 5.14 (2H, s, PhCH₂O), 6.68–6.84 (3H, m, Ar), 7.28–7.46 (5H, m, Ar). ¹³C NMR (CDCl₃, 75 MHz): δ 35.8, 36.4, 53.3, 56.0, 71.2, 112.6, 114.3, 120.6, 127.3, 127.8, 128.5, 133.2, 137.4, 146.6, 149.6. MS (EI, 70 eV): m/z = 271 (M⁺, <1), 228 (46), 137 (18), 137 (18) 91 (58), 44 (100).

3-Benzyloxyphenylacetic Acid (5a). A literature procedure⁴⁰ was adapted for our purpose: A solution of 3-hydroxyphenylacetic acid (6.02 g, 39.6 mmol), KOH (6.0 g, 107 mmol), and NaI (0.2 g, 1.4 mmol) in ethanol (200 mL) was heated to 90 °C. Benzyl bromide (8.01 g, 46.8 mmol) was added, whereupon the mixture was refluxed at 100 °C for 16 h. The resulting suspension was concentrated to 70 mL and poured into water (200 mL) to give a slightly brownish solution from which the product was precipitated by addition of conc hydrochloric

acid. The precipitate was filtered and recrystallized from H₂O/AcOH (1/1, 70 mL) to yield 6.61 g (69%) of 3-benzyloxyphenylacetic acid as a white solid. Mp = 124–125 °C (lit.⁴¹ 119 °C). TLC (EtOAc): R_f = 0.60. The ¹H NMR data are in accordance with literature.⁴¹ ¹³C NMR (CDCl₃, 75 MHz): δ 41.1, 70.0, 113.7, 116.0, 122.0, 127.6, 128.0, 128.6, 129.7, 134.7, 136.9, 159.0, 177.6. MS (EI, 70 eV): m/z = 242 (M⁺, 9), 91 (100), 65 (10).

3-Benzyloxy-4-methoxyphenylacetic Acid (5f). Method A. A literature procedure⁴⁰ was adapted for our purpose: A solution of 3-hydroxy-4-methoxyphenylacetic acid (2.00 g, 11.0 mmol), KOH (1.73 g, 30 mmol), and NaI (0.06 g, 0.4 mmol) in ethanol (60 mL) was heated to 90 °C. Benzyl bromide (2.59 g, 16.5 mmol) was added, whereupon the mixture was refluxed at 100 °C for 16 h. The resulting suspension was poured into water (110 mL) to give a brownish solution from which the product was precipitated by addition of conc hydrochloric acid. The precipitate was filtered and recrystallized from H₂O/AcOH (1/1, 35 mL) to yield 1.99 g (67%) of 3-benzyloxy-4-methoxyphenylacetic acid as an off-white solid. Mp = 117–118 °C (lit.⁴² 124–125 °C). TLC (petroleum ether/EtOAc = 3/1 + 1 drop of AcOH): R_f = 0.63. The ¹H NMR data are in accordance with literature.⁴¹ ¹³C NMR (CDCl₃, 75 MHz): δ 40.5, 56.1, 71.1, 111.9, 115.3, 122.2, 125.6, 127.5, 127.9, 128.5, 137.0, 148.2, 149.1, 177.7.

Method B. A literature procedure^{28,43} was adapted for our purpose: To a stirred solution of isovanillin **10** (20.0 g, 0.131 mol) in ethanol (120 mL) were added K₂CO₃ (20.1 g, 0.145 mol) and benzyl bromide (22.5 g, 0.131 mol). The mixture was stirred for 20 h at room temperature under argon atmosphere. The solution was filtered through Celite and washed with CH₂Cl₂ (3 × 100 mL), and the solvent was evaporated under reduced pressure. The residue was taken up in CH₂Cl₂ (200 mL), washed with 5% NaOH solution (100 mL), and dried over K₂CO₃. Evaporation of the solvent under reduced pressure yielded 31.3 g of a yellow solid. Recrystallization from ethanol gave 3-benzyloxy-4-methoxybenzaldehyde (29.2 g, 91%) as a white solid. Mp: 62–63 °C (lit.²⁴ 61–62 °C). TLC (petroleum ether/EtOAc = 3/1): R_f = 0.29. The ¹H and ¹³C NMR data are in accordance with literature.⁴⁴ MS (EI, 70 eV): m/z = 242 (M⁺, 13), 91 (100), 65 (9).

A solution of 3-benzyloxy-4-methoxybenzaldehyde (29.0 g, 0.120 mol) and chloroform (35 mL) in DMF (120 mL) under argon atmosphere was cooled to –10 °C on an ice/NaCl bath. A solution of KOH (8.88 g, 0.158 mol) in methanol (30 mL) was added dropwise over 30 min and the resulting mixture was stirred for 2 h at –10 °C. The reaction was quenched with 1 N hydrochloric acid (270 mL) and stirred for an additional 30 min at –10 °C. Afterward, the mixture was allowed to warm to room temperature, toluene (100 mL) was added, and the phases were separated. The aqueous phase was extracted with toluene (2 × 100 mL), and the combined organic phases were washed with water (30 mL) and brine (30 mL) and dried over Na₂SO₄. Evaporation of the solvent under reduced pressure gave 42.9 g (97%) of 1-(3-benzyloxy-4-methoxyphenyl)-2,2,2-trichloroethanol **11** as a yellowish solid, which was used in the next step without further purification. TLC (petroleum ether/EtOAc = 3/1): R_f = 0.53. ¹H NMR (CDCl₃, 300 MHz): δ 3.71 (1H, br s, OH), 3.92 (3H, s, OCH₃), 5.09 (1H, s, CH–OH), 5.21 (2H, s, PhCH₂O), 6.89 (1H, d, J = 8.7 Hz, Ar), 7.14–7.21 (2H, m, Ar), 7.26–7.46 (5H, m, Ar). ¹³C NMR (CDCl₃, 75 MHz): δ 55.9, 71.0, 84.1, 103.4, 110.6, 115.1, 122.6, 127.3, 127.4, 127.9, 128.6, 137.0, 147.1, 150.5. MS (EI, 70 eV): m/z = 360 (M⁺, 1), 243 (36), 91 (100).

Diphenyl diselenide (36.9 g, 0.118 mol) was dissolved in deoxygenated ethanol (300 mL); purged with argon for 1 h). NaBH₄ (9.0 g, 0.238 mol) was added in portions over 30 min, upon which the previously orange solution turned colorless. The resulting mixture was stirred for 30 min at room temperature before addition of **11** (40.8 g, 0.113 mol) followed by NaOH (27.1 g, 0.678 mol). The reaction was then stirred for 18 h at 40 °C. The solvent was evaporated under reduced

pressure, and the solid residue was dissolved in water (200 mL). The pH of the solution was adjusted to 1.0 by addition of conc hydrochloric acid, and the product was extracted into EtOAc (5 × 100 mL). The combined organic phases were dried over Na₂SO₄, and the solvent was evaporated under reduced pressure to give an orange solid, which was recrystallized from petroleum ether/acetone to afford **Sf** (11.0 g, 31%) as an off-white solid. The spectroscopic and chromatographic data are identical to those of **Sf** obtained by method A.

Synthesis of Amides 3a–g. A literature procedure⁴⁵ was adapted for our purpose: A solution of phenylacetic acid derivative **5a** or **5f** (10.5–12.0 mmol), oxalyl chloride (1.95 g, 15.4 mmol), and one drop of DMF in dry toluene (40 mL) was stirred at room temperature under argon for 1 h. The solvent was evaporated under reduced pressure to give the acyl chloride (quant), which was used without further purification.

The amine **4a–g** (10.0–13.5 mmol) was dissolved in CHCl₃ (30 mL). A 3% NaOH solution (150 mL) was added, and the mixture was cooled to 0 °C on an ice bath. A solution of the crude phenylacetyl chloride derivative (10.6–12.8 mmol) in chloroform (20 mL) was added dropwise over 1 h to the vigorously stirred mixture. The ice bath was removed, and stirring was continued for 16 h at room temperature. The phases were separated, and the aqueous phase was extracted with CHCl₃ (50 mL). The combined organic phases were washed with dilute HCl solution (100 mL) and then water (100 mL) and dried over Na₂SO₄. Evaporation of the solvent under reduced pressure yielded the crude amide **3a–g**, which was purified by flash chromatography (silica; petroleum ether/EtOAc = 1/1). The product is obtained as a mixture of rotamers, to which NMR signals are assigned based on the peak intensities as well as the DEPT, COSY, and HSQC spectra.

2-(3-Benzyloxyphenyl)-N-(3,4-dimethoxyphenethyl)-N-methylacetamide (3a). Yield: 2.97 g (64%) as an off-white solid. Ratio *trans/cis* = 1.15/1. Mp: 97–98 °C. TLC (petroleum ether/EtOAc = 1/1): *R_f* = 0.55. The ¹H and ¹³C NMR as well as MS data are in accordance with literature.¹⁹ HRMS: calcd for C₂₆H₂₉NO₄ 419.2097; found 419.2099.

2-(3-Benzyloxyphenyl)-N-(3-methoxyphenethyl)-N-methylacetamide (3b). Yield: 2.79 g (68%) as a pale yellowish liquid. Ratio *trans/cis* = 1.05/1. TLC (petroleum ether/EtOAc = 1/1): *R_f* = 0.37. The ¹H and ¹³C NMR as well as MS data are in accordance with literature.¹⁹ HRMS: calcd for C₂₅H₂₇NO₃ 389.1991; found 389.1990.

2-(3-Benzyloxyphenyl)-N-methyl-N-(3,4,5-trimethoxyphenethyl)acetamide (3c). Yield: 3.63 g (63%) as a pale yellowish liquid. Ratio *trans/cis* = 1.05/1. TLC (petroleum ether/EtOAc = 1/1): *R_f* = 0.18. The ¹H and ¹³C NMR as well as MS data are in accordance with literature.¹⁹ HRMS: calcd for C₂₇H₃₁NO₅ 449.2202; found 449.2224.

2-(3-Benzyloxyphenyl)-N-(3,4-methylenedioxyphenethyl)-N-methylacetamide (3d). Yield: 3.88 g (97%) as a pale yellowish liquid. Ratio *trans/cis* = 1.07/1. TLC (petroleum ether/EtOAc = 1/1): *R_f* = 0.37. The ¹H and ¹³C NMR as well as MS data are in accordance with literature.¹⁹ HRMS: calcd for C₂₅H₂₅NO₄ 403.1783; found 403.1796.

2-(3-Benzyloxyphenyl)-N-(4-benzyloxy-3-methoxyphenethyl)-N-methylacetamide (3e). Yield: 5.19 g (78%) as a pale yellowish liquid. Ratio *trans/cis* = 1.11/1. TLC (petroleum ether/EtOAc = 1/1): *R_f* = 0.26. MS (EI, 70 eV): *m/z* = 495 (M⁺, S), 240 (48), 197 (5), 149 (12), 91 (100). HRMS: calcd for C₃₂H₃₃NO₄ 495.2410; found 495.2440. *trans-3e*: ¹H NMR (CDCl₃, 300 MHz): δ 2.76 (2H, t, *J* = 7.5 Hz, CH₂-CH₂-N), 2.82 (3H, s, N-CH₃), 3.56 (2H, t, *J* = 7.5 Hz, CH₂-CH₂-N), 3.65 (2H, s, CH₂-CO), 3.81 (3H, s, OCH₃), 5.04 (2H, s, Ph-C H₂-O), 5.10 (2H, s, Ph-C H₂-O), 6.61–6.64 (1H, m, Ar), 6.74–6.90 (5H, m, Ar), 7.18–7.40 (11H, m, Ar). ¹³C NMR (CDCl₃, 75 MHz): δ 33.3 (CH₂), 36.6 (CH₃), 41.4 (CH₂), 50.3 (CH₂), 56.0 (CH₃), 69.9 (CH₂), 71.1 (CH₂), 112.6 (CH), 113.2 (CH), 114.3 (CH), 115.3 (CH), 120.7 (CH), 121.4 (CH), 127.3 (CH), 127.5 (CH), 127.8 (CH), 128.0 (CH), 128.5 (CH), 128.6 (CH), 129.7 (CH), 132.4 (C), 136.5 (C), 137.0 (C), 137.2 (C), 146.7 (C), 149.7 (C), 159.1 (C), 170.6 (C). *cis-3e*: ¹H NMR (CDCl₃, 300 MHz): δ 2.60 (2H, t, *J* = 7.2 Hz, CH₂-CH₂-N),

2.95 (3H, s, N-CH₃), 3.41 (2H, s, CH₂-CO), 3.42 (2H, t, *J* = 7.1 Hz, CH₂-C H₂-N), 3.84 (3H, s, OCH₃), 5.02 (2H, s, Ph-C H₂-O), 5.10 (2H, s, Ph-C H₂-O), 6.53–6.90 (2H, m, Ar), 6.74–6.90 (4H, m, Ar), 7.18–7.40 (11H, m, Ar). ¹³C NMR (CDCl₃, 75 MHz): δ 33.6 (CH₃), 34.3 (CH₂), 40.8 (CH₂), 52.2 (CH₂), 56.1 (CH₃), 69.9 (CH₂), 71.1 (CH₂), 112.5 (CH), 113.2 (CH), 114.5 (CH), 115.2 (CH), 120.7 (CH), 121.3 (CH), 127.3 (CH), 127.5 (CH), 127.9 (CH), 128.0 (CH), 128.5 (CH), 128.6 (CH), 129.7 (CH), 131.4 (C), 136.9 (C), 137.0 (C), 137.1 (C), 147.0 (C), 149.9 (C), 159.1 (C), 170.8 (C).

2-(3-Benzyloxy-4-methoxyphenyl)-N-(4-benzyloxy-3-methoxyphenethyl)-N-methylacetamide (3f). Yield: 2.33 g (76%) as an off-white solid. Ratio *trans/cis* = 1.14/1. Mp: 126–127 °C. TLC (petroleum ether/EtOAc = 1/1): *R_f* = 0.64. MS (EI, 70 eV): *m/z* = 525 (M⁺, 3), 240 (22), 149 (11), 105 (14), 91 (100). HRMS: calcd for C₃₃H₃₅NO₅; 525.2515; found 525.2523. *trans-3f*: ¹H NMR (CDCl₃, 300 MHz): δ 2.74 (2H, t, *J* = 7.5 Hz, CH₂-CH₂-N), 2.79 (3H, s, N-CH₃), 3.54 (2H, t, *J* = 7.7 Hz, CH₂-CH₂-N), 3.59 (2H, s, CH₂-CO), 3.84 (3H, m, OCH₃), 3.88 (3H, s, OCH₃), 5.13 (2H, s, Ph-C H₂-O), 5.16 (2H, s, Ph-C H₂-O), 6.53–6.86 (6H, m, Ar), 7.28–7.47 (10H, m, Ar). ¹³C NMR (CDCl₃, 75 MHz): δ 33.3 (CH₂), 36.5 (CH₃), 40.8 (CH₂), 50.2 (CH₂), 56.0 (CH₃), 70.9 (CH₂), 71.1 (CH₂), 112.0 (CH), 112.6 (CH), 114.2 (CH), 114.7 (CH), 120.7 (CH), 121.5 (CH), 127.3 (CH), 127.4 (CH), 127.8 (CH), 127.9 (CH), 128.5 (CH), 132.4 (C), 137.1 (C), 146.6 (C), 148.2 (C), 149.6 (C), 170.9 (C). *cis-3f*: ¹H NMR (CDCl₃, 300 MHz): δ 2.58 (2H, t, *J* = 7.2 Hz, CH₂-CH₂-N), 2.94 (3H, s, N-CH₃), 3.35 (2H, s, CH₂-CO), 3.39 (2H, t, *J* = 6.9 Hz, CH₂-CH₂-N), 3.87 (3H, s, OCH₃), 3.88 (3H, s, OCH₃), 5.13 (2H, s, Ph-CH₂-O × 2), 6.53–6.90 (2H, m, Ar), 6.74–6.90 (4H, m, Ar), 7.18–7.40 (11H, m, Ar). ¹³C NMR (CDCl₃, 75 MHz): δ 33.6 (CH₂), 34.2 (CH₂), 40.8 (CH₂), 50.2 (CH₂), 56.0 (CH₃), 70.8 (CH₂), 71.1 (CH₂), 111.9 (CH), 112.6 (CH), 114.5 (CH), 114.5 (CH), 120.7 (CH), 121.3 (CH), 127.3 (CH), 127.4 (CH), 127.7 (CH), 127.8 (CH), 128.5 (CH), 131.4 (C), 137.1 (CH), 137.3 (CH), 147.0 (CH), 148.6 (CH), 149.8 (CH), 171.2 (CH).

2-(3-Benzyloxyphenyl)-N-phenethyl-N-methylacetamide (3g). Yield: 2.30 g (63%) as a pale yellowish liquid. Ratio *trans/cis* = 1.05/1. TLC (petroleum ether/EtOAc = 1/1): *R_f* = 0.51. *trans-3g*: ¹H NMR (CDCl₃, 300 MHz): δ 2.79–2.84 (SH, s + t overlap, N-CH₃ + CH₂-CH₂-N), 3.57 (2H, t, *J* = 7.5 Hz, CH₂-CH₂-N), 3.63 (2H, s, CH₂-CO), 5.03 (2H, s, Ph-C H₂-O), 6.73–6.88 (3H, m, Ar), 7.05–7.07 (1H, m, Ar), 7.14–7.42 (10H, m, Ar). ¹³C NMR (CDCl₃, 75 MHz): δ 33.7 (CH₂), 36.6 (CH₃), 41.4 (CH₂), 50.2 (CH₂), 69.9 (CH₂), 113.2 (CH), 115.3 (CH), 121.5 (CH), 126.3 (CH), 127.5 (CH), 128.0 (CH), 128.6 (CH), 128.8 (CH), 128.9 (CH), 129.7 (CH), 136.6 (C), 137.0 (C), 139.1 (C), 159.1 (C), 170.8 (C). *cis-3g*: ¹H NMR (CDCl₃, 300 MHz): δ 2.66 (2H, t, *J* = 7.3 Hz, CH₂-CH₂-N), 2.95 (3H, s, N-CH₃), 3.40 (2H, s, CH₂-CO), 3.44 (1H, t, *J* = 7.3 Hz, CH₂-CH₂-N), 5.01 (2H, s, Ph-C H₂-O), 6.73–6.88 (3H, m, Ar), 7.05–7.07 (1H, m, Ar), 7.14–7.42 (10H, m, Ar). ¹³C NMR (CDCl₃, 75 MHz): δ 33.6 (CH₂), 34.7 (CH₂), 40.8 (CH₂), 52.0 (CH₂), 69.9 (CH₂), 113.3 (CH), 115.2 (CH), 121.4 (CH), 126.8 (CH), 127.5 (CH), 128.0 (CH), 128.5 (CH), 128.6 (CH), 128.9 (CH), 129.7 (CH), 136.9 (C), 137.0 (C), 138.3 (C), 159.1 (C), 170.7 (C).

Bischler–Napieralski Cyclization of Amides 3a–f. A literature procedure⁴⁶ was adapted for our purpose: A solution of amide **3a–f** (7.0 mmol) and POCl₃ (21.0 mmol) in dry acetonitrile (60 mL) was refluxed for 3 h under argon atmosphere. The solvent and excess POCl₃ were evaporated under reduced pressure, and the residue was dissolved in dry methanol (50 mL), flushed with argon, and cooled to –5 °C on an ice/NaCl bath. NaBH₄ (50.0 mmol) was added in portions to the stirred mixture. The ice bath was then removed, and stirring was continued for 16 h at room temperature. The solvent was evaporated, and the residue was treated with half-saturated Na₂CO₃ solution (60 mL). The product was extracted with CH₂Cl₂ (3 × 30 mL) and the combined organic phases were dried over Na₂SO₄ and evaporated under reduced pressure to give the crude tetrahydroisoquinoline, which was purified by flash chromatography (silica; CH₂Cl₂/MeOH/NH₃(aq) = 96/3/1).

1-(3-Benzyloxybenzyl)-6,7-dimethoxy-2-methyl-1,2,3,4-tetrahydroisoquinoline. Yield: 2.78 g (94%) as a yellowish liquid. TLC ($\text{CH}_2\text{Cl}_2/\text{MeOH}/\text{NH}_3(\text{aq}) = 90/9/1$): $R_f = 0.75$. The ^1H and ^{13}C NMR as well as MS data are in accordance with literature.¹⁹ HRMS: calcd for $\text{C}_{26}\text{H}_{38}\text{NO}_3$ [(M - H)⁺] 402.2069; found 402.2071.

1-(3-Benzyloxybenzyl)-6-methoxy-2-methyl-1,2,3,4-tetrahydroisoquinoline. Yield: 2.43 g (94%) as a pale yellowish liquid. TLC ($\text{CH}_2\text{Cl}_2/\text{MeOH}/\text{NH}_3(\text{aq}) = 90/9/1$): $R_f = 0.61$. The ^1H and ^{13}C NMR as well as MS data are in accordance with literature.¹⁹ HRMS: calcd for $\text{C}_{25}\text{H}_{36}\text{NO}_2$ [(M - H)⁺] 372.1964; found 372.1974.

1-(3-Benzyloxybenzyl)-2-methyl-6,7,8-trimethoxy-1,2,3,4-tetrahydroisoquinoline. Yield: 2.89 g (85%) as a pale yellowish viscous liquid. TLC ($\text{CH}_2\text{Cl}_2/\text{MeOH}/\text{NH}_3(\text{aq}) = 90/9/1$): $R_f = 0.75$. The ^1H and ^{13}C NMR as well as MS data are in accordance with literature.¹⁹ HRMS: calcd for $\text{C}_{27}\text{H}_{40}\text{NO}_4$ [(M - H)⁺] 432.2175; found 432.2194.

1-(3-Benzyloxybenzyl)-6,7-methylenedioxy-2-methyl-1,2,3,4-tetrahydroisoquinoline. Yield: 3.59 g (97%) as a pale yellowish liquid. TLC ($\text{CH}_2\text{Cl}_2/\text{MeOH}/\text{NH}_3(\text{aq}) = 90/9/1$): $R_f = 0.76$. The ^1H and ^{13}C NMR as well as MS data are in accordance with literature.¹⁹ HRMS: calcd for $\text{C}_{25}\text{H}_{24}\text{N}_2\text{O}_3$ [(M - H)⁺] 386.1756; found 386.1740.

1-(3-Benzyloxybenzyl)-7-benzyloxy-6-methoxy-2-methyl-1,2,3,4-tetrahydroisoquinoline. Yield: 4.36 g (88%) as a pale yellowish liquid. TLC ($\text{CH}_2\text{Cl}_2/\text{MeOH}/\text{NH}_3(\text{aq}) = 90/9/1$): $R_f = 0.28$. ^1H NMR (CDCl_3 , 300 MHz): δ 2.56 (3H, s, NCH_3), 2.58–2.90 (4H, m, CH_2), 3.10–3.20 (2H, m, CH_2), 3.68 (1H, dd, $J_1 = 6.9$ Hz, $J_2 = 5.7$ Hz, CH), 3.86 (3H, s, OCH_3), 4.76 (1H, d, $J = 12.3$ Hz, PhCH_2O), 4.86 (1H, d, $J = 12.0$ Hz, PhCH_2O), 5.01 (2H, s, $\text{Ph-CH}_2\text{O}$), 6.13 (1H, s, Ar), 6.60 (1H, s, Ar), 6.69–6.88 (3H, m, Ar), 7.20 (1H, t, $J = 8.0$ Hz, Ar), 7.28–7.45 (10H, m, Ar). ^{13}C NMR (CDCl_3 , 75 MHz): δ 25.7, 41.1, 42.7, 47.0, 55.9, 64.6, 69.9, 70.8, 111.7, 112.3, 113.7, 116.4, 122.6, 126.5, 127.3, 127.5, 127.7, 127.9, 128.4, 128.6, 129.1, 129.4, 137.1, 137.1, 141.9, 145.6, 147.9, 158.7. MS (EI, 70 eV): $m/z = 478$ [(M - H)⁺, <1], 282 (100), 191 (30), 162 (18), 91 (37). HRMS: calcd for $\text{C}_{32}\text{H}_{32}\text{NO}_3$ [(M - H)⁺] 478.2382; found 478.2391.

1-(3-Benzyloxy-4-methoxybenzyl)-7-benzyloxy-6-methoxy-2-methyl-1,2,3,4-tetrahydroisoquinoline. Yield: 1.98 g (97%) as a yellowish liquid. TLC ($\text{CH}_2\text{Cl}_2/\text{MeOH}/\text{NH}_3(\text{aq}) = 90/9/1$): $R_f = 0.56$. ^1H NMR (CDCl_3 , 300 MHz): δ 2.47 (3H, s, NCH_3), 2.50–2.58 (1H, m, CH_2), 2.66–2.83 (3H, m, CH_2), 2.97–3.12 (2H, m, CH_2), 3.55 (1H, dd, $J_1 = 6.9$ Hz, $J_2 = 5.2$ Hz, CH), 3.85 (3H, s, OCH_3), 3.86 (3H, s, OCH_3), 4.80 (1H, d, $J = 12.3$ Hz, PhCH_2O), 4.87 (1H, d, $J = 12.3$ Hz, PhCH_2O), 5.07 (2H, s, $\text{Ph-CH}_2\text{O}$), 6.10 (1H, s, Ar), 6.55–6.57 (2H, m, Ar), 6.64 (1H, d, $J = 1.9$ Hz, Ar), 6.77 (1H, d, $J = 8.2$ Hz, Ar), 7.26–7.38 (8H, m, Ar), 7.42–7.45 (2H, m, Ar). ^{13}C NMR (CDCl_3 , 75 MHz): δ 25.8, 40.5, 42.7, 47.2, 55.9, 56.0, 64.6, 70.8, 70.9, 111.4, 111.6, 113.7, 115.7, 122.5, 126.8, 127.2, 127.3, 127.7, 127.7, 128.4, 128.5, 129.3, 132.4, 137.3, 145.6, 147.7, 147.8, 148.0. MS (EI, 70 eV): $m/z = 507$ [(M - 2H)⁺, <1], 282 (100), 191 (25), 162 (13), 91 (21). HRMS: calcd for $\text{C}_{33}\text{H}_{33}\text{NO}_4$ [(M - 2H)⁺] 507.2410; found 507.2435.

tert-Butyl 3,4-Dihydro-2(1H)-isoquinolinecarboxylate (14)^{22a}. A solution of di-tert-butyl dicarbonate (11.11 g, 50.9 mmol) in CH_2Cl_2 (20 mL) was added dropwise to a solution of 1,2,3,4-tetrahydroisoquinoline **13** (6.66 g, 50.0 mmol) in CH_2Cl_2 (30 mL). After stirring at room temperature for 2 h, the solvent was evaporated under reduced pressure to give 11.74 g (100%) of **14** as an orange liquid. TLC (petroleum ether/EtOAc = 3/1): $R_f = 0.62$. The ^1H NMR data are in accordance with literature.^{22a} ^{13}C NMR (CDCl_3 , 75 MHz): δ 28.5, 29.0, 40.7, 45.9, 85.2, 126.2, 126.3, 128.7, 134.8, 154.9. MS (EI, 70 eV): $m/z = 218$ [(M - CH_3)⁺, <1], 176 (100), 160 (24), 142 (9), 132 (70), 117 (13), 104 (52), 77 (13), 57 (78), 41 (22).

3-Benzyloxybenzyl bromide (16). A literature procedure⁴⁷ was adapted for our purpose: A solution of 3-benzyloxybenzyl alcohol **15** (8.01 g, 37.4 mmol) and tetrabromomethane (13.1 g, 39.4 mmol) in CH_2Cl_2 (60 mL) was cooled to 0 °C on an ice/NaCl bath.

Triphenylphosphine (10.22 g, 39.0 mmol) was added in portions to the stirred mixture, the cooling bath was removed, and the solution was stirred at room temperature for 2 h. The solvent was evaporated under reduced pressure, and the liquid residue was poured into well-stirred petroleum ether (100 mL), resulting in the formation of a white precipitate. The solid was removed by filtration and washed with petroleum ether (3 × 50 mL), and the filtrate was evaporated under reduced pressure to give 18.4 g of an orange liquid. Flash chromatography (silica; petroleum ether → petroleum ether/EtOAc = 9/1) afforded **16** (9.75 g, 94%) as a white crystalline solid. Mp: 54–55 °C (lit.⁴⁸ 37–39 °C). TLC (petroleum ether/EtOAc = 3/1): $R_f = 0.76$. The ^1H and ^{13}C NMR data are in accordance with literature.⁴⁸ MS (EI, 70 eV): $m/z = 276$ (M⁺, 8), 197 (15), 91 (100).

tert-Butyl 1-(3-Benzyloxybenzyl)-3,4-dihydro-2(1H)-isoquinolinecarboxylate (17). A literature procedure^{22a} was adapted for our purpose: A solution of tert-butyl 3,4-dihydro-2(1H)-carboxylate **14** (2.33 g, 10.0 mmol) and tetramethylethylenediamine (1.22 g, 10.5 mmol) in anhydrous THF under argon atmosphere was cooled to –78 °C. tert-Butyl lithium solution (1.7 M in pentane; 6.2 mL, 10.5 mmol) was added dropwise over 30 min, resulting in a deep red solution, which was stirred at –78 °C for 30 min. A solution of 3-benzyloxybenzyl bromide (**5**; 2.77 g, 10.0 mmol) in anhydrous THF (10 mL) was added dropwise over 30 min. The mixture was then stirred for 3 h, during which time the temperature was allowed to rise to –50 °C. The resulting yellow suspension was quenched with saturated NH_4Cl solution (10 mL). Water (30 mL) was added, the phases were separated, and the aqueous phase was extracted with tert-butyl methyl ether (2 × 20 mL). The combined organic phases were dried over Na_2SO_4 and the solvent was evaporated under reduced pressure to give 5.52 g of an orange liquid. Flash chromatography (silica; petroleum ether → petroleum ether/EtOAc = 95/5) afforded **17** (2.21 g, 51%) as a colorless liquid. TLC (petroleum ether/EtOAc = 3/1): $R_f = 0.59$. MS (EI, 70 eV): $m/z = 429$ (M⁺, <1), 232 (16), 176 (57), 132 (100), 91 (38). HRMS: calcd for $\text{C}_{28}\text{H}_{31}\text{NO}_3$ (M⁺) 429.2304; found 429.2333. The product is obtained as a mixture of rotamers (ratio *cis/trans* = 2/1), to which NMR signals are assigned based on the peak intensities as well as the DEPT, COSY, and HSQC spectra. *cis*-17: ^1H NMR (CDCl_3 , 300 MHz): δ 1.25 (9H, s, CH_3), 2.62–3.07 (4H, m, CH_2), 3.22–3.31 (1H, m, $\text{CH}_2\text{CH}_2\text{N}$), 4.19 (1H, ddd, $J_1 = 13.1$ Hz, $J_2 = 5.6$ Hz, $J_3 = 3.5$ Hz, $\text{CH}_2\text{CH}_2\text{N}$), 5.01 (2H, s, PhCH_2O), 5.22 (1H, dd, $J_1 = 8.2$ Hz, $J_2 = 5.6$ Hz, CH), 6.68–6.92 (3H, m, Ar), 7.03–7.19 (5H, m, Ar), 7.32–7.49 (5H, m, Ar). ^{13}C NMR (CDCl_3 , 75 MHz): δ 28.1 (CH_3), 28.5 (CH_2), 37.0 (CH_2), 43.0 (CH_2), 56.7 (CH), 69.9 (CH_2), 79.6 (C), 112.7 (CH), 116.3 (CH), 122.4 (CH), 125.9 (CH), 126.7 (CH), 127.3 (CH), 127.5 (CH), 127.9 (CH), 128.6 (CH), 129.1 (CH), 129.3 (CH), 134.8 (C), 137.0 (C), 137.1 (C), 140.2 (C), 154.4 (C), 158.8 (C). *trans*-17: ^1H NMR (CDCl_3 , 300 MHz): δ 1.42 (9H, s, CH_3), 2.62–3.07 (4H, m, CH_2), 3.22–3.31 (1H, m, $\text{CH}_2\text{CH}_2\text{N}$), 3.78 (1H, dt, $J_1 = 11.3$ Hz, $J_2 = 5.2$ Hz, $\text{CH}_2\text{CH}_2\text{N}$), 4.96 (2H, s, PhCH_2O), 5.38 (1H, t, $J = 6.7$ Hz, CH), 6.68–6.92 (3H, m, Ar), 7.03–7.19 (5H, m, Ar), 7.32–7.49 (5H, m, Ar). ^{13}C NMR (CDCl_3 , 75 MHz): δ 28.4 (CH_2), 28.6 (CH_3), 39.4 (CH_2), 42.7 (CH_2), 55.5 (CH), 69.8 (CH_2), 79.5 (C), 113.0 (CH), 116.0 (CH), 122.5 (CH), 125.9 (CH), 126.6 (CH), 127.3 (CH), 127.5 (CH), 127.9 (CH), 128.4 (CH), 129.0 (CH), 129.3 (CH), 134.6 (C), 137.0 (C), 137.2 (C), 139.8 (C), 154.7 (C), 158.6 (C).

1-(3-Benzyloxybenzyl)-2-methyl-1,2,3,4-tetrahydroisoquinoline (18). A solution of tert-butyl 1-(3-benzyloxybenzyl)-3,4-dihydro-2(1H)-isoquinolinecarboxylate **17** (3.55 g, 8.26 mmol) in anhydrous THF (160 mL) under argon atmosphere was cooled to 0 °C on an ice bath. LiAlH_4 (1.60 g, 42.2 mmol) was added in portions to the stirred solution; afterward the ice bath was removed and the mixture was refluxed for 16 h. The suspension was diluted with THF (50 mL) and cooled to 0 °C on an ice bath. Water (1.6 mL), 15% NaOH solution (1.6 mL), and again water (4.8 mL) were added to the vigorously stirred

mixture, the ice bath was removed, and stirring was continued for 1 h at room temperature. The resulting suspension was filtered through Celite, washed with THF, dried over Na_2SO_4 , and evaporated under reduced pressure to give 2.89 g of a yellow liquid. Flash chromatography (silica; $\text{CH}_2\text{Cl}_2/\text{MeOH}/\text{NH}_3(\text{aq}) = 98/1/1$) afforded **18** (2.09 g, 74%) as a yellowish liquid. TLC ($\text{CH}_2\text{Cl}_2/\text{MeOH}/\text{NH}_3(\text{aq}) = 90/9/1$): $R_f = 0.56$. ^1H NMR (CDCl_3 , 300 MHz): δ 2.54 (3H, s, NCH_3), 2.67–2.83 (2H, m, CH_2), 2.88–2.98 (2H, m, CH_2), 3.14–3.27 (2H, m, CH_2), 3.87 (1H, t, $J = 6.2$ Hz, CH), 5.04 (2H, s, PhCH_2O), 6.78–6.89 (4H, m, Ar), 7.06–7.24 (4H, m, Ar), 7.36–7.46 (5H, m, Ar). ^{13}C NMR (CDCl_3 , 75 MHz): δ 26.1, 41.5, 42.9, 47.1, 65.0, 69.9, 112.4, 116.2, 122.4, 125.4, 126.0, 127.6, 127.9, 128.0, 128.6, 128.8, 129.0, 134.4, 137.3, 137.9, 141.7, 158.6. MS (EI, 70 eV): $m/z = 342$ [(M – H) $^+$, <1], 146 (100), 131 (6), 91 (10). HRMS: calcd for $\text{C}_{24}\text{H}_{24}\text{NO}$ [(M – H) $^+$] 342.1858; found 342.1851.

Hydrogenolytic Deprotection Affording Tetrahydroisoquinolines 1a–g. A literature procedure²⁴ was adapted for our purpose: A mixture of benzyl-protected tetrahydroisoquinoline (5.75–9.16 mmol), Pd 10% on activated charcoal (0.20–0.30 g), acetic acid (12.5–20.0 mmol), and dry methanol (50 mL) was stirred under H_2 atmosphere (balloon) for 16 h. The mixture was filtered through Celite, washed with methanol (100 mL), and evaporated under reduced pressure. The residue was dissolved in CH_2Cl_2 (30 mL) and washed with half-saturated NaHCO_3 solution (40 mL). The organic phase was dried over Na_2SO_4 and evaporated under reduced pressure to afford pure **1a–g**.

6,7-Dimethoxy-1-(3-hydroxybenzyl)-2-methyl-1,2,3,4-tetrahydroisoquinoline (1a). Yield: 2.07 g (98%) as an off-white solid foam. Mp: 127–128 °C (lit.⁴⁹ 135 °C). TLC ($\text{CH}_2\text{Cl}_2/\text{MeOH}/\text{NH}_3(\text{aq}) = 90/9/1$): $R_f = 0.53$. The ^1H and ^{13}C NMR as well as MS data are in accordance with literature.^{19,50} HRMS: calcd for $\text{C}_{19}\text{H}_{22}\text{NO}_3$ [(M – H) $^+$] 312.1600; found 312.1589.

1-(3-Hydroxybenzyl)-6-methoxy-2-methyl-1,2,3,4-tetrahydroisoquinoline (1b). Yield: 1.53 g (94%) as an off-white solid foam. Mp = 113–116 °C. TLC ($\text{CH}_2\text{Cl}_2/\text{MeOH}/\text{NH}_3(\text{aq}) = 90/9/1$): $R_f = 0.51$. The ^1H and ^{13}C NMR as well as MS data are in accordance with literature.¹⁹ HRMS: calcd for $\text{C}_{18}\text{H}_{20}\text{NO}_2$ [(M – H) $^+$] 282.1494; found 282.1499.

1-(3-Hydroxybenzyl)-2-methyl-6,7,8-trimethoxy-1,2,3,4-tetrahydroisoquinoline (1c). Yield: 1.87 g (84%) as a highly viscous yellowish liquid. TLC ($\text{CH}_2\text{Cl}_2/\text{MeOH}/\text{NH}_3(\text{aq}) = 90/9/1$): $R_f = 0.51$. The ^1H and ^{13}C NMR as well as MS data are in accordance with literature.¹⁹ HRMS: calcd for $\text{C}_{20}\text{H}_{24}\text{NO}_4$ [(M – H) $^+$] 342.1705; found 342.1727.

1-(3-Hydroxybenzyl)-6,7-methylenedioxy-2-methyl-1,2,3,4-tetrahydroisoquinoline (1d). Yield: 2.19 g (81%) as a white solid foam. Mp: 143–145 °C (lit.⁴⁹ 145 °C). TLC ($\text{CH}_2\text{Cl}_2/\text{MeOH}/\text{NH}_3(\text{aq}) = 90/9/1$): $R_f = 0.45$. The ^1H and ^{13}C NMR as well as MS data are in accordance with literature.¹⁹ HRMS: calcd for $\text{C}_{18}\text{H}_{18}\text{NO}_3$ [(M – H) $^+$] 296.1287; found 296.1297.

1-(3-Hydroxybenzyl)-7-hydroxy-6-methoxy-2-methyl-1,2,3,4-tetrahydroisoquinoline (1e). Yield: 2.11 g (98%) as an off-white solid foam. Mp: 103–106 °C (lit.⁴⁹ 111–113 °C). TLC ($\text{CH}_2\text{Cl}_2/\text{MeOH}/\text{NH}_3(\text{aq}) = 90/9/1$): $R_f = 0.25$. The NMR data are in accordance with literature.⁵⁰ MS (EI, 70 eV): $m/z = 298$ [(M – H) $^+$, <1], 192 (100), 177 (19), 148 (5). MS (EI, 70 eV): $m/z = 298$ [(M – H) $^+$, <1], 192 (100), 177 (19), 148 (5). HRMS: calcd for $\text{C}_{18}\text{H}_{20}\text{NO}_3$ [(M – H) $^+$] 298.1443; found 298.1450.

Reticuline (1f). Yield: 0.90 g (70%) as an off-white solid foam. Mp: 83–84 °C. TLC ($\text{CH}_2\text{Cl}_2/\text{MeOH}/\text{NH}_3(\text{aq}) = 90/9/1$): $R_f = 0.29$. The NMR data are in accordance with literature.²⁴ MS (EI, 70 eV): $m/z = 328$ [(M – H) $^+$, <1], 192 (100), 177 (21). HRMS: calcd for $\text{C}_{19}\text{H}_{22}\text{NO}_4$ [(M – H) $^+$] 328.1549; found 328.1571.

1-(3-Hydroxybenzyl)-2-methyl-1,2,3,4-tetrahydroisoquinoline (1g). Yield: 1.25 g (94%) as an off-white solid foam. Mp: 129–130 °C. TLC ($\text{CH}_2\text{Cl}_2/\text{MeOH}/\text{NH}_3(\text{aq}) = 90/9/1$): $R_f = 0.47$. ^1H NMR (CDCl_3 , 300 MHz): δ 2.50 (3H, s, NCH_3), 2.73–3.05 (4H, m, CH_2), 3.17 (1H, dd, $J_1 = 13.8$ Hz, $J_2 = 6.0$ Hz, CH_2), 3.28–3.37 (1H, m, CH_2), 3.92 (1H, t, $J = 6.5$ Hz, CH), 6.60–6.63 (3H, m, Ar), 6.76 (1H, d, $J = 7.8$ Hz, Ar), 7.02–7.15 (4H, m, Ar). ^{13}C NMR (CDCl_3 , 75 MHz): δ 24.5 (CH_2), 41.7 (CH_2), 41.9 (CH_3), 46.0 (CH_2), 64.9 (CH), 113.9 (CH), 116.6 (CH), 121.1 (CH), 125.6 (CH), 126.4 (CH), 128.1 (CH), 128.9 (CH), 129.4 (CH), 133.2 (C), 136.8 (C), 140.9 (C), 156.7 (C). MS (EI, 70 eV): $m/z = 252$ [(M – H) $^+$, <1], 146 (100), 131 (7). HRMS: calcd for $\text{C}_{17}\text{H}_{18}\text{NO}$ [(M – H) $^+$] 252.1388; found 252.1403.

BBE-Catalyzed Kinetic Resolution of 1a–g.¹⁹ Substrate **1a–g** (500 mg, 1.5–2.0 mmol) was dissolved in toluene (17.5 mL) and buffer (7.5 mL, 10 mM Tris-HCl, pH 9.0, 10 mM MgCl_2) containing BBE (1.5 mL enzyme solution, final concentration = 1 g/L = 0.017 mM) and crude catalase (125 mg, final concentration 5 g/L). The mixture was shaken in a light-shielded round-bottom flask (50 mL) at 200 rpm and 40 °C for 24 h. The reaction was stopped by phase separation, followed by extraction of the aqueous phase with ethyl acetate (3 × 10 mL). The combined organic phases were dried over Na_2SO_4 and evaporated under reduced pressure to give the crude product. Flash chromatography (silica; a–f, $\text{CH}_2\text{Cl}_2/\text{MeOH}/\text{NH}_3(\text{aq}) = 96/3/1$; g, $\text{CH}_2\text{Cl}_2/\text{MeOH}/\text{NH}_3(\text{aq}) = 98/1/1$) afforded pure (S)-**2a–g** and (R)-**1a–g**.

(S)-2,3-Dimethoxy-9-hydroxyberbine (S)-2a. Yield: 207 mg (42%) as an off-white solid foam. Mp: 90–95 °C. TLC ($\text{CH}_2\text{Cl}_2/\text{MeOH}/\text{NH}_3(\text{aq}) = 90/9/1$): $R_f = 0.78$. $[\alpha]_D^{20} = -273.4$ (CHCl_3 , $c = 1.0$); lit.⁵⁰ (R) +176 (MeOH, $c = 0.34$). The ^1H and ^{13}C NMR as well as MS data are in accordance with literature.^{19,50} HRMS: calcd for $\text{C}_{19}\text{H}_{21}\text{NO}_3$ 311.1521; found 311.1519.

(R)-6,7-Dimethoxy-1-(3-hydroxybenzyl)-2-methyl-1,2,3,4-tetrahydroisoquinoline (R)-1a. Yield: 249 mg (50%) as an off-white solid foam. Mp: 151–153 °C. TLC ($\text{CH}_2\text{Cl}_2/\text{MeOH}/\text{NH}_3(\text{aq}) = 90/9/1$): $R_f = 0.53$. $[\alpha]_D^{20} = -109.4$ (CHCl_3 , $c = 1.0$). The ^1H and ^{13}C NMR as well as MS data are in agreement with those obtained for the racemic compound. HRMS: calcd for $\text{C}_{19}\text{H}_{22}\text{NO}_3$ [(M – H) $^+$] 312.1600; found 312.1591. The NMR data are in accordance with literature.⁵⁰

(S)-9-Hydroxy-3-methoxyberbine (S)-2b. Yield: 177 mg (36%) as an off-white solid foam. Mp: 192–195 °C. TLC ($\text{CH}_2\text{Cl}_2/\text{MeOH}/\text{NH}_3(\text{aq}) = 90/9/1$): $R_f = 0.56$. $[\alpha]_D^{20} = -280.6$ (CHCl_3 , $c = 0.5$). The ^1H and ^{13}C NMR as well as MS data are in accordance with literature.¹⁹ HRMS: calcd for $\text{C}_{18}\text{H}_{19}\text{NO}_2$ 281.1416; found 281.1415.

(R)-1-(3-Hydroxybenzyl)-6-methoxy-2-methyl-1,2,3,4-tetrahydroisoquinoline (R)-1b. Yield: 181 mg (36%) as a highly viscous yellowish liquid. TLC ($\text{CH}_2\text{Cl}_2/\text{MeOH}/\text{NH}_3(\text{aq}) = 90/9/1$): $R_f = 0.47$. $[\alpha]_D^{20} = -76.3$ (CHCl_3 , $c = 0.63$). The ^1H and ^{13}C NMR as well as MS data are in agreement with those obtained for the racemic compound. HRMS: calcd for $\text{C}_{18}\text{H}_{20}\text{NO}_2$ [(M – H) $^+$] 282.1494; found 282.1504.

(S)-9-Hydroxy-1,2,3-trimethoxyberbine (S)-2c. Yield: 194 mg (39%) as an off-white solid foam. Mp: 85–89 °C. TLC ($\text{CH}_2\text{Cl}_2/\text{MeOH}/\text{NH}_3(\text{aq}) = 90/9/1$): $R_f = 0.60$. $[\alpha]_D^{20} = -226.5$ (CHCl_3 , $c = 0.57$). The ^1H and ^{13}C NMR as well as MS data are in accordance with literature.¹⁹ HRMS: calcd for $\text{C}_{20}\text{H}_{23}\text{NO}_4$ 341.1627; found 341.1623.

(R)-1-(3-Hydroxybenzyl)-2-methyl-6,7,8-trimethoxy-1,2,3,4-tetrahydroisoquinoline (R)-1c. Yield: 237 mg (47%) as highly viscous yellowish liquid. TLC ($\text{CH}_2\text{Cl}_2/\text{MeOH}/\text{NH}_3(\text{aq}) = 90/9/1$): $R_f = 0.33$. $[\alpha]_D^{20} = -75.4$ (CHCl_3 , $c = 0.75$). The ^1H and ^{13}C NMR as well as MS data are in agreement with those obtained for the racemic compound. HRMS: calcd for $\text{C}_{20}\text{H}_{24}\text{NO}_4$ [(M – H) $^+$] 342.1705; found 342.1703.

(S)-9-Hydroxy-2,3-methylenedioxyberbine (S)-2d. Yield: 155 mg (31%) as an off-white solid foam. Mp: 177–180 °C. TLC ($\text{CH}_2\text{Cl}_2/\text{MeOH}/\text{NH}_3(\text{aq}) = 90/9/1$): $R_f = 0.50$. $[\alpha]_D^{20} = -342.5$ (CHCl_3 , $c = 0.63$). The ^1H and ^{13}C NMR as well as MS data are in accordance with literature.¹⁹ HRMS: calcd for $\text{C}_{18}\text{H}_{17}\text{NO}_3$ 295.1208; found 295.1209.

(R)-1-(3-Hydroxybenzyl)-6,7-methylenedioxy-2-methyl-1,2,3,4-tetrahydroisoquinoline (R)-1d. Yield: 231 mg (46%) as an off-white solid foam. Mp: 165–167 °C. TLC ($\text{CH}_2\text{Cl}_2/\text{MeOH}/\text{NH}_3(\text{aq}) = 90/9/1$): $R_f = 0.38$. $[\alpha]_D^{20} = -83.2$ (CHCl_3 , $c = 0.31$). The ^1H and ^{13}C NMR as well as MS data are in agreement with those obtained for the racemic compound. HRMS: calcd for $\text{C}_{18}\text{H}_{18}\text{NO}_3$ [(M - H)⁺] 296.1287; found 296.1303.

(S)-2,9-Dihydroxy-3-methoxyberbine (S)-2e. Yield: 129 mg (22%) as an off-white solid foam. Mp: 135 °C (decomp.). TLC ($\text{CH}_2\text{Cl}_2/\text{MeOH}/\text{NH}_3(\text{aq}) = 90/9/1$): $R_f = 0.63$. $[\alpha]_D^{20} = -281.5$ (CHCl_3 , $c = 0.28$); lit.⁵⁰ $[\alpha]_D^{20} = -129.0$ (CHCl_3 , $c = 0.3$). The ^1H and ^{13}C NMR data are in accordance with literature.⁵⁰ MS (EI, 70 eV): $m/z = 297$ (M⁺, 100), 296 (92), 282 (15), 178 (60), 176 (82), 163 (16), 149 (19), 120 (24), 86 (52). HRMS: calcd for $\text{C}_{18}\text{H}_{19}\text{NO}_3$ 297.1365; found 297.1373.

(R)-1-(3-Hydroxybenzyl)-7-hydroxy-6-methoxy-2-methyl-1,2,3,4-tetrahydroisoquinoline (R)-1e. Yield: 247 mg (49%) as an off-white solid foam. Mp: 89–90 °C. TLC ($\text{CH}_2\text{Cl}_2/\text{MeOH}/\text{NH}_3(\text{aq}) = 90/9/1$): $R_f = 0.39$. $[\alpha]_D^{20} = -29.1$ (CHCl_3 , $c = 0.36$); lit.⁵⁰ (S): +43 (MeOH, $c = 0.5$). The ^1H and ^{13}C NMR as well as MS data are in agreement with those obtained for the racemic compound. HRMS: calcd for $\text{C}_{18}\text{H}_{20}\text{NO}_3$ [(M - H)⁺] 298.1443; found 298.1453. The NMR data are in accordance with literature.⁵⁰

(S)-Scoulerine (S)-2f. Yield: 232 mg (47%) as an off-white solid foam. Mp: 194–195 °C. TLC ($\text{CH}_2\text{Cl}_2/\text{MeOH}/\text{NH}_3(\text{aq}) = 90/9/1$): $R_f = 0.49$. $[\alpha]_D^{20} = -248.3$ (CHCl_3 , $c = 0.27$); lit.⁵¹ $[\alpha]_D^{20} = -315$ (MeOH, $c = 0.11$). ^1H NMR (CDCl_3 , 300 MHz): δ 2.63–2.70 (2H, m, CH_2), 2.83 (1H, dd, $J_1 = 15.9$ Hz, $J_2 = 11.4$ Hz, CH_2), 3.11–3.28 (3H, m, CH_2), 3.49–3.57 (2H, m, N- CH_2 -Ar + CH), 3.87 (3H, s, OCH_3), 3.88 (3H, s, OCH_3), 4.25 (1H, d, $J = 15.6$ Hz, N- CH_2 -Ar), 6.61 (1H, s, Ar), 6.68 (1H, d, $J = 8.3$ Hz, Ar), 6.75 (1H, d, $J = 8.3$ Hz, Ar), 6.84 (1H, s, Ar). ^{13}C NMR (CHCl_3 , 75 MHz): δ 29.2 (CH_2), 36.3 (CH_2), 51.6 (CH_2), 53.5 (CH_2), 55.9 (CH_2), 56.2 (CH_3), 59.2 (CH), 109.0 (CH), 110.6 (CH), 111.4 (CH), 119.3 (CH), 121.2 (C), 126.1 (C), 128.2 (C), 130.6 (C), 141.5 (C), 143.9 (C), 144.0 (C), 145.1 (C). MS (EI, 70 eV): $m/z = 327$ (M⁺, 55), 310 (8), 178 (100), 176 (32), 163 (13), 150 (48), 135 (27), 107 (16). HRMS: calcd for $\text{C}_{19}\text{H}_{21}\text{NO}_4$ 327.1471; found 327.1490.

(R)-Reticuline (R)-1f. Yield: 182 mg (37%) as an off-white solid foam. Mp: 74–75 °C. TLC ($\text{CH}_2\text{Cl}_2/\text{MeOH}/\text{NH}_3(\text{aq}) = 90/9/1$): $R_f = 0.29$. $[\alpha]_D^{20} = -64.6$ (CHCl_3 , $c = 0.26$); lit.⁵² $[\alpha]_D^{20} = -55$ (EtOH, $c = 0.44$). The ^1H and ^{13}C NMR as well as MS data are in agreement with those obtained for the racemic compound. HRMS: calcd for $\text{C}_{19}\text{H}_{22}\text{NO}_4$ [(M - H)⁺] 328.1549; found 328.1600. The NMR data are in accordance with literature.²⁴

(S)-9-Hydroxyberbine (S)-2g. Yield: 230 mg (46%) as an off-white solid foam. Mp: 103–104 °C. TLC ($\text{CH}_2\text{Cl}_2/\text{MeOH}/\text{NH}_3(\text{aq}) = 90/9/1$): $R_f = 0.58$. $[\alpha]_D^{20} = -328.8$ (CHCl_3 , $c = 1.0$). ^1H NMR (CDCl_3 , 300 MHz): δ 2.55–2.71 (2H, m, CH_2), 2.86 (1H, dd, $J_1 = 16.3$ Hz, $J_2 = 11.5$ Hz, CH_2), 3.10–3.20 (2H, m, CH_2), 3.26 (1H, dd, $J_1 = 16.5$ Hz, $J_2 = 3.7$ Hz, CH_2), 3.36 (1H, d, $J = 15.6$ Hz, N- CH_2 -Ar), 3.62 (1H, dd, $J_1 = 11.2$ Hz, $J_2 = 3.3$ Hz, CH), 4.09 (1H, d, $J = 15.6$ Hz, N- CH_2 -Ar), 6.21 (1H, d, $J = 7.9$ Hz, Ar), 6.58 (1H, d, $J = 7.6$ Hz, Ar), 6.78 (1H, t, $J = 7.8$ Hz, Ar), 7.04–7.21 (3H, m, Ar). ^{13}C NMR ($\text{DMSO}-d_6$, 75 MHz): δ 29.1 (CH_2), 36.2 (CH_2), 51.3 (CH_2), 53.6 (CH_2), 59.4 (CH), 112.5 (CH), 120.5 (CH), 121.8 (C), 125.5 (CH), 126.1 (CH), 126.3 (CH), 126.8 (CH), 128.9 (CH), 134.4 (C), 135.9 (C), 137.5 (C), 152.4 (C). MS (EI, 70 eV): $m/z = 251$ (M⁺, 70), 132 (100), 130 (50), 130 (32), 91 (27). HRMS: calcd for $\text{C}_{17}\text{H}_{17}\text{NO}$ 251.1310; found 251.1308.

(R)-1-(3-Hydroxybenzyl)-2-methyl-1,2,3,4-tetrahydroisoquinoline (R)-1g. Yield: 247 mg (49%) as an off-white solid foam. Mp: 110–111 °C. TLC ($\text{CH}_2\text{Cl}_2/\text{MeOH}/\text{NH}_3(\text{aq}) = 90/9/1$): $R_f = 0.45$. $[\alpha]_D^{20} = -58.4$ (CHCl_3 , $c = 1.0$). The ^1H and ^{13}C NMR as well as MS data are in agreement with those obtained for the racemic compound. HRMS: calcd for $\text{C}_{17}\text{H}_{17}\text{NO}$ [(M - 2H)⁺]: 251.1310; found 251.1338.

Determination of Absolute Configuration. Absolute configurations of benzyloisoquinolines 1a–g and berbines 2a–g were assigned based on optical rotation, circular dichroism, and HPLC elution order analogies as previously described.¹⁹

Preparation of Racemic Reference Samples for Chiral HPLC Analysis. Racemic samples of berbines 2a–g for use as HPLC reference were prepared as previously described.¹⁹

Enzyme Expression and Purification. BBE expression was carried out in a 7 L glass fermenter according to the following protocol: *Preparation of Inoculum.* Overnight cultures (ONCs) of *Pichia pastoris* colonies containing the BBE expression plasmid [pPICZα-BBE-ER] were grown in 50 mL of YPD medium containing 100 μg/mL zeocin (in 300 mL Erlenmeyer flasks) at 30 °C and 150 rpm for 20 h. The ONC was used to inoculate 300 mL of YPD medium (in 2 L baffled Erlenmeyer flasks) to an initial OD₆₀₀ of 1.0. The cultures were grown to an OD₆₀₀ of 10–15 at 30 °C and 150 rpm.

Preparation of Fermenter. Feeding flasks and tubing for base, antifoam, glycerol, and methanol addition as well as inoculum flasks were autoclaved. The fermenter was equipped with a calibrated pH electrode, a pO₂ electrode, and a sampling nozzle, filled with fermentation basal salts medium (3.5 L, see below), sterilized, and cooled to 30 °C. Trace salts solution (15 mL, for composition see below) and antifoam (Struktol J650, 1:10 dilution; 100 mL) were added, and the pH was adjusted to 5.0 by addition of 25% aqueous ammonia. The pO₂ electrode was calibrated using N₂ and air saturation for adjusting the 0% and 100% values, respectively.

Inoculation and Glycerol Batch Phase. The fermenter was inoculated with the shaking flask culture (300 mL, the initial OD₆₀₀ in the fermenter should be 1.0), and the batch was stirred overnight with automatic control of pO₂ ($\geq 30\%$), pH (pH 5.0) and temperature (30 °C). The next morning, the culture had consumed all glycerol present in the medium (as indicated by a sharp rise in the pO₂ value).

Glycerol Fed-Batch Phase. A glycerol feed (50% w/v; containing 12 mL/L of trace salts solution) was started with an initial feed rate of 15 g/h, causing the pO₂ to drop. After about 5 min, when the pO₂ had reached again a value above 30%, the feed rate was raised continuously to 30 g/h over 30 min. Three hours later, the feed rate was raised continuously to 45 g/h over 30 min. This feed rate was maintained overnight. The next morning, 1000 g of 50% glycerol had been added in total. A sample was taken and analyzed for wet cell weight (WCW). A WCW of 280 g/L was reached at the end of the glycerol batch-phase.

Methanol Fed-Batch Phase (Induction Phase). After approximately 1000 g of glycerol had been added, methanol adaptation was started by pumping 5 g of methanol feed (HPLC grade, methanol containing 12 mL/L of trace salts solution) into the fermenter. Subsequently, the glycerol feed was continuously reduced to 15 g/h over 1 h 59 min and finally reduced to zero within 1 min. During these 2 h of decrease of glycerol feed, the pH value was raised to 6.0 by addition of base. This pH adjustment is crucial for protein expression. As soon as the glycerol feed had been stopped, the methanol feed was started with an initial feed rate of 3 g/h. During the next 12 h, the feed rate was slowly raised to 9 g/h in several steps. This rate was maintained until the end of fermentation. Samples were taken every 24 h and analyzed for WCW and BBE activity. The activity rose over time, while the WCW stayed constant. After addition of 750 g of methanol in total (96 h of induction), pH and pO₂ control were disabled, and (NH₄)₂SO₄ was added to the batch to a final concentration of 1 M. The culture was aliquoted into centrifuge beakers (1 L), and the cells were pelleted by centrifugation (4000 rpm,

30 min, 4 °C). The supernatant was subjected to protein purification (see below).

Protein Purification. Hydrophobic Interaction Chromatography (HIC). The fermentation supernatant was loaded onto a Phenyl Sepharose column (XK50/20, Phenyl Sepharose 6 High Sub) equilibrated with HIC start buffer (50 mM $K_2HPO_4 \cdot 3H_2O$, 1 M $(NH_4)_2SO_4$, pH 7.5; filtered and degassed) with maximum flow rate and the column was washed with HIC start buffer until absorption (280, 375, 450 nm) and conductivity readings were constant. BBE was eluted using a gradient of HIC start buffer against 20% aqueous ethanol (100% start buffer to 50% in 25 min; 50% to 20% in 60 min; 20% to 0% start buffer in 60 min) and a flow rate of 6 mL/min. Fractions of 12 mL were collected, activity assays were performed and the active fractions were pooled and concentrated using the Centriprep centrifugal filtration system.

Gel Filtration (GF). The pooled and concentrated fractions from HIC were loaded onto a Superdex 200 column (XK16/100, Superdex 200, prep grade) equilibrated with GF buffer (100 mM Tris-HCl, 150 mM NaCl, pH 8.0; filtered and degassed) using a 3 mL sample loop. BBE was eluted with GF buffer at a flow rate of 1 mL/min. Fractions of 3 mL were collected, activity assays were performed and the active fractions were pooled and concentrated as above. The protein solution was flash frozen by dripping into liquid nitrogen.

Activity Assay. A mixture of *rac*-reticuline solution (4 μ L, 10 mM in reaction buffer/DMSO = 9/1), 4 μ L BBE solution (protein purification fraction, fermentation supernatant, etc.), and BBE assay buffer (17 μ L, 100 mM Tris-HCl, pH 9.0) were incubated at 37 °C for 10 min. The reaction was analyzed by TLC (silica; $CH_2Cl_2/MeOH/NH_4OH = 90/9/1$; visualization by UV irradiation).

Media and Feed Solutions. YPD Medium (for 1 L). Bacto yeast extract (10 g) and Bacto peptone (20 g) were dissolved and autoclaved in 900 mL of H_2O ; glucose (20 g) was dissolved and autoclaved in 100 mL of H_2O . The two solutions were mixed after autoclaving.

Basal Salts Medium (according to Hartner & Winkler; 3.5 L). A total of 0.6 g $CaSO_4 \cdot 2H_2O$, 8.1 g $MgSO_4 \cdot 7H_2O$, 10 g K_2SO_4 , 7 g KOH, 0.77 g NaCl, 112.8 g glycerol, 44.6 mL phosphoric acid, and water (bidest.) ad 3500 mL.

Trace Salts Solution (200 mL). Dissolve 40 mg biotin, 16 mg NaI, 40 mg $Na_2MoO_4 \cdot 2H_2O$, 4 mg H_3BO_3 , and 146 mg $CoCl_2 \cdot 6H_2O$ in 100 mL H_2O (bidest.). Additionally, 1.2 g $CuSO_4 \cdot 5H_2O$, 590 mg $MnCl_2 \cdot 4H_2O$, 4 g $ZnCl_2$, 13 g $FeSO_4 \cdot 7H_2O$ and 1 mL H_2SO_4 (conc) are dissolved in 100 mL H_2O (bidest.). The two solutions were mixed, filter-sterilized, and stored at 4 °C.

Glycerol Feed (1.5 L). Mix 750 g glycerol, water (bidest.) ad 1500 mL; autoclave, add 18 mL trace salts solution.

Methanol Feed (1.5 L). Mix 1.5 L HPLC grade MeOH and 18 mL trace salts solution.

Base (400 mL). Ammonium hydroxide 25% solution.

Fermenter Settings. Temperature. Setpoint: 30 °C, Mode: AUTO
Stirrer. Mode: CASC, Min: 25% (= 500 rpm), Max: 75% (= 1500 rpm), Ramp: 20%/sec

pH. Setpoint: 5.00, Mode: Auto, Pump: ---/BASE

pO_2 . Setpoint: 30%, Mode: AUTO, CASC: STIRR AIRFL, Parameter: HTTime: 1 min, Dead: 0.5%, Stirr Min: 25%, Stirr Max: 75%, Airfl Min: 25%, Airfl Max: 100%

Foam. Mode: AUTO, Pump: AFOAM, Cycle: 0:10 m:s

Airflow. Mode: CASC, Min: 25% (= 2.5 L/min), Max: 100% (= 10 L/min)

■ ASSOCIATED CONTENT

Supporting Information. General experimental information; analytical methods; 1H and ^{13}C NMR spectra, MS spectra, and HRMS results of new compounds. This material is available free of charge via the Internet at <http://pubs.acs.org>.

■ AUTHOR INFORMATION

Corresponding Author

*E-mail: wolfgang.kroutil@uni-graz.at.

■ ACKNOWLEDGMENT

This study was financed by the Austrian Science Fund (FWF Project P20903-N17 and P22115-N17). The authors would like to thank Bernd Werner for acquiring the NMR spectra. Financial support by NAWI Graz is acknowledged.

■ REFERENCES

- (1) Bentley, K. W. *The Isoquinoline Alkaloids*; Harwood Academic Publishers: Amsterdam, 1998.
- (2) (a) Martin, M. L.; Diaz, M. T.; Montero, M. J.; Prieto, P.; Roman, L. S.; Cortes, D. *Planta Med.* **1993**, *59*, 63–67. (b) Chulia, S.; Ivorra, M. D.; Lugnier, C.; Vila, E.; Noguera, M. A.; D'Ocon, P. *Br. J. Pharmacol.* **1994**, *113*, 1377–1385. (c) Kashiwada, Y.; Aoshima, A.; Ikeshiro, Y.; Chen, Y.-P.; Furukawa, H.; Itoigawa, M.; Sawada, T. *Chem. Pharm. Bull.* **1976**, *24*, 1909–1912. (d) Jang, S. I.; Kim, B. H.; Lee, W.-Y.; An, S. J.; Choi, H. G.; Jeon, B. H.; Chung, H.-T.; Rho, J.-R.; Kim, Y.-J.; Chai, K.-Y. *Arch. Pharm. Res.* **2004**, *27*, 923–929.
- (3) (a) Gao, J.-M.; Liu, W.-T.; Li, M.-L.; Liu, H.-W.; Zhang, X.-C.; Li, Z.-X. *J. Mol. Struct.* **2008**, *892*, 466–469 and references therein. (b) Ko, F. N.; Guh, J. H.; Yu, S. M.; Hou, Y. S.; Wu, Y. C.; Teng, C. M. *Br. J. Pharmacol.* **1994**, *112*, 1174–1180. (c) Eisenreich, W. J.; Hofner, G.; Bracher, F. *Nat. Prod. Res.* **2003**, *17*, 437–440. (d) Yamahara, J.; Konoshima, T.; Sakakibara, Y.; Ishiguro, M.; Sawada, T. *Chem. Pharm. Bull.* **1976**, *24*, 1909–1912. (e) Jang, S. I.; Kim, B. H.; Lee, W.-Y.; An, S. J.; Choi, H. G.; Jeon, B. H.; Chung, H.-T.; Rho, J.-R.; Kim, Y.-J.; Chai, K.-Y. *Arch. Pharm. Res.* **2004**, *27*, 923–929.
- (4) Li, J.; Jin, G.; Shen, J.; Ji, R. *Drugs Fut.* **2006**, *31*, 379–384.
- (5) Chakka, S. K.; Andersson, P. G.; Maguire, G. E. M.; Kruger, H. G.; Govender, T. *Eur. J. Org. Chem.* **2010**, 972–980.
- (6) For a review see Chrzanoska, M.; Rozwadowska, M. *D. Chem. Rev.* **2004**, *104*, 3341–3370.
- (7) (a) Meyers, A. I. *Tetrahedron* **1992**, *48*, 2589–2612. (b) Meyers, A. I.; Nguyen, T. H. *Heterocycles* **1994**, *39*, 513–518. (c) Matulenko, M. A.; Meyers, A. I. *J. Org. Chem.* **1996**, *61*, 573–580.
- (8) (a) Noyori, R.; Ohta, M.; Hsiao, Y.; Kitamura, M.; Ohta, T.; Takaya, H. *J. Am. Soc. Chem.* **1986**, *108*, 7117–7119. (b) Kitamura, M.; Hsiao, Y.; Ohta, M.; Tsukamoto, M.; Ohta, T.; Takaya, H.; Noyori, R. *J. Org. Chem.* **1994**, *59*, 297–310. (c) Mujahidin, D.; Doye, S. *Eur. J. Org. Chem.* **2005**, 2689–2693. (d) Lu, S.-M.; Wang, Y.-Q.; Han, X.-W.; Zhou, Y.-G. *Angew. Chem., Int. Ed.* **2006**, *45*, 2260–2263. (e) Yan, P.-C.; Xie, J.-H.; Hou, G.-H.; Wang, L.-X.; Zhou, Q.-L. *Adv. Synth. Catal.* **2009**, *351*, 3243–3250.
- (9) (a) Ito, K.; Akashi, S.; Saito, B.; Katsuki, T. *Synlett* **2003**, 1809–1812. (b) Shi, C.; Ojima, I. *Tetrahedron* **2007**, *63*, 8563–8570. (c) Teichert, J. F.; Fañanás-Mastral, M.; Feringa, B. L. *Angew. Chem., Int. Ed.* **2011**, *50*, 688–691.
- (10) (a) Ukaji, Y.; Shimizu, Y.; Kenmoku, Y.; Ahmed, A.; Inomata, K. *Bull. Chem. Soc. Jpn.* **2000**, *73*, 447–452. (b) Sasamoto, N.; Dubs, C.; Hamashima, Y.; Sodeoka, M. *J. Am. Chem. Soc.* **2006**, *128*, 14010–14011. (c) Dubs, C.; Hamashima, Y.; Sasamoto, N.; Seidel, T. M.; Suzuki, S.; Hashizume, D.; Sodeoka, M. *J. Org. Chem.* **2008**, *73*, 5859–5871. (d) Taylor, A. M.; Schreiber, S. L. *Org. Lett.* **2006**, *8*, 143–146. (e) Itoh, T.; Miyazaki, M.; Fukuoka, H.; Nagata, K.; Ohsawa, A. *Org. Lett.* **2006**, *8*, 1295–1297. (f) Wang, S.; Seto, C. T. *Org. Lett.* **2006**, *8*, 3979–3982. (g) Li, Z.; MacLeod, P. D.; Li, C.-J. *Tetrahedron: Asymmetry* **2006**, *17*, 590–597. (h) Kanemitsu, T.; Yamashita, Y.; Nagata, K.; Itoh, T. *Synlett* **2006**, 1595–1597.
- (11) Barton, D. H. R.; Kirby, G. W.; Steglich, W.; Thomas, G. M.; Battersby, A. R.; Dobson, T. A.; Ramuz, H. J. *Chem. Soc.* **1965**, 2423–2438.
- (12) Cui, W.; Iwasa, K.; Sugiura, M.; Takeuchi, A.; Tode, C.; Nishiyama, Y.; Moriyasu, M.; Tokuda, H.; Takeda, K. *J. Nat. Prod.* **2007**, *70*, 1771–1778.

- (13) (a) Hawkins, K. M.; Smolke, C. D. *Nat. Chem. Biol.* **2008**, *4*, 564–573. (b) Minami, H.; Kim, J.-S.; Ikezawa, N.; Takemura, T.; Katayama, T.; Kumagai, H.; Sato, F. *Proc. Natl. Acad. Sci. U.S.A.* **2008**, *105*, 7393–7398.
- (14) (a) Savile, C. K.; Janey, J. M.; Mundorff, E. C.; Moore, J. C.; Tam, S.; Jarvis, W. R.; Colbeck, J. C.; Krebber, A.; Fleitz, F. J.; Brands, J.; Devine, P. N.; Huisman, G. W.; Hughes, G. J. *Science* **2010**, *329*, 305–309. (b) Fischer, T.; Pietruszka, J. *Top. Curr. Chem.* **2010**, *297*, 1–43. (c) Woodley, J. M. *Trends Biotechnol.* **2008**, *26*, 321–327. (d) *Biocatalysis in the Pharmaceutical and Biotechnology Industry*; Patel, R. N., Ed.; CRC Press: Boca Raton, 2007. (e) Schoemaker, H. E.; Mink, D.; Wubbolts, M. G. *Science* **2003**, *299*, 1694–1697.
- (15) (a) Resch, V.; Schrittwieser, J. H.; Siirola, E.; Kroutil, W. *Curr. Opin. Biotechnol.* **2011**, Epub ahead of print, doi:10.1016/j.copbio.2011.02.002. (b) Clapés, P.; Fessner, W.-D.; Sprenger, G. A.; Samland, A. K. *Curr. Opin. Chem. Biol.* **2010**, *14*, 154–167. (c) Holt, J.; Hanefeld, U. *Curr. Org. Synth.* **2009**, *6*, 15–37. (d) *Industrial Processes Using Lyases for C–C, C–N, and C–O Bond Formation*; Pohl, M.; Liese, A. in *Biocatalysis in the Pharmaceutical and Biotechnology Industry*; Patel, R. N., Ed.; CRC Press: Boca Raton, 2007, pp 661–676.
- (16) Facchini, P. J. *Annu. Rev. Plant Physiol. Plant Mol. Biol.* **2001**, *52*, 29–66.
- (17) (a) Winkler, A.; Lyskowski, A.; Riedl, S.; Puhl, M.; Kutchan, T. M.; Macheroux, P.; Gruber, K. *Nat. Chem. Biol.* **2008**, *4*, 739–741. (b) Winkler, A.; Kutchan, T. M.; Macheroux, P. *J. Biol. Chem.* **2007**, *282*, 24437–24443.
- (18) (a) Winkler, A.; Hartner, F.; Kutchan, T. M.; Glieder, A.; Macheroux, P. *J. Biol. Chem.* **2006**, *281*, 21276–21285. (b) Winkler, A.; Motz, K.; Riedl, S.; Puhl, M.; Macheroux, P.; Gruber, K. *J. Biol. Chem.* **2009**, *284*, 19993–20001.
- (19) Schrittwieser, J. H.; Resch, V.; Sattler, J. H.; Lienhart, W.-D.; Durchschein, K.; Winkler, A.; Gruber, K.; Macheroux, P.; Kroutil, W. *Angew. Chem., Int. Ed.* **2011**, *50*, 1068–1071.
- (20) For reviews, see: (a) Cox, E. D.; Cook, J. M. *Chem. Rev.* **1995**, *95*, 1797–1842. (b) Whaley, W. M.; Govindachari, T. R. *Org. React.* **1951**, *6*, 151–190. For recent examples, see: (c) Znabet, A.; Zonneveld, J.; Janssen, E.; De Kanter, F. J. J.; Helliwell, M.; Turner, N. J.; Ruijter, E.; Orru, R. V. A. *Chem. Commun.* **2010**, *46*, 7706–7708. (d) Barbero, M.; Bazzi, S.; Cadamuro, S.; Dughera, S. *Tetrahedron Lett.* **2010**, *51*, 6356–6359. (e) Razafindrabe, C. R.; Aubry, S.; Bourdon, B.; Andriantsiferana, M.; Pellet-Rostaing, S.; Lemaire, M. *Tetrahedron* **2010**, *66*, 9061–9066. (f) Awuah, E.; Capretta, A. J. *Org. Chem.* **2010**, *75*, 5627–5634. (g) Magnus, N. A.; Ley, C. P.; Pollock, P. M.; Wepsiec, J. P. *Org. Lett.* **2010**, *12*, 3700–3703.
- (21) For a review, see: (a) Whaley, W. M.; Govindachari, T. R. *Org. React.* **1951**, *6*, 74–150. For mechanistic investigations, see: (b) Fodor, G.; Gal, J.; Phillips, B. A. *Angew. Chem., Int. Ed.* **1972**, *11*, 919–920. (c) Fodor, G.; Nagubandi, S. *Tetrahedron* **1980**, *36*, 1279–1300. For recent examples, see: (d) Zein, A. L.; Dawe, L. N.; Georghiou, P. E. *J. Nat. Prod.* **2010**, *73*, 1427–1430. (e) Zein, A. L.; Dakhil, O. O.; Dawe, L. N.; Georghiou, P. E. *Tetrahedron Lett.* **2010**, *51*, 177–180. (f) Sobarzo-Sánchez, E.; Uriarte, E.; Santana, L.; Tapia, R. A.; Lourido, P. P. *Helv. Chim. Acta* **2010**, *93*, 1385–1394. (g) Jadhav, V. B.; Nayak, S. K.; Row, T. N. G.; Kulkarni, M. V. *Eur. J. Med. Chem.* **2010**, *45*, 3575–3580. (h) Bringmann, G.; Gulder, T.; Hertlein, B.; Hemberger, Y.; Meyer, F. J. *Am. Chem. Soc.* **2010**, *132*, 1151–1158. (i) Zein, A. L.; Dakhil, O. O.; Dawe, L. N.; Georghiou, P. E. *Tetrahedron Lett.* **2010**, *51*, 177–180.
- (22) (a) Coppola, G. M. J. *Heterocycl. Chem.* **1991**, *28*, 1769–1772. (b) Azzena, U.; Pisano, L.; Pittalis, M. *Heterocycles* **2004**, *63*, 401–409. (c) Tokitoh, N.; Okazaki, R. *Bull. Chem. Soc. Jpn.* **1988**, *61*, 735–740. (d) Louafi, F.; Hurvois, J.-P.; Chibani, A.; Roisnel, T. *J. Org. Chem.* **2010**, *75*, 5721–5724. (e) Liermann, J. C.; Opatz, T. *J. Org. Chem.* **2008**, *73*, 4526–4531.
- (23) Bobbitt, J. M.; Steinfeld, S.; Weisgraber, K. H.; Dutta, S. *J. Org. Chem.* **1969**, *34*, 2478–2479.
- (24) Meyers, A. L.; Guiles, J. *Heterocycles* **1989**, *28*, 295–301.
- (25) Johnstone, R. A. W.; Rose, M. E. *Tetrahedron* **1979**, *35*, 2169–2173.
- (26) Mohri, K.; Suzuki, K.; Usui, M.; Isobe, K.; Tsuda, Y. *Chem. Pharm. Bull.* **1995**, *43*, 159–161.
- (27) Jones, B. A.; Bradshaw, J. S.; Nishioka, M.; Lee, M. L. *J. Org. Chem.* **1984**, *49*, 4947–4951.
- (28) Caferio, L. R.; Snowden, T. S. *Org. Lett.* **2008**, *10*, 3853–3856.
- (29) Bailey, K. R.; Ellis, A. J.; Reiss, R.; Snape, T. J.; Turner, N. J. *Chem. Commun.* **2007**, *35*, 3640–3642.
- (30) (a) Chrzanowska, M.; Dreas, A. *Tetrahedron: Asymmetry* **2004**, *15*, 2561–2567. (b) Mujahidin, D.; Doye, S. *Eur. J. Org. Chem.* **2005**, 2689–2693. (c) Boudou, M.; Enders, D. *J. Org. Chem.* **2005**, *70*, 9486–9494. (d) Cheng, J.-J.; Yang, Y.-S. *J. Org. Chem.* **2009**, *74*, 9225–9228.
- (31) Halbsguth, C.; Meissner, O.; Haeblerlein, H. *Planta Med.* **2003**, *69*, 305–309.
- (32) Brown, R. C. D.; Bataille, C. J. R.; Bruton, G.; Hinks, J. D.; Swain, N. A. *J. Org. Chem.* **2001**, *66*, 6719–6728.
- (33) Hashima, H.; Hayashi, M.; Kamano, Y.; Sato, N. *Bioorg. Med. Chem.* **2000**, *8*, 1757–1766.
- (34) Banholzer, K.; Campbell, T. W.; Schmid, H. *Helv. Chim. Acta* **1952**, *35*, 1577–1581.
- (35) Ishibashi, H.; Miki, Y.; Ikeda, Y.; Kiriya, A.; Ikeda, M. *Chem. Pharm. Bull.* **1989**, *37*, 3396–3398.
- (36) Pouységou, L.; Avellan, A.-V.; Quideau, S. *J. Org. Chem.* **2002**, *67*, 3425–3436.
- (37) Bermejo, A.; Andreu, I.; Suvire, F.; Léonce, S.; Caignard, D. H.; Renard, P.; Pierré, A.; Enriz, R. D.; Cortes, D.; Cabedo, N. *J. Med. Chem.* **2002**, *45*, 5058–5068.
- (38) Cheng, J.-J.; Yang, Y.-S. *J. Org. Chem.* **2009**, *74*, 9225–9228.
- (39) Martins, J. E. D.; Clarkson, G. J.; Wills, M. *Org. Lett.* **2009**, *11*, 847–850.
- (40) Jones, B. A.; Bradshaw, J. S.; Nishioka, M.; Lee, M. L. *J. Org. Chem.* **1984**, *49*, 4947–4951.
- (41) Lee, J.; Lee, J.-H.; Kim, S. Y.; Perry, N. A.; Lewin, N. E.; Ayres, J. A.; Blumberg, P. M. *Bioorg. Med. Chem.* **2006**, *14*, 2022–2031.
- (42) Duclos, R. L., Jr.; Tung, J. S.; Rapoport, H. *J. Org. Chem.* **1984**, *49*, 5243–5246.
- (43) Wyratt, J. M.; Hazen, G. G.; Weinstock, L. M. *J. Org. Chem.* **1987**, *52*, 944–945.
- (44) Okano, K.; Tokuyama, H.; Fukuyama, T. *J. Am. Chem. Soc.* **2006**, *128*, 7136–7137.
- (45) Memetizidis, G.; Stambach, J.-F.; Jung, L. *Heterocycles* **1990**, *31*, 341–351.
- (46) Seo, J. W.; Srisook, E.; Son, H. J.; Hwang, O.; Cha, Y.-N.; Chi, D. Y. *Eur. J. Med. Chem.* **2008**, *43*, 1160–1170.
- (47) Baughman, T. W.; Sworen, J. C.; Wagener, K. B. *Tetrahedron* **2004**, *60*, 10943–10948.
- (48) Bender, D. M.; Williams, R. M. *J. Org. Chem.* **1997**, *62*, 6690–6691.
- (49) Faller, J. W.; Phillips, J. P. *Anal. Chim. Acta* **1965**, *32*, 586–589.
- (50) Oger, J. M.; Fardeau, A.; Richomme, P.; Guinaudeau, H.; Fournet, A. *Can. J. Chem.* **1993**, *71*, 1128–1135.
- (51) Slavik, J.; Slavikova, L. *Collect. Czech. Chem. Commun.* **1989**, *54*, 2009–2020.
- (52) Stermitz, F. R.; Teng, L. C. *Tetrahedron Lett.* **1967**, *8*, 1601–1602.

Appendix

Curriculum Vitae



Personal Information

Name	Mag. Wolf-Dieter Lienhart
Adress	Hauptstraße 253, 8591 Maria Lankowitz
E-mail	wolf-dieter.lienhart@tugraz.at
Telephone	0043 650 8142947
Date and place of birth	08. March 1983, Voitsberg (Austria)

Education

2004 -2010 Diploma study Biochemistry - Karl Franzens Universität Graz (Austria)

2007 Temporary employment abroad NIOZ Royal Netherlands Institute for Sea Research

Since 2010 PhD Departments of Biochemistry -Graz University of Technology (Austria)

Awards

2014 Best Poster award on the 12th DocDay-NAWI Graz Doctoral School of Molecular Biosciences and Biotechnology

further Activities

In charge of the computer equipment of the Institute for Biochemistry (Graz Technical University) since 2011

Additional skills

Languages	German – native
	English – business fluent
	Italian – school knowledge
IT knowledge	Good command of office suite (word processor, spread sheet, presentation software)
	Good command of photo editing software gained as an amateur photographer
	Basic knowledge in programming (Visual Studio)

Licenses

- Driving license class B
- License to handle explosives

Publications

Papers:

Schrittwieser JH, Resch V, Sattler JH, Lienhart W, Durchschein K, Winkler A, et al.

Biokatalytische enantioselektive oxidative C-C-kupplung durch C-H-aktivierung mit molekularem sauerstoff. *Angewandte Chemie*. 2011;123(5):1100-3.

Schrittwieser JH, Resch V, Sattler JH, Lienhart WD, Durchschein K, Winkler A, et al.

Biocatalytic enantioselective oxidative C-C coupling by aerobic C-H activation. *Angew Chem Int Ed Engl*. 2011 Feb 1;50(5):1068-71.

Schrittwieser JH, Resch V, Wallner S, Lienhart WD, Sattler JH, Resch J, et al. Biocatalytic organic synthesis of optically pure (S)-scoulerine and berbine and benzyloquinoline alkaloids. *J Org Chem*. 2011 Aug 19;76(16):6703-14.

Lienhart WD, Gudipati V, Macheroux P. The human flavoproteome. *Arch Biochem Biophys*. 2013 Jul 15;535(2):150-62.

Gudipati V, Koch K, Lienhart WD, Macheroux P. The flavoproteome of the yeast *saccharomyces cerevisiae*. *Biochim Biophys Acta*. 2014 Mar;1844(3):535-44.

Lienhart WD, Gudipati V, Uhl MK, Binter A, Pulido SA, Saf R, et al. Collapse of the native structure caused by a single amino acid exchange in human NAD(P)H:Quinone oxidoreductase(1.). *FEBS J*. 2014 Oct;281(20):4691-704.

Presentations:

Schrittwieser, J. H.; Resch, V.; Sattler, J.; Lienhart, W.-D.; Wallner, S.; Gruber, K.; Macheroux, P.; Kroutil, W. Access to novel berbine derivatives employing the berberine bridge enzyme. 17th International Symposium on Flavins and Flavoproteins. San Francisco 27.07.2011

Lienhart, W.-D.; Gudipati, V.; Macheroux, P. The role of NAD(P)H:quinone oxidoreductase 1 in human cancer development. 7th DocDay NAWI Graz Doctoral School of Molecular Biosciences and Biotechnology. Graz 06.02.2012

Posters:

Agogué H., Brink M., Lienhart W-D., Herndl G. J. Distinct archaeoplankton assemblages characterize the meso- and bathypelagic zones of the eastern North Atlantic basin. SAME 10 (10th Symposium on Aquatic Microbial Ecology), Faro, Portugal, Sept 2007

Gudipati, V.; Lienhart, W.-D.; Koch, K.; Macheroux, P. Yeast quinone reductase Lot6p and its interactions with 20S proteasome and Yap4p. Enzymes & Signals - A research summit of the

DK Molecular Enzymology and the DK Molecular Mechanisms of Cell Signaling. Graz,
09.12.2012

Gudipati, V.; Lienhart, W.-D.; Koch, K.; Dohmen, J.; Macheroux, P. Yeast quinone reductase Lot6p mediates the degradation of transcription factor Yap4p by the 20S proteasome. FEBS Special Meeting on "Protein Quality Control and Ubiquitin Systems in Health and Disease". Kusadasi, Turkey 14.11.2012

Macheroux, P.; Gudipati, V.; Uhl, M. K.; Zangger, K.; Gruber, K.; Lienhart, W.-D. The role of NAD(P)H:quinone oxidoreductase 1 (NQO1) in human cancer development. FEBS Congress. St. Petersburg, Russian Federation 08.07.2013

Lienhart, W.-D.; Gudipati, V.; Uhl, M. K.; Zangger, K.; Gruber, K.; Macheroux, P. The role of NAD(P)H:quinone oxidoreductase 1 in human cancer development. 10th DocDay - NAWI Graz Doctoral School of Molecular Biosciences and Biotechnology. Graz 12.07.2013

Lienhart, W.-D.; Strandback, E. S.; Gudipati, V.; Uhl, M. K.; Binter, A.; Pulido, S.; Zangger, K.; Gruber, K.; Macheroux, P. Insight into the structural behavior of a natural variant of NAD(P)H:quinone oxidoreductase 1 (NQO1). Enzyme Mechanisms by Biological Systems. Manchester, UK 01.06.2014

Lienhart, W.-D.; Strandback, E. S.; Gudipati, V.; Uhl, M. K.; Binter, A.; Pulido, S.; Zangger, K.; Gruber, K.; Macheroux, P. Insight into the structural behaviour of a natural variant of NAD(P)H:quinone oxidoreductase 1 (NQO1). 12th DocDay-NAWI Graz Doctoral School of Molecular Biosciences and Biotechnology. University of Graz 18.07.2014

Strandback, E. S.; Lienhart, W.-D.; Gudipati, V.; Uhl, M. K.; Binter, A.; Pulido, S.; Zangger, K.; Gruber, K.; Macheroux, P. Insight into the structural behaviour of a natural variant of NAD(P)H:quinone oxidoreductase 1 (NQO1). - 18th International Symposium on Flavins and Flavoproteins. Cha-Am, Thailand 27.07.2014